Universitat de Girona

UV INDEX MEASUREMENT AND MODEL AGREEMENT: UNCERTAINTIES AND LIMITATIONS

Jordi BADOSA I FRANCH

ISBN: 84-689-6849-8
Dipòsit legal: GI-208-2006

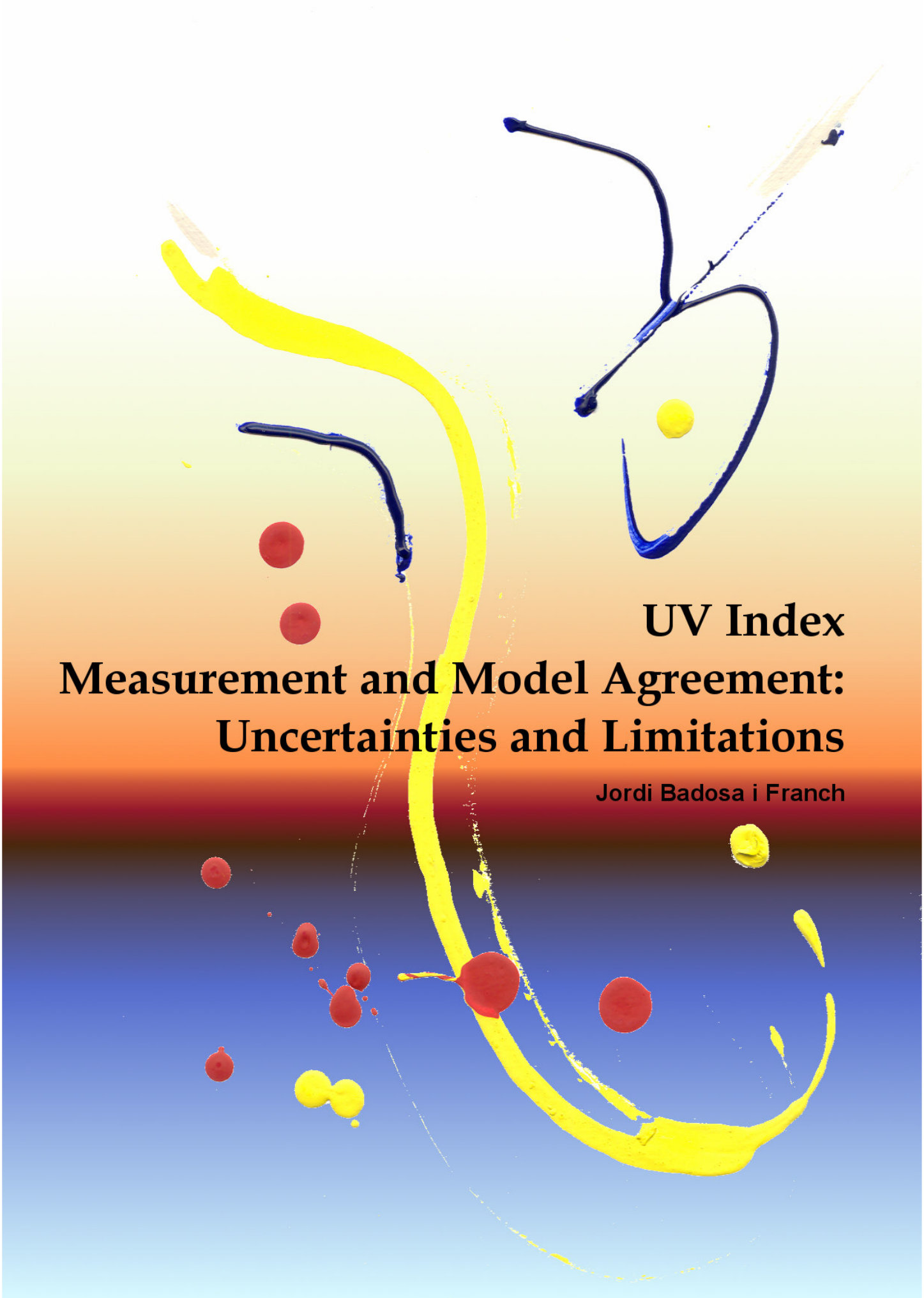

UV Index Measurement and Model Agreement: Uncertainties and Limitations

Jordi Badosa i Franch

UV Index Measurement and Model Agreement: Uncertainties and Limitations

Jordi Badosa i Franch

Thesis work supervised by
Josep Calbó
Josep Abel Gonzàlez

Universitat de Girona

Doctorat de Medi Ambient
Itinerari de Física i Tecnologia Ambiental

Girona, May 2005

Here and Now.

Acknowledgements

This Thesis work has been developed thanks to a pre-doctoral scholarship (FI) from the Ministry of Universities, Research and Information Society (DURSI) of the Government of Catalonia.

This work has been partly funded through projects IMMPACTE from the Ministry of Environment of the Government of Catalonia, and DEPRUVISE (REN2000-0903-C08-01/CLI) from the Ministry of Science and Technology of the Government of Spain.

Part of the work, mainly the Chapter 5, followed on from a three-month research stay in 2002 of the author at the Royal Netherlands Meteorological Institute (KNMI) at De Bilt, The Netherlands, under the supervision of Dr. Michiel van Weele.

Most of the studies presented have been partly developed during research stays of the author at the National Institute of Water and Atmospheric Research (NIWA) at Lauder, New Zealand, in 2003 (three months) and 2004 (four months and a half). For this, we feel very grateful with Dr. Richard McKenzie, who supervised those stays; his trust, enthusiasm and guidance in this work are very much appreciated.

All the individuals and institutions listed in Table 4.2 are gratefully acknowledged for the supply and support of the data used in Chapter 4.

I would also like to thank Dr. Chuck Long of Pacific Northwest National Laboratory (Richland, WA, USA) for the kind assistance in the use of the software for the clear sky selection process presented in Chapter 4.

I would also like to thank Alexander Los from Kipp & Zonen for his kind dedication and efforts in the characterisation of the erythemal radiometer installed in Girona.

I also want to specially thank Josep Calbó and Josep Abel González for the opportunity of undertaken this PhD Thesis, for the support, guidance, trust and understanding during these almost 5 years of working together.

There would be many other names worth mentioning here. I just hope I have been able to show my sincere gratitude because a part of this Thesis belongs to them, and it wouldn't be like this without them.

Publications related to this Thesis

Badosa J., González J.A., Pagès D. and J. Calbó (2002) "Modelling surface UV erythemal irradiance from ozone satellite retrievals", *European Geophysical Society 27th General Assembly. Nice (France). Abstract in Geophysical Research Abstracts.*

Badosa J., González J.A., Pagès D. and J. Calbó (2002) "Sensitivity of UV and VIS cloudless irradiance on variables describing atmospheric aerosols", *European Geophysical Society 27th General Assembly. Nice (France). Abstract in Geophysical Research Abstracts.*

Pagès D., Calbó J., González J.A. and J. Badosa (2002) "Comparison of several ground-based cloud detection techniques", *European Geophysical Society 27th General Assembly. Nice (France). Abstract in Geophysical Research Abstracts*.

Badosa J. (2002) "Mesures d'Irradiància UV Eritemàtica a Catalunya *vs* Modelitzacions per Cels Serens a partir de la Columna d'Ozó d'EP/TOMS (Erythemal UV Irradiance measurements in Catalonia vs. Modelling for Clear Skies Taking the Ozone Column from EP/TOMS)" *Minor Thesis. Doctorate in Environment, University of Girona.*

Badosa J., van Weele M. (2002) "Effects of Aerosols on UV Index", Scientific Report (WR-2002-07), *KNMI.*

Badosa, J., van Weele M., Allaart M. (2003) "Parameterisations for Cloudless UV Index Calculations", *EGS-AGU-EUG Joint Assembly. Nice (France). Abstract in Geophysical Research Abstracts*

Badosa J. Gonzàlez J. A., Calbó J., van Weele M., McKenzie R. L., (2004) "Typical annual UVI values in Catalonia, Spain" *International NIR Workshop &* Symposium, Seville, Spain.

Lorente, J., X. De Cabo, Campmany, E., Sola, Y., González, J.A., Calbó, J., Badosa, J., Alados-Arboledas, L., Martínez-Lozano, A., Cachorro, V., Labajo, A., De La Morena, B., Díaz, J.P., Pujadas, M., Horvath, H., Silva, A.M., Pavese G., (2004), "Altitude effect on UV Index deduced from the veleta-2002 experimental campaign (Spain)" *Internacional Radiation Symposium, Busan, Korea.*

Badosa, J., González J.A., J., Calbó J., van Weele M., McKenzie, R. L. (2005), "Using a parameterization of a radiative transfer model to build high resolution maps of typical clear sky UV index in Catalonia, Spain", *Journal of Applied Meteorology*, *44 (6), 789-803*

McKenzie, R. L., Badosa, J., Kotkamp, M., Johnston, P., (2005), Effects of the temperature dependence in PTFE diffusers on observed UV irradiances, *Geophysical Research Letters*, *32 (L06808)*, doi:10.1029/2004GL022268.

McKenzie, R. L., Johnston, P, Kotkamp, M., Smale, D., Badosa, J., O'Neill, M., Hofmann, D. (2005) "Decadal Time Series of UV Irradiances at two NDSC Sites" *Spring AGU Meeting, New Orleans, USA, 23-27 May, (Ref No. 368) & CMDL Annual Meeting.*

Badosa, J., McKenzie, R.L. , Kotkamp, M., Calbó J., González J. A., Johnston, P. V., O'Neill, M., Anderson, D. J., et al. (2005, in prep), "Erythemal UV irradiance model versus measurement: limitations revealed from a study of clear-sky data from four diverse sites", *Journal of Geophysical Research*, *to be submitted –June 2005*.

Summary

The increase in solar ultraviolet radiation (UVR) levels reaching the Earth surface during the last decades (mostly induced by the stratospheric ozone depletion), together with a detected increase in UVR-related diseases, has lead to a high volume of investigations about this band of the solar radiation and its effects on human beings.

The ultraviolet Index (UVI), which is currently internationally adopted, was defined in order to disseminate information to the public about the risks of exposing the naked body to UVR and to send preventive messages. UVI was initially defined as the maximum daily value. However, the current use of this index has been widened and nowadays it makes sense to refer to an instantaneous value or to the evolution of the measured, modelled, or predicted UVI during the day. The actual value of UVI is affected by the Sun-Earth geometry, clouds, ozone, aerosols, altitude and ground albedo.

High quality UVI measurements are essential as a reference and to study long-term trends; accurate modelling techniques are needed to understand the way factors affect UVR, to predict UVI, and as a quality control of the measurements. For the UVI measurement, best accuracy is expected with data from spectroradiometers. However, since the costs of these devices are expensive, data from erythemal radiometers are more commonly available (most UVI networks are equipped with this latter type of sensors). Best UVI modelling performance is found with multi-scattering radiative transfer models when the input information is well known. However, some relevant input information, such as the aerosol optical properties, is usually not available which can lead to large modelling uncertainties. More simple models are often used for applications such as UVI prediction or elaboration of UVI maps, as they are much faster and require less input parameters.

Considering this framework, **the general objective of this work is to analyse the agreement that can be reached between modelled and measured UVI for cloudless conditions.**

For this, model-measurement comparisons are presented for different modelling techniques, for several input options, and for UVI measured by both erythemal radiometers and spectroradiometers. As a general conclusion, it can be stated that the comparison of modelled vs. measured UVI is very useful to detect limitations and estimate uncertainties in both the modelling and measurements.

As far as modelling is concerned, the main limitations found are the lack of knowledge in the aerosol information considered as input. Also, important differences are found between the ozone column from satellite and from ground based measurements, which lead to important differences in the modelled UVI.

PTUV, a new simple parameterisation for fast UVI calculations for cloudless conditions, has been developed based on radiative transfer calculations. The parameterisation shows a good performance both with respect to the base model and to diverse UVI measurements. PTUV has demonstrated to be useful for particular applications such as to study the annual UVI variation at a particular site (Girona) and to build high resolution maps of typical UVI for a territory (Catalonia).

Regarding the measurements, it is found that the use of the actual spectral response of the erythemal radiometers is very important to avoid large uncertainties in the measured UVI. If well characterised, the erythemal radiometers compare reasonably well with high quality spectroradiometers when measuring UVI. Major issues with respect to the measurements are long term calibration accuracy and stability. Also, a temperature effect in PTFE, a material used as diffuser in some instruments, has been observed, which could have potentially important implications in the experimental field.

Finally, and concerning the model-measurement comparisons, the best agreement has been found when high quality spectroradiometric UVI measurements are considered and radiative transfer models are applied taking into account the best data available regarding aerosol and ozone optical parameters and their changes in time. In this case, the agreement can be as high as 0.1% in UVI, and typically less than 3%. This agreement deteriorates greatly if aerosols are ignored, and depends importantly on the aerosol single scattering albedo. Other data, such as ground albedo or the actual atmospheric temperature and ozone profiles, introduce lower uncertainty in the modelling results.

Resum

En les últimes dècades, l'increment dels nivells de radiació solar ultraviolada (UVR) que arriba a la Terra (principalment degut a la disminució d'ozó estratosfèric) juntament amb l'augment detectat en malalties relacionades amb l'exposició a la UVR, ha portat a un gran volum d'investigacions sobre la radiació solar en aquesta banda i els seus efectes en els humans.

L'índex ultraviolat (UVI), que ha estat adoptat internacionalment, va ser definit amb el propòsit d'informar al públic general sobre els riscos d'exposar el cos nu a la UVR i per tal d'enviar missatges preventius. L'UVI es va definir inicialment com el valor màxim diari. No obstant, el seu ús actual s'ha ampliat i té sentit referir-se a un valor instantani o a una evolució diària del valor d'UVI mesurat, modelitzat o predit. El valor concret d'UVI està afectat per la geometria Sol-Terra, els núvols, l'ozó, els aerosols, l'altitud i l'albedo superficial.

Les mesures d'UVI d'alta qualitat són essencials com a referència i per estudiar tendències a llarg termini; es necessiten també tècniques acurades de modelització per tal d'entendre els factors que afecten la UVR, per predir l'UVI i com a control de qualitat de les mesures. És d'esperar que les mesures més acurades d'UVI s'obtinguin amb espectroradiòmetres. No obstant, com que els costs d'aquests dispositius són elevats, és més habitual trobar dades d'UVI de radiòmetres eritemàtics (de fet, la majoria de les xarxes d'UVI estan equipades amb aquest tipus de sensors).

Els millors resultats en modelització s'obtenen amb models de transferència radiativa de dispersió múltiple quan es coneix bé la informació d'entrada. No obstant, habitualment no es coneix informació d'entrada, com per exemple les propietats òptiques dels aerosols, la qual cosa pot portar a importants incerteses en la modelització. Sovint, s'utilitzen models més simples per aplicacions com ara la predicció d'UVI o l'elaboració de mapes d'UVI, ja que aquests són més ràpids i requereixen menys paràmetres d'entrada.

Tenint en compte aquest marc de treball, **l'objectiu general d'aquest estudi és analitzar l'acord al qual es pot arribar entre la mesura i la modelització d'UVI per condicions de cel sense núvols.**

D'aquesta manera, en aquest estudi es presenten comparacions model-mesura per diferents tècniques de modelització, diferents opcions d'entrada i per mesures d'UVI tant de radiòmetres eritemàtics com d'espectroradiòmeters. Com a conclusió general, es pot afirmar que la comparació model-mesura és molt útil per detectar limitacions i estimar incerteses tant en les modelitzacions com en les mesures.

Pel que fa a la modelització, les principals limitacions que s'han trobat és la falta de coneixement de la informació d'aerosols considerada com a entrada dels models. També, s'han trobat importants diferències entre l'ozó mesurat des de satèl·lit i des de la superfície terrestre, la qual cosa pot portar a diferències importants en l'UVI modelitzat.

PTUV, una nova i simple parametrització pel càlcul ràpid d'UVI per condicions de cel serens, ha estat desenvolupada en base a càlculs de transferència radiativa. La parametrització mostra una bona execució tant respecte el model base com en comparació amb diverses mesures d'UVI. PTUV ha demostrat la seva utilitat per aplicacions particulars com ara l'estudi de l'evolució anual de l'UVI per un cert lloc (Girona) i la composició de mapes d'alta resolució de valors d'UVI típics per un territori concret (Catalunya).

En relació a les mesures, es constata que és molt important saber la resposta espectral dels radiòmetres eritemàtics per tal d'evitar grans incerteses a la mesura d'UVI. Aquest instruments, si estan ben caracteritzats, mostren una bona comparació amb els espectroradiòmetres d'alta qualitat en la mesura d'UVI. Les qüestions més importants respecte les mesures són la calibració i estabilitat a llarg termini. També, s'ha observat un efecte de temperatura en el PTFE, un material utilitzat en els difusors en alguns instruments, cosa que potencialment podria tenir implicacions importants en el camp experimental.

Finalment, i pel que fa a les comparacions model-mesura, el millor acord s'ha trobat quan es consideren mesures d'UVI d'espectroradiòmetres d'alta qualitat i s'usen models de transferència radiativa que consideren les millors dades disponibles pel que fa als paràmetres òptics d'ozó i aerosols i els seus canvis en el temps. D'aquesta manera, l'acord pot ser tan alt dins un 0.1º% en UVI, i típicament entre menys d'un 3%. Aquest acord es veu altament deteriorat si s'ignora la informació d'aerosols i depèn de manera important del valor d'albedo de dispersió simple dels aerosols. Altres dades d'entrada del model, com ara l'albedo superficial i els perfils d'ozó i temperatura introdueixen una incertesa menor en els resultats de modelització.

Table of contents

1
Introduction

General frame

The Sun emits electromagnetic radiation mainly from 200 to 4000 nm. The solar ultraviolet radiation (UVR) (200-400 nm) reaching the top of the atmosphere is about the 8% of the total solar radiation (39% is in the visible band and 53% belongs to the infrared). UVR reaching the Earth surface is even less, both in absolute and in relative terms, as it is strongly absorbed by the atmospheric constituents, in particular ozone. Despite being a small portion of solar radiation, UVR has a decisive role in the atmospheric chemistry and it is necessary for life, though in large amounts it can have serious harmful effects on living organisms. In particular, human exposure to UVR may have serious acute or chronic effects on skin, eyes and immune system.

The research on UVR has its origins in the beginning of the 20th Century. However, the discovery of the stratospheric ozone depletion attributed to emissions of chlorofluorocarbons (CFCs) in mid 1970s unchained a boom in investigation on UVR and its relation to the ozone amount became a very important research field. Simultaneously, and related also with changes in population habits, an increase in skin cancer cases was detected, which lighted a health alarm. Many organisations were created, institutions joined efforts and a lot of research groups focused on the study of this kind of radiation, designing and improving the instrumentation, studying the biological effects of the UV radiation and also disseminating information to advise the population about the UV risks. In this sense, Australia was the first country to promote educational campaigns and to warn the population about the UV levels and their potentially harmful effects. In 1987, New Zealand began prevention campaigns. A UV index (ranging between 0 and 10) was defined in Canada in 1992; daily predictions of this index were disseminated. United States elaborated a similar index.

Nowadays, a single definition of the UV Index (UVI) is accepted by the science community and supported by international organizations such as the World Health Organization (WHO), the United Nations Environment Programme (UNEP), the World Meteorological Organization (WMO) and the International Commission on Non-Ionizing Radiation Protection (ICNIRP).

Overview

This chapter aims to give a general view of UVR, its most known implications on human health and to present UVI and its use as an educational tool. In addition, introduction about different techniques to measure and model UVI and descriptions about the most important factors affecting UVI are exposed briefly in order to set a general frame of this study.

1.1 UV radiation and health effects

The ultraviolet radiation (UVR) is usually discomposed into three ranges, depending on its biological effect: UVC (200-280 nm), UVB (280-315 nm) and UVA (315-400 nm). The boundary between UVB and UVA is somewhat ambiguous, and some authors set it at 320 nm, because there is still ozone absorption between 315 and 320 nm. However, most international agencies and consortia agree in establishing this boundary at 315 nm: the World Health Organization (WHO), the United Nations Environment Programme (UNEP), the World Meteorological Organization (WMO) and the International Commission on Non-Ionizing Radiation Protection (ICNIRP) [*WHO*, 2002], the European Union's action COST 713 [*Vanicek, et al.*, 2000], the *Commission Internationale de l'Eclairage* [*CIE*, 1999] and the International Agency for Research on Cancer [*IARC*, 1992].

The whole UVC and most of UVB are absorbed in the upper atmosphere mainly by the molecules of ozone (O_3) (in the bands of Hartley and Huggins) and oxygen (O_2) (Herzberg band). UVA is much less affected by ozone. Figure 1.1 shows the absorption cross sections for these two molecules as well as for NO_2 in the UV region.

Note that NO_2 has similar absorption cross sections as O_3 and even larger in the UVA region. However, the concentration of NO_2 in the atmosphere is about 1000 times lower than for O_3 so the UV absorption by the former is much less important, even less than the UV absorption by O_2. Actually, since O_2 is more abundant than O_3 (about $3 \cdot 10^5$ times in volume), the oxygen optical depth is about 25 times larger than the ozone optical depth at 200 nm; they are similar around 220 nm and for longer wavelengths the ozone becomes strongly dominant. In this way, O_3 is the most important atmospheric gas to take into account for its effects on UVR on the ground.

It is essential for life that UVC and most of UVB do not reach the surface since they can be very harmful (leading to death) for living beings. However, life would not be possible as we know it without UVB and UVA, since they play a decisive role. As far as human beings are concerned, solar UVB radiation is essential since it promotes the synthesis in the skin of pro-vitamin D (obtained through the diet) to vitamin D [*MacKie*, 1999]. Deficiencies in vitamin D lead to rickets, and the development of soft deformable bones. However, excessive UV radiation exposure may cause both acute and long-term harmful effects on the skin, the eyes and the immunologic system. Probably, the most dangerous effect is the damage to DNA [*Diffey*, 1992].

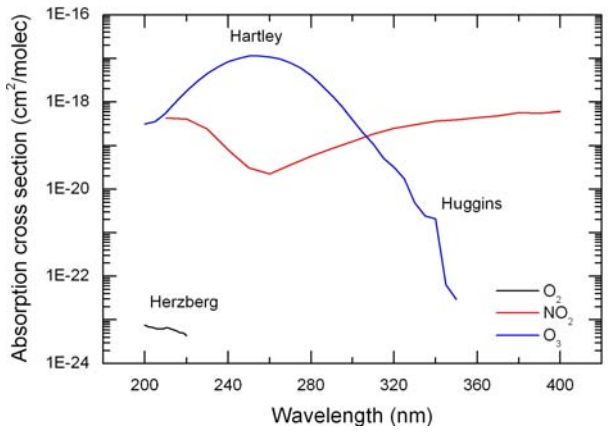

Figure 1.1 Absorption cross sections for the molecules of O_3, O_2, and NO_2 from *Lenoble* [1993, Tables 17.1, 17.3 and 17.4, pp 288-293].

The best known acute effect of excessive UVR exposure on skin is sunburn (erythema), that appears 3-5 hours after exposition if the dose of erythemal irradiance (UVE, see section 1.2) has exceeded (by definition) 1 unit of Minimum Erythemal Dose (MED). The definition of 1 MED ranges from 200 to 500 Jm^{-2} depending on skin type among the European (Caucasian) population [*Vanicek, et al.*, 2000]. Table 1.1 shows characteristics of the six skin phototypes according to *Fitzpatrick* [1988]. Erythema is mainly caused by exposure to UVB

Table 1.1 Skin phototypes classification from *Fitzpatrick* [1988]. Table composition is taken from *WHO* [2002] and MED information is from *Vanicek et al.* [2000]

Skin type		Skin description	Burns in the Sun	Tans after having been in the sun	1MED
I	Melano-compromised	Fair (Caucasians)	Always	Seldom	200 J/m^2
II			Usually	Sometimes	250 J/m^2
III	Melano-competent	Medium (Caucasians)	Sometimes	Usually	350 J/m^2
IV		Dark (Caucasians)	Seldom	Always	450 J/m^2
V	Melano-protected	Asian or Indian	Naturally brown skin		
VI		Afro-Caribbean or Black	Naturally black		

radiation, which also is the main causal factor for various skin cancers, such as non melanocytic carcinoma (including Basal Cell Carcinoma BCC and Squamous Cell Carcinoma SCC) and melanoma skin cancer (MSC) at the pigment cells. On the other hand, UVA radiation has a pronounced effect on the subcutaneous tissue and can alter the structure of collagen and elastin fibres and hence accelerate ageing of the skin. It has been estimated that between two and three million non melanoma skin cancers and approximately 132,000 cases of MSC occur each year worldwide. In the event of a 10% decrease in stratospheric ozone, an additional of 300,000 non-melanoma and 4,500 melanoma skin cancers could be expected worldwide due to the corresponding UV increase, although there is big uncertainty in the relationship between UV and skin cancer [*WHO*, 1995, 2002; *WMO*, 1994].

Eyes can also be affected by excessive UVR exposure. Note that skin has a capacity to adapt to UVR by producing melanin (tan) that protects against UV exposure, while the eye does not. Main effects of exposure to UVR on the eye are cataracts and photo-keratitis (welder's flash, snow blindness). Eye damage is strongly related to UVA, since UVA penetrates deeper than UVB in the eye [*Bruls, et al.*, 1984]. Cataracts are a deformation of the crystalline lens that can result in blindness. Some 20 million people worldwide are currently blind as a result of cataracts, and 12-20% of these cases may be related to excessive UV exposure [*Keeling, et al.*, 1995; *WHO*, 2002]. A decrease by 1% of ozone column is estimated to produce 0.5% increase in new cataract cases. Photo-keratitis is a transient blindness caused by inflammation of the cornea and iris that appears after an acute exposure to UV. Two hours in a place surrounded by snow-covered surfaces can result in photo-keratitis; in comparison, in a sandy area, the effect would appear after 6-8 hours of eye exposition. Other less usual UV-related eye diseases are eye melanoma and photo-conjunctivitis.

Finally, some relations between UV and suppression of immune system have also been reported [*Selgrade, et al.*, 1997; *WHO*, 1995]. Suppression of immune system triggered by UV exposure could lead to increased probability to develop herpes, increased susceptibility to certain infectious diseases, and decreased vaccine effectiveness, as well as the development of illnesses such as contact hypersensitivity response (CHR). More studies are needed to establish UV role in all these effects.

During the second half of the 20th century, a lot of cases of skin cancer and cataracts appeared, not only because of the increase of UV radiation (caused by the decline of stratospheric ozone), but also due to the change in the habits of the population. Indeed, a white skin was a symbol of social status in the beginning of the 20th century, but with the establishment of the concept of holidays and the growing habits for outdoors activities, in particular going to the beach, tanned skins began to be very desirable. This, together with the evolution of the fashion towards less covering clothes, leaded to increased exposition of

the skin to UVR and, as a consequence, so did the health risks. Australia, New Zealand, and Canada are some of the countries where more cases of skin cancer and cataracts have appeared since then. That was influenced by the fact that these countries were mostly colonized by English and French people, who have whiter skin (and therefore less natural protection to high UV levels) than the native people of these areas. In order to advise and warn the population about the risks of exposing the naked body to UVR, these three countries began to disseminate information and gave some simple indices representing the maximum UV level expected for the next day. This was the embryo of the nowadays accepted UV Index.

1.2 UV Index

The UV Index (UVI) is a quantitative approach to account for the UV levels that are important for the effects on the human skin. UVI is a unitless quantity derived from UVE, which is the integration of the monochromatic UV irradiance ($S(\lambda)$) (280-400 nm) weighted by the CIE spectral action function [*McKinlay and Diffey*, 1987]:

$$UVE = \int_{280}^{400} S(\lambda) \cdot CIE(\lambda) \cdot d\lambda \qquad (1.1)$$

Figure 1.2 shows a typical summer noon spectrum of global irradiance at midlatitudes together with the CIE function and the resulting spectral erythemal irradiance. Note that, the contribution of UVB on UVE is larger than the contribution of UVA. For the non-weighted irradiance, 94% (about 52 W/m^2, in this case) of the energy corresponds to UVA and only the 6% (about 3 W/m^2) is in the UVB range. In contrast, for UVE the contribution of the UVB range is 83% while only the 17% is in the UVA. These numbers show the important role of the UVB radiation although it constitutes less than 0.1% of the total solar irradiance. This highlights that small changes in UVB radiation can lead to significant changes in UVE and therefore to strong biological effects and also that the measurement of this radiation is an instrumental challenge, since very precise and sensitive instruments are needed.

Specifically, UVI is found by multiplying UVE (in Wm^{-2}) by 40 and it is usually rounded to the closest integer for its dissemination; for the example in Figure 1.2, UVI would be 9. The UVI scale usually ranges from 0 to 16 although in some regions and seasons it can be even larger. UVI was first defined as the maximum daily-predicted value. However, the current use of this index has been widened and nowadays it makes sense to refer to an instantaneous value and the evolution of the measured, modelled, or predicted UVI during the day.

UVI is the magnitude advised for general information to the public. However, for other purposes, for example related to epidemiology and medicine, erythemal doses (in J/m^2) integrated over hours, days, months or years are preferred.

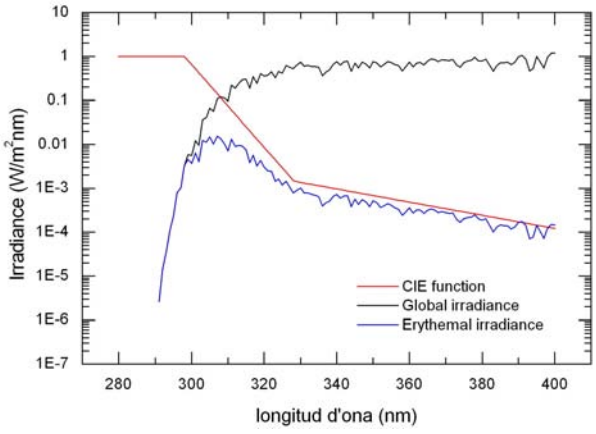

Figure 1.2 Typical summer spectrum of global UV Irradiance and UVE, which results from multiplying the former by the CIE function.

1.3 UVI as an educational tool

A race to a standard ultraviolet index

During the last two decades, continuous efforts have been done to set an international standard ultraviolet index as an educational tool for prevention from the harmful effects of UVR on humans. A first broad discussion on this topic was held in 1994, during the "WMO meeting of experts on UVB measurements, data quality and standardization of UV indices" [*WMO*, 1994]. About the ultraviolet indices, discussions were focused on the method of production, the scale and philosophy as different countries had traditionally adopted different ways.

The countries represented in the meeting were Canada, Germany, New Zealand, Sweden, Finland, UK, USA and Denmark and the Netherlands. Some reported weighted UV doses integrated over several hours, others disseminated the noon UVE, and some also included the effect of clouds through simple correcting factors. Reporting burn times related to different skin types was also common. Some countries initially adopted different weighting functions, such as the ACGIH (American Conference of Governmental Industrial Hygienists) and the DNA action spectra. It was recognized that no one spectrum was appropriate for all effects (on skin, eye, DNA, etc.) and CIE action spectrum appeared to best serve the atmospheric science community at that time. As for the UV index scale, it was adopted the scale used in Canada, that is UVE in Wm^{-2} weighted by 40, as described in section 1.2. From the discussion about which time scales were to be utilized for the UVI calculation, it was recommended to adopt as a minimum requirement the reporting of UVE/UVI at noontime.

This last point was slightly rectified three years later in the frame of another WMO-WHO Meeting [*WMO*, 1998] by stating that "a UV Index forecast should at least present the daily maximum value, whenever it occurs" not at solar noon as stated previously. It was also shown preference on UVI forecasting that include the effects of clouds although it was recognized the complexity and difficulties of considering the cloud effects. There was also some discussion about how burn time information should be disseminated. No clear agreements were reached, although for the countries that decided to disseminate burn times, the recommendation was to do it at least for a "sensitive" skin type. Another outcome of this meeting was that the UV Index should not be associated with a particular sunscreen sun protection factor (SPF) to avoid the interpretation that there is a safe period of sun exposure and that sun exposure can be lengthened with use of sunscreens.

In the frame of the European action COST 713, experts from 13 European countries published a guide for publication and interpretation of solar UV Index forecasts for the public [*Vanicek, et al.*, 2000]. They made recommendations about the kinds of eye and skin protection needed depending on the UVI and the skin type. For the use of sunscreens, a table of SPFs were recommended. In addition, estimations of sunburn times (that is without protection) were also reported as preventive messages. For the estimation of UVI under cloudy conditions, a table of cloud modification factors for different cloud types and amounts of cloud cover was proposed.

In the early 1990s, the WHO, in collaboration with the UNEP, WMO, IARC and ICNIRP had established INTERSUN, a Global UV Project with the mission statement: "To reduce the global burden of disease resulting from exposure to UV radiation". INTERSUN provides scientific information on the health impact and environmental effects of UVR

exposure. The project encourages countries to take action to reduce UVR risks and provides guidance to national authorities.

UVI: an international consensus

In 2002, in the frame of the INTERSUN project, a comprehensive guide on the practical use of UVI was published: "Global solar UV Index. A practical guide" [*WHO*, 2002]. This guide sets recommendations reached by consensus between the above international organizations and currently acts as the reference for the UVI dissemination. Basic recommendations found in previous WMO Meetings and in the COST 713 UVI guide are also stated in this guide. In addition, standard UVR exposure categories and colour scales are recommended as shown in Figure 1.3, which slightly differs from previous recommendations [*Vanicek, et al.*, 2000; *WMO*, 1998]. As a final resolution from previous discussions, the WHO/WMO/UNEP/ICNIRP UVI guide recommends not reporting burn times. The reason behind this is to avoid sending wrong messages to the public since, from the statements "time to burn" or "safe tanning time", it could be interpreted that extending exposure is acceptable, as it had been discussed previously. The guide states that "Although the priority goal of primary skin cancer prevention is to avoid sunburn, cumulative UV radiation exposure plays a major role in developing skin cancer and promotes damage to the eyes and immune system". As a summary of suggestions, Figure 1.4 shows the recommended outdoors habits depending on the value of the actual UVI.

The Basic sun protection messages reported in the guide are:

- Limit exposure during midday hours.
- Seek shade.
- Wear protective clothing.
- Wear a broad-brimmed hat to protect the eyes, face and neck.
- Protect the eyes with wrap-around design sunglasses or sunglasses with side panels.
- Use and reapply broad-spectrum sunscreen of SPF 15+ liberally.
- Avoid tanning beds.
- Protect babies and young children: this is particularly important.

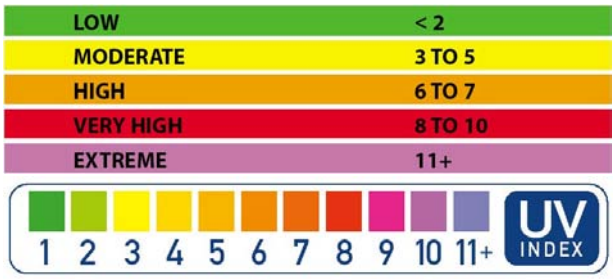

Figure 1.3 UVI colour scales from WHO [2002]. Above: The UV radiation exposure categories Below: colour scale for UVI coded maps

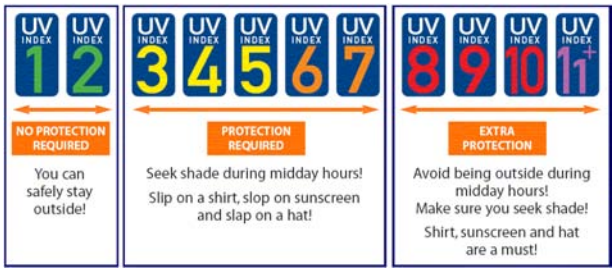

Figure 1.4 Protection recommendations for different intervals of UVI [*WHO*, 2002]

These recommendations are very clear, direct and simple messages in imperative voice. Furthermore, from the INTERSUN project it was advised to use themes for UVR protection in a positive way to have the best impact; for example, using "enjoy the sun safely".

Other simple messages about tips on factors and situations affecting the UV levels to which humans are exposed were shown in a friendly way in the same practical guide (see Figure 1.5). In Section 1.6, the main atmospheric factors that affect UVR reaching the Earth surface are discussed in detail.

The media usually present forecasts of the maximum UV radiation level for the following day. Daily evolutions are also

common when considering measurements or predictions for particular sites. Very often, UVI is presented as the maximum for clear-sky conditions. However, when cloud information is available it is recommended to present UVI as a range of values, corresponding to the plausible effect of clouds.

There are currently many guides and documents giving advice and information about UV effects on human health and how information to different sectors of population should be disseminated. Annex A shows links to several documents from some international organizations. In addition, some Internet links about education on UVI and safety are listed.

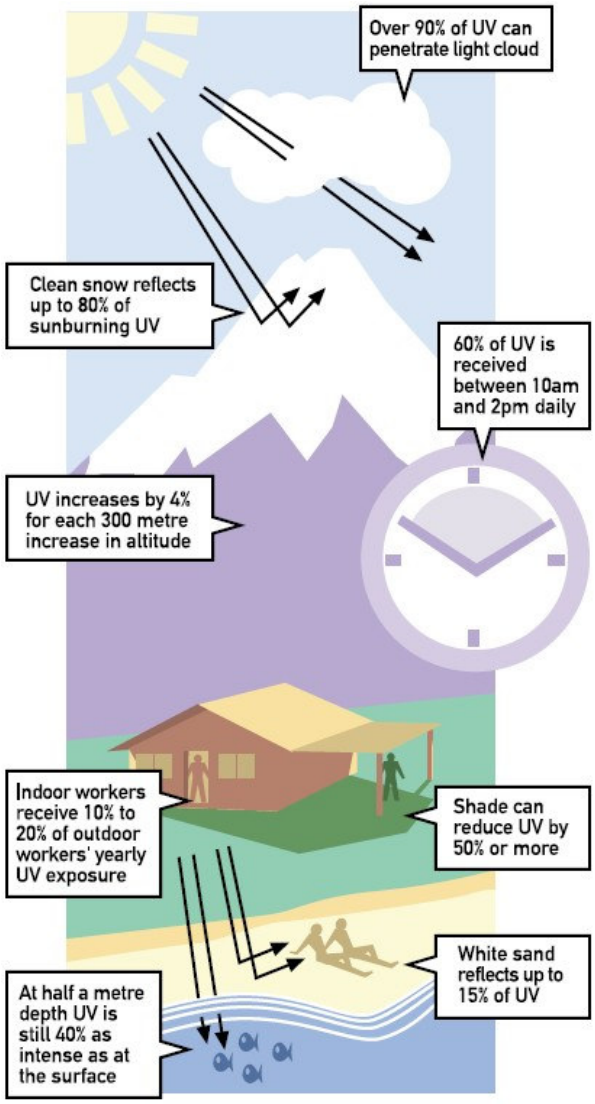

Figure 1.5 Panel that illustrates in a simple way how the UV levels are influenced by several factors [*WHO*, 2002] .

Remaining diversity about the way UVI is presented

National Weather services and institutes from many countries have adopted the UVI scale criteria and advise from WHO [2002]. Examples are Australia, Canada, New Zealand, Hong Kong (China), Norway, Spain, Sweden, Switzerland and USA. However, there is still a large variety of ways to report UVI and give information to the public. As an illustration of this, Table 1.4 shows the colour scales and exposure categories considered by organisations from different countries. Despite of the international recommendations, many of them still report burn times related to the UV levels and skin types. In particular, the UK Met Office reports

Table 1.4 Colour scales and categories of UVI considered by different organisations from diverse countries compared with the standard proposed by WHO [2002]

UVI →	0	1	2	3	4	5	6	7	8	9	10	11+
WHO [2002]	low			moderate			high		very high			extreme
1 LaMMA (Italy)	minimum			Low			medium		high			extreme
2 SIMA (Mexico)	Low						medium		high			extreme
3 Meteo. Insti. (Portugal)	Low						medium		high			extreme
4 Infosolei (France)	low			moderate			High		very high			extreme
5 German Weather Services	low			Medium				high			very high	
6 Met Office UK *	low			moderate			high			very high		

For Portugal, Mexico and Italy, intervals overlap (e.g. for Italy intervals are 0-2, 2-4, 4-7, 7-9 and >9) so the boundary shown here has to be understood like this.

* Scale for fair skin that burns. For fair skin that tans, and for brown and black skins, the labelling is more permissive, being a UVI of 9 considered as high for fair skin that tans and medium for brown and black skins

1 LaMMA: Laboratory for Meteorology and Environmental Modelling. http://www.lamma.rete.toscana.it/previ/ita/stazlam.htm 2 SIMA: Environmental Information System. http://sima.com.mx/sima/df/_zseeng.html 3 http://www.meteo.pt/uv/uvindex.htm 4 http://www.infosoleil.com/ 5 http://www.uv-index.de/ 6 http://www.met-office.gov.uk/weather/uv/uv_uk.html

different exposure categories (low, moderate, high, very high) depending on the skin characteristics. Other countries have not adopted UVI as the magnitude for information to the public. For example, in Argentina, the National Meteorological Service daily reports the expected UV levels using the Solar UV Intensity (ISUV) with cloud effects also taken into account (http://www.meteofa.mil.ar/).

Maps of predicted UVI for continents, large regions and the whole world are also available from different sources. The Institute of Medical Physics and Biostatistics and the University of Veterinary Medicine (hereafter IMPBUVM) in Vienna (Austria) jointly report daily maps of predicted UVI for many specific countries, and also for Europe, the Mediterranean Region and the World (http://www-med-physik.vu-wien.ac.at/uv/uv_online.htm). Alternatively, noon predicted UVI maps for Europe and the World based on assimilated SCIAMACHY (SCanning Imaging Absorption spectroMeter for Atmospheric CartograpHY) [*Bovensmann, et al.*, 2003] total ozone measurements are presented for today and the following 4 days at the TEMIS (Tropospheric Emission Monitoring Internet Service) website (http://www.temis.nl/uvradiation). Figure 1.6 shows two examples of images of predicted UVI for the whole World from the same day and from these two sources. Apart from the possible differences in the reported UVI, note the differences in the format. The upper map (IMPBUVM) follows the colour scale from the WHO [2002] guide (see Figure 1.3) while the lower map (TEMIS) considers a different, continuous colour scale. In this sense, the latter provides more information since the colour scale allows for distinguishing among UVIs higher than 11. Also, whereas the TEMIS map is for cloudless conditions, the IMPBUVM map considers 4 legends taking into account different cloud scenarios.

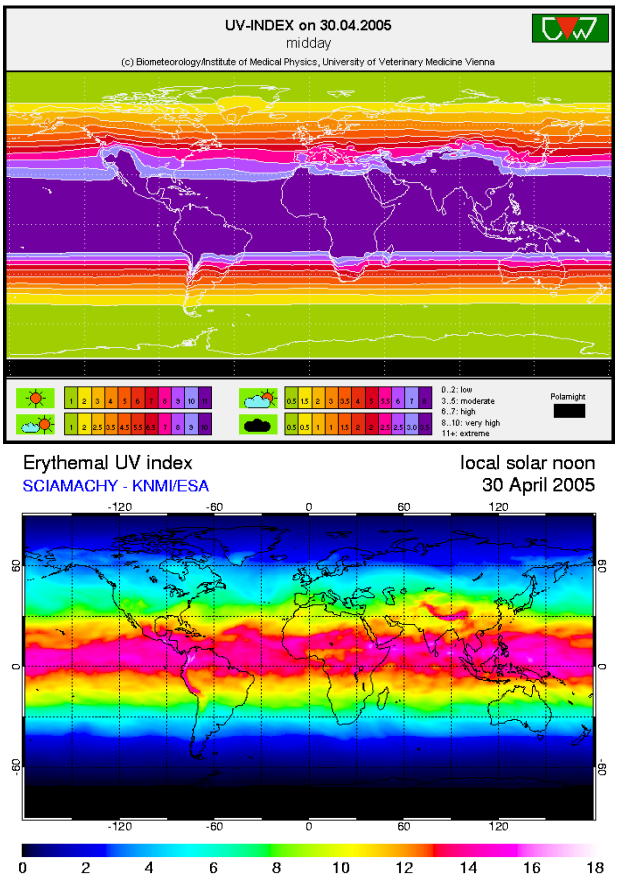

Figure 1.6 Two maps of predicted UVI for the Globe for 30 April 2005 from IMPBUVM (upper) and TEMIS (lower).

This shows that, although very important steps have been done in the last 10 years to standardize the way UVR is reported to the public, there is still a long way to follow before reaching an international uniform way of reporting UVI and give advice. In the present study, however, we will study the UVI as a physical magnitude (that is 40 times UVE) that can be measured and modelled.

1.4 UVI measurement

The solar irradiance on the Earth surface changes by more than five orders of magnitude in the UVB region (see Figure 1.2), which represents less than 0.1% of the total solar irradiance coming from the Sun but more than 80% of UVE (and UVI). Thus, measuring UVI presents an instrumental challenge that, despite of huge improvements already achieved so far, has not been completely solved. Main limitations in UV instrumentation are the calibration accuracy and stability of the

instrument but also the lack of homogeneity among instruments performing the same type of measurement [*Taalas, et al.*, 2000; *Webb*, 2000] .

There are different methodologies for measuring the UV radiation reaching the Earth's surface [*WMO*, 1999]. Ground-based instruments can be classified in four types:

- Dosimeters
- Radiometers
- Multi-band photometers
- High resolution spectroradiometers

Among the instruments measuring UVR, dosimeters are the simplest and cheapest. They are devices designed to measure integrated (through wavelength and time) UV doses. Some dosimeters also respond according to an action spectrum (such as the CIE function), thereby serving as a direct-reading instrument for dose that affects a particular receptor. These instruments are usually based on chemical species sensible to UVR. UV dosimeters are currently widely used as personal meters to investigate the UV doses received by different sectors of the population, such as children, teenagers, workers, golfers, etc. [e.g., *Thieden, et al.*, 2004; *Wright, et al.*, 2004].

Radiometers can measure dose rates with high sampling frequencies. Erythemal radiometers are a particular kind of these radiometers that have a spectral response close to the erythemal (CIE) action spectrum. Erythemal radiometers are often referred as Robertson-Berger (RB) sensors, after the pioneering instrument developed by Don Robertson and Daniel S. Berger [*Berger*, 1976], which was the first used extendedly for monitoring purposes. These instruments, however, have some calibration problems that are not completely solved. For this reason, *Weatherhead* [1997] recommended they not be used in studies of long time UVE trends. In general, it is accepted that their accuracy is within 10% [*Bais, et al.*, 2001a; *Leszczynski, et al.*, 1998].

Multi-band photometers can measure UVR at two or more wavelengths with bandwidths typically ranging from 2 to 10 nm. Some of them incorporate a single detector and use a filter wheel for the measurement at the different wavelengths. Others have one detector for the measurement at each considered wavelengths so all the measurements are taken simultaneously. Principal applications of this type of instruments are the retrieval of the ozone, water vapour, and NO_2 columns as well as the aerosol optical depth. For these purposes they usually offer the same accuracy as spectroradiometers but with lower buying and maintaining costs. If combined with UV modelling, multi-band photometers can be used to estimate UVE and UVI.

High resolution spectroradiometers are much more expensive and, unlike the other instrument types, need long scanning periods (of the order of some minutes). These devices can measure the UV solar spectrum with a typical spectral resolution of 0.2-1 nm. The advantage of spectral data is its versatility so they allow a lot of possible applications, such as getting different weighted irradiances, studying spectral attenuation from atmospheric constituents, etc. The most common problems that affect the irradiance measurements from these instruments (and also the other instruments above mentioned) are calibration and angular deviation from the correct cosine behaviour. Among these spectroradiometers, a classical instrument is the so-called Brewer spectrophotometer manufactured by Kipp & Zonen, which was designed for ozone column measurement using ratios between irradiances at ozone absorbing and non-absorbing wavelengths following the Dobson method [e.g., *Dobson*, 1968]. In addition, Brewer instruments measure the spectral

irradiance from 286.5 nm to 363 nm with 0.5 nm steps. Other state-of-the-art spectroradiometers can measure at wider wavelength ranges, such as the instruments built by the National Institute of Water and Atmospheric Research (NIWA) in New Zealand [e.g., *McKenzie, et al.*, 1997]. It is currently accepted that the best UVI measurements from spectroradiometers have an uncertainty within ±5% [*Bais, et al.*, 2001b; *Seckmeyer, et al.*, 2001]. Ground-based UVI measurements are commonly obtained from erythemal RB radiometers and spectroradiometers and the best accuracy is expected with the latter (see the above discussion). This study will present analyses with UVI from both types of instruments. Figure 1.7 shows pictures of the three different types of erythemal radiometers that will be considered and Figure 1.8 shows pictures of the NIWA spectroradiometer, measurements from which will be also studied in the present work.

To get a complete view about the techniques to measure UVR, satellite based estimation techniques must also be mentioned as a very different approach. These type of measurements combine radiative transfer modelling and measurements of the Earth reflectivity to Sun light [*Mayer, et al.*, 1997; *Ziemke, et al.*, 2000]. Main difficulties with this technique are the effects of clouds and aerosols (particularly sub pixel problems associated to broken and scattered clouds), and low spatial resolution or low frequency depending on the satellite orbit (geostationary or polar, respectively). All UV satellite-based estimations are based on ozone measurement devices. For this purpose, an important sensor is the Total Ozone Mapping Spectrometer (TOMS) from NASA, currently on board of the Earth Probe spacecraft, which has provided estimations of ground erythemal UV daily doses since 1978. Recently, irradiances at single wavelengths (305, 310, 320 and 380 nm) as well as the noon erythemal local-noon irradiances have become available (for inspection only, since these data are in validation process). The Global Ozone Monitoring Experiment, GOME, operated by the European Space Agency (ESA), has also provided a global distribution of UV at the ground since 1995. World UVI maps were first available from the GOME Fast Delivery Service, although this is currently out of service. UVI maps using data from SCIAMACHY, on board of the ENVISAT satellite (launched in 2002) also operated by ESA, are offered instead by the TEMIS team (see Figure 1.6). NOAA and EPA also forecast UV levels from ozone measurements made by TOVS (TIROS Operational Vertical Sounder) or SBUV/2 (Solar Backscatter UltraViolet/2) instruments onboard NOAA polar orbiting satellites.

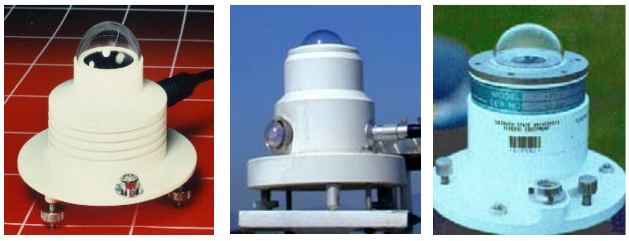

Figura 1.7 Three erythemal radiometers comercially available. (from left to right) Solar Light Company (SLC) 501, Kipp&Zonen UV-S-E-T and Yankee Environmental Systems (YES) UVB-1.

Figure 1.8 Pictures of the NIWA-built spectroradiometer. Top left: Two NIWA systems. Top right: Power Supply & meter. Centre: NIWA system under test. Bottom left: PTFE Diffuser. Bottom right: Interior of temperature stabilized weatherproof box (source: www.niwa.co.nz).

Validation and cross-comparison between ground-based measurements and satellite-based estimations is a very active area of current research, especially for the newest satellite sensors.

1.5 UVI modelling

Model calculations of UV are essential (1) to help understanding the processes affecting UV reaching the ground, (2) to predict UV and (3) to provide quality control of UV measurements.

Three model techniques can be distinguished:

- Empirical
- Parameterized
- Multi-scattering radiative transfer

Empirical models consist of more or less simple relations established between observed data and have a restricted number of input parameters. Usually, they are used for very specific purposes such as to calculate UVR in a particular spectral band and resolution. Furthermore, some empirical models are only applicable to the particular region where they were developed. That is not the case of the *Allaart, et al.* [2004] empirical model, which is based on fitted UVI measurements from a Brewer spectrophotometer. This algorithm is currently used by TEMIS to calculate the predicted UVI for the whole World (see UVI map in Figure 1.6). Also, the algorithm developed by *Schmalwieser et al.*[2002] is based on measurements (at discrete wavelengths) and it is used to calculate the predicted UVI presented in maps by IMPBUVM (see Figure 1.6).

Parameterized spectral models are usually more complex than the empirical models and consider simplifications of the atmospheric radiative transfer physical processes. They are commonly one-dimensional (i.e. they only consider vertical variations) and allow the modification of a wider variety of input parameters, although they rarely consider the effect of clouds. Some of them allow calculations of UVR in different spectral bands (UV, visible and infrared). Two of the freely available parameterised models for the UV spectral calculation (and also UVI) are SPCTRAL2 [*Bird and Riordan*, 1986] and SMARTS2 [*Gueymard*, 1995] (http://rredc.nrel.gov/solar/models/).

Multi-scattering radiative transfer models are computationally more complex; they allow introducing much detailed atmospheric information and most of them give the option of considering effects of clouds. The most common numerical methods used by this type of models to solve the radiative transfer equation are the discrete ordinates, spherical harmonics, successive orders of scattering, the FN method based on eigenfunctions, doubling-adding, and the matrix operator method [*Van Weele, et al.*, 2000]. Most numerical methods treat the atmosphere in a number of horizontal homogeneous vertical layers. To give a more "real" approach, some models incorporate pseudo-spherical corrections. Others also consider complete spherical corrections (3D models) but they are much computationally demanding and offer accuracies that are often not needed for most common applications. Montecarlo methods are widely used for 3D-calculations in atmospheres with horitzontal and vertical inhomogeneous patterns (for example, with scattered clouds). Some of the freely available radiative transfer models are the Santa Barbara DISORT Atmospheric Radiative Transfer model (SBDART) [*Ricchiazzi, et al.*, 1998] (http://www.crseo.ucsb.edu/esrg/pauls_dir/), Libradtran, Library for radiative transfer [*Mayer and Kylling*, 2005] (http://www.libradtran.org/), and the Trophospheric Ultraviolet

and Visible (TUV) radiative transfer model [*Madronich*, 1993b] (http://www.acd.ucar.edu/TUV/).
Multi-scattering radiative transfer models offer better accuracy in calculated UVI than parameterized and empirical models if most relevant input parameters are known. However, the latter are often used for particular applications such as to carry out a large amount of calculations, for the UVI prediction and to generate high-spatial-resolution UVI maps since they are faster and require less input information than the former. In this study, the TUV radiative transfer model will be widely used for the UVI calculations; a simple parameterisation of this model will be also considered for particular applications.

1.6 Factors affecting UVI

The main factors that affect the UV radiation (and UVI) reaching the ground surface are the Sun-Earth geometry, ozone, clouds, surface albedo, altitude and aerosols.

Earth-Sun Geometry
The solar zenith angle (*SZA*) is the main factor that affects UVR. *SZA* is the angle between the solar and the zenith directions, which can be calculated with reasonable accuracy using Sun-Earth simple astronomical formulas given the day, time and the latitude and longitude of the site of interest [e.g., *Iqbal*, 1983; *Lenoble*, 1993]. *SZA* affects both the optical path through the atmosphere and the angular distribution of scattered solar radiation. As *SZA* increases, the path that UVR has to travel through the atmosphere is longer and, therefore, the effects of some constituents like ozone and aerosols become more important. The change in *SZA* strongly affects UVI, leading to a reduction to about 16-19% when *SZA* varies from 0 to 60 degrees and to about 1.5-2.5 % when reaching 80º, depending on the ozone and aerosol loads, as it can be seen in Figure 1.9.
For this study, *SZA* will be considered up to 80º. For greater angles, there are large measurement and modelling errors and UVI is very low (<1), so there is less practical interest.
Another astronomical factor is the variation of Earth-Sun distance due to Earth elliptical orbit around the Sun. As result of this variation, the incoming solar irradiance varies by ±3.5% [*Iqbal*, 1983] throughout the year, and it is a maximum in December and a minimum in June.

Ozone
The role that ozone plays in diminishing UVR is well known [e.g., *Herman, et al.*, 1999; e.g., *Lenoble*, 1993] and has already been mentioned above. The most important parameter for the effect of ozone on UV radiation is the total ozone column (*TOZ*) defined as the thickness of the ozone vertical column if brought to standard temperature and pressure conditions (i.e. 0ºC and 1 atm). The natural units of *TOZ* are atm-cm but usually it is expressed in Dobson Units (DU), such as 1 atm-cm = 1000 DU; 1 DU of ozone corresponds to 2.69 10^{20} molecules per m^2 in an ozone column.
As commented in Section 1.1, ozone strongly absorbs the UVR so UVC and most of UVB do not reach the surface. This absorption has large wavelength dependence in the UVB range in such a way that, for midlatitudes, a 10% reduction in *TOZ* leads to about 2% increase in the surface UV irradiance at 320 nm while at 290 nm the change is approximately of 110% [*Ziemke, et al.*, 1998]. *Herman, et al.* [1999] showed that this spectral dependency of the effect

on UVR induced by a change in *TOZ* is non-linear in *TOZ* and *SZA*. The sensitivity of UVR to changes in *TOZ* can be described by the so-called Radiation Amplification Factor (RAF), which can be defined as the variation rate in UVI due to a relative decrease in *TOZ* as follows:

$$\frac{UVI_1}{UVI_0} = \left(\frac{\mathrm{TOZ}_1}{\mathrm{TOZ}_0} \right)^{-\mathrm{RAF}} \qquad (1.2)$$

For small changes in *TOZ* (less than 5%), this expression is normally simplified as:

$$\frac{UVI_1 - UVI_0}{UVI_0} = -\mathrm{RAF} \cdot \frac{\mathrm{TOZ}_1 - TOZ_0}{\mathrm{TOZ}_0} \qquad (1.3)$$

In general, UVI changes with a RAF close to 1. More specifically, *Thomas and Stamnes* [1999] reported that, for a 10% decrease in *TOZ*, RAF (for annual erythemal UV doses) is 1.17, and for a 20% decrease, RAF is 1.29. The COST-713 Action set the RAF between 1.1 and 1.3, as a guidance range [*Vanicek, et al.*, 2000]. That means that a reduction of 10% in *TOZ* causes an increase in UVI between 11 and 13%. Figure 1.9 shows the combined effect of changing *SZA* and *TOZ* on the UVI value that we found with TUV modelling for aerosol-free and polluted conditions.

The influence of the vertical distribution of ozone on UVI is much less important than *TOZ*. *Krzyscin* [2000] enclosed the effect of changes in the ozone vertical distribution on UVI within 5%. Through modelling with TUV we calculated that UVI was increased by up to 8% (for *SZA* conditions from 0 to 80 degrees) when a mid latitude ozone profile was replaced by a tropical profile, which is an extreme scenario.

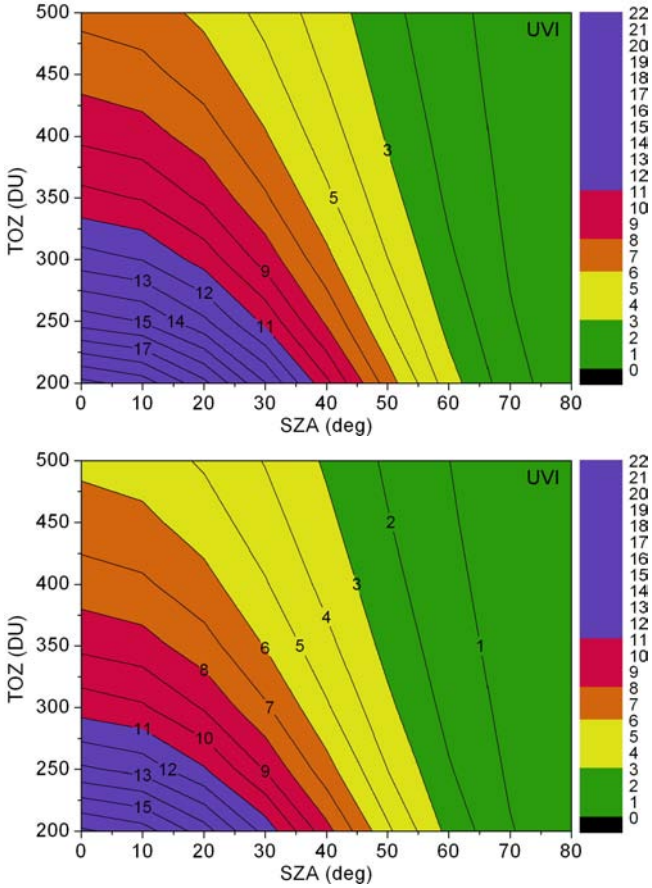

Figure 1.9 UVI calculated with TUV for different values of *SZA* and *TOZ* at ground surface (z=0 km) and ground albedo of 0.05. Upper: No aerosols are considered. Lower: AOD_{368}=0.5, *SSA*=0.9, *alpha*=1.4 and *g*=0.7.

Clouds

The study of the effects of clouds on UVI is complex due to the great temporal and spatial variability of cloud characteristics and the difficulties to characterize its optical properties. It is known that clouds can induce both an increase and decrease in UVI. The reduction effect is the most usual and has a larger effect; for example, *Renaud et al.* [2000] showed decreases in UVI to about 8% of the clear-sky value for thick clouds and 70% for thin clouds in overcast conditions. The COST-713 Action reported reductions down to

20% of the clear sky radiation (for overcast conditions and rain) [*Vanicek, et al.*, 2000]; and the SUVDAMA (Scientific UV Data Management) project found, from UV spectral measurements, reductions down to 30% [*Seckmeyer*, 2000]. *Frederick and Snell* [1990] found mean annual cloud attenuations between 22-38% at several sites in the USA. *McKenzie et al.* [1996; 1991] reported attenuation due to clouds of 25-30% in the global UV reaching the ground. *Lubin et al.* [1998] found attenuations of 10-25% in the rain forest. *Estupiñan et al.* [1996] noted that attenuation may be undetectable for very thin clouds or small cloud amount but it can be as high as 99% under extremely thick clouds. Enhancements of UVR induced by clouds have also been reported. *Tunc* [1999] found enhancements of 16% in UVI for broken clouds; *Sabburg and Wong* [2000] found, from UVB measurements, that 3% of the cases showed enhancements up to 8% mostly (in 86% of the cases) due to the presence of cirrus clouds or turbidity. *Calbó et al.* [2005] recently collected the existing studies about the effects of clouds on UVR in a comprehensive review study.

Cloudy conditions will not be included in this study because of the difficulties in considering the effect of clouds on UVI and the large uncertainty that this can induce in both the measurements and modeling. Moreover, before considering the cloud effects, it is convenient to carry out studies for cloudless skies, so to evaluate the accuracies for these favorable conditions. Thus, in this study, filtering techniques will be applied to select cloudless conditions.

Surface albedo

The surface albedo is defined as the ratio between the reflected and the incident irradiance on a surface, which depends on wavelength. The effect of albedo on UVR depends on the characteristics of the ground both from near and up-to-10-km-away surfaces. For most of the surfaces the surface albedo in the UV region is very small, typically about 2-5% [*Madronich*, 1993a]. Sand (with an albedo up to about 0.25) and snow (up to 1 for fresh snow) are remarkable exceptions. *Renaud et al.* [2000] found, for clear skies and snow conditions, enhancements of about 15 to 25% in UVI due to the multiple ground-atmosphere reflections. They also saw that this relative increment was about 80% larger for overcast conditions. *McKenzie et al.* [1998], for snow-covered grounds, showed increases of 28% for clear skies, and increases exceeding 50% under cloudy skies. The combined factors of snow and aerosols in cloudless situations can lead to enhancements in UVI of about 50% for moderately polluted atmospheres, as we detected through modelling calculations. It is also remarkable that the UV exposure on tilted or vertical surfaces can be doubled when the ground is covered by snow [*Weihs, et al.*, 2000].

High albedo situations, such as from snowy and sandy surfaces, are out of the scope of this study so the most typical situations, with albedo up to 5%, will be considered for the modelling.

Altitude

As altitude increases, a portion of atmosphere is left underneath; this reduces the radiation extinction and thus causes an increase in UVI. The observed altitude effect varies greatly from place to place, due to the influence of the surrounding areas and the degree of aerosol loading, as has been reported by several authors. *Blumthaler et al.* [1997] measured a mean altitude effect on UVI of 15.1% ± 1.8% per km in the Alps; *Schmucki and Philipona* [2002] estimated, from more than three years of measurements in the Alps, yearly mean noon

altitude effect of 11.0% per km with seasonal fluctuations from 8% to 16%; *Zaratti et al.* [2002] found an altitude effect near 7% per km from UVI measurements from two low-polluted sites near La Paz, Bolivia; according to the COST-713 Action, UVI increases about 6-8% per km [*Vanicek, et al.*, 2000]; this also agrees well with *Madronich* [1993a], that exposed values of 5-8% per km as normal altitude effect.

Figure 1.10 shows the dependencies of UVI on *SZA* and altitude that we found using TUV model for two different aerosol scenarios and low surface albedo. From this, an altitude effect of less than 5% is found (from 0 to 1 km above the ground) when no aerosols are considered and it is much larger, about 15%, for the polluted scenario at 30º of *SZA*.

Aerosols

The aerosols scatter and absorb UVR attenuating the direct component and enhancing the diffuse. The global (direct + diffuse) irradiance is typically attenuated. Remarkable exceptions are situations with snow-covered surfaces, as commented above.

The relationship between the incident extraterrestrial solar radiation (I_0) and the transmitted direct component (I) is explained by the Beer-Lambert law:

$$I = I_0 \exp(-\sum_i \tau_i(\lambda, z) \cdot m_i) \qquad (1.4)$$

where τ_i and m_i are the optical depths and air masses of the different processes (absorption and scattering) by the atmospheric components. The aerosol optical depth (*AOD*) accounts for both absorption and scattering and is the most important parameter to explain the effects of aerosols on UVI.

The *AOD* spectral dependence is often described with the coefficient *alpha* of Ångström's formula [*Angstrom*, 1964] as follows:

$$AOD_\lambda = AOD_{\lambda_0} \cdot \left(\frac{\lambda_0}{\lambda}\right)^{alpha} \qquad (1.5)$$

where λ_0 is the reference wavelength at which AOD is set as input to the model; in this study λ_0 = 368 nm, since it is a wavelength in the UV range and out of the ozone influence.

For very clean sites, values of *AOD* (at 368 nm) rarely exceed 0.2, as is the case of Lauder, New Zealand, and Mauna Loa, Hawaii (see discussions in Chapter 4). Girona, Spain, and De Bilt, the Netherlands, are examples of moderately polluted sites, with mean annual AOD_{368} of 0.21 [*González, et al.*, 2001] and 0.35 [*Stammes and Henzing*, 2000]. For highly polluted conditions, AOD_{368} can be larger

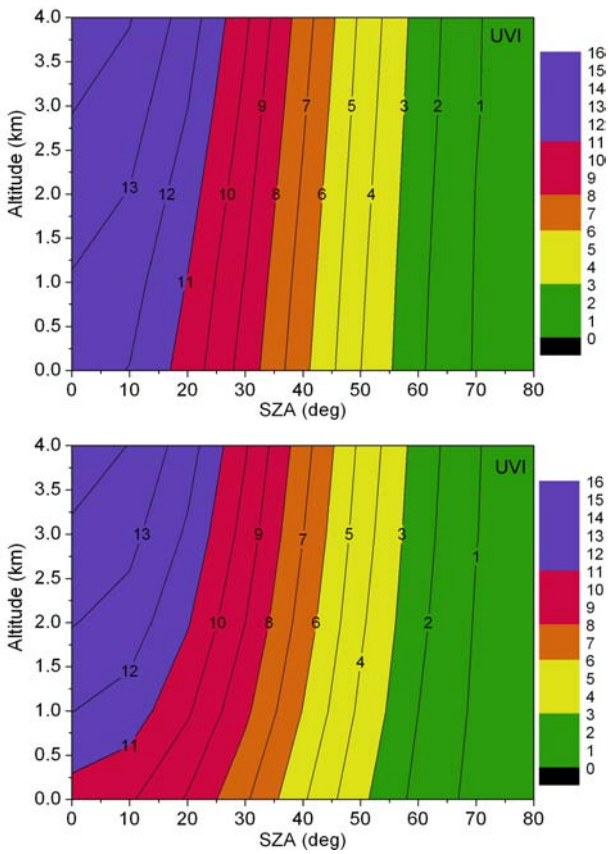

Figure 1.10 UVI calculated with TUV for different values of *SZA* and altitude with *TOZ*=300 DU and ground albedo of 0.05. Upper: No aerosols. Lower: AOD_{368}=0.5 *SSA*=0.9, *alpha*=1.4 and *g*=0.7. A realistic vertical distribution of *AOD* (with a decreasing aerosol amount as altitude increases) is considered. The exact aerosol profile used is described in detail in Chapter 6.

than 2, as is the case of Ispra, Italy, with reported mean and maximum AOD_{368} values of 0.59 and 2.6, respectively, from one year study [*Meleti and Cappellani*, 2000].

Other parameters that characterise the aerosol optical properties are the single scattering albedo (*SSA*) and the aerosol phase function. SSA is defined as

$$SSA = \sigma_s / (\sigma_s + \sigma_a)$$

where σ_s an σ_a are the aerosol scattering and absorption cross sections, respectively. If *SSA*=1, the aerosol only scatters and if it is 0, it is a pure absorber. Typically, *SSA* ranges between 0.8 and 0.999 in the UV range [Madronich, 1993a], although the actual *SSA* values are quite uncertain.

The phase function $P(\theta,\phi,\theta',\phi')$ is defined as the probability that an incident photon from direction described by angles θ' and ϕ' is scattered into a direction with angles θ and ϕ. Usually, considering axial symmetry around the incident direction is enough. For molecular scattering (Rayleigh) the phase function is symmetric in the sense that a photon has the same probability of being back-scattered than forward-scattered. However, the aerosol phase function is somewhat more complicated. The forward-scattering is usually strong for larger aerosols. For radiative transfer purposes, the asymmetry factor (g) is used as a rough descriptor of the phase function. The parameter g is defined as

$$g = \frac{1}{2}\int_{-1}^{1} P(\Theta)\cos(\Theta)d(\cos(\Theta)) \qquad (1.6)$$

and takes values from –1 (perfect back-scattering) to +1 (perfect forward-scattering) and is 0 for Rayleigh scattering. For atmospheric aerosol, typical values of g range between 0.6 and 0.8 [Madronich, 1993a].

Many studies have reported the attenuating effect of aerosols. *McKenzie et al.* [2001] found that aerosols can reduce UVI by more than 30% in some polluted places. From the SUVDAMA project measurements analyses, it was found that the global UV irradiance was reduced by 20% for *AODs* from 0.1 to 1 at 355 nm [*Seckmeyer*, 2000] for moderate *SZA*. Lorente *et al.* [1994] detected reductions of the UVB irradiance up to 14% and 37 % at 30 and 60 degrees of SZA, respectively, due to urban aerosols in Barcelona. *Meleti and Cappellani* [2000], detected maximum decreases in UVB of about 24% and 39% at Ispra (Italy) for the same two values of SZA. *Reuder and Schwander* [1999], identified, from modelling, reductions in UVI of 24% and 30% at 40 and 70 degrees, respectively, for a high-turbidity atmosphere with respect to a low-turbidity scenario. Wenny *et al* [2001] showed (combining aerosol measurements near Black Mountain, North Carolina, and modeling) that for strong absorption aerosols situations, UVI could be decreased by up to 5 units.

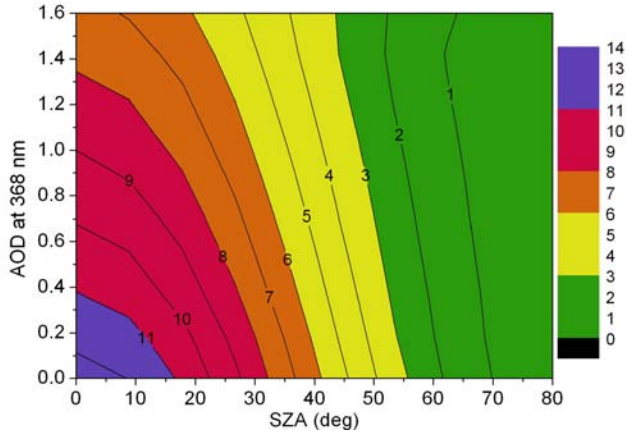

Figure 1.11 UVI calculated with TUV for different values of *SZA* and *AOD* at ground surface (z=0 km) with *TOZ*=300 DU, ground albedo of 0.05, *SSA*=0.9, *alpha*=1.4 and *g*=0.7.

In Figure 1.9, it is shown through model calculations that we performed with TUV model, how UVI is affected by the change of *SZA* and *TOZ* when the effect of aerosols is neglected and when *AOD* is set to 0.5 at 368 nm, *alpha*=1.4, *SSA*=0.9 and g=0.7. Figure 1.11, obtained also by using TUV, shows the

effect of changing *AOD* and *SZA* on UVI. For example, at 30º, it is seen that a change in *AOD* from 0.1 to 1 leads to a change in UVI from about 8 to 6. That is a 25% reduction, which is similar to the reported attenuation by *Seckmeyer* [2000].

1.7 References

Allaart, M., et al. (2004), An empirical model to predict the UV-Index based on the solar zenith angles and total ozone, *Meteorological Applications*, *11*, 59-65.

Angstrom, A. (1964), The parameters of atmospheric turbidity, *Tellus*, *16*, 64-75.

Bais, A., et al. (2001a), Report of the LAP/COST/WMO intercomparison of erythemal radiometers, 54 pp, WMO, Geneva.

Bais, A. F., et al. (2001b), SUSPEN intercomparison of ultraviolet spectroradiometers, *Journal of Geophysical Research*, *106*, 12509-12525.

Berger, D. S. (1976), The sunburning ultraviolet meter: design and performance, *Photochemistry and Photobiology*, *24*, 587-593.

Bird, R. E., and C. Riordan (1986), Simple solar spectral model for direct and diffuse irradiance on horizontal and tilted planes at the Earth's surface for cloudless atmospheres, *Journal of Climate and Applied Meteorology*, *25*, 87-97.

Blumthaler, M., et al. (1997), Increase in solar UV radiation with altitude, *Journal of Photochemistry and Photobiology B: Biology*, *39*, 130-134.

Bovensmann, H. S., et al. (2003), SCIAMACHY on ENVISAT: Some Highlights from the First Year in Orbit, *IGACtivities Newsletter*, *28*, 14-19.

Bruls, W. A. G., et al. (1984), Transmission of UV-radiation through human epidermal layers as a factor influencing the minimal erythema dose, *Photochem. and Photobiol.*, *39*, 63-67.

Calbó, J., et al. (2005), Empirical studies of cloud effects on UV radiation: a review, *Reviews of Gephysics*, *43, RG2002, doi: 10.1029/2004RG000155*, 28 pp.

CIE (1999), Standardization of the Terms UV-A1, UV-A2 and UV-B, Commission Internationale de l'Eclairage, Report 134/1, Vienna.

Diffey, B. L. (1992), Tables of Ambient Solar Ultraviolet Radiation for use in Epidemiological Studies of Malignant Melanoma.

Dobson, G. M. B. (1968), Forty Years' Research On Atmospheric Ozone at Oxford: a History, *Applied Optics*, *7*, 387-.

Estupiñán, J. G., et al. (1996), The effects of clouds and haze on UV-B radiation, *Journal of Geophysical Research*, *101*, 16807-16816.

Fitzpatrick, T. B. (1988), The validity and practicality of sun-reactive skin types I through VI, *Archives of Dermatology*, *124*, 869-871.

Frederick, J. E., and H. E. Snell (1990), Tropospheric Influence on Solar Ultraviolet Radiation: The Role of clouds, *Bulletin of the American Meteorological Society*, 373-381.

González, J. A., et al. (2001), Aplicación de métodos basados en medidas radiativas de banda ancha a la determinación de la turbidez atmosférica en Girona. (Application of methods based on broadband radiative measurements and the atmospheric turbidity determination in Girona.), in *El Tiempo del Clima.*, edited by A. J. Pérez-Cueva, et al, pp. 467-475, Asociación Española de Climatología.

Gueymard, C. (1995), SMARTS2, a simple model of the atmospheric transfer of sunshine, *Florida Solar Energy Center*, Rep. FSEC-PF-270-295.

Herman, J. R., et al. (1999), Ultraviolet radiation at the Earth's surface, in *UNEP/WMO Scientific Assessment of the Ozone Layer: 1998*, edited by D. L. Albritton, et al., pp. 9.1-9.46, WMO Global Ozone Res. and Monit. Proj., Geneva.

IARC (1992), Solar and ultraviolet radiation, *IARC Monographs on the evaluation of carcinogenic risks to humans and their supplements*, *55*, 336 pp.

Iqbal, M. (1983), *An introduction to solar radiation*, 390 pp., Academic Press, Toronto.

Keeling, C. D., et al. (1995), Interannual extremes in the rate of rise of atmospheric carbon dioxide since 1980, *Nature*, *375*, 666-670.

Krzyscin, J. W. (2000), Impact of the ozone profile on the surface UV radiation: analyses of the Umkehr and UVB measurements at Belsk (52N, 21E), Poland, *Journal of Geophysical Research*, *105*, 5009-5015.

Lenoble, J. (1993), *Atmospheric radiative transfer*, A. Deepak Publishing.

Leszczynski, K., et al. (1998), Erythemally weighted radiometers in solar UV monitoring: results from the WMO/STUK intercomparison, *Photochemistry and photobiology*, *67*, 212-221.

Lorente, J., et al. (1994), Influence of urban aerosols on spectral solar irradiances, *Journal of Applied Meteorology*, *33*, 406-415.

Lubin, D., et al. (1998), Global surface ultraviolet radiation climatology from TOMS and ERBE data, *Journal of Geophysical Research*, *103*, 26,061-026,091.

MacKie, R. M. (1999), Effects of Ultraviolet radiation on human health, paper presented at Ultraviolet radiation exposure, measurement and protection, Nuclear Technology Publishing, Oxford, England.

Madronich, S. (1993a), The atmosphere and UV-B radiation at ground level, in *Environmental UV Photobiology*, edited by A. R. Young and et al., pp. 1-, Plenum, New York.

Madronich, S. (1993b), UV radiation in the natural and perturbed atmosphere, in *UV-B Radiation and Ozone depletion. Effects on Humans, Animals, Plants, Microorganisms, and Materials*, edited by M. Tevini, pp. 17-69, Lewis Publishers, Boca Raton.

Mayer, B., and A. Kylling (2005), Technical note: The libRadtran software package for radiative transfer calculations - description and examples of use, *Atmospheric Chemistry and Physics Discussions*, *5*, 1319-1381.

Mayer, B., et al. (1997), Systematic long-term comparison of spectral UV measurements and UVSPEC modeling results, *Journal of Geophysical Research*, *102*, 8755-8767.

McKenzie, R. L., et al. (1996), UV radiation in New Zealand: measured North to South differences, and relationship to other latitudes, *Weather and Climate*, *16*, 17-26.

McKenzie, R. L., et al. (1997), UV spectro-radiometry in the network for the detection of stratospheric change (NDSC), paper presented at Solar Ultraviolet Radiation. Modelling, Measurements and Effects, Springer-Verlag, Berlin, October 1995.

McKenzie, R. L., et al. (1991), The relationship between erythemal UV and ozone derived from spectral irradiance measurements, *Geophys. Res. Lett.*, *18*, 2269-2272.

McKenzie, R. L., et al. (1998), Effects of snow cover on UV radiation and surface albedo: a case study, *Journal of Geophysical Research*, *103*, 28785-28792.

McKenzie, R. L., et al. (2001), Satellite retrievals of erythemal UV dose compared with ground-based measurements at northern and southern midlatitudes, *Journal of Geophysical Research*, *106*, 24051-24062.

McKinlay, A. F., and B. L. Diffey (1987), A Reference Action Spectrum for Ultra-violet Induced Erythema in Human Skin, in *Human Exposure to Ultraviolet Radiation: Risks and Regulations*, edited by W. F. Passchier and B. F. M. Bosnajakovic, pp. 83-87, Elsevier, Amsterdam.

Meleti, C., and F. Cappellani (2000), Measurements of aerosol optical depth at Ispra: Analysis of the correlation with UV-B, UV-A, and total solar irradiance, *Journal of Geophysical Research*, *105*, 4971-4978.

Renaud, A., et al. (2000), Influence of snow and clouds on erythemal UV radiation: Analysis of Swiss measurements and comparison with models, *Journal of Geophysical Research*, *105*, 4961-4969.

Reuder, J., and H. Schwander (1999), Aerosol effects on UV radiation in nonurban regions, *Journal of Geophysical Research*, *104*, 4065-4077.

Ricchiazzi, P., et al. (1998), SBDART: a research and teaching software tool for plane-parallel radiative transfer in the Earth's atmosphere, *Bulletin of the American Meteorological Society*, *79*, 2101-2114.

Sabburg, J., and J. Wong (2000), The effect of clouds on enhancing UVB irradiance at the earth's surface: a one year study, *Geophysical Research Letters*, *27*, 3337-3340.

Schmalwieser, A. W., et al. (2002), World-wide forecast of the biologically effective UV radiation: UV-index and daily dose, *Procedings of SPIE*, *4482*, 259-264.

Schmucki, D. A., and R. Philipona (2002), Ultraviolet radiation in the Alps: the altitude effect, *Optical Engineering*, *41*, 3090-3095.

Seckmeyer, G. (2000), Coordinated ultraviolet radiation measurements, *Radiation Protection Dosimetry*, *91*, 99-103.

Seckmeyer, G., et al. (2001), Instruments to measure solar ultraviolet irradiance. Part 1: spectral instruments, 30 pp, World Meteorological Organisation, Geneva.

Selgrade, M. J., et al. (1997), Ultraviolet radiation-induced immune modulation: protection consequences for infections, allergic and uautoimmune disease, *Environmental Health Perspectives*, *105 (3)*, 332-334.

Stammes, P., and J. S. Henzing (2000), Mulispectral aerosol optical thickness at De Bilt, 1997-1999, *Journal of Aerosol Science*, *31*, S283-S284 [Special Issue EAC 2000].

Taalas, P., et al. (2000), European Conference on Atmospheric UV Radiation: Overview, *Journal of Geophysical Research*, *105*, 47777-44785.

Thieden, E., et al. (2004), Proportion of Lifetime UV Dose Received by Children, Teenagers and Adults Based on Time-Stamped Personal Dosimetry, *Journal of Investigative Dermatology*, *123*, 1147-1150.

Thomas, G. E., and K. Stamnes (1999), *Radiative transfer in the atmosphere and the ocean*, Cambridge University Press.

Tunc, S. (1999), Enhancements of solar and ultraviolet surface irradiance under partial cloudy conditions, 45 pp, KNMI, De Bilt, Holland.

Van Weele, M., et al. (2000), From model intercomparison toward benchmark UV spectra for six real atmopsheres, *Journal of Geophysical Research*, *105*, 4915-4925.

Vanicek, K., et al. (2000), *UV-Index for the public*, 27 pp., European Union, COST-713 Action, Brussells.

Weatherhead, E. C., et al. (1997), Analysis of long-term behaviour of ultraviolet radiation measured by Robertson-Berger meters at 14 sites in the United States, *J. Geophysical Research*, *102*, 8737-8754.

Webb, A. R. (2000), Standardisation of data from ultraviolet radiation detectors, *Radiation Protection Dosimetry*, *91*, 123-128.

Weihs, P., et al. (2000), Measurements of the reflectivity in ultraviolet and visible wavelength range in a mountainous region, *Radiation Protection Dosimetry*, *91*, 123-128.

Wenny, B. N., et al. (2001), Aerosol optical depth measurements and their impact on surface levels of ultraviolet-B radiation, *Journal of Geophysical Research*, *106*, 17311-17319.

WHO (1995), Protection against exposure to ultraviolet radiation, World Health Organization, Geneva, Switzerland.

WHO (2002), *Global solar UV Index: A practical guide*, 28 pp., World Health Organisation (WHO), World Meteorological Organisation (WMO), United Nations Environment Program (UNEP), and International Commission on Non-Ionising Radiation Protection (ICNRP), Geneva.

WMO (1994), Report of the WMO meeting of experts on UV-B measurements, data quality and standardization of UV indices, Les Diablerets, Switzerland.

WMO (1998), Report of the WMO-WHO Meeting of Experts on Standardization of UV Indices and their Dissemination to the Public, 187 pp, WMO, Les Diablerets, Switzerland.

WMO (1999), *Scientific Assessment of Ozone Depletion: 1998*, Geneva.

Wright, C., et al. (2004), Real-time measurements of ultraviolet radiation using portable electronic dosimeters, in *International NIR Workshop and Symposium*, edited, ICNIRP/WHO.

Zaratti, F., et al. (2002), Erythemally weighted UV variations at two high-altitude locations, *Journal of Geophysical Research*, *108*, doi:10.1029/2001JD000918.

Ziemke, J. R., et al. (2000), Erythemally weighted UV trends over northern latitudes derived from Nimbus 7 TOMS measurements, *Journal of Geophysical Research*, *105*, 7373 - 7382.

Ziemke, J. R., et al. (1998), Total ozone/UVB monitoring and forecasting: Impact of clouds and the horizontal resolution of satellite retrievals, *Journal of Geophysical Research*, *103*, 3865-3871.

2

Objectives and methodology

General frame

As stressed in the previous Chapter, solar UVR can have serious effects on living beings and, in particular, on humans. From the social, health and economic points of view, educational and preventive campaigns are needed to stop the increase that has been detected in the occurrence of diseases related to exposure to UVR during the last decades. UVI is the recommended magnitude for the dissemination of the UV levels relevant for the human health.

From the scientific point of view, research on UVR and UVI is needed to:

obtain **reliable estimations of UVI** to be disseminated to the public;
identify and quantify **factors** that affect the UVR;
assess for possible **long-term UV trends**;
to know the **uncertainties** affecting the modelling and measurement of UVR so to
help developing **better techniques** in both fields, and
make a step ahead in the **state of the art of** the science of **UVR**.

Given both the scientific interest and the social impact of this research, there has been recently in Spain a growing number of projects and researchers focused on the topic of UVR. The present work was partially developed in the frame of one of these projects (DEPRUVISE). In addition, the Department of Environment of the Catalan Government launched an initiative to measure UVR and funded the project IMMPACTE, that included among its goals the improvement of the UVI predictions, and in which the author of the present work was involved

Overview

For the UVI measurement, best accuracy is expected with data from spectroradiometers. However, since the buying and maintaining costs of these devices are expensive, data from erythemal radiometers is more commonly available (most UVI networks are equipped with this latter type of sensors).

Best UVI modelling performance is found with radiative transfer models when the input information is well known. However, some relevant input information, such as the aerosol optical properties, is usually not available which can lead to large modelling uncertainties. More simple models are often used for applications such as UVI prediction or elaboration of UVI maps, as they are much faster and require less input parameters.

2.1 Objectives and methodology

The general objective of this study is to analyse the agreement that can be reached between modelled and measured UVI for cloudless conditions.

Best agreement is expected when state-of-the-art spectroradiometric data and radiative transfer modelling incorporating the broadest possible range of input data are used. Since these conditions are rarely available in practice, in one hand, it is convenient to analyse the differences between using spectroradiometric data and measured UVI from erythemal radiometers. On the other hand, it is also necessary to analyse the differences between UVI calculated from a radiative transfer model and other simple UVI models that are useful for particular purposes. Moreover, the effect of different modelling parameters on the calculated UVI and the uncertainties associated to different assumptions need to be evaluated.
Below, the contribution of this study to the above exposed needs is presented. The specific objectives are distributed in three separate but related studies, which will set the structure of the document and the way results will be presented.

Chapter 3 – UVI Measurements by Erythemal Radiometers

Premise
Erythemal radiometers are widely used in many applications, such as for UVI monitoring in networks, for UVI forecast validations, and for diverse investigation purposes since they are easily transportable, cheap and allow instantaneous UVI measurements. These types of instruments have spectral responses that resemble the CIE action function (see section 1.2). Deviations from this function may lead to large errors in the UVI measurement. Actually, this is a major source of uncertainties of the erythemal radiometers. So, it is very important to have the actual spectral response of the instrument well characterised and apply corrections to the measurements.
Objective
The objective sought in Chapter 3 is to quantify errors that can be made when measuring UVI with erythemal radiometers if the spectral response is not conveniently corrected or uncertain. Also, an additional objective of this chapter is to evaluate the performance of different erythemal radiometers.
Methodology
To meet these objectives, spectral responses for three erythemal radiometers from different brands are compared and a methodology for calculating spectral correction factors is presented, based on previous studies. The different correction factors are compared and uncertainties are discussed. UVI measurements from erythemal radiometers are contrasted with spectroradiometric data and model results.

Chapter 4 – UVI model vs. measurement

Premise
The best accuracy in measuring UVI is expected from spectroradiometers. Measurements from these instruments are much less commonly available than data from erythemal radiometers, but they are often used to cross-calibrate the latter sensors. So, the high quality performance of spectroradiometers is required to use them as a reference and to study long term UVI trends. Multi-scattering radiative transfer models offer the best accuracy in

calculating UVI if the most important input information is known. However, this information is rarely available together and rarely concurrent with UVI spectroradiometric data to study model-measurement agreement. Few UVI model-measurement comparisons meeting these requirements have been presented in previous studies, although such comparisons are needed to get a complete picture about the factors, limitations and uncertainties involved in both modelling and measuring UVI.

Objective

The objective of Chapter 4 is to evaluate the agreement between high quality UVI measurements and radiative transfer modelling, when the relevant input information is available. In this sense, it is needed to analyse the effect of making different assumptions when modelling, and to identify the limitations and uncertainties associated to both measurement and modelling.

Methodology

Chapter 4 presents the results of a detailed comparison for clear-sky conditions between measured and modelled UVI at four diverse sites in both hemispheres. For this, state-of-the-art UVI measurements and radiative transfer modelling incorporating the broadest possible range of input data is available. Different modelling tests are considered depending on the most relevant input information (such as ozone and aerosols) and differences in the UVI calculated are analysed. Discussions are raised about uncertainties and limitations in both the model and the measurements.

Chapter 5: PTUV: A new parameterisation for UVI fast calculations – Application to build maps

Premise

Dissemination of UVI to the general public is often presented by means of UVI maps, at least when large geographical and/or diverse areas are under study. One way of building high spatial resolution maps is using UVI models. Multi-scattering radiative transfer models are computationally demanding and require a wide range of input data, most of which are usually not known accurately for the whole territory. So, simple assumptions must be done. This makes it convenient to use simple and fast UVI models that serve the required purpose.

Objective

The main objective of Chapter 5 is to describe a new parameterisation for fast UVI calculations for clear-sky conditions that requires a limited number of (the most important) input parameters, and that can be used under a wide range of conditions worldwide. The practical application of the parameterisation is to build maps of typical UVI for the region of Catalonia.

Methodology

To reach these objectives, the TUV model has been taken as the base model to get the parameterisation (named PTUV). It has been developed by fitting TUV UVI calculations for a broad range of conditions. Differences in performance between PTUV and the full (TUV) model are delimited. Validation tests against measurements from both hemispheres are also presented to further check its performance. Climatology of *TOZ*, *AOD* and UVI is presented for Girona (Catalonia) and seasonal maps of UVI for Catalonia are presented and discussed.

3

UVI Measurements by Erythemal Radiometers

General frame

While ozone has been continuously monitored since 1926, UVB monitoring began in 1962, when Dr. Don Robertson of the University of Queensland (Australia) solved the problem of measuring the biologically effective UVR using an stable and reproducible sensor. In 1973, a network of UV sensors designed by Robertson and Daniel S. Berger was established. In 1983, the network had twenty stations in North America, four in Europe, one in Hawaii, and two each in Australia and New Zealand. The number of these sensors went on growing so that in 1997 there were 400 new erythemal radiometers worldwide.

Current erythemal radiometers follow a similar measure principle to that of the Robertson-Berger (RB) meters: sunshine goes through the protection glass filters that block the visible and infrared light; the UV radiation excites the fluorescent phosphor, which converts UV light to visible light (green), which is measured by photodiodes. UVR is spectrally weighted by the phosphor in a similar way to the erythemal function (CIE). Different erythemal radiometers, and even the devices from the same manufacturer, have different spectral responses. Since the UVI measurement by these instruments is highly dependant on their spectral response, it is very important to have each sensor characterised by its spectral function and to apply corrections for the deviations from the CIE function.

The use of spectroradiometric data greatly reduces the uncertainties resulting from band pass differences between instrument response and the CIE response. So the UVI measurement from spectroradiometers is expected to be more accurate. Actually, the erythemal radiometers are commonly calibrated against spectroradiometers.

Overview

This Chapter aims to quantify errors that can be made when measuring UVI with erythemal radiometers and analyse how they compare with UVI modelling and spectroradiometric data.

For this, especial attention is paid on their spectral responses, as a major source of measurement uncertainty with these sensors. Different spectral responses are studied and a methodology to find spectral corrections, based on previous studies, is presented. The different correction factors found are compared and the effect of having an uncertain measure of the spectral response on the measured UVI is estimated for a particular case. Finally, UVI model-measurement comparisons are presented for UVI measurements from erythemal radiometers and one spectroradiometric system in order to study the performance of the different instruments.

3.1 The role of the erythemal radiometers

The Robertson-Berger (RB) type radiometers [*Berger*, 1976] have been widely used for UVB measurements since mid 1970s. Actually, they are the most common and widely spread instruments for the UVI monitoring. This is mainly because, unlike the spectroradiometers, the erythemal radiometers have low buying and maintaining costs and they require less technical expertise for their operation.

Some of the most common erythemal radiometers used, and that will be commented in this study, are the Yankee Environmnetal Systems (YES) UVB-1, the Solar Light Company (SLC) 501 and the Kipp & Zonen (KZ) UV-S-E-T (see Figure 1.7).

Some applications in which UVI measured from erythemal radiometers are used can be commented. Over the last decades, many countries have established networks with RB type radiometers for UVI monitoring and dissemination. For example, *Martinez-Lozano et al.* [2002] presented two years of UVI measurements from the Spanish broadband UV-B radiometric network with 16 YES UVB-1 radiometers. From those measurements at 11 sites they discussed the territorial distribution of UVI in Spain and the maximum values recorded. *Cede et al* [2002b] presented a climatologic analysis of 2-4 years of UVI measurements of the Argentinean ultraviolet network, equipped with SLC 501 and YES UVB-1 radiometers. *Schmalwieser and Schauberger* [2001] presented an objective method for selecting sites for the Austrian UV monitoring network. Nine stations were considered and equipped with SLC 501 radiometers.

UVI from erythemal radiometers is also used in validation processes to assist UVI forecasting. That was the case, for example, for the verification at some sites of the UVI forecasts for USA issued by the National Weather Service [*Long, et al.*, 1995]. *Schmalwieser and Schauberger* [2000] also presented validation tests of the Austrian forecast model using broadband UVI measurements from Vienna.

When dealing with UVI measurements under cloudy conditions, it is convenient to have an instant UVI measurement since cloud optical properties can significantly change in a matter of seconds. For this, the erythemal radiometers become very useful since the UVI measurements with spectroradiometers tend to be slow-scanning (taking few minutes). *Cede et al* [2002a] presented a study about the effects of clouds on erythemal and total irradiance for the Argentine network. Taking the same dataset, *Cede et al* [2002b] studied the influence of the integration time on the value of UVI as a function of the observed cloud coverage. *Thiel* [1997] presented similar analyses to those by *Cede et al* [2002a] from two sites in Germany.

Other examples of research studies involving measurements from erythemal radiometers are the works from *Blumthaler et al* [1997] and *Zaratti et al* [2002], which analysed the altitude effect on UVE by comparing measurements from two sites at different altitude.

From all the above stated, it is evident that the erythemal radiometers play an important role in the UVI dissemination and research fields so it is important to ensure their measurement quality.

3.2 Erythemal radiometers intercomparison studies

It is known that the spectral response functions (SRFs) of the erythemal radiometers differ from the CIE function and that there can be significant differences between the spectral responses from different sensors, even between sensors from the same manufacturer.
Several international intercomparison campaigns of erythemal radiometers have been hold to test the performance of and agreements between different sensors. *Leszczynski et al* [1998] presented the results from the WMO/STUK intercomparison between 20 erythemal radiometers of six different types from 16 countries carried out in 1995 in Helsinki, Finland. In particular, a total of 15 SLC radiometers were included in this comparison and their SRFs were found to agree within ±10% for most of them, from 290 to 320 nm. In the UVA range, the differences were much larger. To correct for the non-ideal SRFs of the sensors, they calculated correction factors as a function of *SZA* and *TOZ*; these factors were as large as 1.8 for large *SZA* and up to about 1.15 for low *SZA* with a large diversity depending on the sensor. They also measured the angular response of all the radiometers and found deviations from the ideal cosine response within +30 to -20%. From comparisons with spectroradiometric data, they also found re-calibration factors between 0.87 and 1.75 with an uncertainty of ±10%. The calibrations of the 15 SLC radiometers were compatible with each other within 8%.
In 1999 a comparison campaign with 29 erythemal radiometers of five types from 14 countries was carried out in Thessaloniki, Greece [*Bais, et al.*, 2001]. In the study, both the spectral and angular responses of the instruments were characterised. Five of the considered SLC 501 radiometers had already taken part in the WMO/STUK 1995 campaign and the new calibrations against spectroradiometric data showed changes in the calibration factors from -3.3 to 18.7%. For most sensors, the new calibration factors found differed by less than 10% from the ones provided by the manufacturer. However, other sensors showed deviations of more than 20% on both negative and positive side. The calibration factors are expected to increase in time due to the decrease of the instrument sensitivity. According to *Bais et al.*[2001], a decrease in the calibration factor could be the result of a shift in the spectral response to longer wavelengths. In this sense, *di Sarra et al* [2002] found, from the comparison of the SRFs of 11 YES UVB-1 radiometers, that the corresponding SRFs were spread by up to 1.5 nm in the 310-340 nm range. From the particular comparison between two radiometers with normalized SRF shifted by 1.25 nm, differences up to 6% in the measured signal were reported from *SZA* variations alone. This effect also induces both seasonal and latitudinal dependences of the differences in the measure from the two sensors. The relative differences of the signal caused by a 100 DU change in *TOZ* were comparable with or larger than that produced by the *SZA* variations [*di Sarra, et al.*, 2002].

These important changes in calibration, differences between radiometers and the difficulties of having the sensors well characterised and corrected often makes the measured UVI values from such instruments largely uncertain. As commented above, an essential source of uncertainty comes from the spectral response of the instrument. This will be discussed in detail next. The erythemal radiometers also need angular corrections for their deviations from the ideal cosine response. *Leszczynski et al* [1998] showed that, although the angular response could largely deviate from the cosine response, the actual angular correction factors to be applied to the measurements had a dependence on *SZA* typically of less than 5%. Following the method from *Leszczynski et al* [1998], we performed test analyses of the

angular corrections as a function of *SZA* that would be found for typical angular responses for the SLC 501 and the KZ UV-S-E-T sensors. Although the angular response differed by down to -40% for *SZA* down to 80º, the corresponding correction factors were within 3-4%. That is because the diffuse component of the radiation is about the half of the global irradiance in the UV range and becomes even more important than the direct component as *SZA* increases. In this way, the errors for the non-ideal angular response of the instruments are highly attenuated. For this, this Chapter focuses on the spectral responses and the corresponding spectral corrections, as they are a major issue in broadband UVI measuring. Corrections for angular responses will be applied when available but no further analyses will be presented.

3.3 Methodology to calculate spectral response correction: a case study

In this section, a detailed methodology for calculating spectral correction factors is presented. Alternative methodologies have been discussed elsewhere. *Bodhaine et al* [1998] presented a method for determining the calibration of a broadband UV instrument by comparison with a calibrated spectroradiometer. That procedure did not require precise knowledge of the spectral response of erythemal radiometer so the calibration factors for different *SZA* and *TOZ* conditions were inferred through direct comparison with the spectroradiometric data. They showed that a *TOZ* decrease of 100 DU (from 300 to 200 DU) would lead to an increase of the calibration factor by almost 20%. *Los* [2003] discussed a method developed to transfer in the laboratory the outdoor calibrations of several reference instruments to other instruments by means of a well-maintained system including a monochromator with an absolute calibrated photodiode detector.

The method presented here requires both high quality spectroradiometric UVI measurements (to get a calibration for certain *SZA* and *TOZ* conditions) and modelling (to extend the calibration to other conditions, i.e. to obtain the correction factors). The steps required to get the correction factors are commented next. The exposed method is based on a method used by Kipp & Zonen [Alexander Los, personal communication], which is also very similar to one of the methods proposed by *Bais et al* [2001].

3.3.1 Spectral responses

Three instruments from different manufacturers are considered for this analysis: YES UVB-1, SLC 501 and Kipp & Zonen (KZ) UV-S-E-T (see Figure 1.7). One measurement of the SRF was available for each instrument except for the YES UVB-1, for which three measurements were available. Table 3.1 summarises the origin, date and the identification label chosen for each spectral response function.

Table 3.2 summarizes the resolution characteristics of the original spectral functions and the modifications made in order to standardise them at 1 nm resolution from 285 to 400 nm,

Table 3.1 Information about the origin and date of each spectral response function measurement. The selected identifier for each response is also shown.

Instrument	Measuring site	Calibration from	Calibration year	Identifier
		Manufacturer	1992	YES92
YES UVB-1	Lauder (New Zealand	IRL*	1995 (November)	YESIRL
		STUK**	1995 (December)	YESSTUK
SLC 501	Leigh (New Zealand)	IRL	1995 (November)	SLCIRL
KZ UV-S-E-T	Girona (Spain)	Manufacturer	2003	KZ

* Industrial Research Limited, New Zealand

** Radiation and Nuclear Safety Authority, Finland

Table 3.2 Format characteristics of the original spectral function and processes applied in order to standardise them.

Identifier	Original format	Process applied
YES92	2nm steps from 270 to 390 nm. Single measurements at 400, 450 and 500 nm	Linear interpolation to upgrade the resolution to 1nm from 285 to 400 nm.
YESIRL	1 nm steps from 265 to 340 nm. Single measurements at 360, 400, and 500 nm.	Linear interpolation from 340 to 360 nm and from 360 to 400 nm.
YESSTUK	1 nm steps from 270 to 390 nm.	From 391 to 400 nm the response is set to 0.
SLCIRL	1 nm steps from 250 to 340 nm. Single measurements at 400 and 500 nm.	Linear interpolation from 340 to 400 nm.
KZ	0.5 nm steps from 280 to 400 nm.	Selection of the records with integer wavelengths to get 1nm resolution.

according to the specifications chosen for the present study. When possible, the SRFs were considered up to 400 nm although linear interpolations for intervals up to 60 nm had to be done. For the YESSTUK, the SRF was only available up to 391 nm. In this sense, it was estimated that when the SRFs were available for a reduced wavelength range the calibration factors were generally underestimated by 0.5 to 7% [*Bais, et al.*, 2001].

All these spectral responses were also normalized to 1.0 at 297 nm, as suggested by WMO [*WMO*, 1994]. Figure 3.1 shows the five SRFs together with the CIE function. Note the apparent differences between the three SRF for the YES UVB-1 instrument. The three different functions agree with each other within ±3% for wavelengths up to 305 nm and, from this on, differences become much larger. If YESIRL is taken as reference, YES92 and YESSTUK differ from that by up to 24 and down -36%, respectively, for wavelengths up to 320 nm. These are differences considerably larger than those reported by *Leszczynski et al* [1998] for SLC radiometers, as commented above.

3.3.2 Spectral correction calculations

TUV model

As already introduced in Section 1.5, TUV is a multi-scattering radiative transfer model. It incorporates two methods of solving de radiative transfer equation: the two-stream code and the discrete ordinates (DISORT) with n streams (being 8 streams sufficient for irradiances). Both methods allow pseudo-spherical corrections. TUV can be used over the wavelength range 121 - 750 nm, for calculating the spectral irradiance, the spectral actinic flux, photodissociation coefficients (J-values), and biologically effective irradiance (such as UVE and UVI). The code offers a great versatility, and allows setting an arbitrary number of vertical layers for the introduction of gases, aerosol and clouds information. It runs under FORTRAN 77 and it is built from a central program that calls peripheral routines that generate the different atmospheric profiles and the parameters needed for the radiative transfer calculations.

UV spectral Modelling

Both *SZA* and *TOZ* highly affect the shape of the solar spectrum in the UV region so the spectral corrections have to be found as a function of these variables. UV spectra at the ground level were modelled with TUV model version 4.1a for different conditions as specified in Table 3.3.

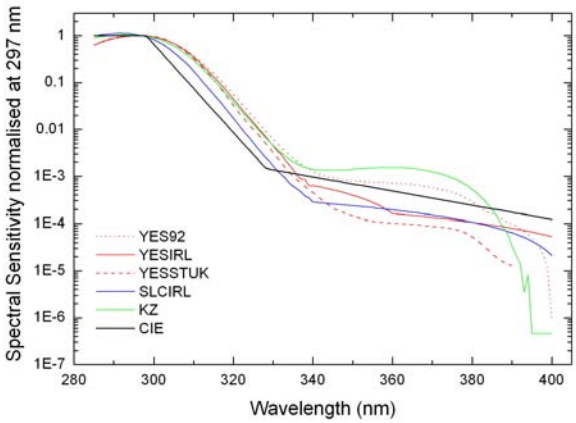

Figure 3.1 Spectral response functions for YES, KZ, SLC instruments together with CIE function.

Aerosols do have a wavelength dependent effect though this is much weaker and consequently its influence on the correction factors will be neglected. A change in altitude certainly affects the shape of the UV spectrum. However, the location of a given instrument is commonly unchanged and the altitude effect could be taken into account when calibrating the sensor.

Table 3.3 Conditions considered in the TUV model to find the spectral correction factors

Wavelength range	285-400 nm
Wavelength resolution	1 nm
SZA	From 0 to 85 degrees with 5 degree steps
TOZ	From 200 to 500 DU with 10 DU steps
Surface albedo	0.02
Altitude	0 km
Aerosol	None
Radiative transfer code	8 streams with pseudo spherical corrections

A total of 558 spectra were obtained from the combination of the 18 different values of *SZA* and the 31 different values of *TOZ*.

Calculation of weighted spectra integrals

All the UV spectra were multiplied by the six weighting functions and each resultant effective spectrum was integrated from 285 to 400 nm. We can express this in a mathematical form as follows. If $S_\lambda(\lambda,SZA,TOZ)$ represents the irradiance for a certain wavelength λ, *TOZ* and *SZA*, and if $SRF_i(\lambda)$ is the spectral response function with i accounting for the different spectral response functions considered, then the integrated weighted irradiances for each i can be expressed as:

$$I_i(SZA,TOZ) = \int_{285}^{400} S_\lambda(\lambda,SZA,TOZ)\ SRF_i(\lambda)\ d\lambda \qquad (3.1)$$

Ratios and normalization

The following ratios were then calculated:

$$R_i(SZA,TOZ) = \frac{I_{CIE}(SZA,TOZ)}{I_i(SZA,TOZ)} \qquad (3.2)$$

where $I_{CIE}(SZA,TOZ)$ represents the "true" erythemal irradiance, calculated with the CIE spectral function for each *SZA* and *TOZ*.

Actually, $R_i(SZA,TOZ)$ could be already used as spectral correction factors. For this, the erythemal radiometers should be calibrated against spectroradiometric data weighted by the $SRF_i(\lambda)$ function instead of the CIE function. In this way, the corrected UVI measurements from the erythemal radiometers would be obtained as:

$$UVI_i(SZA,TOZ,...) = V_i(SZA,TOZ,...)\ f_i\ R_i(SZA,TOZ) \qquad (3.3)$$

where f_i is the calibration factor, "…" accounts for the other factors affecting the signal, and V_i is the directly measured signal by the radiometer in Volts.

Note that, considering this way, the calibration factor f_i only depends on the characteristics of the radiometer (i.e., its SRF) and does not depend on *SZA* or *TOZ* at all. This is because the actual SRF of the radiometer is used for the calibration. In fact, this method could be also used to check the radiometer's SRF. If that was wrongly measured, f_i would vary with *SZA* and *TOZ*, which could be detected after few hours of data, as was discussed by *Bais et al* [2001]. The main disadvantage of this method is that the SRF function has to be known with very high accuracy; otherwise, the calibration can be highly uncertain.

Another way of calibrating the erythemal radiometers against spectral measurements is by weighting the latter by the CIE function. In this way, the calibration factor has to be written as $f_i(SZA_{cal},TOZ_{cal})$ since strictly speaking, it is valid only for the conditions for which it was found. Then, the spectral correction factors have to be referred to SZA_{cal} and TOZ_{cal} as follows:

$$N_i(SZA,TOZ,SZA_{cal},TOZ_{cal}) = \frac{R_i(SZA,TOZ)}{R_i(SZA_{cal},TOZ_{cal})} \qquad (3.4)$$

In this way, UVI_i is obtained as:

$$UVI_i(SZA,TOZ,...) = V_i(SZA,TOZ,...)\ f_i(SZA_{cal},TOZ_{cal})\ N_i(SZA,TOZ,SZA_{cal},TOZ_{cal}) \qquad (3.5)$$

The advantage of this method is that the calibration factor f_i can also be found by comparison with data from another well characterized, reliable erythemal radiometer. The main problem of this method is the possible *TOZ* variations during the calibration, which would add uncertainty in the calibration factor [*Bais, et al.*, 2001]. Using this method it is also important to have an accurate SRF for the sensor, although this is less critical than for the first method, as commented above.

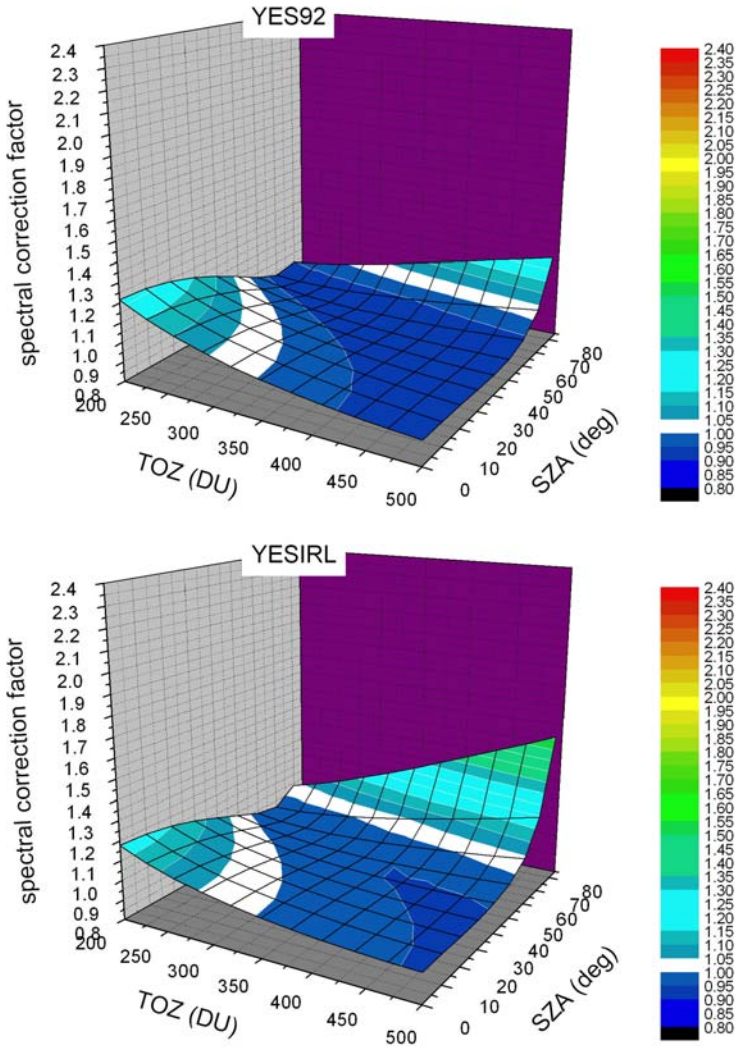

Figure 3.2 Normalized spectral correction factors $N_i(SZA,TOZ,SZA_{cal},TOZ_{cal})$

For this study this latter calibration method will be assumed since the $N_i(SZA,TOZ,SZA_{cal},TOZ_{cal})$ factors are more convenient to visualize the differences between instruments and evaluate how important the corrections factors are. For this, it will be assumed that the calibration factor of the sensor is well known from direct comparisons against a spectroradiometer or an already well characterized erythemal radiometer for the conditions SZA_{cal} and TOZ_{cal}. These reference conditions of *SZA* and *TOZ* have been set at 30º and 300 DU, which implies that the calibration factor must be known for these conditions. Figure 3.2 shows the representation of the obtained spectral calibration factors following this methodology (that is, $N_i(SZA,TOZ,SZA_{cal},TOZ_{cal})$) as a function of *SZA* and *TOZ*. Note that YES92, YESIRL and YESSTUK

present similar correction factors for low *TOZ* and *SZA* and become quite remarkable for large SZA and TOZ. However, the differences at low *SZA* and *TOZ* have a stronger effect on the absolute value of UVI, since as *SZA* and *TOZ* increase, UVI becomes highly reduced (see Figure 1.9).

The shape of the plots in Figure 3.2 can be understood in the following way.

SZA and *TOZ* highly affect the UV spectrum so the larger the values of these parameters, the greater the absorption in the UV spectrum, being more attenuated for short than for long wavelengths.

This means that for large *SZA* and *TOZ* the long-wavelength (thus the UVA region) part of the spectral responses become dominant and for low *SZA* and *TOZ*, the short-wavelength part (the UVB region) become more important.

Using this argument some behaviours found can be easily explained. For instance, the $SRF_{SLCIRL}(\lambda)$ stays very close to the CIE function for low wavelengths but it gets far from it at large wavelengths. In this way, N_{SLCIRL} stay very close to 1 for low *SZA* and *TOZ* but it goes up to 2 for large values of these parameters.

Note that the N_{KZ} surface plot is the flattest even though in Figure 3.1 $SRF_{KZ}(\lambda)$ appears far from the CIE function. This is because the correction factors are normalised, which means that the SRF could be rescaled with no change in these factors. In Figure 3.3 the $SRF_{KZ}(\lambda)$ divided by 2.5 is shown together with the CIE function.

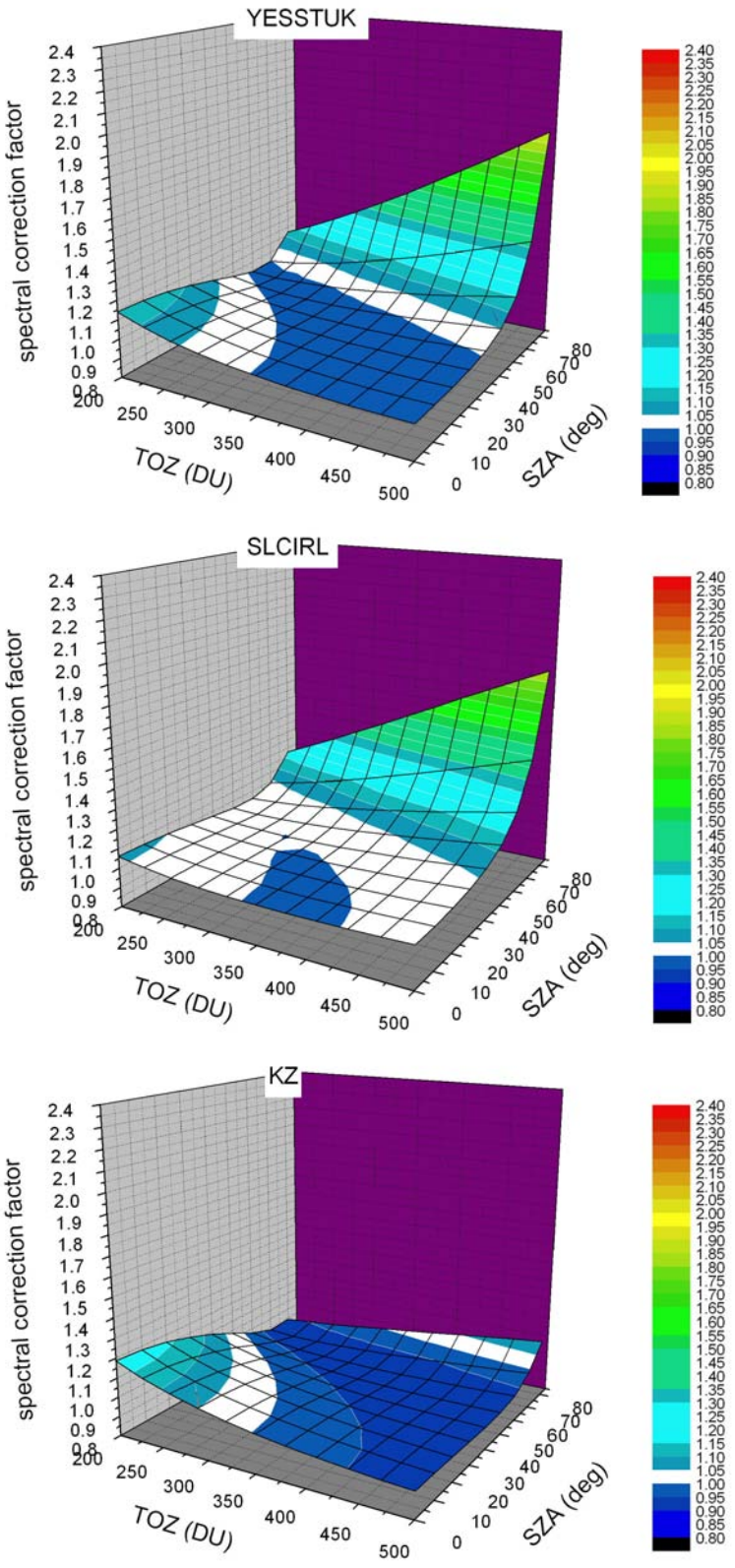

Figure 3.2 (cont). Normalized spectral correction factors $N_i(SZA, TOZ, SZA_{cal}, TOZ_{cal})$

In this way, the two functions appear very close to each other.
The same argument can be used for YES92, which also shows quite low correction factors. The patterns seen for YESSTUK and YESIRL can be explained similarly.
The tables with the values of $N_i(SZA,TOZ,SZA_{cal},TOZ_{cal})$ for the five cases are collected in Annex B.

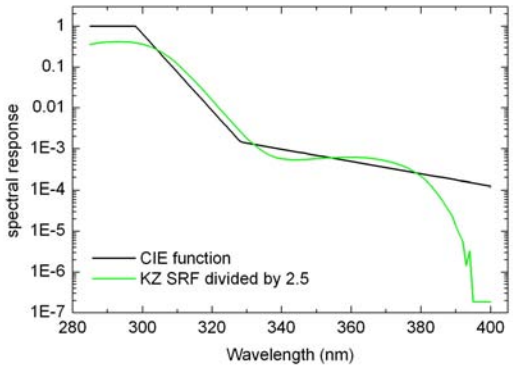

Figure 3.3 Representation of the KZ spectral response function divided by 2.5 and the CIE function

3.4 Importance of the spectral correction factors

The interest is set on which would be the error made in UVI if no spectral correction factors were applied. For this, it will be assumed that a perfect absolute calibration factor (i.e., as $f_i(SZA_{cal},TOZ_{cal})$) is available for each erythemal radiometer and that all the instruments have an ideal cosine response.
As far as relative errors are concerned, these can be directly inferred from the plots in Figure 3.2. If no spectral correction factors were applied (i.e. $N_i(SZA,TOZ) = 1$ for all *SZA* and *TOZ* conditions) the measured UVI would be too low by down to -22 % for low *SZA* and *TOZ* and down to -233 % for large *SZA* and *TOZ*. For moderate values of *SZA* and *TOZ* uncertainties would be about ±10%. Recall that these differences would change if other reference conditions were considered.
In Figure 3.4 the absolute errors in UVI that would arise from not applying the spectral correction factors are represented for the five cases. Error values down to -3 in UVI are found. The smallest errors are found for SLCIRL while the largest are detected for YES92. As expected, the largest absolute errors are detected when UVI is large, i.e., for low *SZA* and *TOZ*.
This shows the high relevance of applying spectral correction factors to the measurements. Indirectly, this also underlines the importance of accurately knowing the actual spectral response of the instrument in order to avoid poor corrections. This point can be clearly discussed here since three different SRFs are available for the YES UVB-1 radiometer, each of them leading to different spectral correction factors.
In Figure 3.5 it has been assumed that YESIRL is the correct (=real) spectral response function for the YES sensor, and the absolute and relative errors, that would be made by taking the YES92 or YESSTUK spectral response functions instead, are plotted. Interestingly, the differences for YES92 and YESSTUK appear very similar and with opposite sign. Maximum absolute and relative differences in UVI are of 0.7 and 25%, respectively. This gives an idea of the uncertainties that could be found related to an uncertain measurement of SRF.

3.5 Model–measurement comparisons

In this section, UVI model-measurement comparisons for clear-sky conditions are shown in order to test the results found when using different measurements for the same site and period.

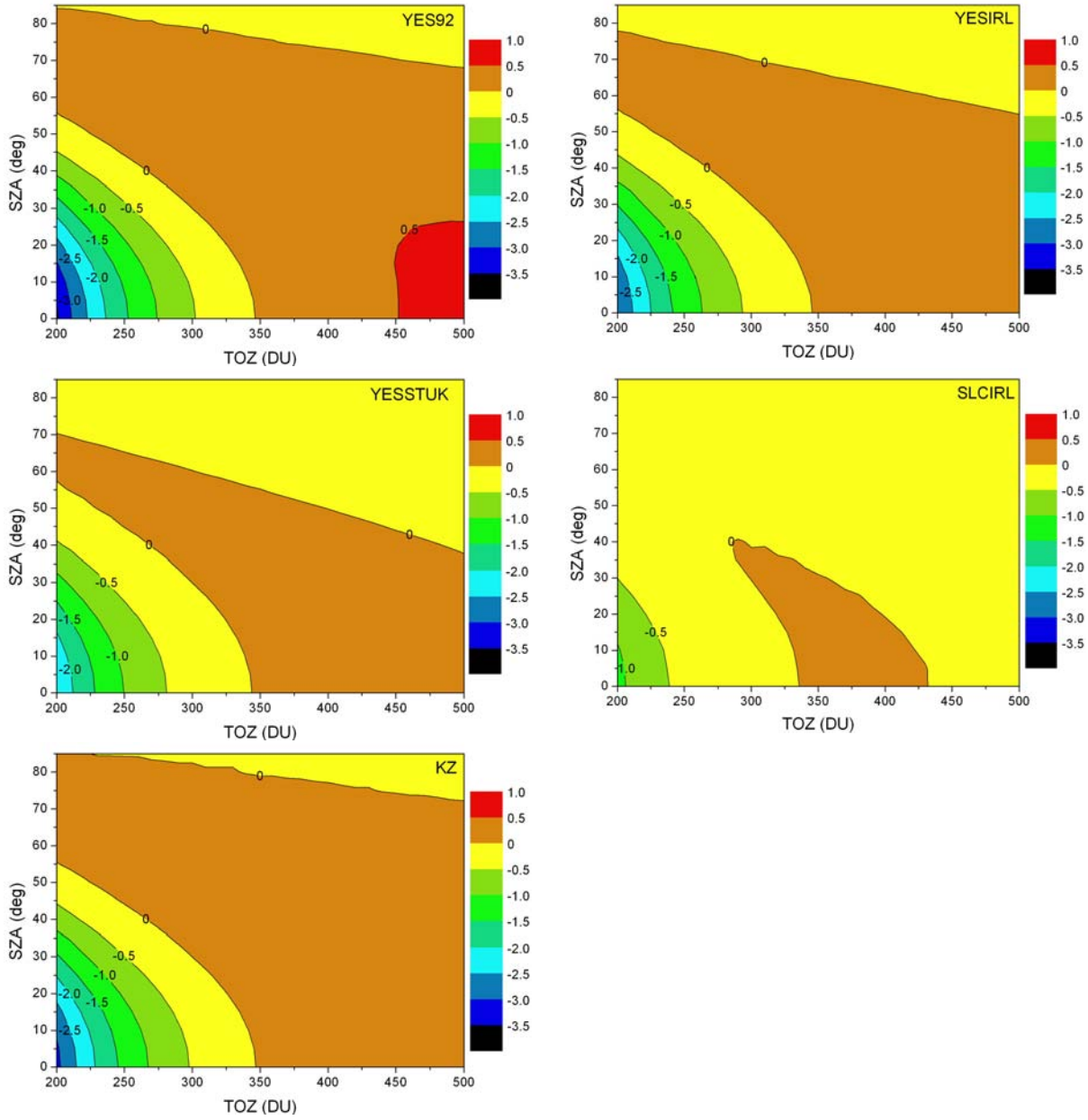

Figure 3.4 Absolute errors in UVI that would be found if no spectral correction was applied

For this, data from Lauder (45.04ºS, 169.684ºE, 370 m above sea level), New Zealand, corresponding to 49 clear-sky days of 2001, were considered. The clear-sky criterion was based on the visual inspection of the UVI measurements and only whole days were selected.

Datasets and measurement treatment

UVI measurements are available from different instruments maintained by the National Institute of Water and Atmospheric Research (NIWA). For this analysis UVI from two erythemal radiometers, YES UVB-1 and SLC 501, and from a NIWA-built spectroradiometric system (hereon referred to as UVM) [*McKenzie, et al.*, 1997] are considered. The YES and SLC data are concurrent and we have used 10 minute means of data taken at 1-minute resolution. The spectroradiometric data are taken every 5 degrees of *SZA* except around midday, where the time interval between measurements is 15 minutes.

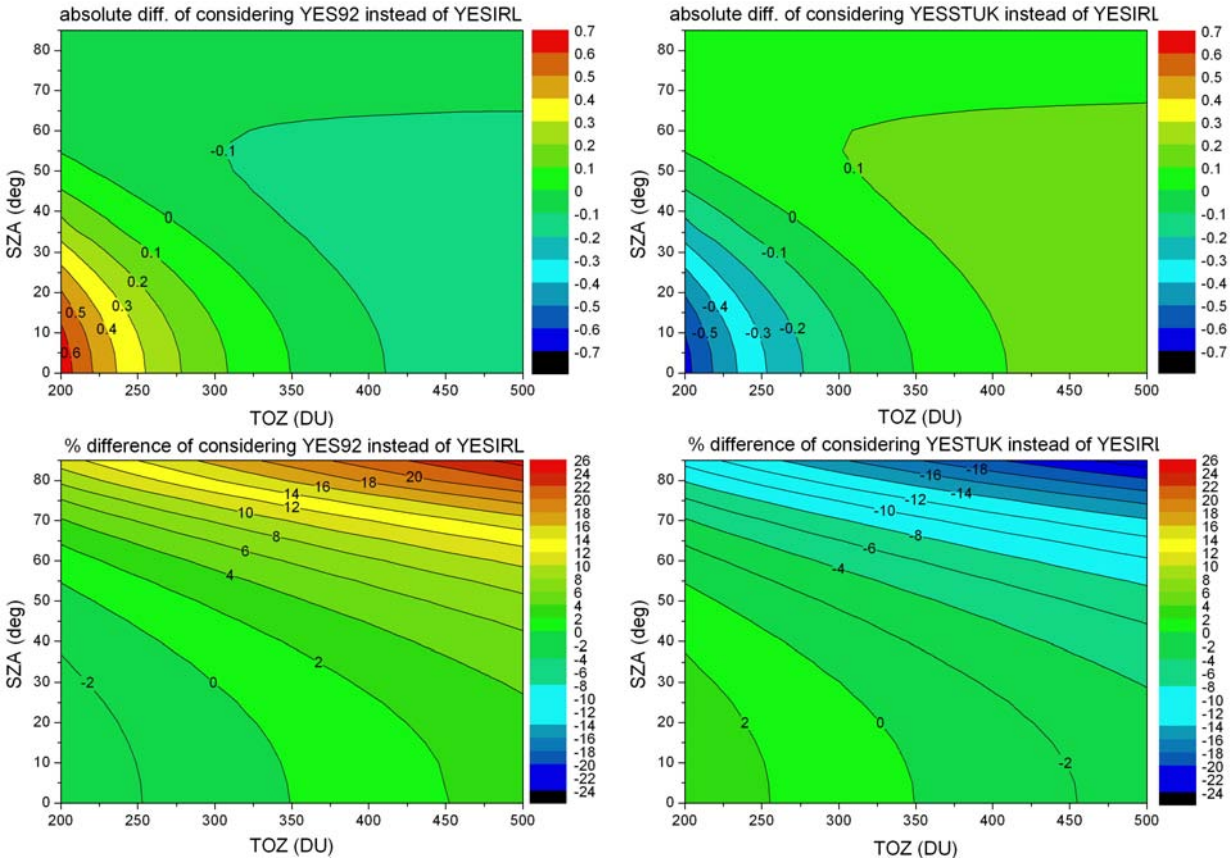

Figure 3.5 Absolute and relative errors that would be found if the YES92 or the YESSTUK spectral response function were considered instead of the YESIRL function, which is supposed to be the good one.

Figure 3.6 shows the histograms of *SZA* for the data considered for the SLC, YES and UVM datasets. Note the different shapes of the histograms, with relatively more measurements for low *SZA* with UVM than with SLC and YES.

The YES SRFs discussed in the previous sections correspond to the sensor in Lauder here considered. However, the SRF for the SLC sensor are for an instrument located at Leigh. For the SLC sensor in Lauder, the SRF was not available so it was assumed to be the same as for the Leigh instrument.

For the spectral correction, the SRFs from IRL (in Figure 3.1) were considered for both the YES and SLC radiometers, being the correction factors developed by NIWA. These correction factors were calculated using the same methodology described in Section 3.3. Cosine (angular) corrections were also applied. For the YES radiometer, the cosine response was measured during the WMO/STUK campaign [*Leszczynski, et al.*, 1998]. The cosine response for the SLC radiometer at Leigh was available from IRL measurements in 1995 and this was considered for the angular corrections of the SLC instrument at Lauder. Cosine corrections were calculated assuming an isotropic atmosphere.

Calibrations for these two radiometers are routinely performed once a year by comparing them against the UVI measurements from UVM. The calibration day for 2001 was day 81. Figure 3.7 shows the measured UVI data with YES, SLC (after being corrected for their spectral and angular responses and the new calibration factor had been applied) and UVM together with the ratios between the first two and the latter. A very good agreement (within 1-2%) is seen among the three instruments around noon, but much worse for the beginning and the end of the day.

Table 3.4 Conditions considered in the TUV model for the UVI model-measurement comparisons

Wavelength range	280-400 nm
Wavelength resolution	1 nm
SZA	From the instrument stamp
TOZ	From TOMS assimilated
Surface albedo	0.05
Altitude	0.37 km
AOD	From sun photometer measurements at 415nm. Two values per day (am/pm)
SSA	0.9
alpha	1.4
G	0.7
Aerosol profile	*AOD* distributed in the first km above ground
Radiative transfer code	8 streams with pseudo spherical corrections

Model vs measurement

The TUV model was used for the UVI calculations. Table 3.4 summarises the input information considered. Two *AOD* estimations per day (am/pm) were available from sun photometer measurements; half days with no *AOD* data were rejected from the analyses.

The asymmetry parameter (g) and the *SSA* were set to 0.7 and 0.9, respectively, as typical reported values in the UV range, as commented in Section 1.6, and consistently with values considered in Chapters 4 and 5. The Ångström's exponent *alpha* is set to 1.4 as a typical value for Lauder (see discussion in Section 4.4). The input options not shown in Table 3.4 were considered as default by the model.

Figure 3.8 shows the results of the UVI model-measurement comparisons. Diverse agreements are found depending on the instrument considered. When using data from the SLC radiometer, the model underestimates the measurements by about 2.3%; that is seen through the regression slope (*B*) value. The opposite happens when using the YES and UVM devices, and overestimations found are about 5.5% and

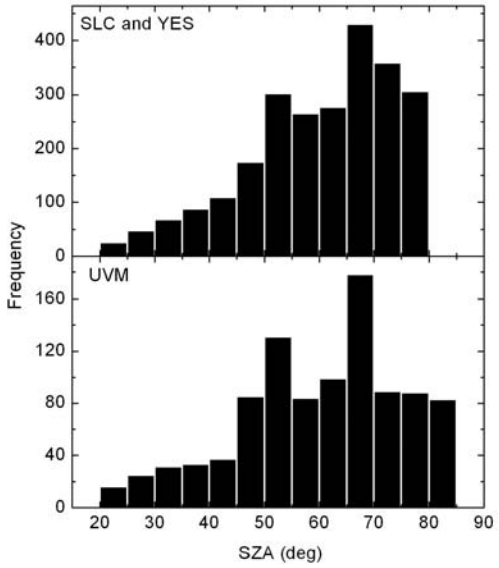

Figure 3.6 Histograms of *SZA* values for the considered measured UVI with SLC YES and UVM.

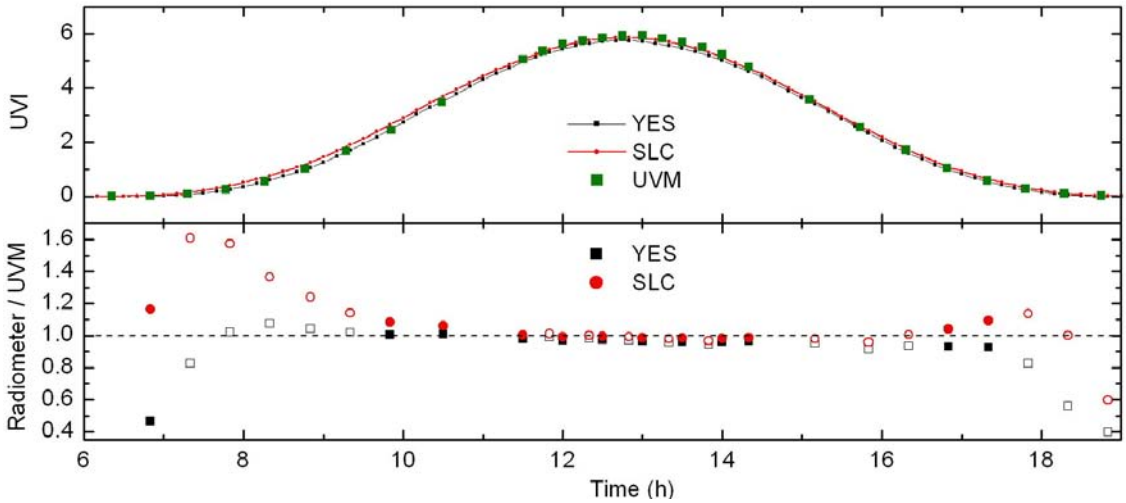

Figure 3.7 Comparison between the data from the YES and SLC radiometers and UVM for day 81 of 2001, during which YES and SLC were calibrated against UVM. Since UVM and the radiometers have different scanning times, only the solid symbols correspond to matching data and for the open circles, differences in time are up to 5 minutes.

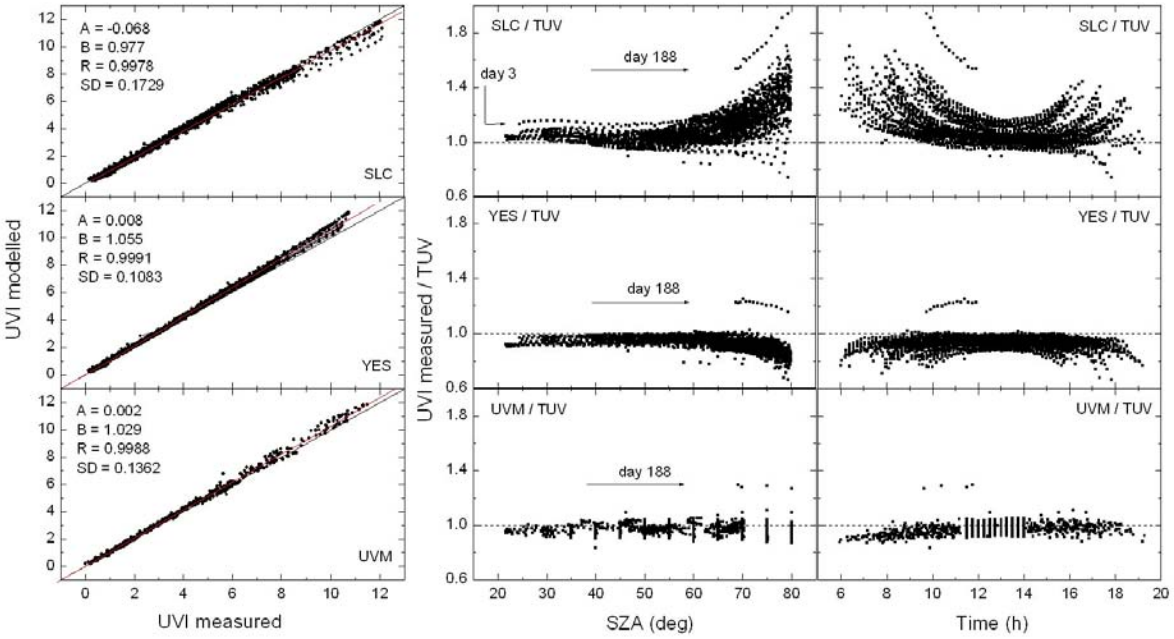

Figure 3.8 Results of the UVI model measurement comparison for clear days in Lauder 2001 using measured UVI from SLC 501 and YES UVB-1 radiometers and the UVM spectroradiometer. Left: Model vs. Measurement plots; the fitted line and the statistics of the linear regression are shown. Right: Measurement-model ratios as a function of SZA and time.

2.9%, respectively. Regression coefficients (R) of the model vs. measurement plots are always larger than 0.997, showing good alignments.

More interesting is the analysis of the dispersion of the points around the fitted line. By visual inspection, similar dispersions are seen for YES and UVM and much larger dispersions occur for SLC. This can be analysed more objectively through the standard deviation (SD) of the regression fit. The lowest SD is found for YES, while for UVM SD is 25% higher. This difference, which a priori was not so evident, arises because the UVM dataset has proportionately more data with low SZA (and thus high UVI, which have a larger contribution to SD) than the measurements from YES (as noted in Figure 3.6). Since the datasets for YES and SLC are concurrent, their SD are directly comparable. The SD for the latter is 60% larger than for the former, which confirms the differences seen.

The measurement/model ratios are also shown as a function of SZA and time in Figure 3.8. The results are significantly worse when using SLC than YES and UVM. This is seen through the larger dispersion of the points and the strongest dependences of the ratios on SZA. For the YES dataset, there is also an angular dependence though much smaller and in the opposite sense. For UVM, no significant angular dependence is seen. The results for YES and UVM are similar for $SZA<60^{o}$. This shows, taking the modelling as a good reference, a very good performance of the YES instrument and a much worse performance of the SLC instrument.

Note that there are few outlying scattered points in the plots. This most likely corresponds to data slightly affected by clouds. Day 188 (marked in Figure 3.8) is an outlier since the measurements read much larger (about 20-30% from the YES and UVM plots) than the model. That was a clear-sky day with the ground covered by frost, so the UVI was enhanced by the large ground albedo for these conditions. Day 3 also appears away from the other days for the SLC comparison (see Figure 3.8). The previous day was rainy and the

corresponding annotations in the log suggest the possibility of electrical problems related with leaks and electrocuted mice.

The remaining angular dependence for YES could be uncertainties in the spectral or/and angular responses and (thus) the corresponding correction factors. As seen in Section 3.3 and also discussed in previous studies [*di Sarra, et al.*, 2002; *Leszczynski, et al.*, 1998] slight errors in the spectral response can lead to important errors in the correction factors.

Regarding the time evolution, higher SLC/TUV ratios are observed in the morning than in the afternoon, which is not seen for the YES/TUV ratios. This is also visible in Figure 3.7 for the SLC and YES 1-day comparisons with UVM. These am/pm differences for the SLC sensor cannot be related to a time error since both YES and SLC instruments are connected to the same data logger and time stamp. The most probable reason for that azimuthal error is an error of the instrument levelling. It could be also related to the positioning of the Peltier element on the SLC sensor which aims to stabilise the sensor temperature at 25ºC. If it is not axially symmetric, the active heating or cooling could lead to different responses from different parts of the sensor. For the YES radiometer, the whole instrument cavity is heated and the temperature is stabilised at 40ºC.

The UVM/TUV ratio also has a slight morning-afternoon asymmetry. In this case, the reason is related to a time stamp error. For the UVM spectroradiometer, the time stamp corresponds to the centre of the scan, at wavelength 370 nm. The time that would correspond to the effective wavelength of UVI, which is in the UVB region (around 310 nm, see Figure 1.2), is about 1 minute before the considered time stamp. This lag induces an uncertainty of ±3% at 75 degrees of *SZA*. Thus, if this time error was corrected results for UVM in Figure 3.8 would improve. In Chapter 4, this time stamp issue is commented in more detail and corrected leading to higher measurement accuracy and better model-measurement comparison results.

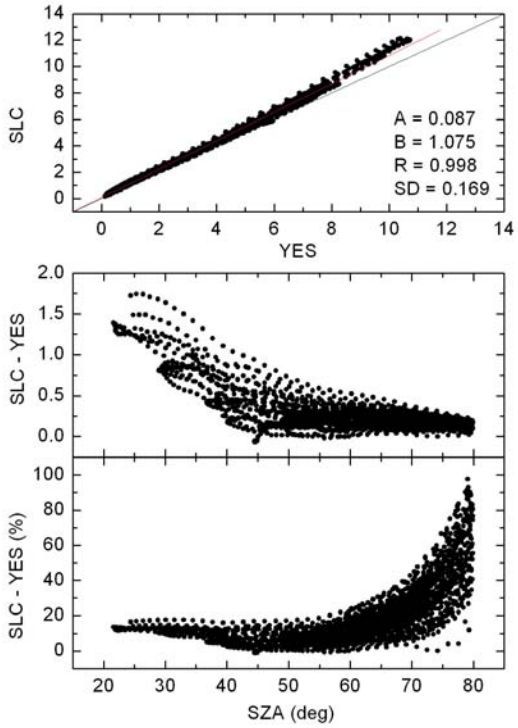

Figure 3.9 Absolute and relative differences between concurrent UVI measured with one SLC 501 and one YES UVB-1 in Lauder 2001.

In order to show more evidence about the differences between data from the two radiometers, Figure 3.9 shows the results from the direct comparison between the measured UVI by SLC and by YES. The linear regression shows good correlation between SLC and YES but with large dispersion and a systematic bias of about 7.5%. Absolute differences found are up to 1.8 in UVI. Relative differences are within 20% for *SZA*<60º. For larger angles, differences go up to 100%. This highlights the different performance of the two instruments.

Analysis for data at noontime

Since the radiometric measurements are not concurrent with the UVM data, the strict comparison between them can only be reliable around noon, when UVM measures with higher frequency and more matches are found (see Figure. 3.7). Also, UVI changes more slowly around noon, so the comparison

between the measurements is then more reliable. Figure 3.10 shows the cross comparisons between the three sources of UVI measurements. From the YES vs. UVM comparison, the points appear very well aligned but the former underestimates the UVM measurements by about 4% (B =0.959). Mean relative differences are -3.1 ± 3.2% (being the interval given by one SD) with peak values down to -11%, and do not show a clear dependence on SZA for angles up to 60º. Absolute differences are down to -0.84 in UVI.

The SLC vs. UVM comparison show worse agreements, with lower regression coefficient and, in this case, SLC overestimating UVM by about 5.5%. Moreover, the SD of the linear fit is twice as large as the SD found for the YES vs. UVM comparison. The SLC-UVM relative differences are larger, more dependent on SZA, and, thus, more dispersed. The mean difference is 7.2 ± 5.1% with peak values up to 16%. Maximum absolute differences are of 1.7 in UVI.

To complete this analysis, the noon data from SLC and YES are also compared showing systematic deviations of 10% (B=1.10), which is sensibly larger than what has been found for the whole datasets (see Figure 3.9). The dependence of the relative differences on SZA has the same pattern that for the SLC-UVM comparison but with larger values. Mean relative differences are 11.3 ± 7.4% with peak values up to 27.4%. Maximum absolute differences are the same as for the SLC-UVM comparison.

In order to analyse the annual variations of the relative differences shown in both Figure 3.8 and 3.10, Figure 3.11 shows the cross-comparison between UVI measured with YES, SLC and UVM and the TUV UVI calculations for data around noon. Note that SLC has a clear annual evolution both with respect to UVM and TUV. The YES data seems to have also some annual evolution though this is less evident than for the SLC data. In comparison with both UVM and TUV, the SLC instrument reads much higher (up to about 20%) in the wintertime than in summer. The relative YES data also seems to have maximum values around the equinoxes and minimum values around summer solstice. The maximum amplitude of YES evolutions is about the half (11%) of the SLC evolutions. The UVM instrument has no apparent annual pattern with respect to TUV and the range of values is

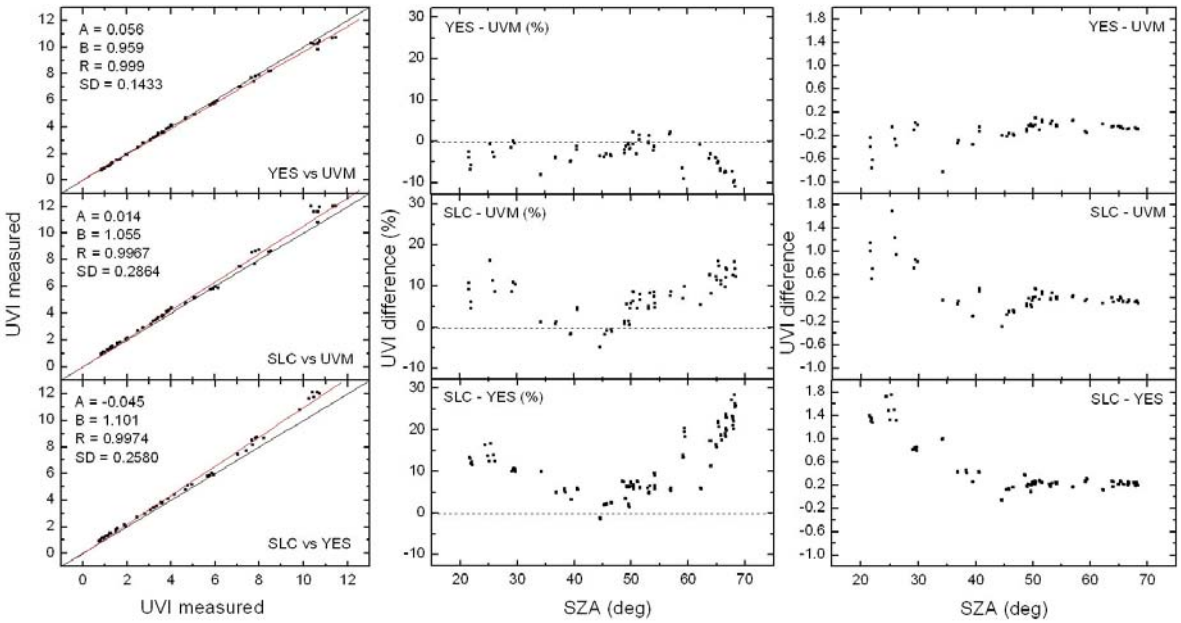

Figure 3.10 Comparison between UVI measured by the YES, SLC and UVM instruments for noon conditions. For the comparisons against UVM, data from noon ±15 min is included in order to get at least one match per day.

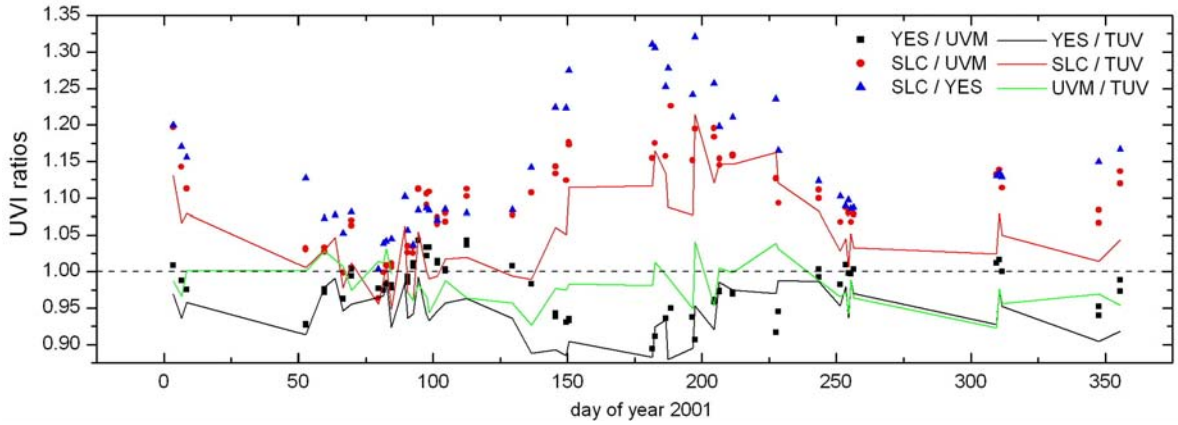

Figure 3.11 Different ratios between measured and modelled UVI around noon. For the comparisons against UVM, data from noon ±15 min is included in order to get at least one match per day, as in Figure 3.10. Data for day 188 are here not shown as this day is an outlier (see Figure 3.8).

similar to that for YES, about 12%. Note that the maximum differences shown in Figure 3.11 are from the SLC/YES comparison.

All these analyses lead us to believe that there is an error in the characterisation (and thus in the applied corrections) for the SLC instrument. That is most likely because both the angular and spectral responses were taken from another SLC instrument (the sensor at Leigh), which probably differ from the actual responses for the instrument in Lauder. This confirms the above commented result about the necessity of characterizing each particular instrument. That is, despite of being the same brand and model, two UVI radiometers may have SRF and angular responses different enough to result in unacceptable errors in the measurements if standard, generic or typical corrections are used. Errors in the angular response corrections lead to errors in the measurement as a function of *SZA* while errors in the spectral response lead to errors as a function of both *SZA* and *TOZ*. These two sources of error appear in the above comparison as both systematic and random differences between SLC data and UVM and TUV values.

In addition to this, dependencies observed in the spectral response of the SLC 501 radiometers on both temperature and relative humidity have recently been reported in the literature [*Huber, et al.*, 2003; 2002]. In particular, *Huber et al* [2002] reported reductions in the spectral response of 10% in the UVB range and of a factor 2 in the UVA range due to temperature increase of 20ºC at the outside of an instrument's housing. *Huber et al* [2003] detected a reduction of up to 5% in the instrument sensitivity in the UVB region and a reduction of a factor more than 2 in the UVA region when the internal relative humidity of a SLC 501 radiometer experimented an extreme change, from 9 to 70%.

Figure 3.12 shows the annual evolutions of the noon *SZA*, *TOZ*, relative humidity, and air temperature. In Figure 3.13, these evolutions are compared against the measurement/model ratios from Figure 3.11 in order to explore possible correlations. No statistically significant correlation is found for the YES/TUV and UVM/TUV ratios. However, SLC/TUV ratios appear correlated (with R > 0.5) with *TOZ*, air temperature and relative humidity.

It has to be noted that air temperature is also correlated with relative humidity (R = -0.784) and *TOZ* (R=-0.643) and also well correlated with *SZA* (R = -0.821). Relative humidity is related to *SZA* and *TOZ* with R =0.521 and R=0.502, respectively. Obviously, these latter correlations correspond to the seasonal variation of the four variables. Therefore, the

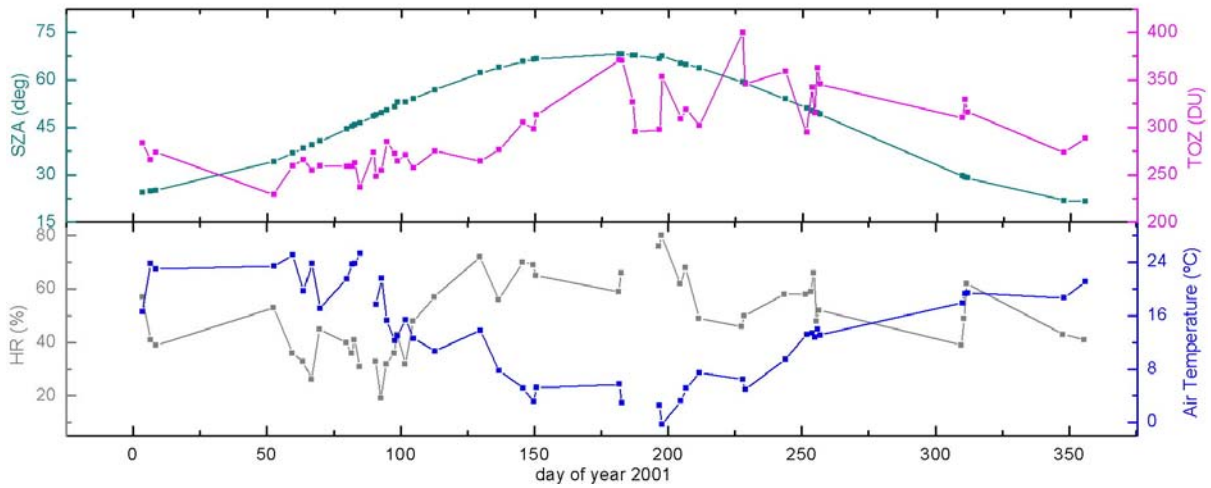

Figure 3.12 Upper: Noon measurement-model ratios for the YES, SLC and UVM data for the days of the study. Lower: Noon *SZA*, air temperatures (ºC) and relative humidity (%) values for the days of study.

contribution of each variable to the annual variation of the SLC/TUV ratio is difficult to establish.

However, it can be noted that, around winter, there are the highest values of *SZA* and *TOZ*, both contributing to higher absorption of UVR in the UVB region and thus, increasing the contribution of UVA in UVE and UVI. That certainly affects the spectral corrections, as has been discussed in Section 3.3. The contributions that changes of air temperature and relative humidity could have in the annual evolution of the SLC/TUV ratio are difficult to specify since the actual temperature and relative humidity within the sensor case are not known, despite the temperature is expected to be stabilized at 25ºC and the relative humidity minimized through the desiccant.

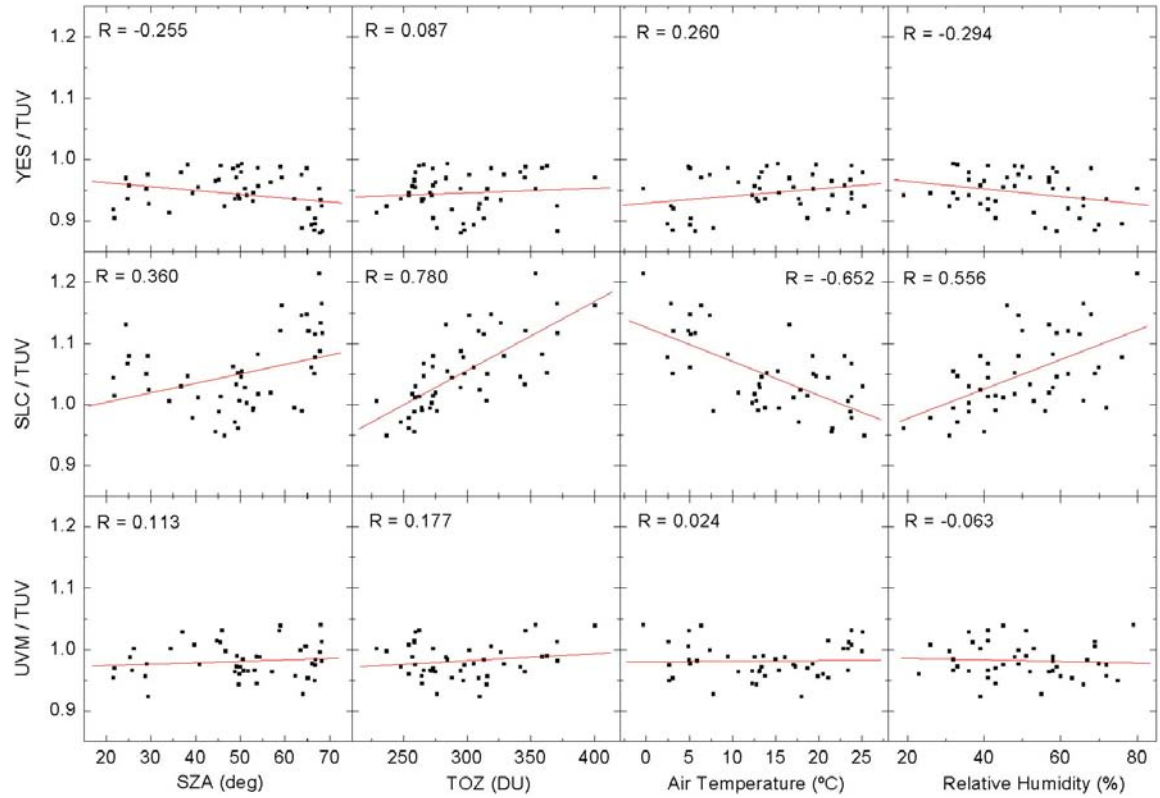

Figure 3.13 Measurement/model ratios vs. *SZA*, *TOZ*, air temperature and relative humidity for noon conditions.

3.6 Conclusions

In this chapter, the SRFs from three different types of erythemal radiometers have been shown and a methodology for the corresponding spectral corrections has been presented. The developed analysis and obtained results confirm the need of having the erythemal radiometers well characterised to apply the adequate correction and to avoid important errors in the UVI measurements.

Correction factors found range from 0.90 to 2.33. If no spectral corrections were applied, UVI would be underestimated by down to -22% and -3 units of UVI for the conditions associated to larger UV levels (i.e., low *SZA* and *TOZ*). These differences are relative to the considered reference conditions (*SZA* = 30º and *TOZ* = 300 DU).

Due to differences among the three SRFs available for the YES sensor, differences of ±0.7 in UVI have been obtained, which highlights the measurement errors that could be associated with an uncertain characterisation of the instrument.

Model-measurement comparisons for clear-sky conditions have been carried out with UVI data from two erythemal radiometers in Lauder (one YES UVB-1 and one SLC 501) together UVI from the UVM spectroradiometric data. The regression slopes from the model vs. measurement comparison have shown bias of -2.3%, +5.5% and +2.9%, when using the SLC, YES and UVM data, respectively, showing a large difference between the results with SLC and YES. Actually, UVI measurements from SLC are systematically larger than YES values (7.5%) being the relative differences up to 100% for large *SZA*; the absolute differences are up to 1.7 in UVI.

Moreover, the dispersion of the points around the regression line, is much larger (*SD* about 60% larger) for SLC in comparison with YES; the latter has shown similar dispersions to UVM. The SLC data have shown a large angular dependence whereas a much smaller dependence is found with YES and no dependence is seen for UVM. An azimuthal dependence has been detected in the SLC data leading to much larger values in the morning than in the afternoon. A time error has also been detected for the UVM data, though with a much lower effect.

From the analysis of noon data, an even higher bias (about 10%) has been found between both radiometers. Mean differences (plus minus one *SD*) between the erythemal radiometers and the UVM data are -3.1 ± 3.2% for the YES and much worse, 7.2 ± 5.1% for the SLC. Maximum YES - UVM and SLC - UVM differences are of -0.84 and 1.7 in UVI, respectively.

Both the SLC/TUV and the SLC/UVM ratios have shown a clear annual variation, being larger by up to about 20% in winter than in summer. For the YES data, an annual pattern is not so clear and for UVM, there is no visible pattern, being (for these two) the maximum amplitude of the annual variations about the half of that for the SLC data.

In order to investigate the annual changes of the SLC performance, the SLC/TUV ratio has been plotted against *SZA*, *TOZ*, air temperature and relative humidity. The SLC/TUV ratio correlates with all these variables, although the relation with SZA is clearly non linear. However a causal dependence can not be derived from this analysis, since it is difficult to separate the contribution of each of these variables on the annual evolution of the SLC measurements. The YES/TUV and UVM/TUV ratios did not show any significant correlation.

The most probable reason of (or the main cause for) the poor performance of the SLC is an error in the considered SRF. Both the spectral and angular responses and correction factors

were considered from a different SLC instrument, and this is probably a poor assumption. An error of this type leads to errors in the measured UVI as a function of *SZA* and *TOZ* as it has been observed.

It has to be pointed out that the main aim of this chapter was to evaluate the performance of the erythemal radiometers. Model-measurement comparisons have been useful here to see the differences when considering measured data from different instruments and no much attention has been paid on the actual model-measurement agreement. Moreover, the model-measurement comparisons presented here were affected by important limitations such as a not strict cloud filtering and time and azimuthal errors of the data.

Despite these limitations, we have confirmed that the best performance in the UVI measurement-model comparison is found with spectroradiometric data; good agreements were also found for a well characterized erythemal radiometer (YES).

Next chapter aims to present a much more accurate model-measurement analysis in order to investigate which type of agreements can be found when using the best possible measured data and the best modelling input information.

3.7 References

Bais, A., et al. (2001), Report of the LAP/COST/WMO intercomparison of erythemal radiometers, 54 pp, WMO, Geneva.

Berger, D. S. (1976), The sunburning ultraviolet meter: design and performance, *Photochemistry and Photobiology*, *24*, 587-593.

Blumthaler, M., et al. (1997), Increase in solar UV radiation with altitude, *Journal of Photochemistry and Photobiology B: Biology*, *39*, 130-134.

Bodhaine, B. A., et al. (1998), Calibrating broadband UV instruments: ozone and solar zenith angle dependence, *Journal of Atmospheric and Oceanic Technology*, *15*, 916-926.

Cede, A., et al. (2002a), Effects of clouds on erythemal and total irradiance as derived from data of the Argentine Network, *Geophysical Research Letters*, *29*, 10.1029/2002GL015708.

Cede, A., et al. (2002b), Monitoring of erythemal irradiance in the Argentina ultraviolet network, *J. Geophys. Res.*, *107*, 10.1029/2001JD001206.

di Sarra, A., et al. (2002), On the Importance of spectral responsivity of Robertson-Berger-type ultraviolet radiometers for long-term observations, *Photochemistry and Photobiology*, *76(1)*, 64-72.

Huber, M., et al. (2003), Solar UV measurements with Robertson-Berger type instruments: influence of the detector's humidity status, *Agricultural and Forest Meteorology*, *120*, 39-43.

Huber, M., et al. (2002), Effects of ambient temperature on Robertson-Berger type erythemal dosimeters, *Applied Optics*, *41*, 4273-4277.

Leszczynski, K., et al. (1998), Erythemally weighted radiometers in solar UV monitoring: results from the WMO/STUK intercomparison, *Photochemistry and photobiology*, *67*, 212-221.

Long, C. S., et al. (1995), Ultraviolet index forecasts issued by the National Weather Service, *Bulletin of the American Meteorological Society*, *77*, 729-748.

Los, A. (2003), A Laboratory calibration transfer method for broadband UV filter radiometers, paper presented at EGS-AGU-EUG Joint Assembly, Nice.

Martinez-Lozano, J. A., et al. (2002), UV Index experimental values during the years 2000 and 2001 from the Spanish broadband UV-B Radiometric Network, *Photochemistry and Photobiology*, *76(2)*, 181-187.

McKenzie, R. L., et al. (1997), UV spectro-radiometry in the network for the detection of stratospheric change (NDSC), paper presented at Solar Ultraviolet Radiation. Modelling, Measurements and Effects, Springer-Verlag, Berlin, October 1995.

Schmalwieser, A. W., and G. Schauberger (2000), Validation of the Austrian forecast model for solar, biologically effective UV radiation - UV index for Vienna, *Journal of Geophysical Research*, *105*, 26661-26667.

Schmalwieser, A. W., and G. Schauberger (2001), A monitoring network for erythemally-effective solar ultraviolet radiation in Austria: determination of the measuring sites and visualisation of the spatial distribution, *Theoretical and Applied Climatology*, *69*, 221-229.

Thiel, S., et al. (1997), Modification of global erythemally effective irradiance by clouds, *Photochemistry and Photobiology*, *65(6)*, 969-973.

WMO (1994), Report of the WMO meeting of experts on UV-B measurements, data quality and standardization of UV indices, Les Diablerets, Switzerland.

Zaratti, F., et al. (2002), Erythemally weighted UV variations at two high-altitude locations, *Journal of Geophysical Research*, *108*, doi:10.1029/2001JD000918.

4

UVI Model vs. Measurement

General frame

In Chapter 3, discussions have been presented about the characterisation and performance of different erythemal radiometers. UVI model-measurement comparisons using concurrent measurements from two erythemal radiometers and using spectroradiometric data have been analysed. Large errors were found with one radiometer while the other showed reasonable good performance; the best model-measurement agreements, however, were found with UVI measured with a spectroradiometric system.

High quality spectroradiometers are needed as a reference (for example, erythemal radiometers are usually calibrated against them) and to study long-term trends (such as UV increases induced by the ozone depletion). Moreover, their accuracy set the state of the art in UVI measuring.

In addition, accurate modelling techniques are needed to better understand the way factors affect UV radiation, to predict UVI, and as a quality control of the measurements. Multi-scattering radiative transfer models offer better accuracy in calculated UVI than parameterized and empirical models if most of the relevant input parameters are known.

Few comparisons between UVI high quality measurements and multi-scattering models have been presented so far since this kind of measurements concurrent with other measured quantities needed as input to the model are rarely available.

Overview

This study presents the results of a detailed comparison between measured and modelled UVI for clear sky conditions and solar zenith angle (*SZA*) ≤ 80º. For this, state-of-the-art spectroradiometric data and state-of-the-art radiative transfer modelling incorporating the broadest possible range of input data are used. One year of data from Lauder (New Zealand), Boulder (Colorado, USA), Mauna Loa (Hawaii, USA) and Melbourne (Australia) are analysed. A total of fifteen modelling cases have been compared with these measurements.

Special attention is paid on uncertainties associated with both the UVI modelling and measuring and limitations of their comparison are highlighted.

4.1 Contribution of this study

Several studies have previously discussed about the accuracy of both model and measurement in the UV range. For this, several intercomparison analyses have been carried out between different type of measurements, among several modelling approaches, and between model results and measurements.

Model vs. Model
Several radiative transfer models are freely available allowing UVI modelling. Several intercomparisons of UV spectral models have been performed in order to evaluate agreements between different codes. *Van Weele et al.* [2000] compared global and direct spectral UV calculations from 12 numerical models for six benchmark spectra corresponding to diverse conditions. They found agreements within ± 3% for wavelengths longer than 320 nm and for high sun conditions. For low sun conditions, agreement was within ±10% for wavelengths longer than 300 nm. *Koepke et al.* [1998] presented an intercomparison between models calculating UVI. From the comparison of six numerical radiative transfer models, agreements within 5% and 0.5 units in UVI were found for the 80% of considered conditions. That study assumed the same input options, such as the same simplification of the aerosol phase function and the extraterrestrial (ET) irradiance spectrum, for all considered models. So, absolute errors of radiative transfer models could be larger.

Measurement vs. Measurement
As discussed in Chapter 3, the actual spectral response of erythemal radiometers deviates from the CIE response [*McKinlay and Diffey*, 1987]. This can lead to large uncertainties in the measured UVI. In contrast, if spectral UV data is used from spectroradiometric systems, the exact erythemal function from the CIE can be applied to obtain the erythemal UV irradiance and UVI. This highly reduces the measurement uncertainties. High quality UV measurements are needed as they represent the best accuracy. Long term UV measurements provide essential information about changes in the atmosphere such as the ozone depletion. Many devices have been developed for UV measurement, and several intercomparison campaigns have shown the agreements that can be expected between different instruments. *Seckmeyer et al.* [1995] presented a comparison between spectral UV measurements from five instruments at Garmisch-Partenkirchen (Germany) for three consecutive days in August 1994. The instruments generally agreed within ±5 % for wavelengths longer than 310 nm. The daily doses of erythemal UV were also compared showing agreements within ±7%. *Bais et al* [2001] compared UV measurements from 19 spectroradiometers for two days in July 1997 in Greece, in the frame of SUSPEN (Standardization of Ultraviolet Spectroradiometry in Preparation of a European Network) intercomparison. The range of deviations found between them was ±20%, although 16 instruments agreed within ±10%.

Model vs. Measurement
Comparisons between UV spectral models and measurements have been carried out in several studies for cloudless conditions. *Zeng et al.* [1994] reported model-measurement differences in New Zealand within ±8% in the UVB region and within ±4% for longer wavelengths for the cases in which the atmospheric optical properties were best known.

Weihs and Webb [1997] found deviations about ±10% or slightly more in Panorama, Greece (385 m asl) and ±5% to ±10% at Jungfraujoch, Switzerland (3580 m asl), which, in most of cases, were within the measurement uncertainties. Differences up to 14% in modelled UV were found between runs with estimated and climatic values of SSA, respectively. *Van Weele et al.* [2000] compared the above mentioned UV calculations against observed spectra. In four of the six benchmark conditions they found agreements within ±13% over the whole UV spectral region. These studies showed that model uncertainties are comparable with, but slightly greater than, measurement uncertainties.
Few studies have compared measured and modelled broadband erythemal UV. *De Backer et al* [2001] performed a comparison between UVI from spectral measurements from five instruments at four locations and calculations from eleven radiative transfer models and two empirical models. For the modelling, only *TOZ* measurements were available while aerosol and ground reflectivity information was estimated. In many cases model-measurements deviations were less than 0.5 units of UVI, although deviations of more than 10% were not uncommon, with absolute deviations up to 2 units of UVI for radiative transfer models and occasionally reaching 5 units of UVI. *Mayer et al* [1997] showed comparisons between two years of erythemal UV irradiance measurements from a high quality spectrometer in Garmisch-Partenkirchen and radiative transfer calculations. For this analysis, *AOD* measurements were also available. Systematic deviations ranged from 8 to 12% depending on the modelling code used. It was also shown that model-measurement agreement was greatly improved (dispersion of the differences were reduced by a factor of 4) when aerosol measurements were considered instead of estimations of the visibility. All these studies highlighted the important influence of the uncertainty of aerosol input information on the accuracy of UV calculations.

The present study shows the results from a more detailed comparison between measurements and model calculations of UVI for selected clear sky conditions during one year at four sites. The study differs from previous ones in the following senses:

- UVI measurements from the same kind of spectroradiometers (same manufacturer) are used for all sites, and these instruments represent state-of-the-art in UV measurement.
- The four considered sites are diverse in terms of altitude, latitude (from both hemispheres) and atmospheric characteristics.
- A strict and objective criterion for clear-sky selection is developed so to avoid the clouds effects.
- The most important required input information (such as about ozone and aerosols) for UVI modelling is available at each site.
- Fifteen modelling cases are performed so the effect of considering different input information into the model can be assessed.
- Apart from evaluating the general model-measurement agreement at each site for different modelling cases, special attention is paid to the daily variation of the model-measurement comparison for particular days.

4.2 Sites and datasets

For this study, one year of data was analysed for the following sites and periods: Lauder, New Zealand (2001), Boulder, Colorado (2000), Mauna Loa, Hawaii (2001) and Melbourne,

Australia (2002). Table 4.1 summarizes information about these sites. A wide range of different types of measurements have been involved, as summarised in Table 4.2.
The UVI measurements are derived from spectral irradiance measurements at the four sites. As input for the UVI modelling, an estimation of *TOZ* is also available from those spectral measurements using a previously discussed method [*Stamnes, et al.*, 1991] (hereafter called TOZ_S). In addition to this, *TOZ* from Dobson Ozone Spectrophotometers (hereinafter called TOZ_D) and from the TOMS version 8 (hereafter called TOZ_T) are also considered. *AOD* measurements are available for all sites. Measured ozone and temperature profiles from ozone sondes are also used as input to the model. Other ancillary data, which support to the analysis, are discussed below.

4.3 UVI Measurement dataset

Measurements of UVI from the four sites were taken from spectroradiometers manufactured at the National Institute of Water and Atmospheric Research (NIWA) in Lauder, New Zealand (see Figure 1.8). These instruments represent state-of-the-art for precision long-term measurements of UV irradiances, and they meet the exacting requirements of the Network for the Detection of Stratospheric Change (NDSC) [*McKenzie, et al.*, 1997].

4.3.1 Uncertainties associated with the UVI measurements

It was shown in the SUSPEN intercomparison of spectroradiometers that NIWA-built spectroradiometer agreed within ±5% with the reference spectra and with the other two instruments built with the same double monochromator (Bentham DTM300) [*Bais, et al.*, 2001]. This range is currently accepted as the state-of-the-art uncertainty of UV measurements. Table 4.3 shows known random uncertainties of measured UVI with NIWA spectroradiometers [*McKenzie, et al.*, 1997]. The total uncertainty (Root Summed Square, RSS) is found at the level of about 5.5%.
The lamps used to calibrate these instruments are traceable to primary standards of the National Institute of Standards and Technology (NIST) [*Walker, et al.*, 1987]. Further systematic uncertainties of about 1% can also be traced to changes in the NIST irradiance scale [*Yoon, et al.*, 2002] .
For the wavelength alignment in NIWA instruments, the LOWTRAN ET spectrum [*Kneizys, et al.*, 1983] was previously used as the reference spectrum. Actually, this is the case for the UVM data used in Chapter 3. For this study, however, in order to be consistent with ET spectrum used in the UV modelling (see below), the SUSIM-ATLAS 3 ET spectrum [*Woods, et al.*, 1996] was considered instead. This spectrum was found to be shifted 0.04 nm to the red in comparison with LOWTRAN spectrum. Consequently, this made measured UVI ~1-2% systematically lower than previous estimations from the NIWA group.

Table 4.1 Geographical information about the four sites considered for this study. Also identification names of NIWA spectroradiometers at each site are given.

	Lauder	Boulder	Mauna Loa	Melbourne
Country	New Zealand	Colorado (USA)	Hawaii (USA)	Australia
Year studied	2001	2000	2001	2002
Latitude	45.04 S	40.01 N	19.53 N	37.69 S
Longitude	169.68 E	105.25 W	155.58 W	144.95 E
UT	NZST -12h	LMT+7h	LMT+10h	LMT-10h
Altitude	370 m	1650 m	3400 m	110 m
Instrument ID	UVM	UV4	UV3	UV7

Table 4.2. Details of data sources used for this study from Lauder, Boulder, Mauna Loa, Hilo and Melbourne

Data	Use	Site	Time resolution	Contact	Affiliation (place)	Contact point
Spectral UV	UVI measurements TOZ estimation	Lauder Boulder Mauna Loa Melbourne	5º steps of SZA but 15 min steps around noon	R. McKenzie M. O'Neill " D. Anderson	NIWA[T] (Lauder) NOAA[T]-CMDL[T] (Boulder) " BoM[T] (Melbourne)	r.mckenzie@niwa.co.nz michael.o'neill@noaa.gov " d.anderson@bom.gov.au
Glob / Diff / Dir total irradiance	Clear-sky filtering	Lauder Boulder Mauna Loa Melbourne	1 minute	B. Forgan NOAA-CMDL " B. Forgan	BoM (Melbourne) NOAA-CMDL (Boulder) " BoM (Melbourne)	b.forgan@bom.gov.au http://www.cmdl.noaa.gov/infodata/ftpdata.html " b.forgan@bom.gov.au
Aerosol optical depth	Model input	Lauder Boulder Mauna Loa* Melbourne	2 x day (am/pm) 1 minute " 2 x day (am/pm)	B. Liley E. G. Dutton " B. Forgan	NIWA (Lauder) NOAA-CMDL (Boulder) " BoM (Melbourne)	b.liley@niwa.co.nz ellsworth.g.dutton@noaa.gov " b.forgan@bom.gov.au
Total Ozone Assimilated from TOMS	Model input	All Sites	1 day	G. Bodeker	NIWA (Lauder)	g.bodeker@niwa.co.nz
Total ozone from Dobson sunphotometer	Model input	Lauder Boulder Mauna Loa Melbourne	1 day	NOAA-CMDL " " J. Easson	NOAA-CMDL (Boulder) " " BoM (Melbourne)	http://www.cmdl.noaa.gov/ozwv/dobson/select.html " " j.easson@bom.gov.au
Ozone and temperature profiles from ozone sonde	Model input	Lauder Boulder Mauna Loa (Hilo) Melbourne	1 week aprox.	G. Bodeker S. Oltmans " A. Downey	NIWA (Lauder) NOAA-CMDL (Boulder) " BoM (Melbourne)	g.bodeker@niwa.co.nz samuel.j.oltmans@noaa.gov " a.downey@bom.gov.au
Temperature and wind	Ancillary data	Lauder Boulder Mauna Loa Melbourne	10 minutes 1 hour " 1 minute	Climate database NOAA-CMDL " P. Dyson	NIWA (New Zealand) NOAA-CMDL (Boulder) " BoM (Melbourne)	http://cliflo.niwa.co.nz http://www.cmdl.noaa.gov/infodata/ftpdata.html " p.dyson@bom.gov.au
Webcam images	Ancillary data	Mauna Loa	10 minutes	D. T. Kuniyuki	NOAA-CMDL (Mauna Loa)	Darryl.T.Kuniyuki@noaa.gov

*Data were obtained using a Precision Filter Radiometer supplied to GAW network stations by Christoph Wehrli of the World Radiation Center and Physical Meteorological Observatory Davos (PMOD) in Davos, Switzerland. The data were processed and analyzed by NOAA/CMDL Solar and Thermal Atmospheric Radiation group.

[T]NIWA: National Institute of Water and Atmospheric Research (New Zealand); NOAA: National Oceanic and Atmospheric Administration (USA); CMDL: Climate Monitoring and Diagnostics Laboratory (USA); BoM: Bureau of Meteorology (Australia)

Table 4.3 Uncertainties of measured UVI with NIWA spectroradiometers

	Associated uncertainty	**Uncertainty in UVI (± %) For SZA<80º**
Irradiance calibration		
NIST uncertainty		1.0
NIST ticket value		3.0
Transfer to lamp		2.0
Transfer to spectroradiometer		1.5
Stability	± 2 %	2.0
PTFE temperature (*)	± 10ºC	2.0
Wavelength alignment		
accuracy in UVA	± 0.01 nm	0.5
From non linearities	± 0.02 nm	1.0
Cosine response	± 0.02 (for SZA<<65º)	2.0
Levelling	± 0.02º	<0.2
Time stamp	10 s	<0.2
Photon noise		<0.1
Total Uncertainty (RSS)		**5.5**

* This error will be significantly reduced in future analyses when PTFE sensitivity is known and temperature is logged.

4.3.2 Clear Sky Selection

Strict criteria were used to filter the UVI data for clear-sky conditions using a previously discussed algorithm [*Long and Ackerman*, 2000]. To run this algorithm, 1-minute data of diffuse and global total irradiances were considered for Boulder and Mauna Loa. For Lauder and Melbourne, 1-minute diffuse, direct and global total irradiances were available (see Table 4.2). An available UVI measurement was selected as clear if (1) the algorithm had labelled 70% or more minutes as clear for that day and if (2) the estimated cloud fraction (by the same algorithm) associated to the time of the measurement was less or equal to 2%. Condition (1) was imposed in order to avoid having only few samples selected per day, so daily evolutions and changes could be studied.

Figure 4.1 shows the UVI measurements for the times that passed the clear-sky criteria. There were 31 days for Lauder, 23 days for Boulder (note that for this year there was no UVI data available from days 110 to 165), 98 days for Mauna Loa and 11 days for Melbourne. Note that for Lauder in 2001, 49 clear-sky days had been selected from visual inspection (Chapter 3). This gives evidence that the criteria used here are stricter. The histograms of *SZA* corresponding to these selected measurements are also shown in Figure 4.1. The ranges of *SZA* are: 22.0-75.4º for Lauder, 16.6-75.0º for Boulder, 0.0-80.0º for Mauna Loa and 17.7-75.0º for Melbourne. Conditions was larger *SZA* were filtered by Long and Ackerman algorithm.

Any UVI data for which concurrent measured *AOD* was not available were rejected from the study and are not shown in Figure 4.1. After this filtering process, the percentages of data that remained (for SZA≤80º) were: 6.5% for Lauder, 4.8% for Boulder, 17.8% for Mauna Loa, and 2.5% for Melbourne.

4.4 Modelling

The TUV radiative transfer model version 4.1a was used for the UVI calculations. We used the DISORT radiative transfer solver with 8 streams and pseudo spherical corrections. The spectral range was 280 to 400 nm with 1 nm steps. The TUV default ET spectrum (ATLAS3-SUSIM 13 Nov 94 high resolution) was selected, as commented above.

The following parameters were taken into account in this study

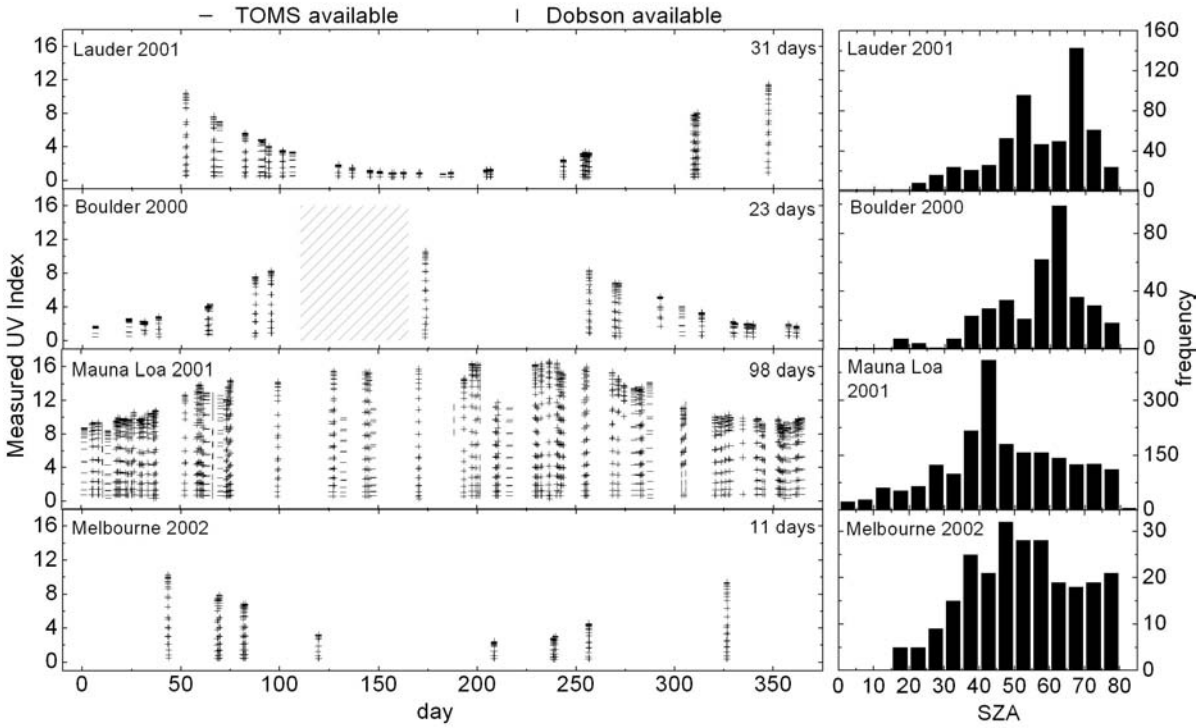

Figure 4.1 Left panel: Clear-sky measured UVI for the four sites as a function of day, representing the considered datasets for this study. Availability of *TOZ* from TOMS and Dobson is shown through horizontal and vertical dashes, respectively. No UVI measurements were available from day 110 to 165 of 2000 in Boulder (hatched zone). Right Panel: Corresponding histogram of *SZA*

- solar zenith angle (*SZA*),
- total ozone column amount (*TOZ*),
- ozone profile (OP),
- temperature profile (TP),
- ground surface albedo (*galb*)
- ground level,
- aerosol optical depth (*AOD*),
- aerosol single scattering albedo (*SSA*),
- aerosol asymmetry factor (*g*),
- aerosol Ångström exponent (*alpha*) [*Angstrom*, 1964],
- aerosol profile.

The way of introducing *SZA,* ground level, *g, alpha* and the aerosol profile into the model remained invariable throughout this Chapter. The other input parameters were introduced in several different ways, leading to different modelling cases that will be discussed in the next section.

For most of the instruments (see Table 4.1), each measurement consists of the average of a reverse scan followed by a forward scan. Consequently the *SZA* is simply calculated from the time stamp logged with the data, which corresponds to the turnaround time between the pair of scans. However, for the older UVM instrument at Lauder, which measures the spectral irradiance doing a single forward scan only, the *SZA* stamp corresponds to the centre of the scan, at wavelength 370 nm, as commented in Section 3.5. A correction of 65 seconds was applied to the instrument time stamp in order to make it correspond to the measurement at 310 nm (which approximates the effective wavelength for UVI), and *SZA*

was recalculated using the incorporated routines in TUV 4.1. It is estimated that an error of about 1 minute in the time leads to maximum errors about ±0.2º in *SZA* for Lauder which corresponds to an error in UVI up to 3% at 75º of *SZA*.

The ground level in the model was usually specified as the altitude of each site (see Table 4.1). However, in the case of Mauna Loa Observatory, the ground level was set to 2.4 km and the output was taken from 1 km above (i.e. at the actual altitude of the site) to account for the multi-scattering with the air layer underneath the measurement site as suggested by *McKenzie et al* [2001].

The aerosol asymmetry factor *g* was set constant to 0.7 for all sites as a typical and commonly used value, as in Section 3.5. It was also assumed here that both *g* and *SSA* are spectrally uniform as a common simplification since their dependence on wavelength is supposed small. This is discussed in more detail in Chapter 5.

The wavelength dependence of aerosol scattering (Ångström's *alpha)* was estimated for Lauder and Melbourne by calculating the slope between the *AOD* measured at 412, 500 and 778 nm. Values from 0.59 to 2.2 for Lauder and from 0.35 to 1.8 for Melbourne were found for the days of study. The mean values and their standard deviation were 1.4±0.3 and 1.1±0.4, respectively. However, for Boulder and Mauna Loa, *AOD* measurements were available at one single wavelength only. A decision was made to set *alpha* constant to 1.4 for all the modelling cases and sites.

The aerosol profile was considered the same way for all the sites, with the *AOD* distributed in the first kilometre above the altitude level, as a simplification of the boundary layer. Another more realistic option of vertically distributing *AOD* is presented and discussed in Section 5.2.

The uncertainties associated with these parameters that are kept invariable, and with the decisions taken about their values, are discussed in section 4.4.2.

4.4.1 Modelling cases

Fifteen modelling cases were considered, by changing the way that *TOZ, AOD, SSA*, OP, TP

Table 4.4 Fifteen modelling cases considered for this study. Considered *TOZ*, *AOD*, *SSA*, OP, TP and *galb* conditions for each case are collected together with the number of days and data points considered for each case. The availability of estimated *TOZ* from each source rules the differences in the number of data points and days considered for each case. Particular cases TUV(10) to TUV(15) correspond to tested modelling conditions that were rejected for this study.

Case						**Number of days (data points)**			
TUV(i)	**TOZ**	**AOD**	**SSA**	**OP&TP**	**galb**	**Lauder**	**Boulder**	**Mauna Loa**	**Melbourne**
1	TOZ_T	Yes	0.9	USSA	0.05	30 (551)	23 (370)	86 (1812)	11 (241)
2	**TOZ_D**	**Yes**	**0.9**	**USSA**	**0.05**	**26 (477)**	**16 (273)**	**72 (1524)**	**11 (241)**
3	TOZ_S	Yes	0.9	USSA	0.05	31 (569)	23 (370)	98 (2034)	11 (241)
4	TOZ_T	0	-	USSA	0.05	30 (551)	23 (370)	86 (1812)	11 (241)
5	TOZ_D	0	-	USSA	0.05	26 (477)	16 (273)	72 (1524)	11 (241)
6	TOZ_S	0	-	USSA	0.05	31 (569)	23 (370)	98 (2034)	11 (241)
7	TOZ_T	Yes	0.7	USSA	0.05	30 (551)	23 (370)	86 (1812)	11 (241)
8	TOZ_D	Yes	0.7	USSA	0.05	26 (477)	16 (273)	72 (1524)	11 (241)
9	TOZ_S	Yes	0.7	USSA	0.05	31 (569)	23 (370)	98 (2034)	11 (241)
16	TOZ_T	Yes	0.9	Sonde	0.05	30 (551)	23 (370)	86 (1812)	11 (241)
17	TOZ_D	Yes	0.9	Sonde	0.05	26 (477)	16 (273)	72 (1524)	11 (241)
18	TOZ_S	Yes	0.9	Sonde	0.05	31 (569)	23 (370)	98 (2034)	11 (241)
19	TOZ_T	Yes	0.9	USSA	0.02	30 (551)	23 (370)	86 (1812)	11 (241)
20	TOZ_D	Yes	0.9	USSA	0.02	26 (477)	16 (273)	72 (1524)	11 (241)
21	TOZ_S	Yes	0.9	USSA	0.02	31 (569)	23 (370)	98 (2034)	11 (241)

and *galb* were introduced into the model. Table 4.4 summarises the modelling conditions and the number of days and data points involved in each case (noted as TUV(i), where "i" represents the case). In fact, one can think of the fifteen modelling cases as five sets of cases, where the three different sources of ozone (TOZ_T, TOZ_D and TOZ_S) are considered. These different modelling options allow study the separate effects of a wide diversity of input information that is usually not available together.

The five sets of cases are variations of the first set (TUV(1,2,3)), for which aerosol information is considered in the modelling, *SSA* is set to 0.9 as a reasonable value [*Madronich*, 1993], the OP and TP are set as default (from USSA) and *galb* = 0.05 is considered (typical for snow-and-sand-free surfaces). Among these three cases, TUV(2) is taken as the base case. TOZ_D is preferred to TOZ_T, even though availability of the former is more limited, mostly because the latter has important errors for high altitude sites; this becomes relevant in the present study (see discussion below). Differences in the input information (*TOZ, AOD, SSA,* OP, TP and *galb*) and output (UVI) relative to base case TUV(2) are analysed next.

TOZ

Figure 4.2 shows the absolute differences of *TOZ* from the three sources and the associated relative difference in the modelled UVI against TOZ_D. The statistics of these differences are summarised in Table 4.5. Significant divergences are found, with TOMS measuring significantly larger *TOZ* for Mauna Loa (9.5 DU in average), but lower for Boulder and Melbourne (-6.4 and -4.9 DU, respectively) and slightly higher for Lauder (2.5 DU). The maximum differences are 24 DU (in Mauna Loa) and –15 DU (in Boulder). These large differences are related to an error in the assigned altitude value for these sites due to the averaged altitude considered in the TOMS footprints. In terms of modelled UVI, differences down to -10% in Mauna Loa and up to 5.5 % in Boulder are found when TOZ_T used is instead of TOZ_D in the model. These differences are smaller for Lauder and Melbourne. Larger TOZ_T - TOZ_D differences are expected to be associated with larger dependencies of the differences in UVI as a function of *SZA*. The mean TOZ_S - TOZ_D differences are positive for Lauder, Boulder and Mauna Loa and not significant for Melbourne. The maximum changes are -17 DU (for Boulder) and +26 DU (for Lauder). In terms of UVI, mean changes are down to -2.5 % for Lauder and Mauna Loa and less important for Boulder and Melbourne. The range of differences is -8.0% to 4.8%. The largest dispersions (i.e. *SD* values) are found in Mauna Loa and Boulder. Unlike the comparison between TOZ_D and TOZ_T, the latter differences should not be considered as an evaluation of the accuracy of TOZ_S (they are less accurate), but rather as an estimation of the deviations in UVI expected when real daily variations in TOZ are considered (as seen in Figure 4.2). TOZ_D (like TOZ_T) is measured near noon and considered constant for the whole day in this study whereas TOZ_S is estimated for each record. This means that, unlike the TOZ_T vs. TOZ_D comparison, the TOZ_S-TOZ_D differences are highly dependent, for example, on the range of *SZA* considered.

On average, the daily TOZ_S range is 11 ± 5.4 DU (the interval is given by one standard deviation of the mean) for Lauder, 7.6 ± 6.0 DU for Boulder, 4.7 ± 2.7 DU for Mauna Loa and 12 ± 2.0 for Melbourne. The maximum TOZ_S variation, 28 DU, was found for day 63 in Boulder, as noted in Figure 2 (this day will be studied in detail later). As seen in the right panel of Figure 4.2, these daily TOZ variations can lead to UVI changes up to 9% in one day.

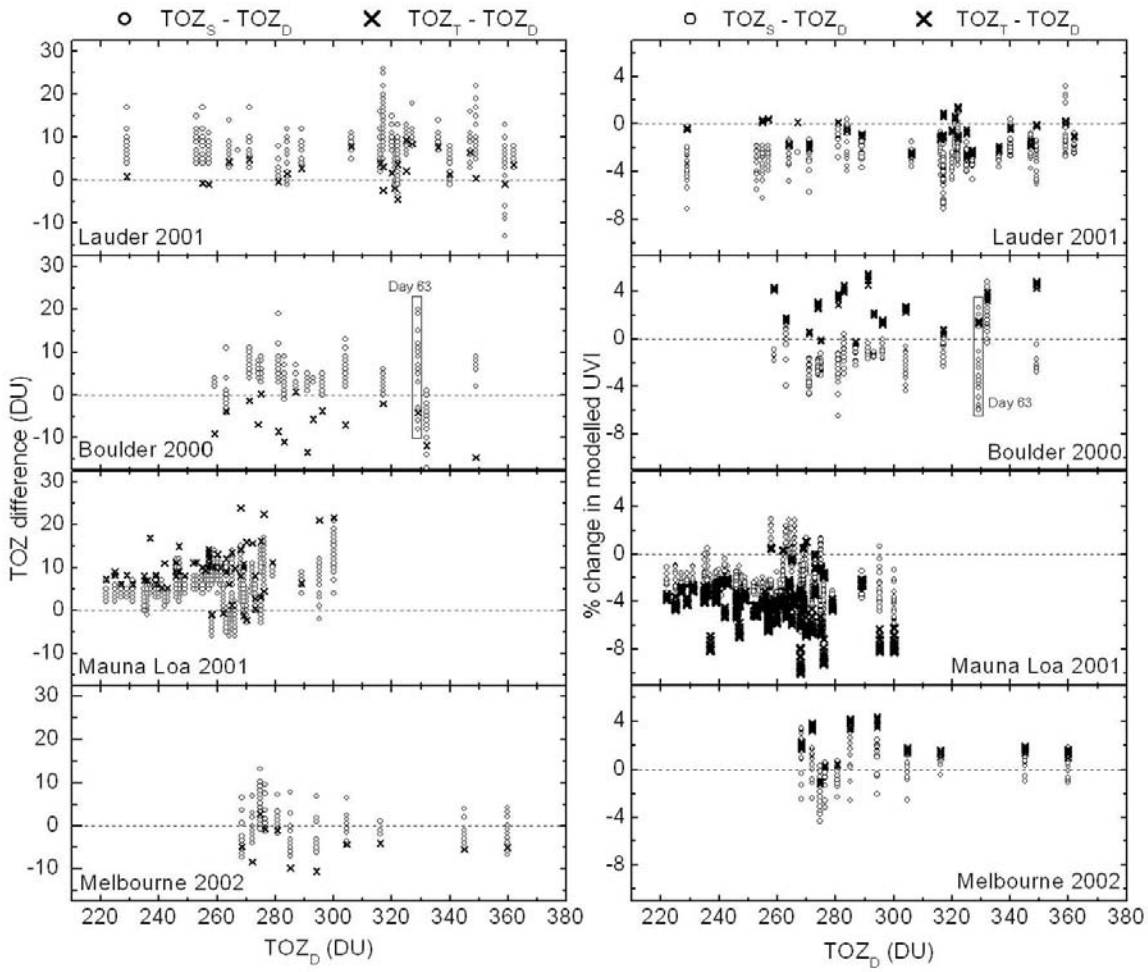

Figure 4.2 Left panel: Differences in ozone measurements: TOZ_T – TOZ_D (crosses) and TOZ_S – TOZ_D (circles) in DU for the datasets in Figure 4.1. Right Panel: Relative differences (in %) in calculated UVI from using TOZ_T (crosses) and TOZ_S (circles) instead of TOZ_D as input to the model.

Table 4.5 (Upper) Minimum, maximum, mean and standard deviation for the comparison between TOZ_T and TOZ_D in terms of TOZ and percentage change in modelled UVI (TUV(1)-TUV(2)) from Figure 4.2. (Lower) The same information but for TOZ_S and TOZ_D (TUV(3)-TUV(2)) is shown

	TOZ_T – TOZ_D (DU)				**% change in UVI**			
	Min	**Max**	**Mean**	**Sd**	**Min**	**Max**	**Mean**	**Sd**
Lauder	-4.4	9.3	2.5	3.6	-2.9	1.5	-0.63	1.0
Boulder	-15	0.70	-6.4	4.7	-0.30	5.5	2.3	1.7
Mauna Loa	-2.3	24	9.5	5.5	-10	1.1	-4.2	2.3
Melbourne	-11	2.8	-4.9	3.9	-1.2	4.3	1.7	1.5

	TOZ_S – TOZ_D (DU)				**% change in UVI**			
	Min	**Max**	**Mean**	**Sd**	**Min**	**Max**	**Mean**	**Sd**
Lauder	-13	26	7.2	4.2	-7.1	3.2	-2.5	1.3
Boulder	-17	20	4.0	4.5	-6.5	4.8	-1.5	1.6
Mauna Loa	-6	21	5.6	4.4	-8.0	3.0	-2.5	1.9
Melbourne	-7.6	13	-0.76	3.8	-4.3	3.4	0.31	1.5

AOD and SSA

The *AOD* measurements (see Table 4.2) at the shortest wavelength available at each site (412 nm for Lauder and Melbourne, 415 nm for Boulder and 367 nm for Mauna Loa) were

considered and converted to those at 368 nm (using an *alpha* of 1.4 for all sites). Quality controls were applied to these measurements based on the visualization of the data against time which leaded us to reject the 1.8% of the records for Mauna Loa, corresponding to unreasonably large optical depths. Figure 4.3 shows the histograms of remaining *AOD* values. None of the sites can be considered as highly-polluted; the most polluted sites are Boulder and Melbourne (with mean *AOD* 0.074 and 0.088, respectively) and the most pristine was Mauna Loa (0.019). The mean *AOD* for Lauder is 0.06. The maximum *AOD*s are: 0.16 for Lauder, 0.23 for Boulder, 0.07 for Mauna Loa and 0.18 for Melbourne. Figure 4.3 also shows histograms of the daily ranges in AOD. Lauder and Mauna Loa have a very low *AOD* variation, with ranges mostly smaller than 0.02. The *AOD* variability is much higher in Boulder, being up to 0.16 (day 63). Melbourne is intermediate, with a maximum range of 0.1. Since for Lauder and Melbourne only two *AOD* estimations (am/pm) are available for each day, the *AOD* daily variability here shown for these sites will be less representative than for Boulder and Mauna Loa, for which 1-minute measurements are used.

Figure 4.3 also shows the effect on modelled UVI of not considering aerosols in the model and considering *SSA* = 0.7, through the ratios TUV(5)/TUV(2) and TUV(8)/TUV(2), respectively. Interestingly, the differences for TUV(5) and TUV(8) appear to be almost symmetric (i.e. similar differences but with opposite sign). These values are up to 9-13% except for Mauna Loa, for which maximum differences are about 3% due to the much lower *AOD* found there. We note that the uncertainty in *SSA* (from 0.9 to 0.7) leads to an uncertainty in the effect of aerosols in UVI up to 11%.

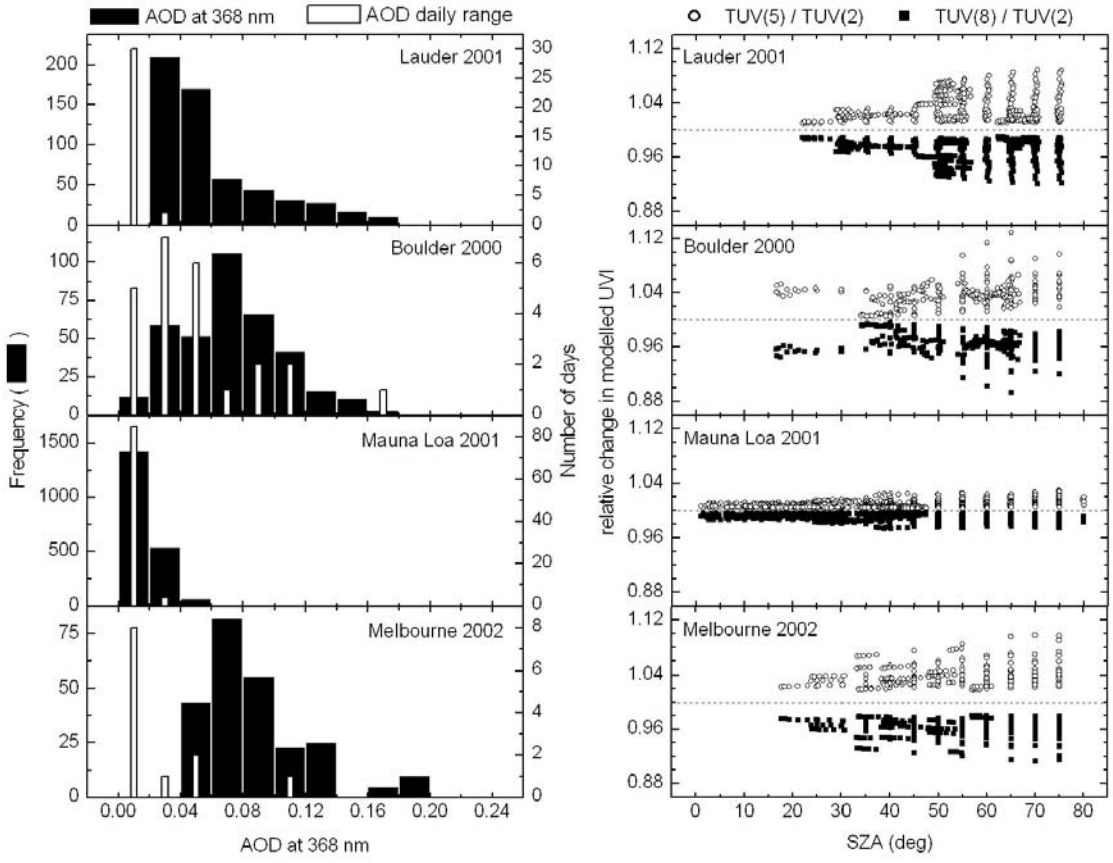

Figure 4.3 Left panel: Histograms of *AOD* at 368 nm (in black) and its daily range (in white) for the datasets in Figure 4.1. Right panel: TUV(i)/TUV(2), for i=5 (no aerosols, circles), and i=8 (*SSA*=0.7, squares).

OP and TP

Ozone sondes are available from each site with typically weekly operational frequency (see Table 4.2). For Mauna Loa, ozone sondes are taken from Hilo (19.75 ºN, 155.25º W, 370 m above sea level), located at the foot of Mauna Loa volcano. The closest sonde to each studied day was used for modelling cases TUV(16,17,18). The maximum lag was 4 days for Lauder and Boulder and 12 days for Melbourne due to a failed launch. For Hilo, maximum lags would have been about 9 days, except that from day 239 to 319 there were no ozone sondes available, leading to a maximum lag of 41 days. This lack of profile data is less critical than for the other sites, since the atmosphere above Mauna Loa is less changeable and measured changes in OP and TP are smaller. For the modelling, sonde OP and TP were re-gridded and smoothed to 2 km steps (the same way as TUV considers the USSA OP and TP). Since sondes only reach altitudes of 30-35 km, the measured OP and TP were filled to 80 km using the USSA profiles as a base. As for the USSA OP, the sonde OPs were renormalized to the TOZ for the modelling. Figure 4.4 shows the effect of using the measured OP and TP instead of the USSA profiles.

The effect on UVI is less than 2.5% for *SZA*≤75º for all sites. Unexpectedly, the USSA profiles work similarly (or even slightly better for low *SZA*) at Lauder and Melbourne than at Boulder or Mauna Loa. One might have expected it to work better in the Northern

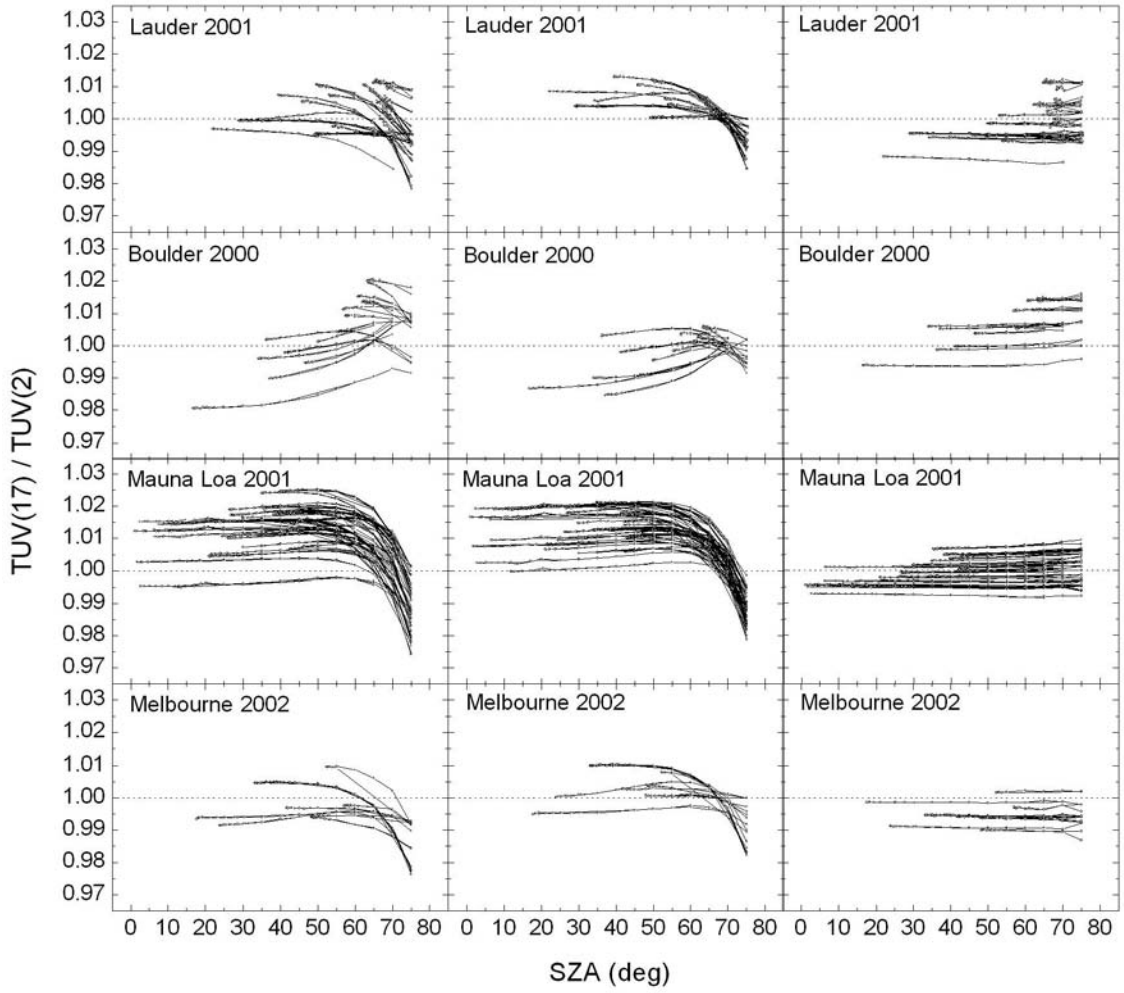

Figure 4.4 Calculated effect on modelled UVI of using measured profiles of ozone and/or temperature, compared with using the USSA profiles for the datasets in Figure 4.1. Plots are restricted to *SZA* ≤ 75º. Column 1: measured OPs and TPs are used. Column 2: measured OPs, but USSA TPs. Column 3: measured TPs, but USSA OPs.

Hemisphere since USSA was based on USA data. Two extra columns of plots are shown in order to assess the effect of changing OP and TP separately. Almost all the dependence on *SZA* comes from changing OP. In particular the tropospheric/stratospheric ozone ratio seems to be important. Mauna Loa shows similar *SZA* dependences for all days, while more diverse patterns are found for the other sites, especially for Boulder. The change in TP acts as an almost constant factor which is independent on SZA. Furthermore, we found that this factor is very well correlated with the mean temperature difference (from the altitude level to 80 km) between the USSA and the sonde TPs scaled by the OP (either from USSA or sonde); each 10 K increase (decrease) of this scaled mean temperature leads to a decrease (increase) of 2% in the calculated UVI. This corresponds to the strong temperature dependence of the ozone absorption cross section [*Molina and Molina*, 1986]. Figure 4.5 shows two extreme examples of the combined effect of changing both OP and TP: day 173 in Boulder and day 18 in Mauna Loa. OP and TP from USSA and the sondes are plotted and the corresponding ratios from Figure 4.4 are shown again.

galb

The ground albedo was changed from 0.05 to 0.02 since the latter might be more realistic for some sites or/and periods, such as for some kind of grass, trees, etc [*Madronich*, 1993; *McKenzie, et al.*, 1996]. Figure 4.6 shows the impact of this change through the ratio TUV(20)/TUV(2) as a function of SZA. The effect is about 1% in UVI and it becomes less important as altitude increases due to the less air above to take part in the ground-atmosphere multi-scattering. At larger *SZA* the dispersion increases (up to ± 0.2%).

4.4.2 Uncertainties associated with the UVI modelling

There are many sources of uncertainties associated with the radiative transfer modelling. There are intrinsic uncertainties (e.g. simplifications assumed for the radiative transfer calculation, the parameterisations of the cross sections, geometric simplifications to the

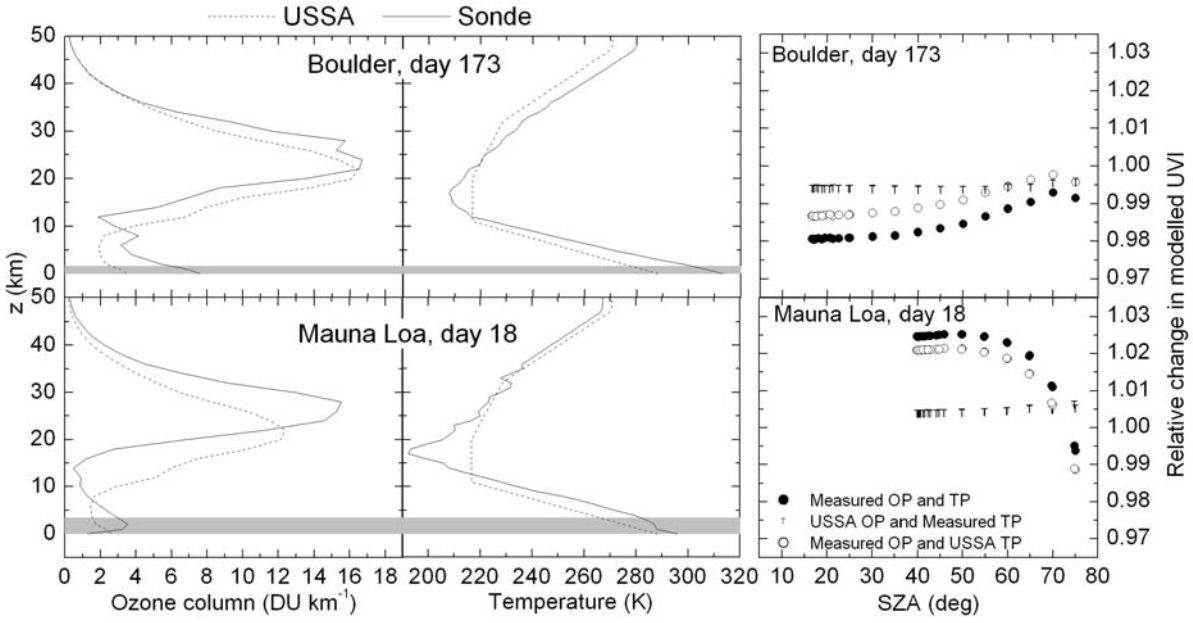

Figure 4.5 Left panel: USSA profiles and measured OP and TP from 0 to 50 km for day 173 in Boulder and day 18 in Mauna Loa. Shaded regions show the parts of the profiles underneath the altitude level of each site. Right panel: Relative change in modelled UVI from considering measured OP and USSA TP (open circles), USSA OP and measured TP (T) and measured OP and TP (solid circles) in relation to case TUV(2) (USSA OP and TP).

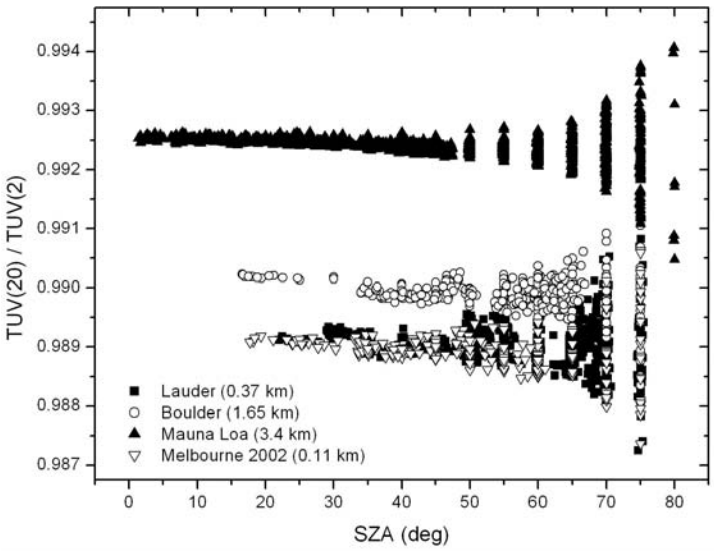

Figure 4.6 Relative change in the calculated UVI caused by changing *galb* from 0.05 (TUV(2)) to 0.02 (TUV(20)) for the datasets in Figure 4.1.

phase function, etc.). Additionally, uncertainties in the input information also propagate through to uncertainties in derived irradiances. When input parameters are well known, the estimated uncertainty in modelled UVI is about ±5%, as discussed above from the study by *Koepke et al* [1998].

In this study, the Ångström exponent *alpha* is set constant to 1.4 for all modelling cases considered. A sensitivity study was carried out for Boulder, since the largest *AOD*s are found at this site. An uncertainty of ±1 in *alpha* (i.e., 0.4 to 2.4), which seems reasonable at least for Lauder and Melbourne, was assumed. This lead to a maximum change in the calculated UVI (relative to the calculation with *alpha*=1.4) of ±3%. This can be taken as a maximum uncertainty from *alpha* in this study.

In addition, the uncertainty of setting $g = 0.7$ must be also taken into account. From a study about the effects of aerosols on UVI [*Badosa and van Weele*, 2002] we found that an uncertainty of about 0.1 units in g can lead to an uncertainty of about 1% in UVI. The results from that study are discussed in more detail in Chapter 5.

Finally, the uncertainty associated to the aerosol profile considered was estimated by changing the vertical *AOD* distribution from the ground level to 3 km above it. The *AOD* was set to 0.23 at 368 nm, which is the extreme value found for this study. Also the more realistic aerosol profile proposed in Section 5.2 was considered. It was found that changes in calculated UVI were always less than 1% for *SZA* from 0 to 75º.

Table 4.6 summarizes the uncertainties in calculated UVI arising from the uncertainties associated to the inputs. In addition, the expected differences in UVI from different input choices are shown as a summary of the results from section 4.4.1.

The largest potential uncertainties are associated with uncertainties in ozone and aerosol information. In particular, lack of knowledge about *SSA* of the aerosols becomes a major source of uncertainty in the modelling.

4.5 General Model–Measurement comparisons

All fifteen modelling cases have been compared with the UVI measurements for the four sites. Figure 4.7 shows histograms of modelled – measured relative differences in UVI, for TUV(2) and all the variations of this base modelling case. With TUV(2), similar average agreements are found for Lauder, Boulder and Mauna Loa, with model overestimations from 2.0 to 2.8 %. For Melbourne, much larger overestimation is found (9.0%). When considering TOZ_T (TUV(1)) and TOZ_S (TUV(3)), mean agreements change in accordance with those expected from Table 4.5. This leads to much more diverse comparisons when

using TOZ_T. Best agreements for Lauder, Boulder and Mauna Loa together are found when using TOZ_S, with model-measurement differences within 5% for 90%, 77% and 98% of the data, respectively. Actually, for the comparisons for all the cases that consider the aerosol contribution and TOZ_S, mean agreements of 0.1-3% are found, depending on the value of *SSA*. Overestimations remain large for Melbourne. When no aerosols are considered in the model (TUV(5)), the model overestimations increase from +0.8%, for Mauna Loa, to +3-4% for the other sites, in comparison with TUV(2). Similar changes, but with opposite sign are found when *SSA* is set to 0.7 (TUV(8)), which was expected from results shown in Figure 4.3. For Melbourne, the best agreement (an overestimation of 4.8%) is found when considering *SSA*=0.7. The effect of considering measured OP and TP (TUV(17)) has a very small effect for all sites except for Mauna Loa, for which mean model-measurement differences increase by 1.1%, showing consistency with what is seen in Figure 4.4. Setting *galb* to 0.02 (TUV(20)) has the expected decreasing effect on the model of about -1%.

The dispersion of histograms also provides information of the model-measurement comparison. To quantify this, the standard deviation (*SD*) can be used. Lowest *SD* values are found for Mauna Loa, followed by Lauder, Melbourne and Boulder. This order is in agreement with mean *AOD*s found at each site, showing that clean sites are easier to model than polluted sites.

When no aerosols are considered, *SD* values significantly increase for all sites, except for Mauna Loa where aerosol effects are small. When *SSA* is 0.7, highest *SD* are found for Lauder; for Boulder *SD* slightly decrease; and for Mauna Loa and Melbourne *SD* are similar to those for TUV(2). For Mauna Loa, the largest increase in *SD* occurs when considering

Table 4.6 Uncertainties in modelled UVI

Uncertainties associated to the measurement	**Estimated uncertainty in modelled UVI**
TOZ_T	3% [*Herman, et al.*, 1991](but precision ~1%)
TOZ_D	3% [*Basher*, 1982]
TOZ_S	3% [*Houët and Brogniez*, 2004]
OP and TP	<1% [*Johnson, et al.*, 2002]
AOD	<1% [*Dutton, et al.*, 1994]
Uncertainties since input value is not measured	
Ground albedo for not snow-covered nor sandy surfaces	1%
Actual single scattering albedo not known	From ±3% (Mauna Loa) to ± 9-11%
alpha	3%
g	1%
Aerosol profile	< 1%
Ozone variation through the day (TOMS & Dobson)	~5%
Expected differences from modelling cases	
If TOZ_T is used instead of TOZ_D	< 5.5% (< 10% for Mauna Loa)
If TOZ_S is used instead of TOZ_D	< 8%
If the actual OP and TP are not used in the modelling	< 2.5% for SZA ≤ 75º
If no aerosols are introduced into the model	With *SSA*=0.9: to -9-13 % (to -3 % for Mauna Loa) With *SSA*=0.7: to -19-24% (to -6 % for Mauna Loa)
Total Uncertainty (RSS for TOMS or Dobson ozone)	**<8%** for clean sites like Lauder and Mauna Loa **>12%** for more polluted sites like Melbourne and Boulder

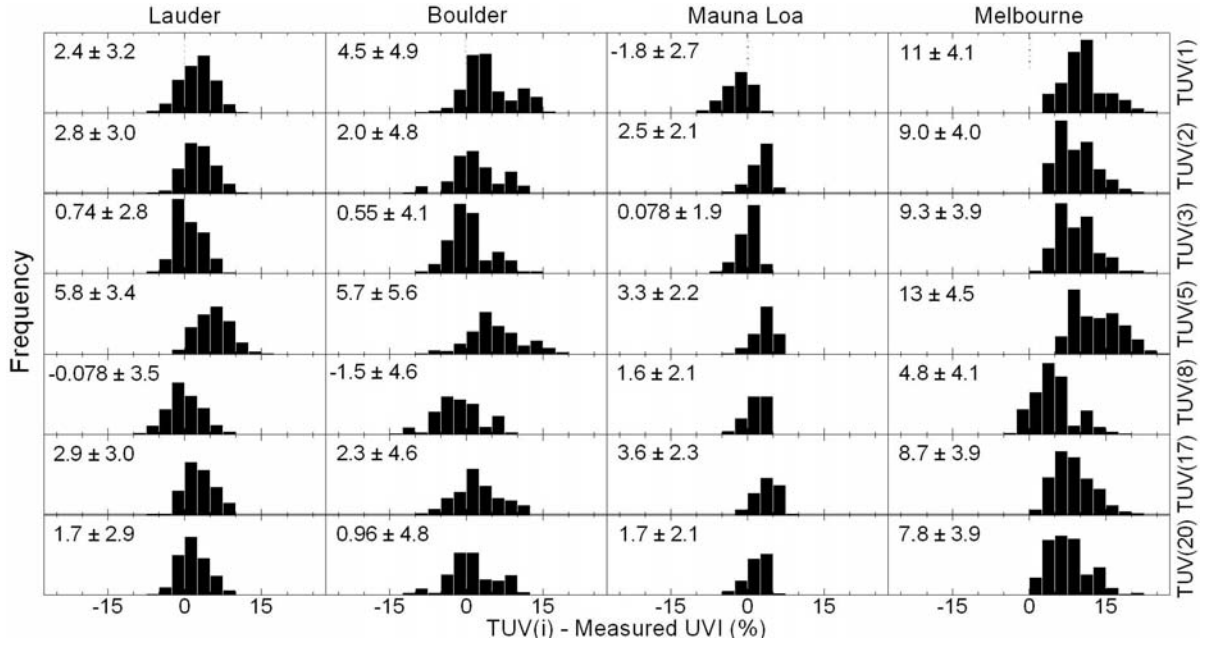

Figure 4.7 Histograms of model – measurement relative differences for all sites and modelling cases TUV(1,2,3,5,8,17,20). Mean differences plus minus their standard deviations are shown for each case.

TOZ_T; showing that, at this site, ground-based measurements of ozone should be preferred over the TOMS ozone data.

The range of differences (i.e. max – min) is about 19% for Lauder and Melbourne, 25% for Boulder and 14% for Mauna Loa for TUV(2) and slightly change depending on the modelling case. Largest ranges of differences are found when no aerosols are considered for the modelling.

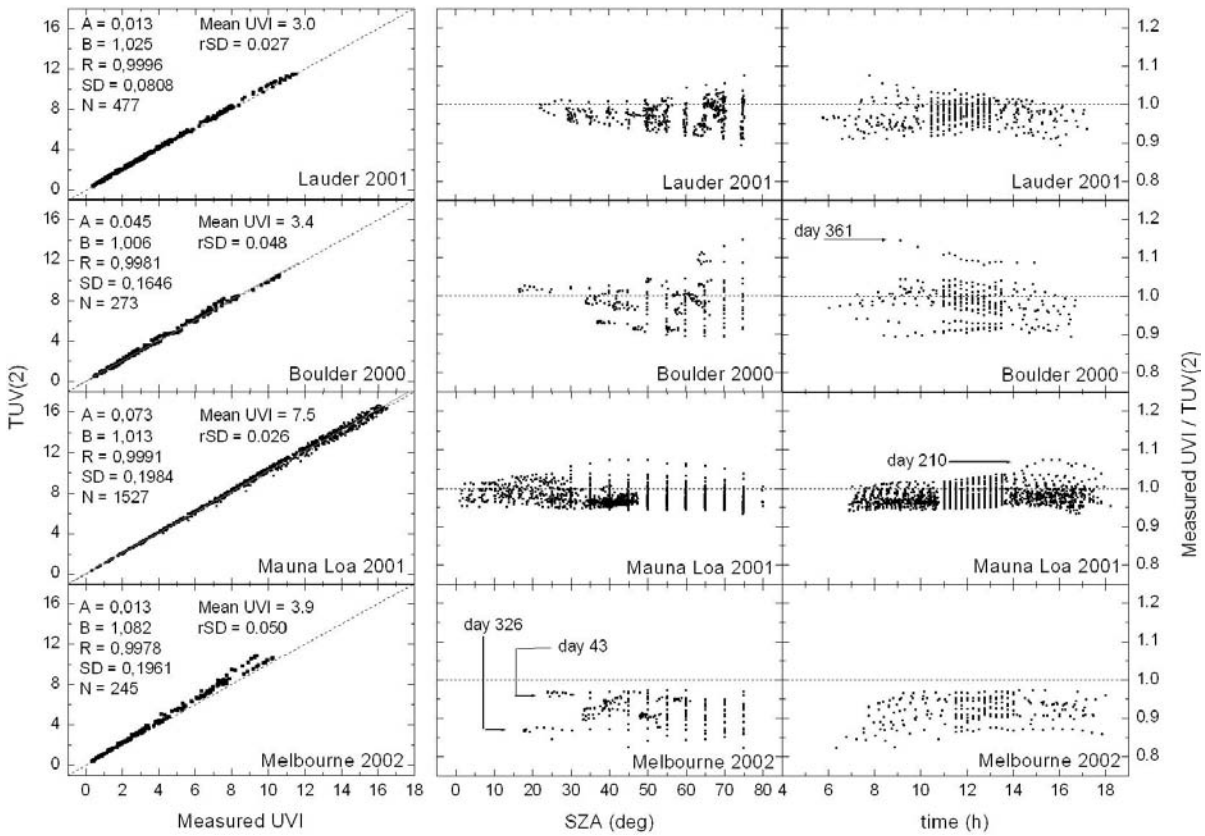

Figure 4.8 Left panel: Regression plot of modelled (TUV(2)) versus measured UVI for four sites. Statistic parameters for regressions are shown. Right panel: Measured UVI / TUV(2) as a function of *SZA* and local time.

The comparison between measured UVI and the modelling base case for the four sites is shown in detail in Figure 4.8. From the TUV(2) vs. measured UVI plot, regression coefficients approaching unity are found in particular for Lauder and Mauna Loa, for which the points are very well aligned (R > 0.999). The regression slopes (*B)* show diverse TUV(2) overestimations of the measurements, which are slightly different from the mean relative model-measurement differences shown in Figure 4.7; this corresponds to the greater weighting from points with higher UVI for the linear fit. The standard deviations, normalised to the mean measured UVI (called *rSD*), show more dispersion around the fitted line for Boulder and Melbourne than for Lauder and Mauna Loa, which is consistent with the dispersions seen in Figure 4.7.
Also, the ratio of measured UVI over TUV(2) (hereafter called R2) are shown against *SZA* and time in Figure 4.8. Several daily evolutions of R2 can be identified both as a function of *SZA* and time. In average, the daily change of R2 is about 0.05 (5%) for all sites except for Mauna Loa, for which this is about 0.03 (3%). This is in agreement with the lower *TOZ* and *AOD* daily variations found for this site. Maximum daily range of R2 is 10% for all sites. Factors that contribute to these daily variations including marked outliers are discussed next.

4.6 Daily evolutions

Below, we will analyze some particular effects that are found through detailed analysis of some specific daily evolutions at the considered sites. In addition, and in order to give complete information about the results obtained, Annex E shows the daily evolutions of *TOZ, AOD*, measured UVI, TUV(1,2,3), and the model-measurement differences and ratios for each day considered from each site in this study.

TOZ and AOD daily evolutions
The largest observed daily variations in the model/measurement ratios are mainly associated with large diurnal changes in *TOZ* (which are not taken into account for TUV(2)). Also, if the aerosol properties considered in TUV(2) are not accurate (such as errors in *SSA*), this would lead to errors that are dependent on *AOD* and *SZA*. A good example of these two factors acting together is found in day 63 in Boulder. This day registered both the largest daily variations in TOZ_S (28 DU) and *AOD* (0.16) among all days from all sites considered in this study. Figure 4.9 shows the measured UVI, TOZ_S, and *AOD* as a function of time on this day. Despite this being a completely clear day some points were rejected from the study since the *AOD* was not available. Relative differences between TUV(2) (*SSA*=0.9 and TOZ_D=329 DU) and measured UVI (hereafter called D2: representing the difference between measurements and model case TUV(2)) are plotted as a function of time in the lower panel of Figure 4.9. In this case, there is an important overestimation by the model. However, a small daily variation of the relative differences is found (values range from 8.8 to 11.9%) due to compensation between the *TOZ* and aerosol effects. In order to see separately the effects of not considering aerosols and not considering the daily evolution of *TOZ*, cases TUV(6) (no aerosols, TOZ_S) and TUV(8) (*SSA*=0.7, TOZ_D) are considered, respectively. From the former, important model-measurement differences are found, with D6 changing from 9.0 to 27.2% through the day; from the latter, D8 goes from 7.9% down to -1.9% due to not considering changes in *TOZ*. The choice of *SSA* at 0.7 seems to work best, as is apparent from a comparison of the analyses of the results using TUV(3) (*SSA*=0.9,

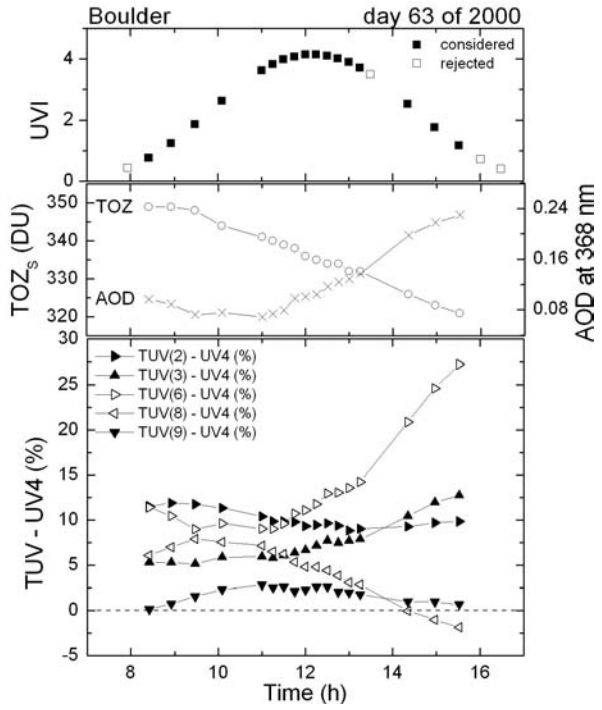

Figure 4.9 Upper panel: Measured UVI on day 63 in Boulder as a function of time. Open squares were rejected from the study due to lack of *AOD* measurements for those times. Center panel: Concurrent TOZ_S and *AOD* as a function of time. Lower panel: relative differences between UVI model and measurement for modelling cases TUV(2,3,6,8,9) as a function of time.

TOZ_S) and TUV(9) (*SSA*=0.7, TOZ_S). With the former, the relative difference (D3) increases through the day from 5.1 to 12.7%. In contrast, with the latter, a much better agreement is found together with a low daily variation of the difference (D9), which changes from 0.13 to 2.8 %. So it seems that for this day, the *SSA* was more likely to be around 0.7 than 0.9.

Effect of snow

Day 361 in Boulder is also worth discussing, as it is an outlier (see Figure 4.8). For this day the UVI measurements are larger than TUV(2) by 14.5% in the morning, and by 8.2% in the afternoon. These changing enhancements in measured UVI were caused by the increase in ground albedo due to snow that partly melted through the day. It has been shown previously that snow cover can lead to substantial increases in UVI [*McKenzie, et al.*, 1998]. As an outlier, this day has an important contribution to the statistics reported in Figure 4.7 for Boulder. If it is excluded from the statistics for TUV(2), although the mean UVI model-measurement difference increases to 2.6%, the *SD* decreases to 4.1 % and the range of differences decrease (from -25%) to 16.2%. This makes Boulder more similar to Melbourne in terms of the *SD* values and the range of differences.

PTFE temperature effect

In Lauder, for some days around summer we detected a step-change in measured UVI of 2-3% around noon. Figure 4.10 shows measured and modelled (case TUV(2)) UVI and their ratio (R2) as a function of time for six days around summer. This was found to be related to an increment in transmittance of the PTFE diffusers used in the spectroradiometers as the temperature changed from about 15 to 21ºC. This effect was first demonstrated in a laboratory study by *Ylianttila and Schreder* [2005]. Using the data from this current work, we demonstrated this effect both for sky irradiance measurements and in the laboratory, for the PTFE diffusers used in NIWA spectroradiometers [*McKenzie, et al.*, 2005]. Evidence of this effect in the field was shown there through a particular case (day 66) and the averaged step from the same six days (the ones in Figure 4.10) as a function of air temperature. Here the data from each of these days are shown separately. The air temperature and wind speed are plotted together with R2 for each day. A 2-3% step in R2 that occurs around a temperature of 20ºC can be observed for each day. There is no obvious relationship between this effect and wind speed. For the days under study, *TOZ* and *AOD* showed low variability around noon; maximum variations from 1000 to 1400 NZST were 3 DU and 0.01 in AOD.

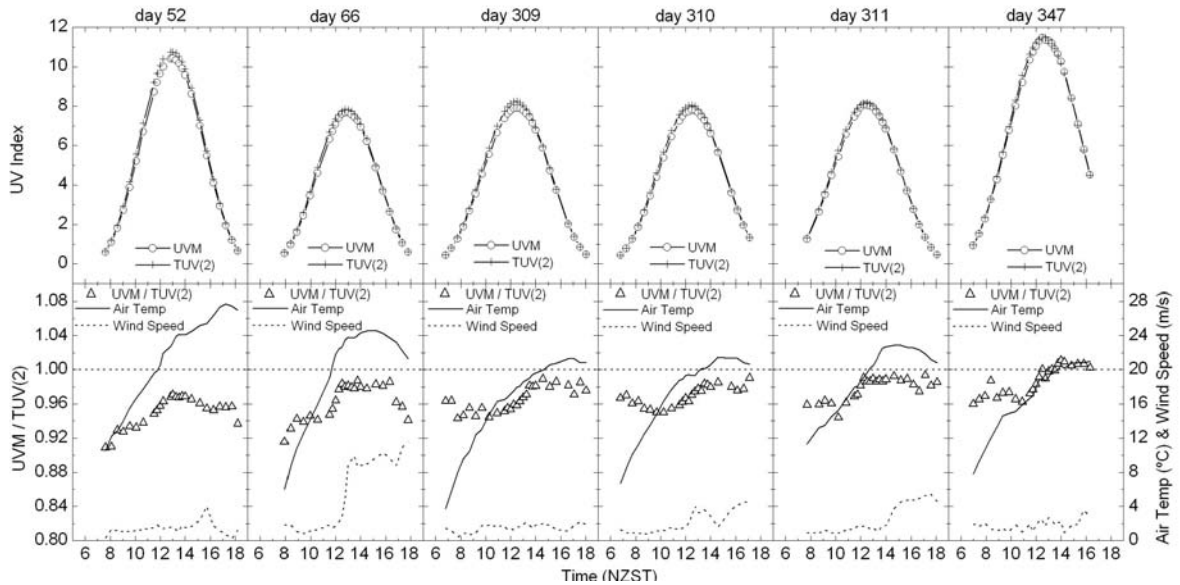

Figure 4.10 UVI model vs measurement comparison for six days of 2001 in Lauder for which air temperature clearly exceeded 20ºC and diurnal variations in *TOZ* and *AOD* were small. Upper: Measured (circles) and modelled (crosses) UVI as a function of time. Lower: Measured over modelled UVI ratio (triangles), air temperature (solid line) and wind speed (dashed line) as a function of time.

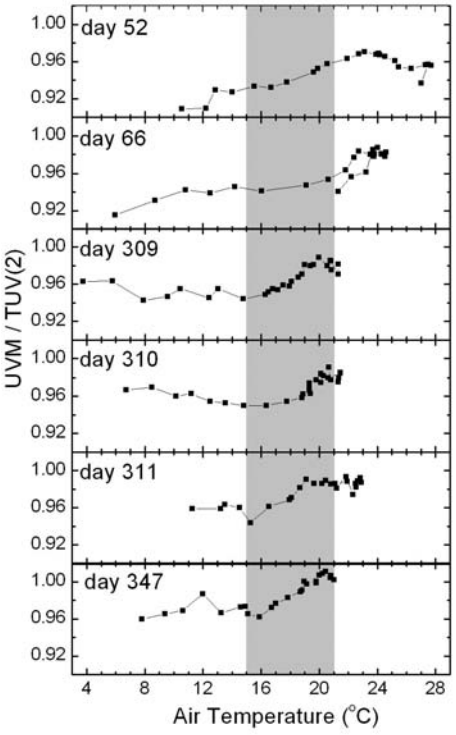

Figure 11. From days represented in Figure 10, measured over modelled UVI as a function of air temperature. The range of temperatures for which the PTFE temperature effect is expected to occur (15 to 21ºC) is shaded.

To see this effect more clearly, Figure 4.11 shows R2 against air temperature, in which the interval of temperatures of interest is shaded. Despite the noise found at this 1-2% level of detail, the step can be clearly seen. For days 309, 310, 311 and 347 the steps occur in the shaded region and reverse when temperature decreases. For days 52 and 66 there seems to be a shift of this effect to higher temperatures. For these days there was a very rapid increase of the air temperature over the period when the step takes place (see Figure 4.10). So it could be that the diffuser temperature had responded more slowly to this increase. Note too that air temperature may not match the actual diffuser temperature.

We recently carried out a differential scanning calorimetric (DSC) experiment with a PTFE sample from a NIWA-built diffuser in collaboration with the Research Group of Materials and Thermodynamics of the University of Girona. This experiment showed an endothermic peak around 18.5 ºC when heating the sample, resulting from a structural change in PTFE, which has been previously discussed in the literature [*Billmeyer*, 1984]. This showed consistency with the optical effect noted here. Annex C describes the details of that experiment and compares the calorimetrical and the optical changes observed in PTFE.

As the observed temperature effect is small it can only be detected in very stable conditions, with low aerosol and ozone variability and with all supporting data available for the radiative transfer modelling. Lauder meets these requirements. In Boulder and Melbourne there is larger aerosol variability and this effect does not show so clearly there. For Mauna Loa, air temperature never exceeded 16.3 ºC for the period studied. Although the diffuser could be warmer than this by a couple of degrees or so (based on measurements at Lauder), clear evidence of the effect was not observed because another factor must be considered at this site, as discussed next.

Effect of clouds built-up underneath

Mauna Loa Observatory is situated on a face of the volcano at 3.4 km above sea level, and there are many clear-sky days in which clouds build-up beneath the site during the day, mostly in the afternoon. This leads to enhancements in measured UVI caused by the increase of the effective albedo of the underlying surface. In Figure 4.8, a larger dispersion of R2 is found in the afternoon than in the morning due to these cloud-induced enhancements. On day 210 (identified in Figure 4.8) this effect is largest.

Figure 4.12 shows the measured UVI, TUV(2) and R2 as a function of time. An increase of about 9% in the R2 ratio is seen from mid-morning to mid-afternoon. TOZ_S did not change much that day, from 272 to 278 DU, and *AOD* was very low (from 0.010 to 0.013).

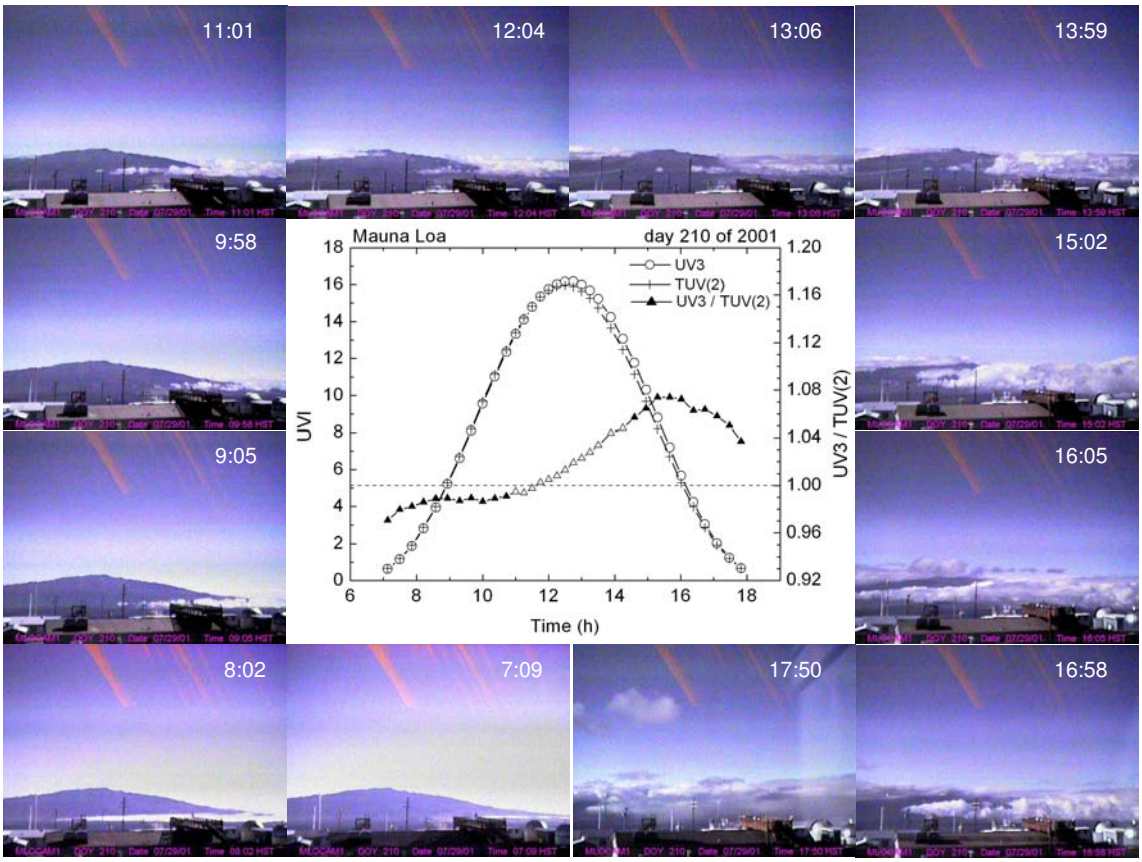

Figure 4.12 (Centre) Measured (circles) and modelled (crosses) UVI and their ratio (triangles) for day 210 of 2001in Mauna Loa. Open triangles account for data that was initially excluded from the study because *AOD* measurements were missing. Modelling for this period has been done using an *AOD* of 0.011 (*AOD* for that day ranged from 0.010 to 0.013) so to have an estimation of the increase in UVI measurements that happened around noon. (Surrounding Pictures) Web cam images from Mauna Loa Observatory facing Mauna Kea for different times of the day.

Webcam images facing volcano Mauna Kea (see Table 4.2) showed evidence that clouds were building-up during this day, as seen in Figure 4.12. From inspection of webcam images from other days with clouds underneath the site, different types of clouds were seen corresponding to different enhancements in UVI. It seems that broken cumuliform clouds were more effective in reflecting UVI than stratiform clouds. However, since the field of view of these images is quite limited, it is difficult to unequivocally establish conclusive relations.

Model overestimations for Melbourne

For Melbourne, large overestimations of the model over the measurements have been found, as discussed above. Day 326 (marked in Figure 4.8) was the day for which the model-measurement agreement was worst among all the days considered in this study. On this day, low *AOD* was measured and it did not change much through the day (the *AOD* at 368 nm was 0.070 in the morning and 0.073, in the afternoon). TOZ_T was 300 DU, TOZ_D was 305 DU and TOZ_S ranged from 300 to 307 DU, showing good agreement between the three sources of ozone data, and not much daily TOZ variation. Some data in midmorning and around noon did not pass the clear sky filter since the deduced cloud fraction rose to 7%.

Figure 4.13 shows the measured UVI together with TUV(2,5,8) and their relative differences (in percent) as a function of time. When considering TUV(2), overestimations from 14 to 22 % were found. If no aerosols were considered (TUV(5)), these became from 17 to 26 % and when *SSA* was set to 0.7, the model-measurement differences slightly improved (they were from 11 to 18 %). Maximum absolute differences are 1.45 in UVI for TUV(2), 1.69 for TUV(5) and 1.17 for TUV(8). UVI modelled for day 326 is very similar to UVI modelled for day 43 (also marked in Figure 8) due to the combined contributions of *SZA*, *TOZ*, and *AOD* in calculated UVI. However, measurements for the former are about 8.5% lower than for the latter and much better UVI model-measurement agreement is found for day 43 (mean agreement is about +4.5%) than for day 326. Therefore, we suspect that there are some issues with either the UVI measurements, or the ancillary data that was used as input to the model on this day.

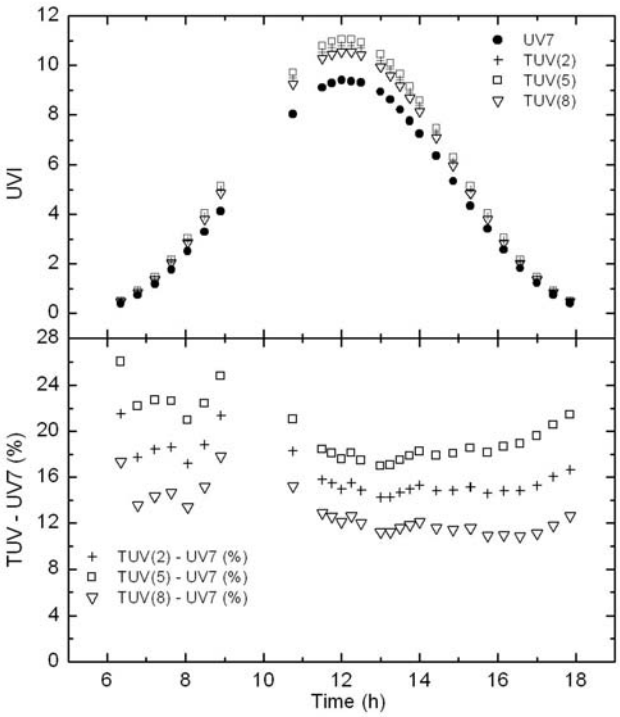

Figure 4.13 Upper panel: UVI measurements and calculations for modelling cases TUV(2,5,8) as a function of time. Lower panel: Relative model – measurement differences for the three modelling cases as a function of time.

4.7 Conclusions

This study is one of the most comprehensive model-measurement intercomparisons undertaken so far for estimations of UVI. It uses state-of-the-art instrumentation, and state-of-the-art radiative transfer modelling incorporating the broadest possible range of ancillary data.

From the general comparisons, best

model-measurement agreements have been found when considering both the daily evolutions of *TOZ* and *AOD*, for which mean agreements are within 0.1-3% depending on the value of *SSA*, except for Melbourne. The corresponding *SD* values are up to 4.2% and model and measurements agree within 5% for the 77% to 98% of the data depending on the site. It is expected that these differences would be larger at more polluted sites, since some of the necessary aerosol parameters are not adequately specified. In this sense we conclude that polluted sites are good to test the model while clean sites are good to test the measurements. Worst model-measurement agreements are found when aerosols are not considered for the UVI calculations, leading to deviations up to 27.2%.

In Melbourne, larger mean model-measurement deviations have been found (5-9%) with maximum deviations of 26% and about 1.5 units of UVI. The reason for this is suspected to be errors either in the calibration of measured UVI or the input aerosol data used at this site.

From the comparison TOZ_T and TOZ_D important systematic deviations have been found for the high altitude sites, with peak differences of -15 DU for Boulder and up to 24 DU for Mauna Loa, leading to deviations of 5.5 and -10 % in UVI, respectively. Mean deviations in calculated UVI were 2.3% for Boulder and -4.2% for Mauna Loa. The difference in sign probably results from the differences in surrounding topography. Mauna Loa is higher than the average altitude surrounding area, while Boulder is lower.

A major issue with respect to modelling is the uncertainty in the input parameters. Uncertainty in the value of *SSA* is particularly important, and can modify the effect of aerosols on UVI up to 11%. Some sites (such as Lauder) have shown better results with SSA=0.9 while other (such as Boulder) have shown better results with SSA=0.7.

For sites where clouds build-up underneath (such as Mauna Loa), errors in modelling can be up to 9% if the induced increment of the effective albedo is not considered. The daily change in *TOZ*, if not taken into account through considering one value for the whole day, can introduce an uncertainty of about 5% in UVI. Uncertainties associated to other input information such as *alpha*, OP and TP affect UVI less than 2.5% for $SZA \leq 75^o$ and uncertainties of aerosol profile, *g*, and ground albedo are about 1%.

The major issues with respect to the measurements were the long term calibration accuracy and stability. In addition, the temperature effect of the PTFE diffusers was studied in detail having a 2-3% effect in throughput between 15 to 21ºC. This may affect all instruments with foreoptics constructed from PTFE and no temperature stabilisation (i.e. most instruments).

All these considerations make uncertainties associated to the UVI modelling comparable with uncertainties associated to the UVI measurement for clean sites and larger for more polluted sites.

Under cloudy conditions (which represents most of the time), very much larger errors are expected in the radiative transfer modelling. Under these conditions, the slow-scanning spectrometers are also subject to significant errors. However, unlike the radiative transfer modelling, no overall bias in the measurements would be expected. Nevertheless, until spectrometers with much faster scan rates become available, or integrating spectrographs become available, direct measurements of UV with broad band instruments (erythemal radiometers) probably provide the most reliable way of estimating UVI under these conditions. That is provided that such instruments are well characterised, corrected and calibrated; otherwise large errors would be expected, as discussed in Chapter 3.

4.8 References

Angstrom, A. (1964), The parameters of atmospheric turbidity, *Tellus*, *16*, 64-75.

Badosa, J., and M. van Weele (2002), Effects of aerosols on uv-index, 48 pp, KNMI, De Bilt.

Bais, A. F., et al. (2001), SUSPEN intercomparison of ultraviolet spectroradiometers, *J. Geophys. Res.*, *106*, 12509-12526.

Basher, R. E. (1982), Review of the Dobson Spectrophotometer and its Accuracy. WMO Global Ozone Research and Monitoring Project, WMO Report No. 13.

Billmeyer, F. W. (1984), *Textbook of Polymer science*, 608 pp., Wiley-Interscience, New York.

De Backer, H., et al. (2001), Comparison of measured and modelled uv indices for the assessment of health risks, *Meteorol. Appl.*, *8*, 267-277.

Dutton, E. G., et al. (1994), Features and effects of aerosol optical depth observed at Mauna Loa Hawaii: 1982-1992, *Journal of Geophysical Research*, *99*, 8295-8306.

Herman, J. R., et al. (1991), A new self-calibration method applied to TOMS and SBUV backscattered ultraviolet radiation data to determine long-term global ozone change, *Journal of Geophysical Research*, *96*, 7531-7545.

Houët, M., and C. Brogniez (2004), Ozone column retrieval from solar UV irradiance measurements at ground level: Sensitivity tests and uncertainty estimation, *J. Geophys. Res.*, *109*, D15302 15310.11029/12004JD004703.

Johnson, B. J., et al. (2002), Electrochemical concentration cell (ECC) ozonesonde pump efficiency measurements and tests on the sensitivity to ozone of buffered and unbuffered ECC sensor cathode solutions, *Journal of Geophysical Research*, *107*, 4393,doi:4310.1029/2001JD000557.

Kneizys, F. X., et al. (1983), Atmospheric Transmittance/Radiance: Computer Code LOWTRAN 6, Air Force Geophysics Laboratory.

Koepke, P., et al. (1998), Comparison of models used for UV index calculations, *Photochemistry and Photobiology*, *67*, 657-662.

Long, C. N., and T. P. Ackerman (2000), Identification of clear skies from broadband pyranometer measurements and calculation of downwelling shortwave clouds effects, *Journal of Geophysical Research*, *105*, 15609-15626.

Madronich, S. (1993), UV radiation in the natural and perturbed atmosphere, in *UV-B Radiation and Ozone depletion. Effects on Humans, Animals, Plants, Microorganisms, and Materials*, edited by M. Tevini, pp. 17-69, Lewis Publishers, Boca Raton.

Mayer, B., et al. (1997), Systematic long-term comparison of spectral UV measurements and UVSPEC modeling results, *Journal of Geophysical Research*, *102*, 8755-8767.

McKenzie, R. L., et al. (2005), Effects of the temperature dependence in PTFE diffusers on observed UV irradiances, *Geophysical Research Letters*, *32 (L06808)*, doi:10.1029/2004GL022268.

McKenzie, R. L., et al. (1997), UV spectro-radiometry in the network for the detection of stratospheric change (NDSC), paper presented at Solar Ultraviolet Radiation. Modelling, Measurements and Effects, Springer-Verlag, Berlin, October 1995.

McKenzie, R. L., et al. (2001), Altitude effects on UV spectral irradiance deduced from measurements at Lauder, New Zealand, and at Mauna Loa Observatory, Hawaii, *Journal of Geophysical Research*, *106*, 22845-22860.

McKenzie, R. L., et al. (1996), Upwelling UV spectral irradiances and surface albedo measurements at Lauder, New Zealand, *Geophysical Research Letters*, *23*, 1757-1760.

McKenzie, R. L., et al. (1998), Effects of snow cover on UV radiation and surface albedo: a case study, *Journal of Geophysical Research*, *103*, 28785-28792.

McKinlay, A. F., and B. L. Diffey (1987), A Reference Action Spectrum for Ultra-violet Induced Erythema in Human Skin, in *Human Exposure to Ultraviolet Radiation: Risks and Regulations*, edited by W. F. Passchier and B. F. M. Bosnajakovic, pp. 83-87, Elsevier, Amsterdam.

Molina, L. T., and M. J. Molina (1986), Absolute absorption cross-sections of ozone in the 185 to 350 nm wavelength range, *Journal of Geophysical Research*, *91*, 14501-14508.

Seckmeyer, G., et al. (1995), Geographical differences in the UV measured by intercompared spectroradiometers, *Geophysical Research Letters*, *22*, 1889-1892.

Stamnes, K., et al. (1991), Derivation of total ozone abundance and cloud effects from spectral irradiance measurements, *Applied Optics*, *30*, 4418-4426.

Van Weele, M., et al. (2000), From model intercomparison toward benchmark UV spectra for six real atmopsheres, *Journal of Geophysical Research*, *105*, 4915-4925.

Walker, J. H., et al. (1987), Spectral irradiance calibrations, NBS Special Publication, National Bureau of Standards, US Dept. of Commerce.

Weihs, P., and A. R. Webb (1997), Accuracy of spectral UV model calculations 2. comparison of UV calculations with measurements, *Journal of Geophysical Research*, *102*, 1551-1560.

Woods, T. N., et al. (1996), Validation of the UARS solar ultraviolet irradiances: comparison with the ATLAS and 2 measurements, *Journal of Geophysical Research*, *101*, 9541-9569.

Ylianttila, L., and J. Schreder (2005), Temperature effects on PTFE diffusers, *Journal of Optical Materials, in press*.

Yoon, H. W., et al. (2002), Realisation of the national Institute of Standards and technology detector-based spectral irradiance scale, *Applied Optics*, *41*, 5879-5890.

Zeng, Z., et al. (1994), Measured UV spectra compared with discrete ordinate method simulations, *Journal of Geophysical Research*, *99*, 23019-23030.

5

A New Parameterisation for UVI Fast Calculations: Application to Build Maps

General frame

As commented in Chapter 1, UVI maps for a particular region are often presented to general public for disseminating both typical (climatic) UV levels and predicted UV index values for next days. For UVI forecasting, modelling techniques have to be used and predictions of the most relevant input information need to be available. For the estimation of the past, present or climatic UVI values, both measurements and modelling can be used. Well calibrated measurements offer the best accuracy though they are rare and often available only at low-spatial resolution; modelling can be done at any spatial resolution but the major limiting factor is the lack of the needed input information. When considering the latter option (i.e. modelling), it becomes convenient to simplify the model, so to allow for fast calculations and consider only the most relevant input information.

Relative errors of UVI estimations are very important for scientific analyses such as the ones presented in the previous Chapters but for practical purposes they become less relevant. When disseminating UVI, efforts should be set on getting accurate estimations in the absolute sense. Specifically, it should be aimed to report UVI with an uncertainty within ±0.5 in UVI, since for larger differences there is a turn in the rounded (and so presented) value of UVI.

Overview

This Chapter presents a climatic analysis of the annual UV Index (UVI) variations in Catalonia (North-East of the Iberian Peninsula) using a new simple parameterisation scheme based on the TUV radiative transfer model.

First, the way the parameterisation was retrieved is described in detail, giving arguments for the input parameters chosen, paying special attention on the aerosol information, and the mathematical structure considered. Then, the parameterisation is compared against the base model. Validation tests are also presented with UVI measurements from two sites, one using high spectral UV measurements and the other from an erythemal radiometer.

Then, the parameterisation is applied to a climatic analysis of the annual UVI variation in Catalonia, showing the contributions of *SZA*, *TOZ* and aerosols. High resolution seasonal maps of typical UV Index values in Catalonia are presented.

5.1 Previously adopted methodologies to build UVI maps

The use of UVI maps is necessary to entirely cover a particular region. However, there is usually a lack of high-density spatial UVI measurements to represent all the territory. So, other sources (such as meteorological ground-based and satellite-based information) and methods (such as empirical algorithms and radiative transfer modelling) usually become necessary.

Some authors have solved the lack of UVI ground-based measurements by combining UVE and total solar irradiance measurements, since the latter are more usually measured than the former. *Bodeker and McKenzie* [1996] used radiative transfer modelling and empirical relations between these two magnitudes to develop an algorithm that retrieves UVI for all cloud conditions considering total irradiance, *TOZ*, altitude, surface pressure, temperature and humidity measurements. This algorithm is currently used in the NIWA's UV Atlas project to produce maps and time series of UVI over New Zealand (see http://www.niwa.cri.nz/services/uvozone/atlas). *Schmalwieser and Schauberger* [2001] established relationships between UVE measurements available from 9 sites and total irradiance measurements available from 39 other sites in Austria to cover the whole country. Cloud effects were also included through relationships between UVE and total irradiance. For the visualization of the data, daily maps of noon UVI were then created with a spatial resolution of approximately 1 km. *Fioletov et al.* [2003] found a statistical relationship between total irradiance and UVE, considering *TOZ*, snow cover, dew point temperature and altitude. They applied this algorithm to 45 stations with total irradiance measurements in Canada to estimate a UVI Climatology. Different types of statistical maps were produced, such as monthly mean daily UV dose, mean noon UVI, 95-percentile of the noon UVI and hourly mean UVI.

Some other studies have produced UVI maps based on radiative transfer modelling and using satellite measurements as input. For example, Verdebout [2000] presented a method to produce UVI maps over Europe with 0.05 degrees of spatial resolution (about 5 km) and half an hour of potential temporal resolution. The method is based on a look-up table generated with a radiative transfer model, whose inputs are *SZA*, *TOZ*, cloud liquid water thickness, near-surface horizontal visibility, altitude and surface UV albedo.

Concerning satellite-derived information, daily UV dose maps and values are available worldwide from TOMS (http://toms.gsfc.nasa.gov), as commented in Chapter 1. The algorithm developed for these calculations uses a table of solutions of the radiative transfer equation. This table also serves for TOMS total ozone column retrievals and takes into account cloud effect (assuming that cloud conditions at noon are representative for the whole day) and surface albedo, using a method to assess the probability of snow presence.

Two examples of predicted UVI maps have been already discussed in Chapter 1 (see Figure 1.6). The UVI maps presented by IMPBUVM are built using the modelling technique described by *Schmalwieser et al.* [2002]. That is an empirical model based on ground-based spectral measurements that calculates the spectral irradiance for 16 wavelengths between 297.5 and 380 nm. The model takes into account *SZA*, altitude, and forecasted *TOZ*. The UVI predictions daily presented by TEMIS uses the empirical algorithm developed by *Allaart et al.* [2004] (as introduced in Section 1.5) that takes into account *SZA*, *TOZ*, and altitude.

The work in this Chapter is directed to retrieve seasonal maps of typical UVI under clear sky and snow-free conditions for Catalonia, North-East of Spain. In this relatively small area (32000 km^2) there is a complex topography, from a coastal line facing to the Mediterranean Sea to the Pyrenees Mountains, with a maximum altitude of 3143 m (see Fig. 5.1). Because of this, Catalonia experiences a large meteorological and climatic variability giving rise to many different climatic conditions within a radius of few kilometres; this diversity also allows people to practice very different activities, from sun bathing on the beach to mountain hiking and skiing, all these with important potential exposures to UV radiation (see Figure 1.5).

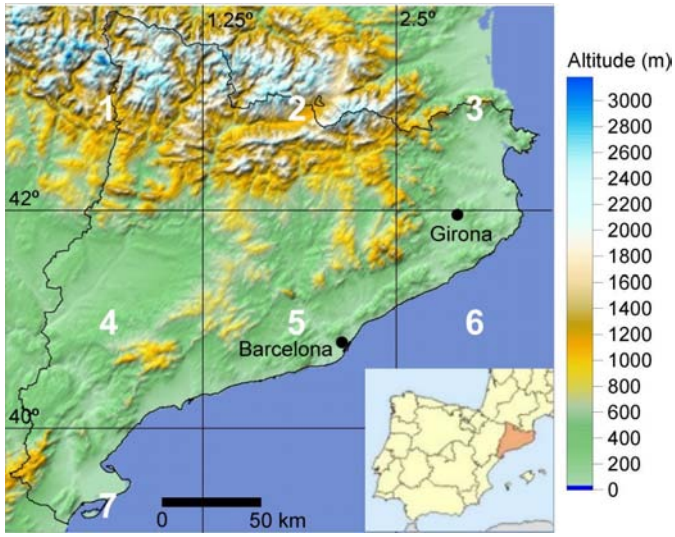

Figure 5.1 Topographic map of Catalonia with 1 km resolution. The low-right square shows the situation of Catalonia in the Iberian Peninsula. Latitude and longitude lines are also shown. The numbers in white indicate the TOMS cells.

Thus, to have a complete characterisation of the meteorological and climatic phenomena in Catalonia, a large density of measuring sites is required. Currently, there are only 5 sites where erythemal UV irradiance is measured in Catalonia, all of them with a short data-record. A possible alternative could be to retrieve typical UVI values based on radiative transfer calculations. However, on one hand, we want high spatial resolution coverage (which involves an important computational cost) and, on the other hand, no accurate high-resolved information about some input variables (such as the aerosol) is available. So it seems reasonable to simplify models through their parameterisation, to make adequate assumptions, and then to perform fast calculations.

The parameterisation here presented considers *SZA*, *TOZ*, altitude (*z*), *AOD* at 368 nm (AOD_{368}) and *SSA* as input parameters. It is named PTUV, Parameterisation of the TUV model, since calculations from this radiative model are used to find the mathematical expressions of the parameterisation.

5.2 Methodology

5.2.1 Parameters considered

Although the application discussed here is only for the small region of Catalonia, the parameterisation was developed in order to be able to explain a wide range of conditions under cloudless skies. Because of this, SZA, TOZ, z, AOD_{368} and SSA were taken with wide ranges (as shown in Table 5.1).

However, some particular situations are omitted from the coverage of this study. Particular surface types with large albedo such as snow and sand are not taken into account here. It has been seen in Section 1.6 that the effect of surface albedo on UVI depends on topography, type of soil and also turbidity of the surroundings; this makes it difficult to find the actual surface albedo values that represent each site at each moment. *Weihs et al.* [2002] considered

Table 5.1 Values considered for *SZA*, *TOZ*, *z*, AOD_{368} and *SSA* to retrieve and validate the parameterisation; this leads to 15120 different cases. The sea level AOD_{368} range is written here since this range is altitude dependent (see equation 5.1). For *alpha* and *g*, constant values are considered.

Parameter	Values considered
SZA	0, 10, 20, 30, 40, 50, 60, 70, 80 deg
TOZ	200, 250, 300, 350, 400, 450, 500 DU
z	0, 1, 2, 3, 4 km
AOD_{368}	0, 0.1, 0.2, 0.4, 0.6, 0.9, 1.2, 1.5
SSA	0.6, 0.7, 0.8, 0.9, 0.95, 1
alpha	1.4
g	0.7

three inversion methods to retrieve surface albedo from UV measurements in spring in Germany and surroundings. They found differences of ±0.15 in the albedo retrieved with the three methods which lead, according to the authors, to an uncertainty in the UV irradiance calculation (in UVB and UVA) of approximately ±3 to 5%. In our study, there is a lack of information about climatic estimations of surface albedo and snow cover for Catalonia; because of this, considering large-albedo cases would be too subjective and thus non-representative of the real situation. Most common surfaces have surface albedo less than 10%, as commented in Section 1.6. In this work, a typical value of 5% is set constant for all the UV calculations.

Also, the conditions of very high turbidity (AOD_{368} *>1.5)* have not been considered for the retrieval of PTUV since these situations are rare (especially in Catalonia) and parameterise them would add extra complexity.

In the following, the parameters and their ranges considered for the elaboration of the parameterisation are discussed.

SZA

As discussed in Chapter 1, *SZA* is the most important parameter affecting UVI. For the parameterisation, the range 0 to 80 degrees of *SZA* is considered

TOZ

The considered range of *TOZ* is 200 to 500 DU. Concerning the vertical ozone profile, TUV default information (from the standard atmosphere USSA 1976) is assumed to be representative. The uncertainties associated to this choice have been discussed in Section 4.4.

Altitude

For an imaginary case with an infinite snow-free flat surface, an increase of about 5.5% per km in UVI occurs for clear skies without aerosols; this is what we find with TUV modelling from 0 to 1 km, *SZA* of 30 degrees and TOZ of 350 DU. The change of *SZA* and *TOZ* separately can slightly affect this value, up to ±0.3%. This is in agreement with experimental findings from *McKenzie et al.* [2001]. When the effect is calculated for 3 to 4 km of altitude, a smaller percentage, 4.8%, is found due to the nonlinear air density vertical distribution. However, these considerations are of minor importance compared with what changes in atmospheric and surface properties can induce. Above sea level, ground surfaces are often mountainous, sometimes being semi snow-covered, and the atmosphere always contains some pollution which varies vertically, horizontally and temporally. Because of this, the observed altitude effect varies greatly from place to place, as has been reported in Section 1.6.

In this study we will split the altitude effect in two contributions: on one hand, the effect for an aerosol-free atmosphere only due to the less molecular extinction as altitude increases;

and on the other hand, the change in UVI due to the lower amount of aerosols. The way this is done is described below.

The range 0-4 km is considered in this study since it covers the most altitudes of human activity. All Pyrenees Mountains are within these limits, so this range includes all of Catalonia.

Aerosols: AOD and SSA

Aerosols attenuate the direct component of radiation and enhance the diffuse component. The total (diffuse + direct) irradiance is normally reduced by aerosols except for especial cases (such as with particular snow-covered surfaces) not considered further in this study.

As discussed in Section 1.6, the aerosol optical properties at each wavelength for the radiative transfer calculations can be explained through the *AOD, SSA,* and *g*. The *AOD* spectral dependence will be described using *alpha*, as it has been done in Chapters 3 and 4. As stated above, the *AOD* value is again referred to 368 nm, which is explicitly indicated for this study.

In practice, as it has been considered in the previous chapters, *g* and *SSA* are considered spectrally uniform because their dependence on wavelength is supposed to be small. *Reuder and Schwander* [1999] reported, from Mie-calculations, variations in *SSA*, from 280 to 400 nm, of about +3% for both low and high pollution conditions considered. For this, continental maritime and continental polluted aerosol types were taken respectively. For *g*, the variations were 1.2% and 2.7%, respectively. However, the works of *Jacobson* [1998; 1999] suggested that *SSA* might increase markedly at shorter wavelengths in the presence of organic (pollutant) aerosols. *Petters et al.* [2003] reported for a site in North Carolina that *SSA* increased from about 0.8 to 0.9 between 300 and 368 nm. The *SSA* values were estimated from an inversion method combining diffuse and direct irradiance measurements at seven wavelengths together with radiative transfer modelling.

In order to decide which aerosol parameters to include in the parameterisation, we performed a study of AOD_{368}, *alpha*, *g* and *SSA* effects on UVI with TUV model. Also, the dependencies of this effect on *SZA* (from 0 to 80 degrees) and *TOZ* (from 250 to 450 DU) were considered. Table 5.2 summarizes the maximum effects on UVI found for the four aerosol parameters. These maximum effects were found at the lowest *SZA* and *TOZ* values, i.e., when UVI takes maximum values. Table 5.2 shows the UVI values for the extreme values of each parameter. Notice that for *SSA*, *g* and *alpha* very wide ranges were taken. For AOD_{368}, values up to 1.5 were included, leaving out the extremely polluted cases, as pointed out above. Table 5.2 shows that, as expected, AOD_{368} is the most important parameter affecting UVI, inducing a maximum change of 6 units of UVI for the full range (AOD_{368} from 0 to 1.5). *SSA* appears to be the second more important parameter, leading to effects in UVI of 2.8 at maximum. The effects of g and *alpha* are much smaller: up to 0.8 and 0.7, respectively. These results are consistent with what has been discussed in Section 4.4.

It was also found that, while *SZA* logically plays an important role in the effect of

Table 5.2 Maximum absolute effects on UVI observed for *SSA*, *g*, *alpha* and AOD_{368} in the range considered. The reference values of each of these parameters considered for this analysis are also shown. In brackets there is UVI calculated for the extreme values of each parameter for *SZA* = 0 deg and *TOZ* = 250 DU, which are the conditions for which the maximum absolute effects are found

Parameter	Ref.	Range	Absolute effect on UVI
SSA	0.9	0.6-1	2.8 (12.3 - 15.1)
g	0.7	0.5-0.9	0.8 (13.9 - 14.7)
alpha	1.4	0-2.9	0.7 (14.6 - 13.9)
AOD_{368}	0.3	0-1.5	6.0 (15.6 – 9.6)

aerosols on UVI, *TOZ* influence is negligible, which allows separate treatment of the aerosol and ozone effects on UVI. Further details about the analyses performed and the results obtained can be found in *Badosa and van Weele* [2002].
These results suggested that three parameters were sufficient to explain the aerosol effect on UVI: AOD_{368}, *SSA* and *SZA*. The ranges considered for AOD_{368} and *SSA* are the same than in Table 5.1: 0-1.5 and 0.6-1.0, respectively; *g* and *alpha* are set constant at 0.7 and 1.4, respectively, as it has also been assumed in the previous chapters.
The *AOD* is generally lower at higher altitudes, so it would be quite unrealistic to consider the same range of *AOD* at all altitudes. Moreover, this would add much complexity to the parameterisation. So, a decision was made to further limit the *AOD* range to be accounted by the parameterisation as altitude increases; for this, the following formula representing an aerosol vertical profile was developed:

$$AOD_{368}(z) = (AOD_{368}(0) - 0.074) \cdot e^{-z/1.3} + 0.074 \cdot e^{-z/8} \qquad (5.1)$$

where $AOD_{368}(z)$ is the AOD_{368} at each altitude and z is given in km.
Equation (5.1) has two exponential functions with two different scale factors, 1.3 and 8 km, accounting for the variable aerosol optical depth near sea level and the assumed constant contribution outside the mixing layer, respectively. To derive these scale factors the vertical profile of *McClatchey et al.* [1972] for 23 km of visibility and normalized to the sea level value was fitted. The multiplying factors of the exponential functions were found by requiring that at 6 km above sea level, the overhead *AOD* at 550 nm is 0.02 when *AOD* at sea level is around 0.1. This is consistent with the specifications of the Radiation Commission of International Association of Meteorology and Atmospheric Physics (IAMAP) (1986), for the continental II aerosol profile plus the background contribution. It is also consistent with *d'Almeida et al.*'s [1991] recommendations for clean continental aerosols.
Strictly, Eq. (5.1) has physical meaning only when $AOD_{368}(0) > 0.074$. This means that this expression might not be useful for low polluted sites, such as the sites considered in Chapter 4 (see Figure 4.3). Further, when using Eq. (5.1) to produce *AOD* profiles, we recommend setting $AOD_{368}(0) = 0.074$ if a lower value had to be considered.
Applying formula (5.1), the maximum value of AOD_{368} considered for the parameterisation is 1.5 for z=0 km, 0.73 for z=1 km, 0.36 for z=2 km, 0.19 for z=3 km and 0.11 for z=4 km. Of course this is a simplification of reality and it has to be understood as such.

5.2.2 Mathematical expression

PTUV consists of three basic multiplying factors: the main factor (UVI_0), which gives UVI at sea level as a function of *SZA* and *TOZ* for aerosol-free conditions; a factor considering the altitude effect for a clean atmosphere (f_z); and a term to account for the aerosol effect (f_{aer}) that also allows for a reduction of AOD_{368} with altitude. The equation that expresses the fitted UVI is then:

$$UVI_f = UVI_0 \cdot f_{aer} \cdot f_z \qquad (5.2)$$

UVI_0 was found using the same fitting formula as *Allaart et al.* [2004]:

$$UVI_0 = \left[E_0 \cdot S \cdot \mu_x \cdot \exp(-\frac{\tau}{\mu_x}) \right] \cdot \left[F \cdot X^G + \frac{H}{TOZ} + J \right] \qquad (5.3)$$

where

$$\mu_x = \mu_0 \cdot (1-\varepsilon) + \varepsilon \qquad \mu_0 = \cos(SZA) \qquad X = 1000\,DU \cdot \mu_0 / TOZ$$

and E_0 accounts for the Sun-Earth distance seasonal variation, which affects UVI by ±3.5% at maximum, as commented in Section 1.6.

The values of the coefficients in formula (5.3) were found by fitting UVI calculated from TUV for *SZA* and *TOZ* ranging from 0 to 80 degrees (with eight steps) and 200 to 500 DU (with six steps), respectively (see Table 5.1). The altitude was set at sea level and no aerosols were considered. The values found for the coefficients were: ε = 0.14, S = 1.22, τ = 0.48, F = 3.17, G = 1.32, H = -126 DU and J = 1.43.

The fitting was achieved using the Levenberg-Marquardt nonlinear fitting method (under Microcal Origin 6.0 software) and using a weighting factor proportional to UVI in order to reduce the absolute errors. The coefficients values found here differ from those at *Allaart et al.* [2004] because of the different dataset used, the inclusion of aerosol contribution, and differences in the fitting methods.

To explain the relative effect of aerosols on UVI, we consider the following exponential function:

$$\frac{UVI(SZA, TOZ, AOD_{368}, SSA)}{UVI(SZA, TOZ, AOD_{368} = 0)} \cong f_{aer} = e^{-b(SZA,SSA)\,AOD_{368}} \qquad (5.4)$$

In equation (5.4), b is a function of *SZA* and *SSA* that can be expressed in two separate polynomial terms:

$$b(SZA, SSA) = (0.344 + 0.773\mu_0 - 1.368\mu_0^2 + 0.580\mu_0^3) \cdot (1 - 5.33(SSA - 0.9) - 2.77(SSA - 0.9)^2) \qquad (5.5)$$

Coefficients in equation (5.5) have been found by fitting TUV calculations for sea level altitude and for the same *SZA* and *TOZ* conditions as for equation (5.3), together with AOD_{368} ranging from 0 to 1.5 (with seven steps) and SSA from 0.6 to 1 (five steps, see Table 5.1) using the Levenberg-Marquardt nonlinear fitting method.

As seen in section 1.6, a wide range of ratios have been reported from different studies to explain the altitude effect. Here, this effect has been divided in two parts: one accounting for the reduction of aerosol optical depth as altitude increases and the other, explaining the enhancement produced as the atmosphere becomes thinner when altitude increases. The first contribution is taken into account in equation (5.4) by introducing the actual AOD_{368} value estimated or measured at the considered altitude. This value should lie within the limits marked by equation (5.1) for which the parameterisation is valid. The AOD_{368} in equation (5.4) can be estimated through equation (5.1) if required. For the second contribution, an increment of 5% per km is assumed, which represents what is found in average with TUV model calculations (see discussion above). This ratio was also recommended by *Allaart et al.* [2004] to describe the altitude effect. The altitude factor is then:

$$f_z = 1 + 0.05 \cdot z \qquad (5.6)$$

The comparison of the results given by equation (5.3) and (5.4) with TUV calculations separately showed maximum absolute errors of ±0.2 in UVI. As these two equations had been retrieved for sea level conditions, the next step was to combine them with equation (5.6), so finally comparing results from equation (5.2) with TUV UVI calculations that considered the altitude change. The UVI calculations were done for all of the 15,120 conditions listed in Table 5.1. The considered AOD_{368} value was changed with altitude according to equation (5.1). Figure 5.2 shows the mean differences between the parameterisation and the TUV model through bins of UVI (square points); the parameterisation deviated from the model systematically down to -0.3 in UVI. So, in order to improve the agreement, the following correction was applied to UVI_f giving the final expression of PTUV:

$$PTUV = 0.0713 + 0.9471UVI_f + 0.005213UVI_f^2 - 1.565E\text{-}4^* UVI_f^3 \quad (5.7)$$

After this correction the mean differences remain very close to 0 for the whole UVI range, as shown in Figure 5.2 (triangle points).
In comparison with TUV with 8 streams, PTUV performs calculations with a speed about 2000 times higher. Compared with the two streams code, the PTUV is about 50 times faster.

5.2.3 Model vs parameterisation

To estimate the errors arising from approximating TUV results by a parameterization such as PTUV, values from the same 15,120 cases in Table 5.1 have been carefully compared. As a result of the comparison, absolute errors are found to range from -0.26 to 0.34, although 88% of cases are within ±0.1, and 99% are within ±0.2 in UVI. Useful information about the maximum absolute errors can be found in their representation as functions of different parameters. Figure 5.3 shows the distribution of averaged absolute errors through bins of *SZA*, *TOZ*, *z* and UVI. Error bars representing the standard deviation and two curves accounting for the maximum errors are also shown. As expected, the maximum absolute errors take place for low *SZA*; however, the largest of these errors are found for very low values of *TOZ*, around 200 DU, which are in general rare conditions. The largest discrepancies between the model and the parameterisation occur for low altitude sites, where a large fraction of aerosol load is present. Also largest absolute errors are found for very low values of *SSA*. In the case of AOD_{368} (not shown) no significant tendency has been detected. Thus, maximum absolute errors of the parameterisation are found when combining very low values of *SZA*, *TOZ* and *SSA*, which are extreme cases, together with low altitude.
Concerning relative errors, in 95% percent of cases with UVI larger than 2 the errors are within ±3%. For lower

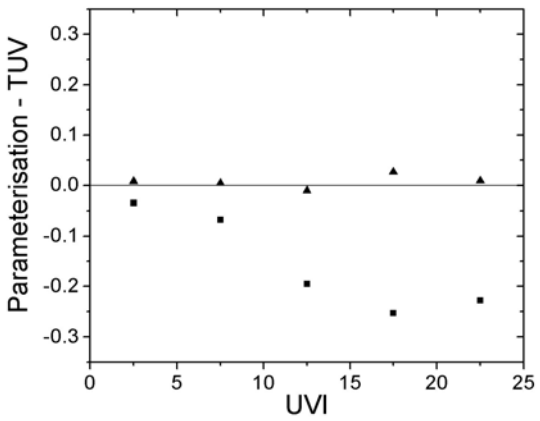

Figure 5.2 Mean errors committed by the parameterisation through bins of TUV UVI before (squares) and after (triangles) the application of Eq. (5.7).

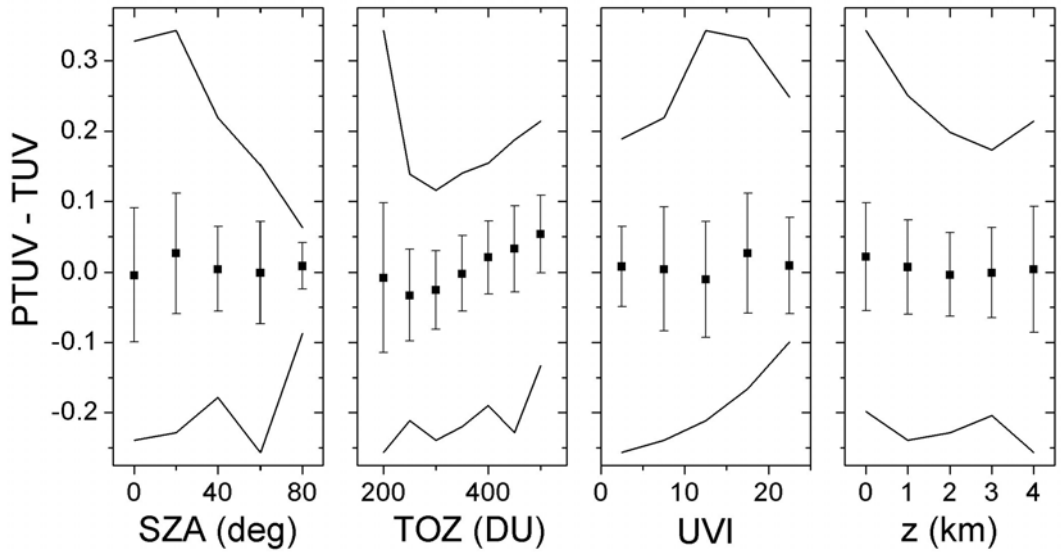

Figure 5.3 Mean absolute errors as function of *SZA*, *TOZ*, *z* and TUV UVI. Standard deviation is showed through the vertical error bars and maximum absolute errors are represented in lines.

values of UVI (and thus larger *SZA*) the relative errors take much larger values. This is due to the model fitting criterion of giving more importance to the points with larger UVI value. The points with largest relative differences are also associated with non common conditions and with very low absolute errors, which are within ±0.19 for UVI<2.

5.3 Validation test

Above, it has been shown that absolute differences between PTUV and TUV remain small for a wide range of hypothetic conditions. Now, the interest is set on testing the performance of PTUV for real conditions. For this, two model-measurement comparisons were carried out. First, high quality UVI measurements are considered for low aerosol load conditions and the general performance of PTUV is tested; second, UVI measurements under more diverse aerosol conditions are used and the availability of PTUV to account for the aerosol contribution is tested.

5.3.1 Comparison with UVI from high quality spectral measurements

PTUV was first compared against high quality spectroradiometric data. For this, the clear-sky UV data used in Chapter 4 from UVM for Lauder 2001 (see Figure 4.1) was considered. Same type of comparisons to that shown in Figure 4.8 was considered so the modelling conditions for case 2 (see Section 4.4 and Table 4.4) were considered for the PTUV modelling. Figure 5.4 shows the model-measurement results when considering both TUV(2) (repeated from Section 4.4 and Figure 4.8) and PTUV; these results can be directly compared.

From the model vs. measurement plot, same regression coefficients are found with both models and similar *SD* values, being slightly better for PTUV. The regression slopes (B) show a slightly larger overestimation of the measurements with PTUV, though the difference is very small, the order of 0.6%. When looking at the relative difference (mean and SD of the data), this was (see Figure 4.7) of 2.8 ± 3.0% when considering TUV(2); for PTUV, the mean relative difference is slightly lower and the SD is similar, 1.9 ± 2.9 %. This

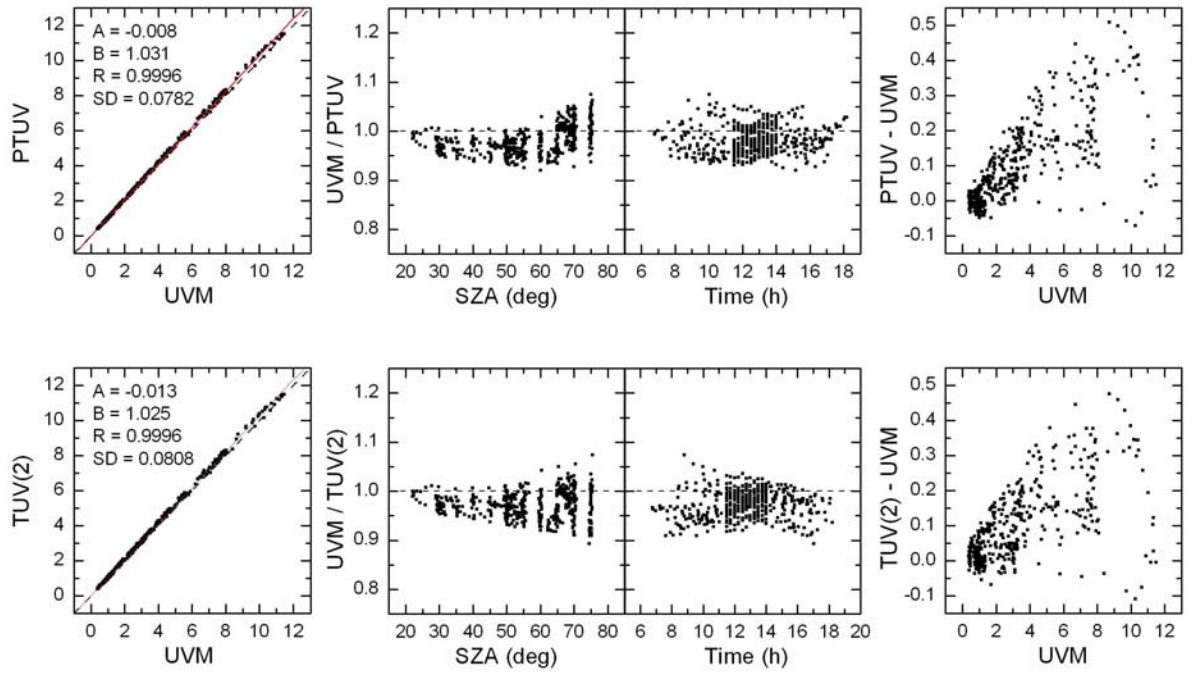

Figure 5.4 Comparison between the UVI calculated with PTUV and TUV(2) and measured with UVM for the clear-sky days in Lauder 2001 from Chapter 4.

can be understood when plotting the UVM/Model ratios against *SZA* and time. It is seen that, with PTUV, there is a larger dependence of the ratios on *SZA* than with TUV, with lower UVI values (in relative terms) for large *SZA*. This poorer accuracy of PTUV for lower UVI was expected since it was retrieved in order to minimize the absolute errors in UVI, as discussed above.

The absolute model-measurement differences (i.e. the residuals) are very similar with PTUV and TUV, as shown in Figure 5.4 as a function of measured UVI. Maximum residuals are 0.51 for PTUV and 0.48 for TUV. The absolute differences between PTUV and TUV are from -0.077 to 0.072 in UVI, which is a much lower interval than that found for the wide range of conditions considered in Section 5.2.3 (see Figure 5.3). This shows the good performance of PTUV in absolute terms.

5.3.2 Comparison with UVI from a Robertson-Berger type meter

Here the attention will be focused on testing the performance of PTUV for diverse *AOD* conditions. For this, the dataset used is a fifteen month period (December 2001 – February 2003) of 1-minute resolution UVI measurements with the Kipp & Zonen UV-S-E-T broad band erythemal radiometer in Girona (41.97ºN, 2.82ºE, 100 m a.s.l.), which has already been presented in Chapter 3.

In order to avoid systematic deviations in the model-measurement comparison, these measurements from Girona were calibrated against TUV model. This makes it easier to study how different ways of introducing the aerosol information affects the model vs. measurement comparison through the change in the dispersion of the residuals.

The UVI measurements were corrected for the non-ideal spectral response of the sensor (see Figure 3.1) by applying the factors found in Section 3.3 (see Figure 3.2). For this, daily TOZ values were taken from TOMS. Strictly, the angular response of the instrument, which deviates from the cosine response, should be corrected, as also noted in Chapter 3. However, here this correction was not applied for the UV-S-E-T instrument, since its angular response

is assumed to be very good, of less than ±4% from 0 to 70 degrees of *SZA* according to the manufacturer. *Leszczynski et al.* [1998] showed that such a deviation induces an angular correction in UVI much lower than this ±4%, which makes it reasonable to neglect this correction (see also discussion in Section 3.2).

Cloudless records were selected through visual inspection of concurrent measurements of both total global and diffuse radiation. This selection reduced the dataset to 11% of its original size; the final dataset contains 25,766 records and involves 104 days, 34 in winter, 34 in spring, 22 in summer and 14 in autumn. Because of non-smooth variations usually observed in UVI around noon mostly in the hotter months, records between 1100 and 1300 TST could be selected only in 18 days, almost all from winter and spring.

For the modelling, assimilated retrievals of *TOZ* from TOMS were used as input to the model. Again, *SSA* was kept constant at 0.9. Concerning AOD_{368}, no specific measurements of *AOD* are available in Girona. However, concurrent measurements of total global irradiance and diffuse irradiance were available from two Kipp & Zonen CM11 pyranometers (one of them, shaded to get the diffuse component), so estimations of Angstrom's β (i.e. AOD at 1000 nm) were possible. The simple algorithm suggested by *Gueymard and Vignola* [1998] was used:

$$K = 0.04 + 1.45 \cdot \beta \qquad (5.8)$$

where K is the ratio between the diffuse and direct normal irradiances. An *alpha* of 1.4 was used to convert *AOD* at the UV wavelengths. *Gueymard and Vignola* [1998] recommend that Equation (5.8) is used for SZA<75º and β<0.35. However, here SZA conditions up to 80º are considered.

The AOD_{368}, TOZ and SZA histograms are presented in Figure 5.5. In Girona, despite being a semi-rural site, there is much more turbidity than in Lauder (see Figure 4.3) which is shown through the wide range of AOD_{368} found up to 1. Regarding *TOZ*, values from 246 to 486 DU are found although most of the records lay around 325 DU, mostly due to the higher frequency of winter and spring days.

Figure 5.6 shows the results of the model-measurement comparison through the plots model vs. measurement and residuals vs. *SZA*. Apart from the results considering PTUV with the aerosol information described above, there are two additional comparisons using different types of modelling that consider two other ways of taking into account (implicitly and explicitly) the aerosol contribution.

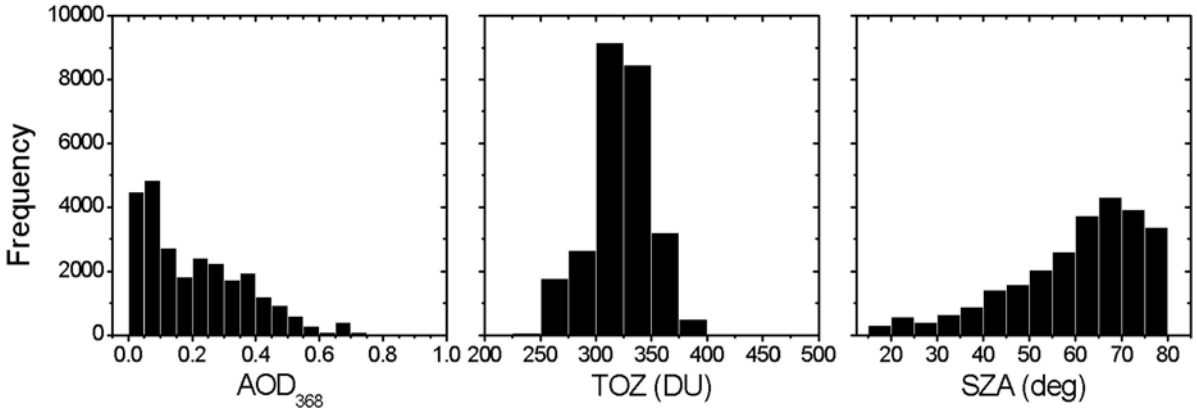

Figure 5.5 AOD_{368}, *TOZ* and *SZA* histograms for the dataset considered for Girona.

On one hand, the results with UVI calculated with the empirical algorithm from *Allaart et al.* [2004] are also shown. As commented above, this formula considers *SZA*, *TOZ*, E_0 and a 5% per km altitude effect as input information and is a result of fitting UVI from Brewer spectrophotometer measurements from De Bilt (Netherlands) and Paramaribo (Surinam).
Thus, the algorithm from *Allaart et al.* (hereon called ALUVI) has implicit aerosol information. On the other hand, PTUV is used with climatic information of AOD_{368} as input. Monthly typical values of Angstrom's β in Girona are considered from *Gonzalez et al.* [2001] based on an algorithm more rigorous [*Gueymard*, 1998] than the one in equation (5.8) that was applied to four years of broadband total and diffuse measurements. Despite of the limited period, these typical values will be considered as climatic hereafter. An *alpha* value of 1.4 is used then to convert *AOD* to 368 nm. This annual variation of AOD_{368} is shown in Figure 5.7.
As shown in Figure 5.6, for the three cases the model vs. measurement plots (5.6a1, 5.6b1, 5.6c1) show excellent correlations, with *R* always larger than 0.996. For plot 5.6a1, which corresponds to the comparison using ALUVI, a good slope is found, with B=0.991. In 5.6b1, for which PTUV with climatic *AOD* is used, a lower slope is found, with B=0.976. The linear fit for 5.6c1 gives B very close to 1 (B=1.003), which is logical given the way the measurements were calibrated. Note that using climatic *AOD* in PTUV leads to underestimate the UVI measurements by about 2.4% (from the comparison between plots 5.6b1 and 5.6c1). The most remarkable aspect is the clear differences observed in the dispersion of the points, mathematically expressed through *SD*. The largest dispersion is found for ALUVI (*SD*=0.167) due to its implicit and site-based treatment of aerosols. When climatic values for AOD are introduced to PTUV a lower *SD* value is found (*SD*=0.131). The

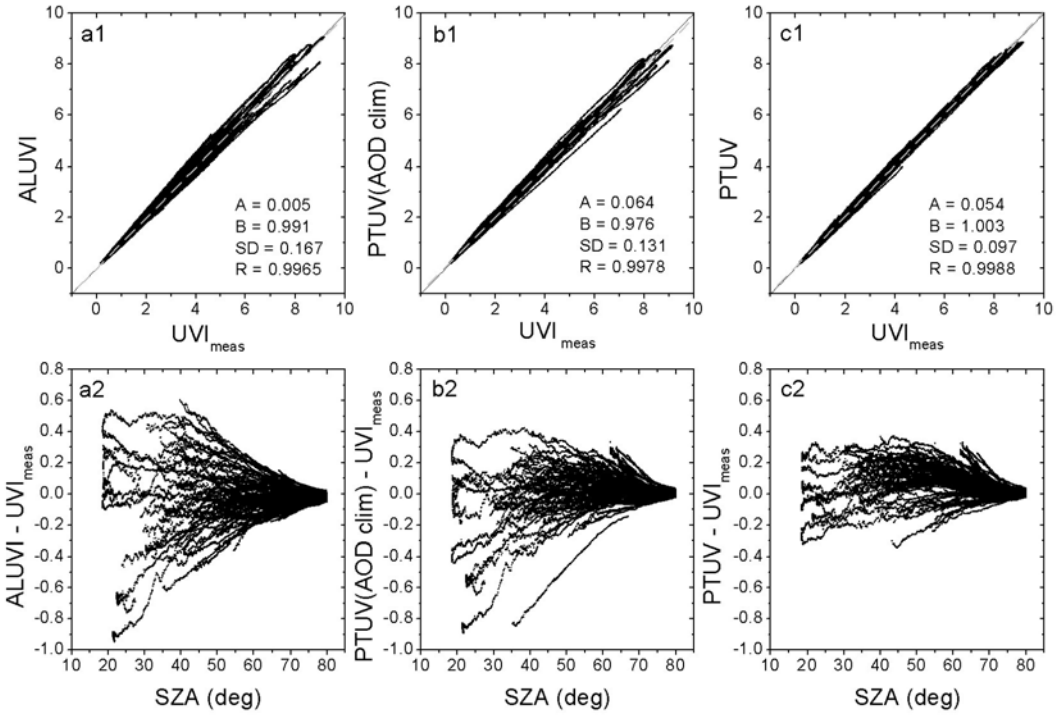

Figure 5.6 UVI modelled vs. UVI measured (1) and the residues vs. SZA (2) plots for with the dataset from Girona and three different ways of modelling (from left to right):a) UVI algorithm from *Allaart et al.* [2004] b) PTUV with AOD climatic from *Gonzalez et al.* [2001] ; c) PTUV with the actual *AOD* conditions from equation (5.8). Dashed lines and solid lines are represented in model vs measurement plots accounting for the linear fit and perfect agreement lines, respectively. The linear fit statistical parameters are also shown

lowest dispersion is found when more aerosol information is considered into the model, that is, in the plot 5.6c1, where *SD*=0.097. This implies a reduction *in SD* of 27% with regard to the *SD* for PTUV with climatic AOD.
These differences in the dispersion are also clearly evident in the residuals vs. *SZA* plots (5.6a2, 5.6b2, 5.6c2). For the comparison with ALUVI, the widest range of residuals is found: -0.95 +0.60 in UVI. In plot 5.6b2, from the comparison using PTUV with climatic *AOD*, a slightly narrower range is found, -0.90 +0.42 in UVI. The residuals for PTUV with concurrent AOD_{368} from equation (5.8) (plot 5.6c2) take values within a limited range in UVI of ±0.37. Thus, a clear relation appears between *SD* and the residuals range, so the larger is *SD* the larger is the residuals range.
These analyses show that the PTUV model is able to explain different (but not extreme) *AOD* situations, giving a good model-measurement agreement. Moreover, from Figure 5.6 it is apparent that considering concurrent information for *AOD* into the model gives much better results than taking into account climatic values or implicit contributions. Slightly better results in the dispersion of the points are found when climatic aerosol information from the working site is explicitly introduced to PTUV, compared with the *Allaart et al.* algorithm which implicitly considers aerosol information from a different site. In spite of this, a better model vs. measurement agreement (i.e. a value of *B* closer to 1) is found for ALUVI than for PTUV with climatic *AOD*.
The reason why PTUV with climatic *AOD* and ALUVI give similar results for Girona is because the aerosol characteristics (mean and annual evolution of AOD) for this site are similar to those in the measurements used to retrieve ALUVI. The latter algorithm, when applied to the dataset from Lauder (Section 5.3.1), gives UVI values 6% lower than PTUV (both with climatic *AOD* estimations and the *AOD* actual measurements available), since the aerosol contribution that is implicitly accounted for by ALUVI overestimates the actual aerosol contribution at Lauder.

5.4 Seasonal UVI maps

5.4.1 Climatic annual variation of UVI

In order to know the typical UVI values for Catalonia it is interesting to see the seasonal variation of some of the variables that affect UVI most, i.e., *SZA*, *TOZ* and *AOD*. For this analysis, Girona has been chosen since for this site there is some data available about typical turbidity, in monthly basis [*González, et al.*, 2001], as commented above. *TOZ* is calculated through moving averages of ±5 days from 25 years (1979-2003) of Earth Probe TOMS assimilated measurements. As these measurements have a latitude-longitude resolution of 1-1.25 degrees, Catalonia is completely covered by seven cells (see Figure 5.1). Girona is very close to the border between cell 3 and 6 so *TOZ* for this site has been calculated as the mean value of these two cells.
Figure 5.7 shows the annual change of noon *SZA*, *TOZ* and AOD_{368}. Maximum *TOZ* values are detected in April and minimum values at the end of October and beginning of November; the range is 284-370 DU. Monthly climatic values of AOD_{368} range from 0.04 (in January) to 0.47 (in July). It is seen that the shape of the curve shows more aerosols during spring than in autumn. The range of noon *SZA* for the considered dataset is from 18.5 to 65.4º.

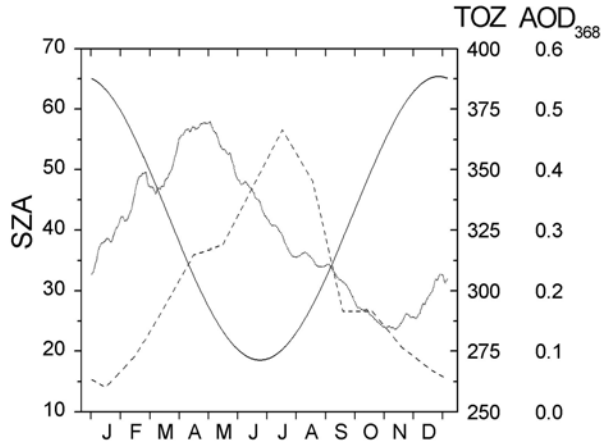

Figure 5.7 Annual variation of *SZA* (solid line) in degrees, *TOZ* (dotted line) in DU and AOD_{368} (dashed line) for Girona.

Note that the maximum and minimum values take place in different months depending on the variable. Consequently, although *SZA* is the dominant factor to describe the annual UVI variation, this is also considerably affected by the shifted variations of AOD_{368} and, most of all *TOZ*. Figure 5.8 shows the resulting UVI annual curve calculated with PTUV considering these variations of *SZA*, *TOZ* and AOD_{368} (thick line). The UVI curve calculated with the summer solstice mean *TOZ* (337 DU) and AOD_{368} (0.39) values (solid grey line) is also plotted. Differences in the shapes of the curves are clear. The "realistic" line is asymmetric in respect to summer solstice, with UVI values about 1 unit larger in autumn equinox than in spring equinox and some oscillations, mainly caused by the *TOZ* annual and day to day variations. Moreover, the maximum UVI of the curve, around 8, is detected during the whole June and July and not only around the summer solstice, which is an important aspect to take into account for UV damage prevention purposes. This fact is produced by the reduction in *TOZ* in summer that partly compensates the effect of the increase of the noon *SZA*.

Figure 5.8 also shows the UVI curves for *TOZ* and AOD_{368} from Figure 5.7 plus and minus one standard deviation. The standard deviations of *TOZ* are around 34-44 DU in winter, 19-41 DU in spring, 12-20 DU in summer and 16-31 DU in autumn. This leads to much larger day-to-day variability of UVI in the first two seasons than for the latter two, which is clearly seen in Figure 5.8 (dashed curves). Concerning AOD_{368}, the standard deviation is around 0.17 in summer and much lower, around 0.05, in winter. Near summer, this aerosol variability induces variability in UVI (dotted curves) that is comparable with variability induced by TOZ, but is much lower for the rest of the year. This gives evidence that it is important to know the aerosol (or turbidity) properties mainly in summer to characterise UVI accurately.

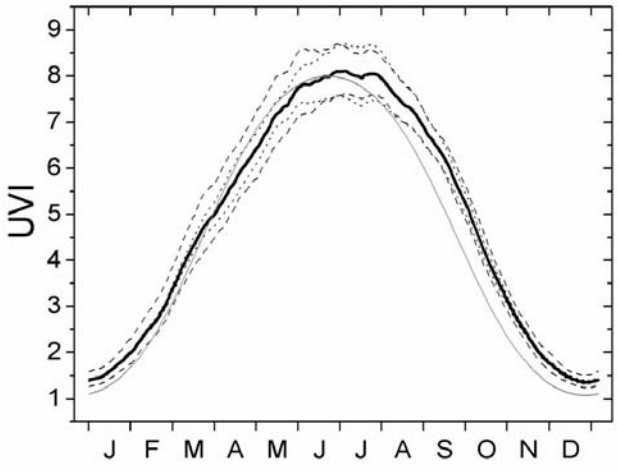

Figure 5.8 Annual variations in UVI (for Girona) calculated with PTUV with the values of Fig. 5.7 (solid thick line), with *TOZ* plus minus one standard deviation (dashed lines), with AOD_{368} plus minus one standard deviation (dotted lines) and with *TOZ* and AOD_{368} set constant to 337 DU and 0.39, respectively (solid grey line).

While the annual UVI considering the climatological mean values of *TOZ* and AOD_{368} reaches a maximum of 8 units, when introducing *TOZ* and AOD_{368} minus their standard deviations into PTUV, a June-July UVI of 9.3 is reached (the corresponding curve is not shown here), which is 16% larger.

All these considerations show the complexity of UVI values expected. For the construction of typical UVI maps in Catalonia, climatological mean values of *TOZ* and AOD_{368} will be used, but

the comments above have to be taken into account.

5.4.2 Construction of seasonal UVI maps

Four maps are presented, corresponding to the solstices and equinoxes at noon for cloudless conditions, in order to see the seasonal differences (see Figure 5.9). A resolution of 1x1 km is taken which involves 268x278 nodes.

The values of *TOZ* have been found also from moving averages of ±5 days of 25 years and averaging together the 7 values that TOMS gives for all the region of Catalonia each day (see Figure 5.1). In this way, for each day one value of *TOZ* is taken to represent all the territory. In Annex E it is shown that the *TOZ* from the seven cells of TOMS are highly correlated and with no significant systematic differences. Consequently, it is a good approximation to assign only one *TOZ* value for Catalonia, although this simplification is poorer in spring and winter when there is the maximum *TOZ* variability.

Since we do not have any climatic information about aerosols for Catalonia, the monthly values of Figure 5.7 have been considered to represent all the territory. Although this situation is far from ideal, we note that this annual turbidity evolution is very similar to what other authors found from analyses for Mediterranean sites such as Barcelona and Valencia [*Lorente*, 1978; *Pedrós, et al.*, 1999; *Pinazo, et al.*, 1995]. Equation (5.1) is used to extrapolate AOD_{368} for different altitudes.

In Figure 5.9 much larger UVI values for 21 June (UVI up to 10.5) than for 21 December (UVI up to 2) are reported, as expected. It is also seen that UVI for 21 September and 21 March is around 6.5 and 5.5 respectively, showing about 1 point in UVI of difference as also appeared in the above analysis for Girona.

Figure 5.10 shows (in grey) all of the UVI values for each map plotted as a function of altitude. The particular case of UVI simulated over a range of altitudes from 0 to 3325 m at 42.88 ºN and 0.04 ºE (north-east corner of the maps) is shown through the black lines. Since Catalonia is a relatively small territory the latitudinal effect is rather weak. This effect appears in Figure 5.10 as the vertical dispersion of the points, which is larger for the equinoxes than for the solstices.

The altitude effect is less obvious for the non-summer maps. Even the relative changes with altitude are smaller in winter than in summer because of the reduced aerosol loading in the boundary layer in winter (relative changes are up to 17% in winter and up to 30% in summer, as calculated from Figure 5.10). For the autumn, winter, and spring maps a maximum difference less than 1.5 in UVI is found for the whole territory. In summer the altitude effect strongly appears with differences up to 2.5 between the coast and the highest mountains. This shows firstly the need of taking into account the altitude effect in Catalonia and, secondly that high and harmful UV levels may occur in the mountain regions.

Situations with large albedo, such as snow-covered surfaces are not considered here. It is known that UVI in these situations is considerably enhanced (as commented in Section 1.6).

Also, it cannot be forgotten that these analyses are only valid for cloudless conditions. If a seasonal cloud climatology was available for Catalonia and used to get typical maps of UVI for all-cloud conditions, that would certainly show lower UVI values than those in Figure 5.9 and with a more or less complex spatial variation.

5.5 Conclusions

In this study a new fast parameterisation of the UV Index, PTUV, is presented, which is based on the TUV radiative transfer model. It has been applied to construct seasonal maps of UV Index for the region of Catalonia. PTUV requires limited input information: *SZA*, *TOZ* and altitude, which can be easily known for a given site. Further, AOD_{368} can either be measured or estimated, and for *SSA*, which is not well known in the UV range, a typical value as reported in the literature can be taken. Despite its simple formulation which is very simple to implement in a computational code, PTUV is able to explain a wide range of cloudless situations although the current implementation excludes cases where the turbidity or surface albedo is high.

An advantage of this parameterisation is the increase in computational speed. In turn this can facilitate, for example, the generation of daily regional forecasts of clear-sky UVI. An alternative approach would have been to pre-calculate multi-dimensional lookup table of UVI values. The advantage of the procedure described here is that it is computational efficient and storage requirements are greatly reduced.

From the comparison with full radiative transfer model calculations using TUV it is concluded that the UVI calculated with PTUV has maximum absolute errors from -0.26 to

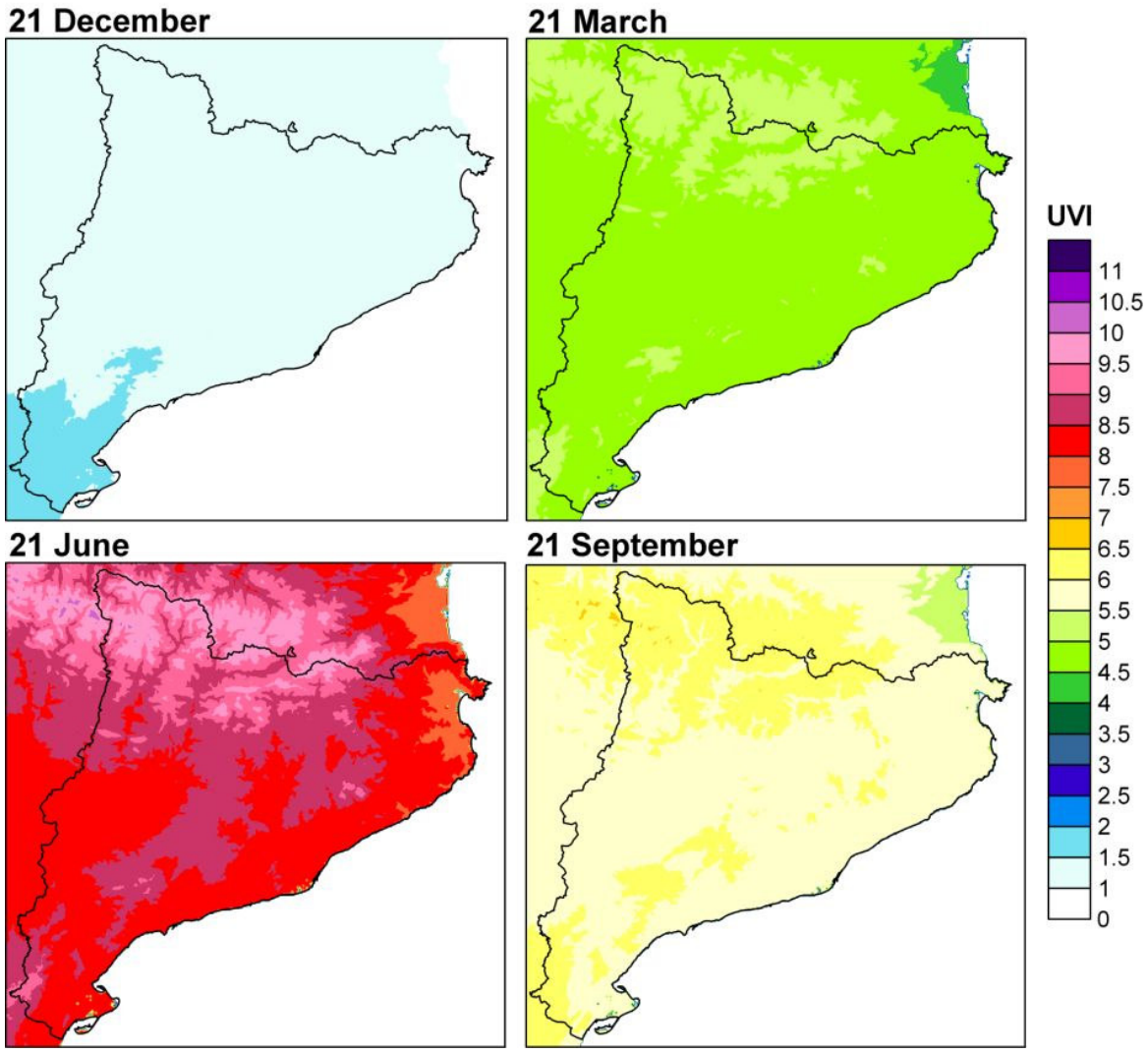

Figure 5.9 Maps of typical UVI for cloudless and snow-free conditions in Catalonia at the solstices and equinoxes with 1x1 km spatial resolution.

0.34 and 99% of the cases within ±0.2. The maximum absolute errors are found for very low values of *SZA*, *TOZ* and *SSA*, which are extreme conditions, together with low values of z.

From the comparison with high quality UVI measurements obtained by the spectroradiometer at Lauder, it is concluded that PTUV performs very similarly to TUV, especially in absolute terms, with maximum model-measurement differences of 0.51 in UVI. From the comparison of PTUV with the UVI measurements in Girona the ability of PTUV to explain quite different aerosol scenarios is illustrated. To estimate *AOD* a simple formula was used, which despite it is not very accurate, resulted to be very useful to explain the changes in aerosol optical depth. Absolute differences of ±0.37 in UVI are found when for each measurement this estimation of AOD_{368} is used. Considerably larger dispersions and absolute errors are found either when climatic AOD_{368} values are used or when the measurements are compared with an empirical formula that implicitly considers aerosols. This result underlines the importance of including aerosol variability when computing UVI.

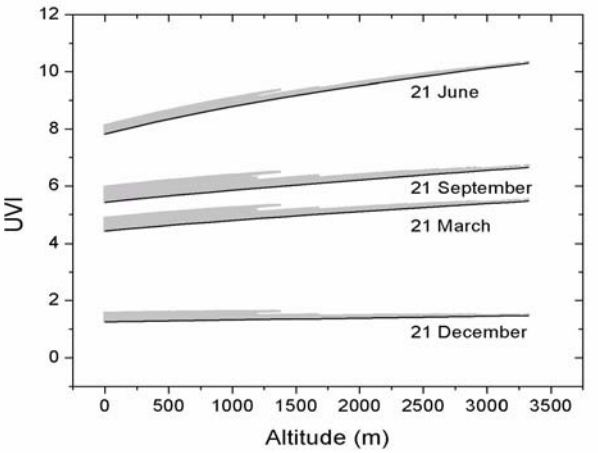

Figure 5.10 UVI for the equinoxes and solstices as a function of altitude. All the values from the maps in Figure 9 are shown in grey; in black, the UVI simulation from 0 to 3325 m at 42.88 degrees of latitude and 0.04 degrees of longitude.

None of the sites considered here is representative of heavily polluted conditions, which would have posed a further challenge for PTUV. Unfortunately, the availability of relevant data from heavily polluted sites is rare. In the future, when suitable data become available, we plan to test PTUV further under more polluted conditions.

Concerning the modelling of the typical UV conditions at Girona, it has been found that the combination of the different annual variations of *SZA*, *TOZ* and *AOD* causes an asymmetric seasonal variation in the noontime UVI annual mean curve, and leads to a long period of about two months (June-July) where the UVI remains close to its maximum values. These results are particularly relevant for the coast of Girona (i.e. Costa Brava) which is a very popular summertime tourist destination.

Another important result from this analysis is that at Girona in summertime the (rather low) *TOZ* variability and the *AOD* variability contribute about equally to the UVI variability. The variability in the total ozone column dominates in the other seasons.

Four seasonal noontime UVI maps for the region of Catalonia have been presented. The winter solstice map shows about 6 times lower values for UVI than the summer solstice map. The spring equinox map has UVI values around one point below the autumn equinox map due to the difference in *TOZ*. The range of UVI over the whole territory is typically less than 1.5, except in the summer when differences up to 2.5 in UVI are found between the coast and the highest mountains. If snow presence had been considered more variation would have been found in wintertime due to the higher UVI values at the mountainous areas.

PTUV could also be used to develop maps of forecasted UVI for a particular region. We expect to be able to test this in future works. For this, the current form of PTUV can be applied directly making assumptions about next day's *TOZ*, *AOD* and *SSA*. For the *TOZ*

prediction, several options are discussed in Annex E for the region of Catalonia. Also, an extension of PTUV to include the surface albedo and cloud effects should be investigated.

5.6 References

Allaart, M., et al. (2004), An empirical model to predict the UV-Index based on the solar zenith angles and total ozone, *Meteorological Applications*, *11*, 59-65.

Badosa, J., and M. van Weele (2002), Effects of aerosols on uv-index, 48 pp, KNMI, De Bilt.

Bodeker, G. E., and R. L. McKenzie (1996), An algorithm for inferring surface UV irradiance including cloud effects, *Journal of Applied Meteorology*, *35*, 1860-1877.

D'Almeida, G. A., et al. (1991), *Atmospheric aerosols: global climatology and radiative characteristics*, 561 pp., A. Deepak Publishing, Virginia, USA.

Fioletov, V. E., et al. (2003), Estimating UV Index Climatology over Canada, *Journal of Applied Meteorology*, *42*, p417.

González, J. A., et al. (2001), Aplicación de métodos basados en medidas radiativas de banda ancha a la determinación de la turbidez atmosférica en Girona. (Application of methods based on broadband radiative measurements and the atmospheric turbidity determination in Girona.), in *El Tiempo del Clima.*, edited by A. J. Pérez-Cueva, et al, pp. 467-475, Asociación Española de Climatología.

Gueymard, C. A. (1998), Turbidity determination from broadband irradiance measurements: A detailed multicoefficient approach, *Journal of Applied Meteorology*, *37*, 414-435.

Gueymard, C. A., and F. Vignola (1998), Determination of atmospheric turbidity from the diffuse-beam broadband irradiance ratio, *Solar Energy*, *63*, 135-146.

Jacobson, M. Z. (1998), Isolating the causes and effects of large ultraviolet reductions in Los Angeles, *J. Aerosol Sci.*, *29*, S655-S656.

Jacobson, M. Z. (1999), Isolating nitrated and aromatic aerosols and nitrated aromatic gases as sources of ultraviolet light absorption, *Journal of Geophysical Research*, *104*, 3527-3542.

Leszczynski, K., et al. (1998), Erythemally weighted radiometers in solar UV monitoring: results from the WMO/STUK intercomparison, *Photochemistry and photobiology*, *67*, 212-221.

Lorente, J. (1978), Contribución al estudio de la turbiedad atmosférica en Barcelona (Contribution to the study of atmospheric turbidity in Barcelona), *Revista de Geofísica*, *2*, 155-167.

McClatchey, R. A., et al. (1972), Optical properties of the atmosphere, *Environment Research Papers*, *411*, 108 pp.

McKenzie, R. L., et al. (2001), Altitude effects on UV spectral irradiance deduced from measurements at Lauder, New Zealand and at Mauna Loa Observatory, Hawaii, *J. Geophys. Res.*, *106*, 22845-22860.

Pedrós, R., et al. (1999), Values of broad band turbidity coefficients in a Mediterranean coastal site, *Solar Light*, *66*, 11-20.

Petters, J. L., et al. (2003), Aerosol single scattering albedo retrieved from measurements of surface UV irradiance and a radiative transfer model, *Journal of Geophysical Research*, *108*, 4288, 4210.1029/2002JD002360.

Pinazo, J. M., et al. (1995), A new method determine Angstrom's turbidity coefficient: its application for Valencia, *Solar Energy*, *54*, 219-226.

Reuder, J., and H. Schwander (1999), Aerosol effects on UV radiation in nonurban regions, *Journal of Geophysical Research*, *104*, 4065-4077.

Schmalwieser, A. W., and G. Schauberger (2001), A monitoring network for erythemally-effective solar ultraviolet radiation in Austria: determination of the measuring sites and visualisation of the spatial distribution, *Theoretical and Applied Climatology*, *69*, 221-229.

Schmalwieser, A. W., et al. (2002), World-wide forecast of the biologically effective UV radiation: UV-index and daily dose, *Procedings of SPIE*, *4482*, 259-264.

Verdebout, J. (2000), A method to generate surface UV radiation maps over Europe using GOME, Meteosat, and ancillary geophysical data, *Journal of Geophysical Research*, *105*, 5049-5058.

Weihs, P., et al. (2002), Effective surface albedo due to snow cover of the surrounding area, *Procedings of SPIE*, *4482*, 152-159.

6
Conclusions

General frame

In the frame of this work, analyses that use different UVI modelling and measuring techniques have been presented. The main objective of the work was to evaluate the agreement that can be obtained between measurements and models for clear-sky conditions.

In Chapter 3, we have discussed the importance of considering spectral correction factors when measuring UVI with erythemal radiometers. Uncertainties associated to a poor characterization of the instruments have been analysed. Measurements from two erythemal radiometers were concurrent together with spectroradiometric UVI measurements. Model-measurement comparisons have been undertaken; for this purpose, the TUV model has been used as the reference.

In Chapter 4, a close model-measurement comparison has been performed between state-of-the-art UVI measurements and modelling considering a broadest range of input information. A strict criterion was used for cloud filtering. Fifteen modelling cases have been considered (1) to analyse the effects of changing different input options and (2) to evaluate the model-measurement agreement. Daily evolutions of the model-measurement agreements have been analysed in detail, showing limitations in both the measurements and the modelling.

In Chapter 5, a new simple parameterisation (PTUV) for fast UVI calculations has been presented. PTUV calculates UVI from a reduced number of input variables: *SZA*, *TOZ*, AOD_{368}, *SSA*, and altitude. PTUV has been compared with the base model (TUV) and also two validation tests have been carried out in order to evaluate its performance against experimental data. As a practical application, PTUV has been used to study the UVI annual evolution for Girona and to build seasonal maps of typical UVI for the region of Catalonia.

6.1 Conclusions

In this study, we have demonstrated the good performance of state-of-the-art clear-sky modelling combined with high quality input information to calculate the erythemal UVI. We have also evaluated the performance that can be expected when simplifications in modelling and input information are assumed. A number of specific conclusions have also been obtained, and are classified here into three topics: UVI modelling, UVI measuring, and the UVI model and measurement comparison.

UVI modelling (from Chapters 4 and 5)

- We have found systematic differences in calculated UVI when considering *TOZ* from TOMS and from Dobson Sunphotometers as input to the model. These differences were in average 2.3% for conditions at Boulder and -4.2% for conditions at Mauna Loa; maximum differences were up to 5.5% and -10%, respectively. The reason for these differences in UVI is the systematic differences in the *TOZ* from TOMS and from Dobson Sunphotometers, with peak differences of -15 DU for Boulder and +24 DU for Mauna Loa. High altitude sites are more affected by differences in the TOZ estimation, probably due to errors in the averaged altitude considered in the TOMS footprints. The opposite sign probably results from the differences in surrounding topography (i.e., Mauna Loa site is higher than most of its surroundings and Boulder site is at lower altitude than part of its surroundings).
- It has been estimated that if the daily change in *TOZ* is not taken into account, that is a single value is considered for the whole day, the corresponding errors of the calculated UVI can be about 5%.
- Knowledge about aerosol information is essential when modelling UVI. Otherwise, if aerosols are neglected, errors up to 27% in UVI can be made, for the range of AOD explored in the present study.
- In this sense, a major modelling issue is the uncertainty in *SSA*. The value of *SSA* has been assumed at 0.9 for the model comparisons in both Chapter 3 and 5. That is a common assumption since the actual value of *SSA* for a certain place and time is usually not known (since it cannot be directly measured). In Chapter 4, we have shown that for some specific sites and days, $SSA = 0.7$ worked better than $SSA = 0.9$, while for other sites and days the opposite is true. We have found that the uncertainty in the actual value of *SSA* can induce uncertainties in modelled UVI up to 11%.
- Still regarding aerosol information, the values of *g* and *alpha* have been considered constant at 0.7 and 1.4, respectively, for all the UVI modelling presented in this work. In Chapter 4, it has been estimated that the uncertainties associated to these assumptions are up to ±3% for *alpha* and ±1% for *g*.
- Related to considering standard ozone and temperature profiles in the modelling instead of introducing measured profiles, the uncertainty in modelled UVI has been estimated to be up to 2.5% for $SZA \leq 75^{o}$.
- The uncertainties associated to considering a typical ground albedo (for non snowy nor sandy surfaces) are estimated to affect by ±1% the value of UVI.

- For Mauna Loa, it has been seen that the effect of clouds that often build up underneath the site on clear days could lead to errors in modelling of up to 9% if the induced increase of effective albedo is not taken into account.
- PTUV, a new simple parameterisation for fast UVI calculations, has been developed by fitting TUV UVI calculations for a wide range of conditions. The main parameters considered by PTUV are *SZA*, *TOZ*, AOD_{368}, *SSA* and altitude. In comparison with TUV, no systematic differences are expected and absolute PTUV-TUV differences are within -0.26 and 0.34 in UVI for all the considered conditions, and are within ±0.2 in UVI for the 99% of conditions.
- PTUV has demonstrated to be useful for particular applications such as to study the annual UVI variation at a particular site (Girona) and to build high resolution maps of typical UVI for a territory (Catalonia), although only for clear-sky conditions. From the first application, we have shown that the maximum annual noon UVI values are extended throughout June and July months and not only around the summer solstice. From the second study, we have found that, in Catalonia, UVI at noon is about 6 times larger in summer than in winter, and that the effect of altitude is relevant, as in summer the UVI on the highest mountains can be up to 2.5 units of UVI larger than the UVI at the coast.

UVI measuring (from Chapters 3 and 4)

- We have confirmed that is essential to know the actual SRF of erythemal radiometers and apply the corresponding spectral correction factors to avoid important errors in the measurement. These errors can be up to 3 units of UVI, depending on the instruments, their SRF, and conditions explored in the present work.
- An erroneous or uncertain measurement of the SRF of an erythemal radiometer can lead to uncertainties in the measured UVI of up to 0.7 in UVI and 25% in relative terms. This was found when comparing three different measurements of the SRF that were available for the same erythemal radiometer.
- From the comparison between concurrent UVI measurements by two erythemal radiometers (a SLC 501 and a YES UVB-1), systematic differences of 7.5% have been found when comparing the whole available datasets and about 10% when comparing the noon data subset. Maximum absolute differences were 1.7 in UVI. Relative differences between the measurements by both erythemal radiometers appeared highly dependent on *SZA* and with values up to 100% for large angles.
- Errors in the spectral and angular corrections applied to the SLC data are most likely the reason for the apparent poor performance of this sensor. Those corrections were calculated taking the spectral and angular responses from a different SLC instrument, which means that it is very important to have each instrument well characterised and that standard, typical, or from-other-instruments responses do not serve the characterisation of a particular sensor. In the particular case of the SLC sensor, its performance could also be affected by changes on ambient temperature and relative humidity, as reported in previous studies and discussed in Chapter 3.
- We have shown that the PTFE diffusers used in the optics of the NIWA spectroradiometers have a temperature dependant transmittance, which has a step change (increment) of 2-3% from about 15 to 21ºC. This temperature dependence

could potentially affect a broad range of geophysical data where PTFE diffusers were used.

UVI model-measurement comparison (from Chapters 3, 4 and 5)

- The best UVI model-measurement global agreements are found when state-of-the-art measurements are considered and both the daily evolutions of *TOZ* and *AOD* are taken into account in the modelling. With these prerequisites, mean agreements range from 0.1 to 3% depending on the considered value of *SSA* (either 0.7 or 0.9). The model results and measurements agree within 5% for more than 90% of the data at pristine sites and for 77% of the data at more polluted sites.
- Data from Melbourne is an exception of the above stated, since larger model-measurement deviations have been found (5-9%), with maximum deviations of 26% and about 1.5 units of UVI. The reason for this is suspected to be errors in either the calibration of the measured UVI or the input aerosol data used at this site.
- As expected, the worst model-measurement agreements are found when the aerosol contribution is not taken into account in the modelling.
- From UVI model vs. measurement analyses that we have carried out by using data from erythemal radiometers, diverse agreements have been found, with regression slopes of -2.3% and +5.5% when using a SLC 501 and a YES UVB-1, respectively. Large dispersions in the model vs. measurement plots have been detected for the SLC data while dispersion is much smaller for the YES data. The relative model-measurement differences shown angular dependence for both SLC and YES data, being much larger the dependence for the former. These dependences were not seen with UVM spectroradiometric data.
- When comparing PTUV with high quality spectroradiometric UVI data, the results turn to be very similar to those when using TUV, with maximum differences between PTUV and TUV of lower than 0.08 in UVI. Maximum differences between the PTUV estimations and the measurements were 0.51 in UVI.
- If PTUV is compared with UVI measurements affected by more aerosols (data measured by an erythemal radiometer at Girona), model and measurements agreements are within -0.90 and +0.42 in UVI when climatic *AOD* information is considered in the modelling. When concurrent *AOD* estimations are taken into account, the agreement is highly improved, to ±0.37 in UVI.

All these conclusions, along with other more specific conclusions, are more extensively explained at the end of Chapters 3, 4, and 5.

In general, and from the above conclusions, it can be stated that the comparison of modelled vs. measured UVI is very useful to detect limitations and estimate uncertainties in both the modelling and the measurements. More specifically, modelling has been used here as a contrast method to reinforce the adoption of spectroradiometry as a reference for the comparison between measurements (as in Chapter 3, comparison between erythemal radiometers and spectroradiometric data); for pristine sites, models can be used for quality control of the measurements (as in Chapter 4, detection of the PTFE temperature effect). Measurements are indispensable to test modelling performance, in particular for polluted conditions (as in Chapter 4, model-measurement for Boulder); in addition, measurements are also very useful to validate new modelling techniques (as in Chapter 5, validation of

PTUV). Regarding the UV measurements, we must insist that calibration accuracy and stability should be improved, as this is a major issue (as commented in Chapter 4).

6.2 Extensions of this work

Next, we list some topics in which the present study could be extended by future research.

Conditions with SZA>80º

For all of the analysis presented in this study, conditions have been restricted to *SZA*<80º. As stated in Chapter 1, main reasons for this choice were that for larger *SZA* conditions, both the modelling and measurements have large errors and there is minor practical interest as the UVI is very close to 0 for these conditions. However, for scientific and technical interests, analyses for *SZA*>80º should be considered in future works.

Higher Aerosol Load

None of the sites considered in this work can be considered as highly polluted. Maximum AOD_{368} value considered for the analyses in Chapter 3 is 0.16 (Lauder), in Chapter 4 is 0.23 (Boulder) and in Chapter 5 is 1.0 (Girona), although the AOD_{368} for Girona rarely exceeds 0.6. Analyses with higher *AOD* values are needed in order to test the performance of UVI modelling by comparing with UVI measurements affected by a larger aerosol load. It is expected that for larger *AOD*s the modelling accuracy becomes more compromised since the above commented uncertainties in *alpha*, and most of all, in *SSA*, have larger effect for larger *AOD*s. Also, the performance of PTUV for larger *AOD* scenarios should be tested in order to extend its validation.

Investigation of the actual value of SSA

As commented above, for some sites and moments, considering *SSA* = 0.7 improves the model-measurement agreement in respect of assuming *SSA* = 0.9 and vice versa. The actual effective *SSA* value in the UV range for a particular place and time is highly uncertain and we have shown that this is an important source of uncertainty in the UVI modelling. The *SSA* value depends on the type of aerosols and this could be linked with the type and origin of air masses. In this sense, it could be investigated how the *SSA* value is related to the different catalogued types of air masses brought by the wind; results of this investigation could then be used to have a more accurate estimation of the actual *SSA* value at any time..

High albedo conditions

For all the analyses presented, low ground albedo values (0.02 and 0.05) have been considered for the UVI modelling. When the ground was covered by frost (one day in Chapter 3) or by snow (one day in Chapter 4), large model-measurement differences, down to about - 20-30%, were obtained, due to not considering the increase in the albedo. Analysis of the ground albedo values to be considered in such conditions should be carried out. Moreover, an extension of PTUV to account for changes in ground albedo should also be considered.

Cloudy conditions

Cloudy situations have been filtered out for all the presented analyses because of reasons commented in Chapter 1. However, clouds highly affect UVI reaching the ground and,

actually, the great majority of situations are somehow affected by clouds. Since the cloud effects on UVI are highly variable in time, measuring UVI with slow scanning spectroradiometers (that take few minutes for each scan) can lead to large and random uncertainties. Therefore, erythemal radiometers (provided that they are well characterised) can be very useful as they can take instantaneous measurements. Also, since PTUV is only prepared to calculate UVI under cloudless conditions, the incorporation of the cloud effects in the parameterisation should be investigated.

Instrumental improvements

In Chapter 3 we have investigated the performance of two erythemal radiometers paying special attention on the spectral corrections and just briefly commenting the angular corrections. The latter should be investigated in more detail, in particular to see its contribution on the results obtained in the model-measurement comparisons. In this sense, more analyses are needed in order to better understand the dependences observed for both the YES data (mainly angular dependences) and the SLC data (model-measurement differences, were found to be correlated with *SZA*, *TOZ*, air temperature and relative humidity).

In relation to the recently discovered temperature effect of the PTFE diffusers, the possibility that this affects other instruments (such as some spectroradiometers and some erythemal radiometers) should be investigated. Also, corrections should be applied to the existing datasets so relations of the change in the throughput with the air temperature and maybe other variables (such as wind speed and thermal couplings) should be established. In the future, the best option would be to stabilise the PTFE diffusers at temperatures above 21ºC when possible or to start monitoring the actual temperature of the PTFE diffusers and apply corrections to the data.

Annex A: Web Resources on UVI, health effects of UVR and protection advises

Institution	Year	Document titles and internet link
ICNIRP	2004	Guidelines on limits of exposure to ultraviolet radiation of wavelengths between 180 nm and 400 nm (incoherent optical radiation) http://www.icnirp.de/documents/UV2004.pdf
WHO	2003	Sun protection and schools – How to make a difference http://www.who.int/uv/publications/en/sunprotschools.pdf Sun protection: A primary teaching resource http://www.who.int/uv/publications/en/primaryteach.pdf Evaluating school programmes to promote sun protection http://www.who.int/uv/publications/en/schoolprog.pdf
INTERSUN	2003	The global UV project. A guide and compendium http://www.who.int/uv/publications/en/Intersunguide.pdf
WHO	2002	Guidelines for tour operators http://www.who.int/uv/publications/en/touroperators.pdf Sun protection message for tourists http://www.who.int/uv/publications/en/tourists.pdf
WHO / WMO UNEP / ICNIRP	2002	Global solar UV Index. A practical guide http://www.who.int/uv/publications/en/GlobalUVI.pdf The UV index sun protection table—notes on supplied clipart http://www.who.int/uv/publications/en/UVIclip.pdf http://www.who.int/docstore/peh-uv/UVIndex_Graphics/gif/
INM*	2002	Indice UV para la población (UV Index for the population) http://www.inm.es/uvi/manual_UVI_nacional.pdf
IARC	2001	IARC Summary Recommendations for Public Health Action http://www.iarc.fr/IARCPress/general/prev.pdf http://www.who.int/uv/resources/recommendations/en/IARCSum.pdf
COST-713	2000	UV-Index for the public http://www.lamma.rete.toscana.it/uvweb/uvbooklet/index.htm
IPCS	1994	Environmental Health Criteria (EHC) 160: Ultraviolet radiation http://www.inchem.org/documents/ehc/ehc/ehc160.htm

*National Meteorological Institute, Spain

Other educational resources on Internet (in English)

Organization, Country	Internet site
The Cancer council, Victoria, Australia	www.sunsmart.com.au
Cancer Council, South Australia, Australia	www.cancersa.org.au/
Irish cancer society, Ireland	www.cancer.ie/sunsmart/
Health Sponsorship Council, New Zealand	www.sunsmart.co.nz
Cancer Research UK, United Kingdom	www.sunsmart.org.uk

Annex B: Spectral Correction Factor Tables For Three Erythemal Radiometers

The following are tables with the spectral correction factors ($N_i(SZA,TOZ,SZA_{cal},TOZ_{cal})$) as a function of *SZA* (in degrees, columns) and *TOZ* (in DU, rows) for the five spectral response functions discussed in Chapter 3. The factors are normalised to 1 at 30º of *SZA* and 300 DU. Plots in Figures 3.1 and 3.2 are shown again.

Table B.1 Spectral correction factors for YES92

	0	5	10	15	20	25	30	35	40	45	50	55	60	65	70	75	80	85
200	1.22	1.22	1.21	1.20	1.19	1.17	1.15	1.12	1.10	1.07	1.04	1.00	0.97	0.94	0.93	0.92	0.95	1.03
210	1.19	1.19	1.19	1.18	1.16	1.15	1.13	1.11	1.08	1.05	1.02	0.99	0.96	0.94	0.92	0.92	0.95	1.04
220	1.17	1.17	1.16	1.16	1.14	1.13	1.11	1.09	1.06	1.03	1.01	0.98	0.95	0.93	0.92	0.92	0.96	1.05
230	1.15	1.15	1.14	1.14	1.12	1.11	1.09	1.07	1.05	1.02	0.99	0.97	0.94	0.93	0.92	0.93	0.97	1.06
240	1.13	1.13	1.13	1.12	1.11	1.09	1.07	1.05	1.03	1.01	0.98	0.96	0.94	0.92	0.92	0.93	0.97	1.07
250	1.12	1.11	1.11	1.10	1.09	1.08	1.06	1.04	1.02	1.00	0.97	0.95	0.93	0.92	0.92	0.93	0.98	1.09
260	1.10	1.10	1.09	1.09	1.07	1.06	1.05	1.03	1.01	0.99	0.96	0.94	0.93	0.92	0.92	0.94	0.99	1.10
270	1.08	1.08	1.08	1.07	1.06	1.05	1.03	1.01	1.00	0.98	0.96	0.94	0.92	0.91	0.92	0.94	1.00	1.11
280	1.07	1.07	1.06	1.06	1.05	1.04	1.02	1.00	0.99	0.97	0.95	0.93	0.92	0.91	0.92	0.95	1.01	1.13
290	1.06	1.06	1.05	1.05	1.04	1.02	1.01	0.99	0.98	0.96	0.94	0.93	0.92	0.91	0.92	0.95	1.02	1.14
300	1.05	1.04	1.04	1.03	1.02	1.01	1.00	0.99	0.97	0.95	0.94	0.92	0.91	0.91	0.92	0.96	1.03	1.15
310	1.03	1.03	1.03	1.02	1.01	1.00	0.99	0.97	0.96	0.95	0.93	0.92	0.91	0.91	0.93	0.96	1.04	1.17
320	1.02	1.02	1.02	1.01	1.00	0.99	0.98	0.97	0.95	0.94	0.93	0.92	0.91	0.91	0.93	0.97	1.05	1.18
330	1.01	1.01	1.01	1.00	1.00	0.99	0.97	0.96	0.95	0.93	0.92	0.91	0.91	0.91	0.93	0.98	1.06	1.20
340	1.01	1.00	1.00	1.00	0.99	0.98	0.97	0.96	0.94	0.93	0.92	0.91	0.91	0.92	0.94	0.98	1.07	1.21
350	1.00	1.00	0.99	0.99	0.98	0.97	0.96	0.95	0.94	0.93	0.92	0.91	0.91	0.92	0.94	0.99	1.08	1.22
360	0.99	0.99	0.98	0.98	0.97	0.96	0.95	0.94	0.93	0.92	0.91	0.91	0.91	0.92	0.95	1.00	1.09	1.24
370	0.98	0.98	0.98	0.97	0.97	0.96	0.95	0.94	0.93	0.92	0.91	0.91	0.91	0.92	0.95	1.01	1.10	1.25
380	0.97	0.97	0.97	0.97	0.96	0.95	0.94	0.93	0.92	0.92	0.91	0.91	0.91	0.92	0.96	1.02	1.11	1.27
390	0.97	0.97	0.96	0.96	0.95	0.95	0.94	0.93	0.92	0.91	0.91	0.91	0.91	0.93	0.96	1.02	1.13	1.28
400	0.96	0.96	0.96	0.95	0.95	0.94	0.93	0.93	0.92	0.91	0.91	0.91	0.91	0.93	0.97	1.03	1.14	1.30
410	0.96	0.96	0.95	0.95	0.94	0.94	0.93	0.92	0.92	0.91	0.91	0.91	0.91	0.93	0.97	1.04	1.15	1.31
420	0.95	0.95	0.95	0.94	0.94	0.93	0.93	0.92	0.91	0.91	0.90	0.91	0.92	0.94	0.98	1.05	1.16	1.33
430	0.95	0.95	0.94	0.94	0.94	0.93	0.92	0.92	0.91	0.91	0.90	0.91	0.92	0.94	0.98	1.06	1.17	1.34
440	0.94	0.94	0.94	0.94	0.93	0.93	0.92	0.91	0.91	0.90	0.90	0.91	0.92	0.95	0.99	1.07	1.18	1.35
450	0.94	0.94	0.94	0.93	0.93	0.92	0.92	0.91	0.91	0.90	0.90	0.91	0.92	0.95	1.00	1.07	1.19	1.37
460	0.93	0.93	0.93	0.93	0.92	0.92	0.91	0.91	0.91	0.90	0.90	0.91	0.93	0.95	1.00	1.08	1.21	1.38
470	0.93	0.93	0.93	0.93	0.92	0.92	0.91	0.91	0.90	0.90	0.91	0.91	0.93	0.96	1.01	1.09	1.22	1.40
480	0.93	0.93	0.92	0.92	0.92	0.91	0.91	0.91	0.90	0.90	0.91	0.91	0.93	0.96	1.02	1.10	1.23	1.41
490	0.92	0.92	0.92	0.92	0.92	0.91	0.91	0.91	0.90	0.90	0.91	0.92	0.94	0.97	1.02	1.11	1.24	1.42
500	0.92	0.92	0.92	0.92	0.91	0.91	0.91	0.90	0.90	0.90	0.91	0.92	0.94	0.97	1.03	1.12	1.25	1.44

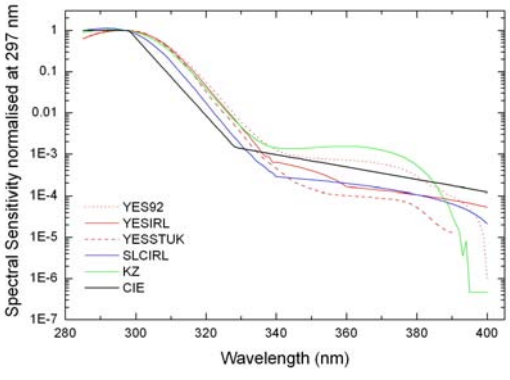

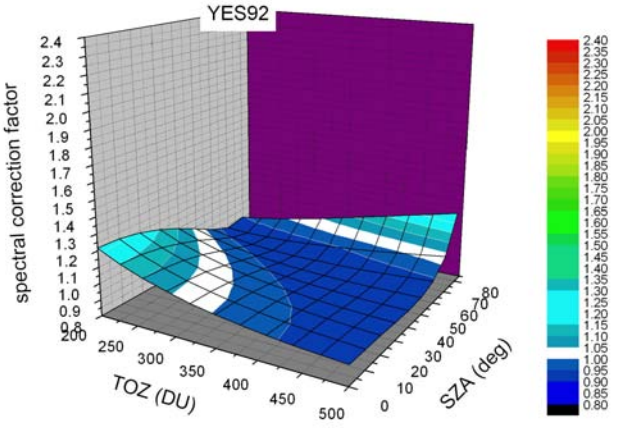

Table B.2 Spectral correction factors for YESIRL

	0	5	10	15	20	25	30	35	40	45	50	55	60	65	70	75	80	85
200	1.18	1.18	1.17	1.16	1.15	1.14	1.12	1.10	1.08	1.05	1.03	1.00	0.98	0.97	0.96	0.98	1.03	1.15
210	1.16	1.16	1.15	1.14	1.13	1.12	1.10	1.09	1.06	1.04	1.02	0.99	0.98	0.96	0.96	0.98	1.04	1.17
220	1.14	1.14	1.13	1.13	1.12	1.10	1.09	1.07	1.05	1.03	1.01	0.99	0.97	0.96	0.96	0.99	1.06	1.19
230	1.12	1.12	1.12	1.11	1.10	1.09	1.07	1.06	1.04	1.02	1.00	0.98	0.96	0.96	0.97	1.00	1.07	1.21
240	1.11	1.10	1.10	1.09	1.08	1.07	1.06	1.04	1.02	1.01	0.99	0.97	0.96	0.96	0.97	1.01	1.08	1.23
250	1.09	1.09	1.09	1.08	1.07	1.06	1.05	1.03	1.01	1.00	0.98	0.97	0.96	0.96	0.97	1.01	1.10	1.25
260	1.08	1.08	1.07	1.07	1.06	1.05	1.04	1.02	1.01	0.99	0.98	0.96	0.96	0.96	0.98	1.02	1.11	1.28
270	1.07	1.07	1.06	1.06	1.05	1.04	1.03	1.01	1.00	0.98	0.97	0.96	0.96	0.96	0.98	1.03	1.13	1.30
280	1.06	1.05	1.05	1.04	1.04	1.03	1.02	1.00	0.99	0.98	0.97	0.96	0.95	0.96	0.99	1.04	1.15	1.32
290	1.04	1.04	1.04	1.03	1.03	1.02	1.01	1.00	0.98	0.97	0.96	0.95	0.95	0.97	0.99	1.05	1.16	1.34
300	1.04	1.03	1.03	1.03	1.02	1.01	1.00	0.99	0.98	0.97	0.96	0.95	0.96	0.97	1.00	1.06	1.18	1.37
310	1.03	1.03	1.02	1.02	1.01	1.00	0.99	0.98	0.97	0.96	0.96	0.95	0.96	0.97	1.01	1.08	1.20	1.39
320	1.02	1.02	1.01	1.01	1.00	1.00	0.99	0.98	0.97	0.96	0.95	0.95	0.96	0.98	1.02	1.09	1.21	1.42
330	1.01	1.01	1.01	1.00	1.00	0.99	0.98	0.97	0.96	0.96	0.95	0.95	0.96	0.98	1.02	1.10	1.23	1.44
340	1.00	1.00	1.00	1.00	0.99	0.98	0.98	0.97	0.96	0.95	0.95	0.95	0.96	0.99	1.03	1.11	1.25	1.47
350	1.00	1.00	0.99	0.99	0.98	0.98	0.97	0.96	0.96	0.95	0.95	0.95	0.97	0.99	1.04	1.13	1.27	1.49
360	0.99	0.99	0.99	0.98	0.98	0.97	0.97	0.96	0.96	0.95	0.95	0.96	0.97	1.00	1.05	1.14	1.29	1.52
370	0.99	0.98	0.98	0.98	0.97	0.97	0.96	0.96	0.95	0.95	0.95	0.96	0.97	1.00	1.06	1.15	1.31	1.54
380	0.98	0.98	0.98	0.97	0.97	0.97	0.96	0.96	0.95	0.95	0.95	0.96	0.98	1.01	1.07	1.17	1.32	1.57
390	0.98	0.98	0.97	0.97	0.97	0.96	0.96	0.95	0.95	0.95	0.95	0.96	0.98	1.02	1.08	1.18	1.34	1.59
400	0.97	0.97	0.97	0.97	0.96	0.96	0.96	0.95	0.95	0.95	0.95	0.96	0.98	1.02	1.09	1.19	1.36	1.62
410	0.97	0.97	0.97	0.96	0.96	0.96	0.95	0.95	0.95	0.95	0.95	0.97	0.99	1.03	1.10	1.21	1.38	1.64
420	0.96	0.96	0.96	0.96	0.96	0.95	0.95	0.95	0.95	0.95	0.96	0.97	0.99	1.04	1.11	1.22	1.40	1.67
430	0.96	0.96	0.96	0.96	0.96	0.95	0.95	0.95	0.95	0.95	0.96	0.97	1.00	1.04	1.12	1.24	1.42	1.69
440	0.96	0.96	0.96	0.96	0.95	0.95	0.95	0.95	0.95	0.95	0.96	0.98	1.00	1.05	1.13	1.25	1.44	1.72
450	0.96	0.96	0.95	0.95	0.95	0.95	0.95	0.95	0.95	0.95	0.96	0.98	1.01	1.06	1.14	1.26	1.46	1.74
460	0.95	0.95	0.95	0.95	0.95	0.95	0.95	0.95	0.95	0.95	0.96	0.98	1.02	1.07	1.15	1.28	1.48	1.77
470	0.95	0.95	0.95	0.95	0.95	0.95	0.95	0.95	0.95	0.96	0.97	0.99	1.02	1.08	1.16	1.29	1.50	1.79
480	0.95	0.95	0.95	0.95	0.95	0.95	0.95	0.95	0.95	0.96	0.97	0.99	1.03	1.08	1.17	1.31	1.52	1.82
490	0.95	0.95	0.95	0.95	0.95	0.95	0.95	0.95	0.95	0.96	0.97	1.00	1.03	1.09	1.18	1.32	1.54	1.85
500	0.95	0.95	0.95	0.95	0.95	0.95	0.95	0.95	0.95	0.96	0.98	1.00	1.04	1.10	1.19	1.34	1.56	1.87

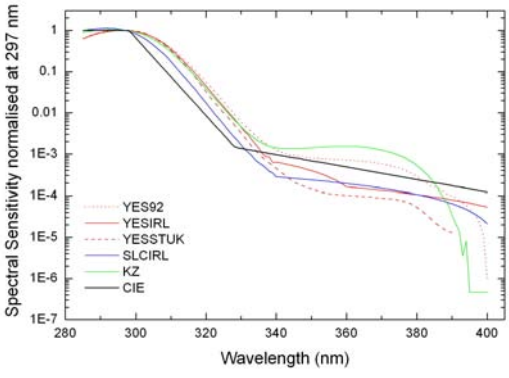

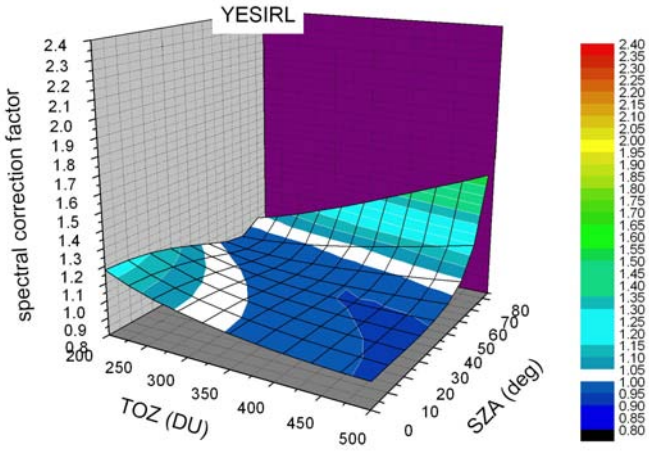

Table B.3 Spectral correction factors for YESSTUK

	0	5	10	15	20	25	30	35	40	45	50	55	60	65	70	75	80	85
200	1.14	1.14	1.13	1.13	1.12	1.11	1.09	1.08	1.06	1.04	1.02	1.01	0.99	0.99	1.00	1.04	1.12	1.28
210	1.12	1.12	1.12	1.11	1.10	1.09	1.08	1.07	1.05	1.03	1.01	1.00	0.99	0.99	1.00	1.05	1.14	1.31
220	1.11	1.11	1.10	1.10	1.09	1.08	1.07	1.05	1.04	1.02	1.01	0.99	0.99	0.99	1.01	1.06	1.16	1.34
230	1.09	1.09	1.09	1.08	1.08	1.07	1.05	1.04	1.03	1.01	1.00	0.99	0.99	0.99	1.02	1.07	1.18	1.37
240	1.08	1.08	1.08	1.07	1.06	1.05	1.04	1.03	1.02	1.01	0.99	0.99	0.98	0.99	1.02	1.08	1.20	1.40
250	1.07	1.07	1.07	1.06	1.05	1.04	1.03	1.02	1.01	1.00	0.99	0.98	0.99	1.00	1.03	1.10	1.22	1.43
260	1.06	1.06	1.05	1.05	1.04	1.04	1.03	1.02	1.00	0.99	0.99	0.98	0.99	1.00	1.04	1.11	1.25	1.46
270	1.05	1.05	1.05	1.04	1.03	1.03	1.02	1.01	1.00	0.99	0.98	0.98	0.99	1.01	1.05	1.13	1.27	1.49
280	1.04	1.04	1.04	1.03	1.03	1.02	1.01	1.00	0.99	0.99	0.98	0.98	0.99	1.01	1.06	1.15	1.29	1.53
290	1.03	1.03	1.03	1.02	1.02	1.01	1.01	1.00	0.99	0.98	0.98	0.98	1.00	1.02	1.07	1.16	1.32	1.56
300	1.02	1.02	1.02	1.02	1.01	1.01	1.00	0.99	0.99	0.98	0.98	0.99	1.00	1.03	1.08	1.18	1.34	1.60
310	1.02	1.02	1.02	1.01	1.01	1.00	1.00	0.99	0.98	0.98	0.98	0.99	1.00	1.04	1.09	1.20	1.37	1.63
320	1.01	1.01	1.01	1.01	1.00	1.00	0.99	0.99	0.98	0.98	0.98	0.99	1.01	1.04	1.11	1.21	1.39	1.67
330	1.01	1.01	1.00	1.00	1.00	0.99	0.99	0.98	0.98	0.98	0.98	0.99	1.01	1.05	1.12	1.23	1.42	1.70
340	1.00	1.00	1.00	1.00	0.99	0.99	0.99	0.98	0.98	0.98	0.98	1.00	1.02	1.06	1.13	1.25	1.45	1.74
350	1.00	1.00	1.00	0.99	0.99	0.99	0.98	0.98	0.98	0.98	0.99	1.00	1.03	1.07	1.15	1.27	1.47	1.77
360	0.99	0.99	0.99	0.99	0.99	0.98	0.98	0.98	0.98	0.98	0.99	1.00	1.03	1.08	1.16	1.29	1.50	1.81
370	0.99	0.99	0.99	0.99	0.98	0.98	0.98	0.98	0.98	0.98	0.99	1.01	1.04	1.09	1.17	1.31	1.53	1.85
380	0.99	0.99	0.99	0.98	0.98	0.98	0.98	0.98	0.98	0.98	0.99	1.01	1.05	1.10	1.19	1.33	1.56	1.88
390	0.98	0.98	0.98	0.98	0.98	0.98	0.98	0.98	0.98	0.99	1.00	1.02	1.05	1.11	1.20	1.35	1.58	1.92
400	0.98	0.98	0.98	0.98	0.98	0.98	0.98	0.98	0.98	0.99	1.00	1.02	1.06	1.12	1.22	1.37	1.61	1.96
410	0.98	0.98	0.98	0.98	0.98	0.98	0.98	0.98	0.98	0.99	1.00	1.03	1.07	1.13	1.23	1.39	1.64	1.99
420	0.98	0.98	0.98	0.98	0.98	0.98	0.98	0.98	0.98	0.99	1.01	1.04	1.08	1.14	1.25	1.41	1.67	2.03
430	0.98	0.98	0.98	0.98	0.98	0.98	0.98	0.98	0.99	1.00	1.01	1.04	1.09	1.15	1.26	1.43	1.70	2.07
440	0.98	0.98	0.98	0.98	0.97	0.98	0.98	0.98	0.99	1.00	1.02	1.05	1.09	1.17	1.28	1.45	1.73	2.11
450	0.97	0.97	0.97	0.97	0.97	0.98	0.98	0.98	0.99	1.00	1.02	1.05	1.10	1.18	1.29	1.48	1.76	2.14
460	0.97	0.97	0.97	0.97	0.98	0.98	0.98	0.98	0.99	1.01	1.03	1.06	1.11	1.19	1.31	1.50	1.79	2.18
470	0.97	0.97	0.97	0.97	0.98	0.98	0.98	0.99	1.00	1.01	1.03	1.07	1.12	1.20	1.33	1.52	1.82	2.22
480	0.97	0.97	0.97	0.97	0.98	0.98	0.98	0.99	1.00	1.01	1.04	1.08	1.13	1.21	1.34	1.54	1.84	2.26
490	0.97	0.97	0.97	0.98	0.98	0.98	0.98	0.99	1.00	1.02	1.04	1.08	1.14	1.23	1.36	1.56	1.87	2.29
500	0.97	0.97	0.98	0.98	0.98	0.98	0.99	0.99	1.01	1.02	1.05	1.09	1.15	1.24	1.38	1.59	1.90	2.33

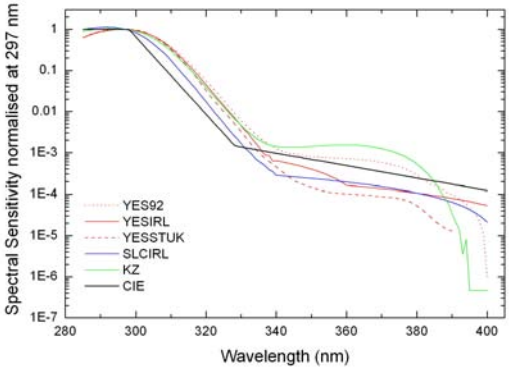

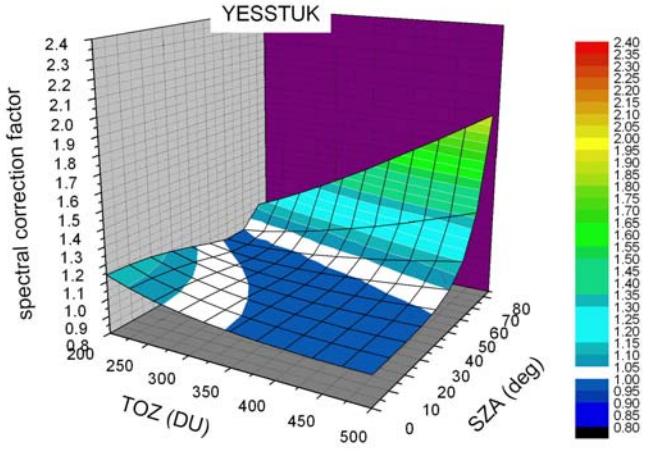

Table B.4 Spectral correction factors for SLCIRL

	0	5	10	15	20	25	30	35	40	45	50	55	60	65	70	75	80	85
200	1.06	1.06	1.06	1.05	1.05	1.04	1.04	1.03	1.02	1.01	1.01	1.00	1.01	1.02	1.04	1.09	1.18	1.31
210	1.05	1.05	1.05	1.05	1.04	1.04	1.03	1.03	1.02	1.01	1.01	1.00	1.01	1.02	1.05	1.10	1.20	1.34
220	1.04	1.04	1.04	1.04	1.04	1.03	1.02	1.02	1.01	1.01	1.00	1.00	1.01	1.02	1.06	1.12	1.22	1.37
230	1.04	1.04	1.04	1.03	1.03	1.02	1.02	1.01	1.01	1.00	1.00	1.00	1.01	1.03	1.07	1.13	1.24	1.40
240	1.03	1.03	1.03	1.03	1.02	1.02	1.01	1.01	1.01	1.00	1.00	1.01	1.02	1.04	1.08	1.15	1.26	1.42
250	1.03	1.03	1.02	1.02	1.02	1.02	1.01	1.01	1.00	1.00	1.00	1.01	1.02	1.04	1.09	1.16	1.28	1.45
260	1.02	1.02	1.02	1.02	1.01	1.01	1.01	1.01	1.00	1.00	1.00	1.01	1.02	1.05	1.10	1.18	1.30	1.48
270	1.02	1.02	1.02	1.01	1.01	1.01	1.01	1.00	1.00	1.00	1.00	1.01	1.03	1.06	1.11	1.19	1.33	1.51
280	1.01	1.01	1.01	1.01	1.01	1.01	1.00	1.00	1.00	1.00	1.01	1.02	1.04	1.07	1.12	1.21	1.35	1.54
290	1.01	1.01	1.01	1.01	1.01	1.00	1.00	1.00	1.00	1.00	1.01	1.02	1.04	1.08	1.13	1.23	1.37	1.57
300	1.01	1.01	1.01	1.00	1.00	1.00	1.00	1.00	1.00	1.00	1.01	1.02	1.05	1.09	1.15	1.24	1.39	1.60
310	1.00	1.00	1.00	1.00	1.00	1.00	1.00	1.00	1.00	1.01	1.01	1.03	1.05	1.10	1.16	1.26	1.42	1.62
320	1.00	1.00	1.00	1.00	1.00	1.00	1.00	1.00	1.00	1.01	1.02	1.03	1.06	1.11	1.17	1.28	1.44	1.65
330	1.00	1.00	1.00	1.00	1.00	1.00	1.00	1.00	1.00	1.01	1.02	1.04	1.07	1.11	1.19	1.30	1.46	1.68
340	1.00	1.00	1.00	1.00	1.00	1.00	1.00	1.00	1.01	1.01	1.02	1.04	1.08	1.13	1.20	1.32	1.49	1.71
350	1.00	1.00	1.00	1.00	1.00	1.00	1.00	1.00	1.01	1.02	1.03	1.05	1.08	1.14	1.21	1.33	1.51	1.74
360	1.00	1.00	1.00	1.00	1.00	1.00	1.00	1.00	1.01	1.02	1.03	1.06	1.09	1.15	1.23	1.35	1.53	1.77
370	1.00	1.00	1.00	1.00	1.00	1.00	1.00	1.01	1.01	1.02	1.04	1.06	1.10	1.16	1.24	1.37	1.56	1.80
380	1.00	1.00	1.00	1.00	1.00	1.00	1.00	1.01	1.01	1.03	1.04	1.07	1.11	1.17	1.26	1.39	1.58	1.82
390	1.00	1.00	1.00	1.00	1.00	1.00	1.00	1.01	1.02	1.03	1.05	1.08	1.12	1.18	1.27	1.41	1.60	1.85
400	1.00	1.00	1.00	1.00	1.00	1.00	1.01	1.01	1.02	1.03	1.05	1.08	1.13	1.19	1.28	1.42	1.62	1.88
410	1.00	1.00	1.00	1.00	1.00	1.00	1.01	1.02	1.02	1.04	1.06	1.09	1.14	1.20	1.30	1.44	1.65	1.91
420	1.00	1.00	1.00	1.00	1.00	1.01	1.01	1.02	1.03	1.04	1.07	1.10	1.14	1.21	1.31	1.46	1.67	1.93
430	1.00	1.00	1.00	1.00	1.00	1.01	1.01	1.02	1.03	1.05	1.07	1.10	1.15	1.22	1.33	1.48	1.69	1.96
440	1.00	1.00	1.00	1.00	1.01	1.01	1.02	1.02	1.04	1.05	1.08	1.11	1.16	1.24	1.34	1.50	1.72	1.99
450	1.00	1.00	1.00	1.01	1.01	1.01	1.02	1.03	1.04	1.06	1.08	1.12	1.17	1.25	1.36	1.52	1.74	2.02
460	1.00	1.00	1.01	1.01	1.01	1.01	1.02	1.03	1.04	1.06	1.09	1.13	1.18	1.26	1.37	1.54	1.76	2.04
470	1.01	1.01	1.01	1.01	1.01	1.02	1.02	1.03	1.05	1.07	1.10	1.14	1.19	1.27	1.39	1.55	1.79	2.07
480	1.01	1.01	1.01	1.01	1.01	1.02	1.03	1.04	1.05	1.07	1.10	1.14	1.20	1.28	1.40	1.57	1.81	2.09
490	1.01	1.01	1.01	1.01	1.02	1.02	1.03	1.04	1.06	1.08	1.11	1.15	1.21	1.30	1.42	1.59	1.83	2.12
500	1.01	1.01	1.01	1.02	1.02	1.03	1.03	1.05	1.06	1.09	1.12	1.16	1.22	1.31	1.43	1.61	1.85	2.15

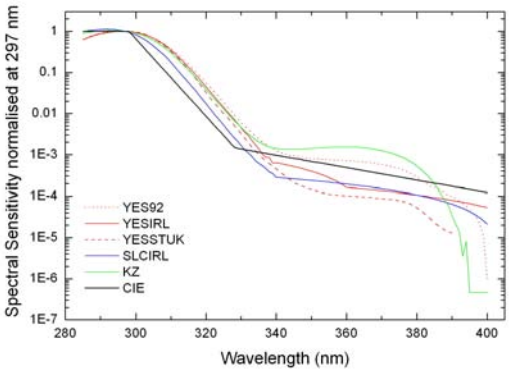

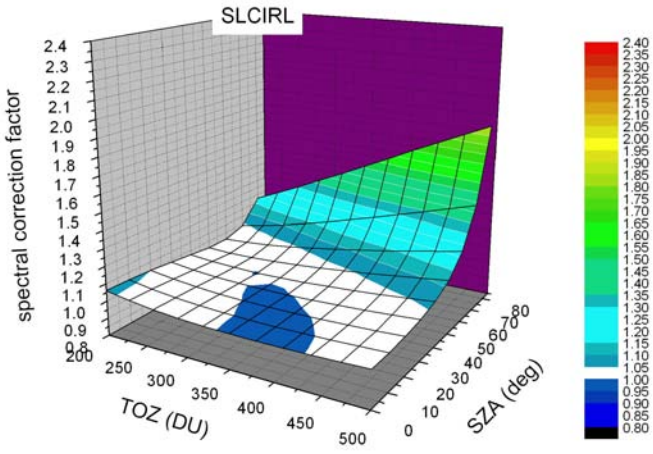

Table B.5 Spectral correction factors for KZ

	0	5	10	15	20	25	30	35	40	45	50	55	60	65	70	75	80	85
200	1.19	1.18	1.18	1.17	1.16	1.15	1.13	1.11	1.08	1.06	1.03	1.00	0.97	0.95	0.93	0.93	0.94	0.99
210	1.17	1.16	1.16	1.15	1.14	1.13	1.11	1.10	1.07	1.04	1.02	0.99	0.97	0.94	0.93	0.93	0.94	1.00
220	1.15	1.15	1.14	1.13	1.12	1.11	1.09	1.07	1.05	1.03	1.00	0.98	0.96	0.94	0.93	0.93	0.95	1.00
230	1.13	1.13	1.12	1.12	1.11	1.09	1.08	1.06	1.04	1.02	0.99	0.97	0.95	0.93	0.92	0.93	0.95	1.01
240	1.11	1.11	1.11	1.10	1.09	1.08	1.06	1.05	1.03	1.01	0.98	0.96	0.94	0.93	0.92	0.93	0.96	1.01
250	1.10	1.10	1.09	1.09	1.08	1.07	1.05	1.03	1.02	1.00	0.98	0.96	0.94	0.93	0.92	0.93	0.96	1.02
260	1.09	1.08	1.08	1.07	1.06	1.05	1.04	1.03	1.01	0.99	0.97	0.95	0.93	0.92	0.92	0.93	0.96	1.03
270	1.07	1.07	1.07	1.06	1.05	1.04	1.03	1.01	1.00	0.98	0.96	0.94	0.93	0.92	0.92	0.93	0.97	1.03
280	1.06	1.06	1.06	1.05	1.04	1.03	1.02	1.00	0.99	0.97	0.95	0.94	0.93	0.92	0.92	0.94	0.98	1.04
290	1.05	1.05	1.05	1.04	1.03	1.02	1.01	0.99	0.98	0.96	0.95	0.93	0.92	0.92	0.92	0.94	0.98	1.05
300	1.04	1.04	1.04	1.03	1.02	1.01	1.00	0.99	0.97	0.96	0.94	0.93	0.92	0.92	0.92	0.94	0.99	1.05
310	1.03	1.03	1.03	1.02	1.01	1.00	0.99	0.98	0.97	0.95	0.94	0.93	0.92	0.92	0.93	0.95	0.99	1.06
320	1.02	1.02	1.02	1.01	1.00	1.00	0.98	0.97	0.96	0.95	0.93	0.92	0.92	0.92	0.93	0.95	1.00	1.07
330	1.01	1.01	1.01	1.00	1.00	0.99	0.98	0.97	0.95	0.94	0.93	0.92	0.92	0.92	0.93	0.96	1.00	1.07
340	1.00	1.00	1.00	1.00	0.99	0.98	0.97	0.96	0.95	0.94	0.93	0.92	0.92	0.92	0.93	0.96	1.01	1.08
350	1.00	1.00	0.99	0.99	0.98	0.97	0.97	0.96	0.94	0.93	0.93	0.92	0.92	0.92	0.93	0.96	1.01	1.09
360	0.99	0.99	0.99	0.98	0.98	0.97	0.96	0.95	0.94	0.93	0.92	0.92	0.92	0.92	0.94	0.97	1.02	1.09
370	0.98	0.98	0.98	0.98	0.97	0.96	0.96	0.95	0.94	0.93	0.92	0.92	0.92	0.92	0.94	0.97	1.03	1.10
380	0.98	0.98	0.98	0.97	0.97	0.96	0.95	0.94	0.93	0.93	0.92	0.91	0.92	0.92	0.94	0.98	1.03	1.10
390	0.97	0.97	0.97	0.97	0.96	0.95	0.95	0.94	0.93	0.92	0.92	0.91	0.92	0.93	0.95	0.98	1.04	1.11
400	0.97	0.97	0.96	0.96	0.96	0.95	0.94	0.94	0.93	0.92	0.92	0.91	0.92	0.93	0.95	0.99	1.04	1.12
410	0.96	0.96	0.96	0.96	0.95	0.95	0.94	0.93	0.93	0.92	0.91	0.91	0.92	0.93	0.95	0.99	1.05	1.12
420	0.96	0.96	0.96	0.95	0.95	0.94	0.94	0.93	0.92	0.92	0.91	0.91	0.92	0.93	0.96	1.00	1.05	1.13
430	0.95	0.95	0.95	0.95	0.94	0.94	0.93	0.93	0.92	0.92	0.91	0.91	0.92	0.93	0.96	1.00	1.06	1.13
440	0.95	0.95	0.95	0.94	0.94	0.94	0.93	0.92	0.92	0.92	0.91	0.91	0.92	0.94	0.96	1.01	1.07	1.14
450	0.95	0.95	0.94	0.94	0.94	0.93	0.93	0.92	0.92	0.91	0.91	0.92	0.92	0.94	0.97	1.01	1.07	1.15
460	0.94	0.94	0.94	0.94	0.93	0.93	0.93	0.92	0.92	0.91	0.91	0.92	0.92	0.94	0.97	1.01	1.08	1.15
470	0.94	0.94	0.94	0.93	0.93	0.93	0.92	0.92	0.92	0.91	0.91	0.92	0.93	0.94	0.97	1.02	1.08	1.16
480	0.94	0.94	0.93	0.93	0.93	0.93	0.92	0.92	0.91	0.91	0.91	0.92	0.93	0.95	0.98	1.02	1.09	1.16
490	0.93	0.93	0.93	0.93	0.93	0.92	0.92	0.92	0.91	0.91	0.91	0.92	0.93	0.95	0.98	1.03	1.09	1.17
500	0.93	0.93	0.93	0.93	0.92	0.92	0.92	0.92	0.91	0.91	0.91	0.92	0.93	0.95	0.99	1.03	1.10	1.17

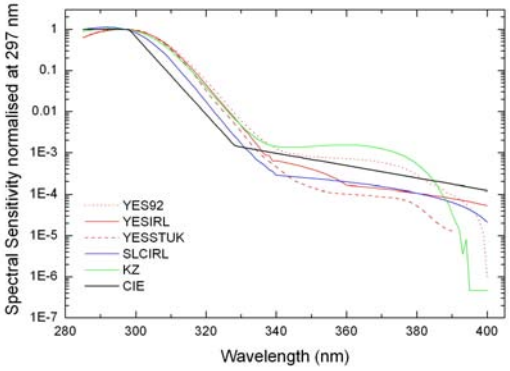

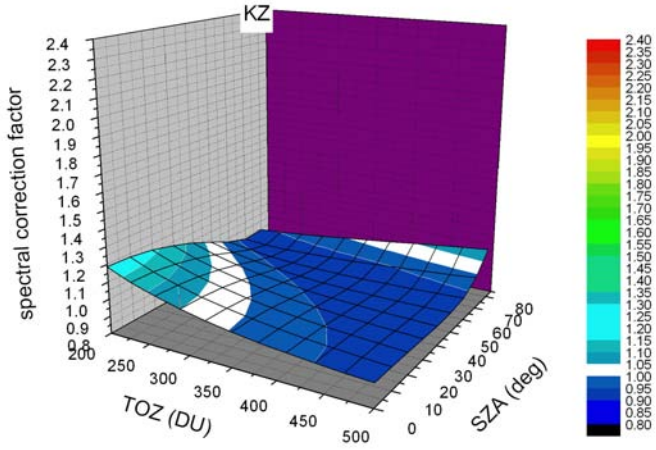

Annex C: DSC Calorimetric Experiment with a PTFE Sample from a NIWA Diffuser

After the work by *McKenzie et al.* [2005] had been published, we did some studies by Differential Scanning Calorimetry (DSC) with a sample from a NIWA-built diffuser (see Figure 1.8) in collaboration with the Research Group of Materials and Thermodynamics of the University of Girona. Here, the results found are described and compared with the change in the throughput reported by *McKenzie et al.* [2005].

C.1 Description of the DSC calorimetric experiment

A sample of the NIWA PTFE diffuser was cut into sheets and put into a platinum crucible of 30 µl. The net mass of the sample was 83.8 mg. In the DSC technique an empty crucible is considered as a reference and the heat flow absorbed or emitted by the sample is inferred through the difference of temperature between the two crucibles. For this, a Mettler DSC30 calorimeter was used.

The crucibles were first cooled from 50 to -30ºC using liquid nitrogen and afterwards heated from -30ºC to 50ºC. The heating rate was set at 2 ºC/min and the crucibles were exposed to 100mL/min flow of synthetic air during the experiment.

C.2 Results and discussion

Two thermograms were obtained (cooling/heating), as shown in Figure C.1. See that for both the cooling and heating thermograms two peaks appear, one of them much larger than the other. This shows that the process is reversible and that the process is exothermic when cooling the sample and endothermic when heating it. Note that the peaking temperatures appear shifted by about 6ºC. That is characteristic of the calorimetric experiments and it is mainly due to a lag in the response of the calorimeter when heating and cooling. In this way, the slower the heating/cooling rate was the smaller the shift would be. Thus, the average of these two thermograms is usually considered as the closest answer to reality. Figure C.2 shows the resulting averaged thermogram that would correspond to heating. Now the two peaks appear with the centre at 18.5ºC and around 28ºC, respectively, which is at halfway between the peaking temperatures for the thermograms in Figure C.1. The total heat involved in the processes (that is the area under the red base line in Figure C.2) is -278 mJ. The interesting value, however, is the enthalpy of the process usually given as the normalised area to the mass. That is the characteristic amount of heat absorbed by the PTFE during the process. This value (-3.3 J/g) is low compared with its heat of fusion (57 J/g) showing that the process under study involves low energy.

The same experiment was repeated several times and the same results were obtained, showing that the processes are perfectly reproducible and reconfirming

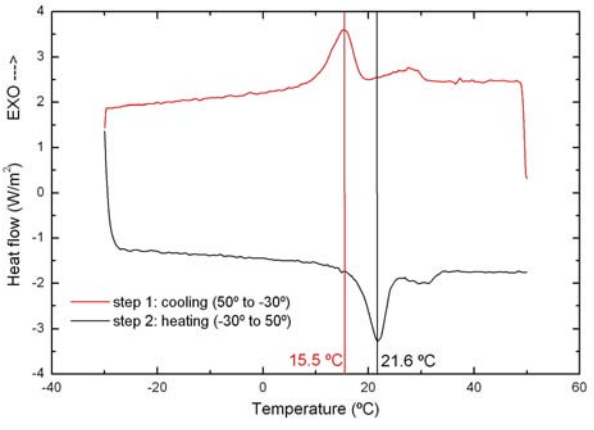

Figure C.1 Thermograms obtained from cooling (red) and heating (black) the PTFE sample.

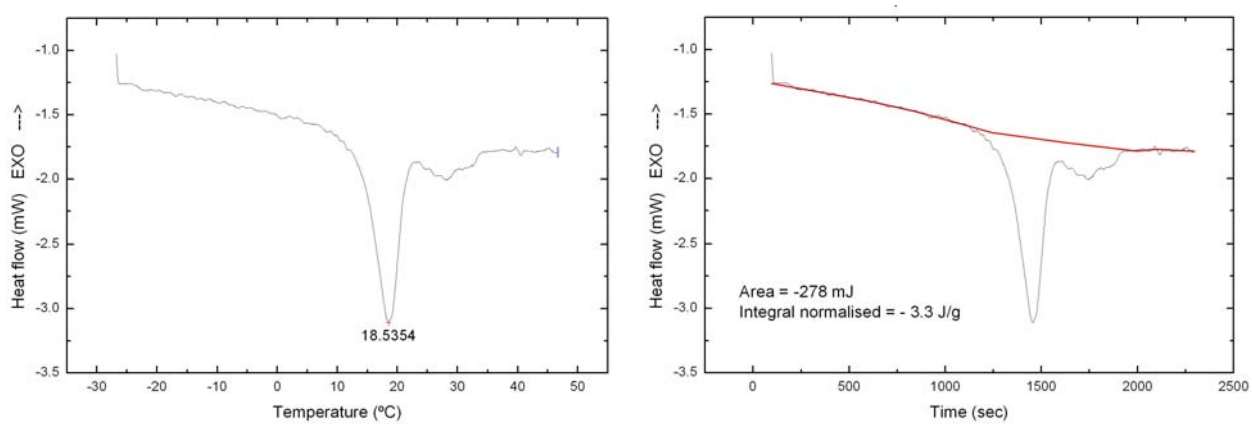

Figure C.2 Thermograms as a function of temperature (left) and time (right).

their reversibility. Also, different heating ratios were considered, as commented below.
Note that the small peak is not well defined. That is because the considered heating rate is low, which makes the measurement of heat flow more uncertain.
In order to see how the thermogram depends on the heating rate, the same experiment was done with 5ºC/min and 10ºC/min. For the latter rate, the range of temperatures was widened (from -50 to 50ºC) to explore lower temperatures. Figure C.3 shows the comparison between the resulting (also averaged) thermograms. See that the heat flow highly increases with the heating rate with the large peak always located around 18.5ºC. The peaks become wider as the heating rate increases and the smallest peak becomes more diffused and hided. No other processes were found when extending the temperature range (for the 10ºC/min thermogram). Note that enthalpy is very similar for the three curves, as expected.

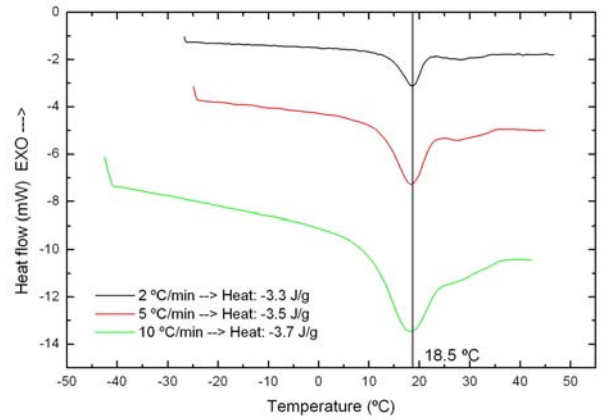

Figure C.3 Thermograms for different heating rates.

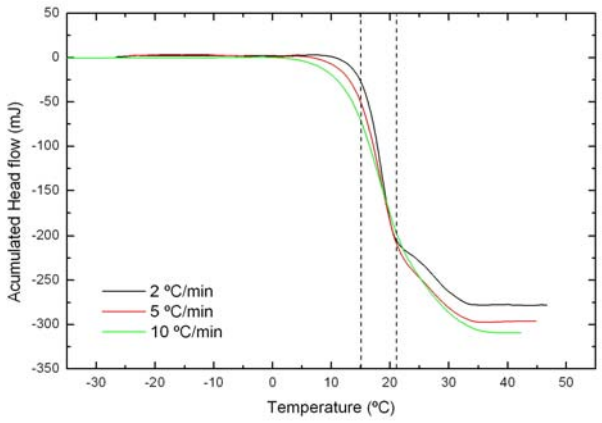

Figure C.4 Acumulated heat flows from Figure C.3 as a function of temperature

Another way of seeing the results is by plotting the accumulated heat flow as a function of temperature, which gives a better idea of the heat change. This is shown in Figure C.4. See that as the heat rate decreases, the step becomes narrower and, thus, steeper. Note that the maximum heat change takes place from 15 to 21ºC, which is the range of temperatures for which the change in the transmittance of the PTFE was observed by both *Ylianttila and Schreder* [2005] and *McKenzie et al.* [2005].

In order to see the relation between the observed calorimetric and optical changes in PTFE, the two changes are directly compared. Figure C.5 shows the accumulated heat flow (for 2ºC/min) and the change in the UVA diode signal from Figure 2 in *McKenzie et al.* [2005]. As

expected, the change in UVA signal and the change in heat flow occur virtually at the same temperatures. If these two curves are differentiated the agreement between these two changes becomes more evident so the endothermic peak and the UVA signal peak appear at the same temperature. Moreover, the second peak also appears in the UVA signal change. Unfortunately, the temperature for the experiment described by *McKenzie et al.* [2005] did not exceed 30ºC so to have the complete peak.

In summary, there is a clear consistency between the results from these two different ways of detecting the same process.

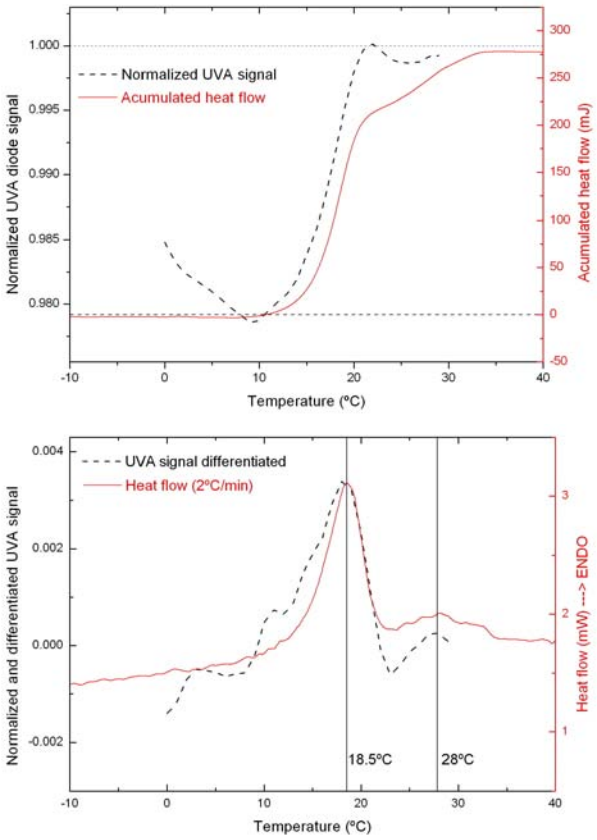

Figure C.5 Comparison between the throughput changes reported by *McKenzie et al.* [2005] and the calorimetric results for 2ºC/min heating rate. Upper: Change in UVA signal as in Figure 2 of *McKenzie et al.* [2005] and accumulated heat flow from Figure C.3. Lower: Differentiation of the upper black curve and eat flow from Figure C.2 with the sign changed.

C.3 Explanation of the process

The observed calorimetric and optical changes in the PTFE are caused by a well known structural change that has been reported in detail in the literature. For example, this is the description given by [*Billmeyer*, 1984]:

"This polymer exists in two helical conformations that may be described as twisted ribbons in which the fully extended planar form is distorted to have a 180ºC twist in 13 CF_2 units in the more stable (low temperature) form. Above 19ºC this form is replaced by a slightly untwisted conformation with 15 CF_2 units per half-twist. Above 19ºC the x-ray diffraction pattern shows diffuse streaks that are interpreted as resulting from small angular displacements of molecular segments about their long axes. Above 30ºC more diffuseness occurs in the x-ray pattern, increasing as the temperature is raised to and above the melting point, 327ºC. This additional diffuseness is attributed to random angular displacement of the molecules about their long axes.

In terms of molecular motion, (…) between 19ºC and 30ºC the molecules are "locked" into the threefold helix corresponding to the 15 CF_2 repeat distance; their motion is restricted to small-angle oscillations about their "rest positions". (…) Above 30ºC torsional motion increases, with the twisting and undertwisting becoming more pronounced, until at Tm (melting point) all crystalline order is lost"

From this, it is clear that there are two processes, around 19 and 30ºC, being the first the most important. That is in agreement with what it has been found in the experiments. As far as the change in transmittance is concerned it can be stated that whereas the change in transmittance of PTFE around 19ºC is about 2-3%, as discussed by *McKenzie et al.* [2005] and *Ylianttila and Schreder* [2005], the change in transmittance around 30ºC is expected to be much lower, of 0.3% the most, from what is seen in Figure C.4.

C.4 Acknowledgements

We would like to kindly thank Alex Gonzàlez from the Research Group of Materials and Thermodynamics of the University of Girona for his essential help and assistance in the calorimetric experiences.

C.5 References

Billmeyer, F. W. (1984), *Textbook of Polymer science*, 608 pp., Wiley-Interscience, New York.

McKenzie, R. L., et al. (2005), Effects of the temperature dependence in PTFE diffusers on observed UV irradiances, *Geophysical Research Letters*, *32 (L06808)*, doi:10.1029/2004GL022268.

Ylianttila, L., and J. Schreder (2005), Temperature effects on PTFE diffusers, *Journal of Optical Materials, in press*.

Annex D: Daily plots for all the days considered in the Model vs. Measurement analyses in Chapter 4

In the following pages, daily plots for all the days and sites considered in the study presented in Chapter 4 are collected in order to complement the analyses presented there.
In the following an example of the plots is shown and a diagram explains the format and contents of the plots. Although the modelling base case in Chapter 4 was TUV(2), here the daily evolution of the modelled UVI is plotted for TUV(3). That is because, on one hand, TUV(3) is available for every day (for both TUV(2) and TUV(1) there are missing days, see Table 4.4) and, on the other hand, best modelling results have been found when considering TUV(3) since it considers the daily evolution of *TOZ* (by considering TOZ_S). However, absolute and relative model-measurement differences are presented for TUV(1), TUV(2) and TUV(3), as the reference set of cases. The UVI, *AOD*, air temperature and wind speed measurements are shown for each day together with the three sources of *TOZ*: TOZ_T, TOZ_D and TOZ_S.

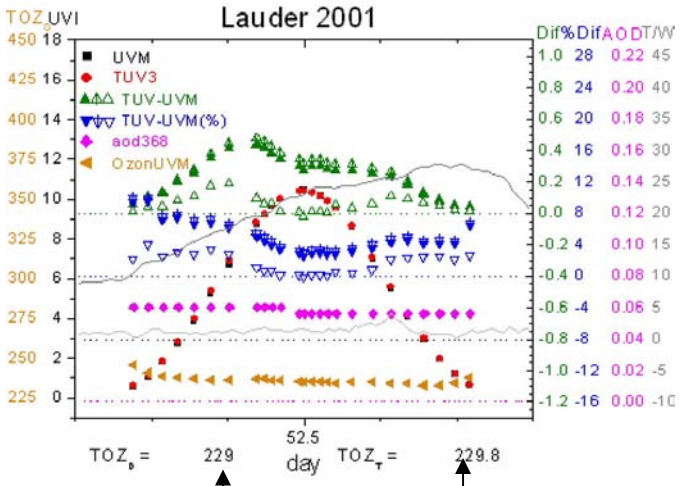

TOZ from TOMS TOZ (DU)

TOZ from Dobson Sunphotometer (DU)

Measured UVI

TUV(3)

TUV(1) – Measured UVI

TUV(2) – Measured UVI

TUV(3) – Measured UVI

TUV(1) – Measured UVI (in %)

TUV(2) – Measured UVI (in %)

TUV(3) – Measured UVI (in %)

Measured AOD_{368}

TOZ_S (DU)

Air temperature (ºC)

Wind speed (m/s)

D.1
Daily plots for clear days in Lauder 2001

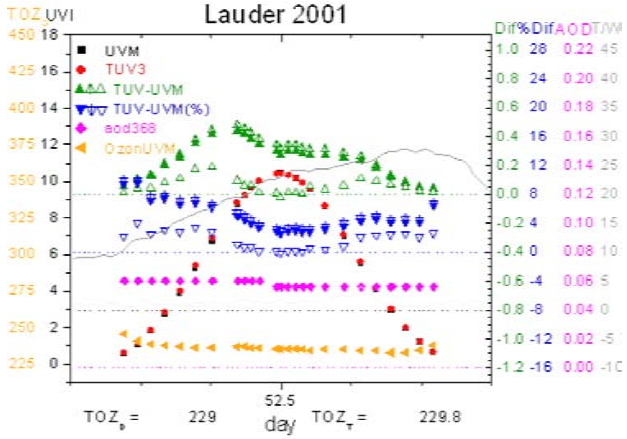
Lauder 2001
TOZ UVI
Dif%Dif AOD T/W
UVM
TUV3
TUV-UVM
TUV-UVM(%)
aod368
OzonUVM
52.5
day
TOZp = 229
TOZT = 229.8

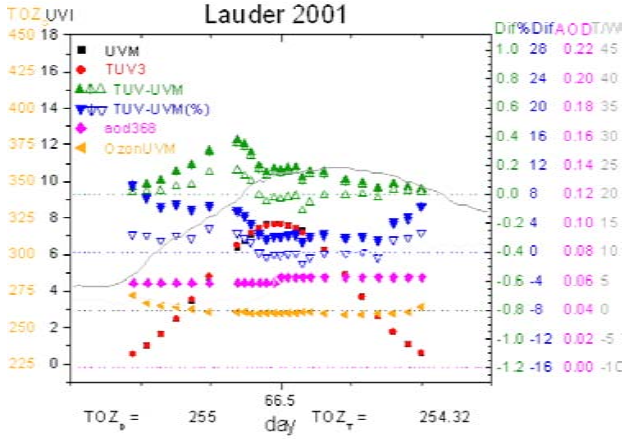
Lauder 2001
TOZ UVI
Dif%Dif AOD T/W
UVM
TUV3
TUV-UVM
TUV-UVM(%)
aod368
OzonUVM
66.5
day
TOZp = 255
TOZT = 254.32

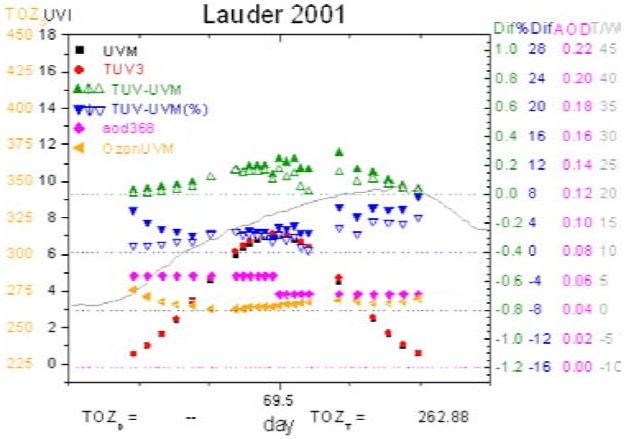
Lauder 2001
TOZ UVI
Dif%Dif AOD T/W
UVM
TUV3
TUV-UVM
TUV-UVM(%)
aod368
OzonUVM
69.5
day
TOZp = --
TOZT = 262.88

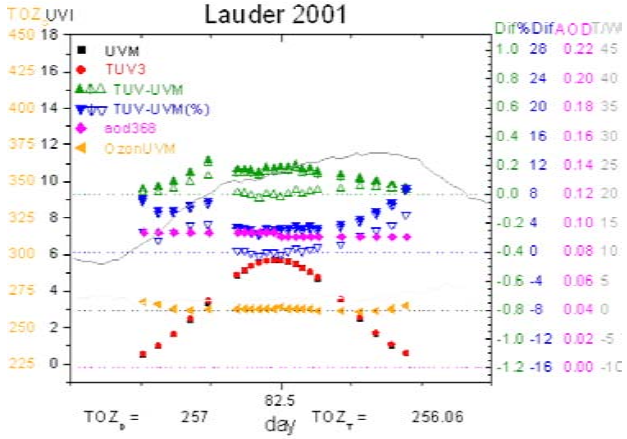
Lauder 2001
TOZ UVI
Dif%Dif AOD T/W
UVM
TUV3
TUV-UVM
TUV-UVM(%)
aod368
OzonUVM
82.5
day
TOZp = 257
TOZT = 256.06

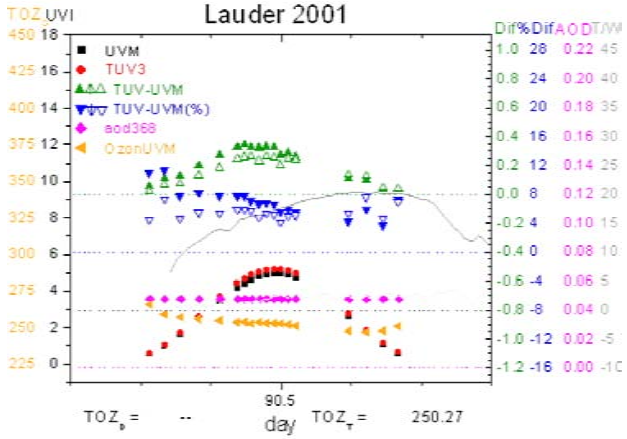
Lauder 2001
TOZ UVI
Dif%Dif AOD T/W
UVM
TUV3
TUV-UVM
TUV-UVM(%)
aod368
OzonUVM
90.5
day
TOZp = --
TOZT = 250.27

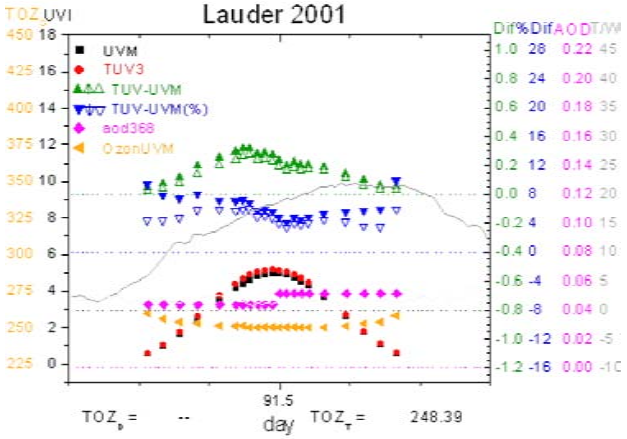
Lauder 2001
TOZ UVI
Dif%Dif AOD T/W
UVM
TUV3
TUV-UVM
TUV-UVM(%)
aod368
OzonUVM
91.5
day
TOZp = --
TOZT = 248.39

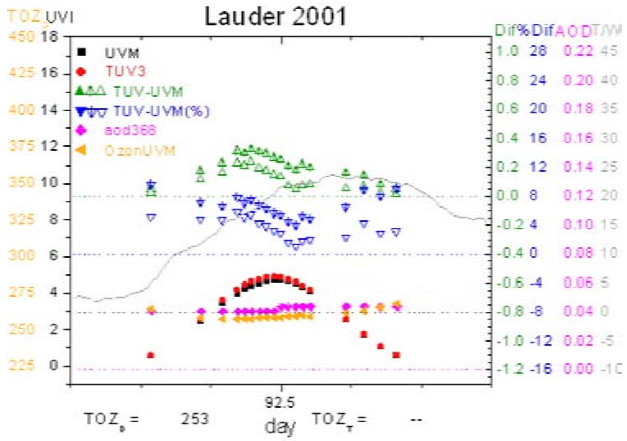
Lauder 2001
TOZ UVI
Dif%Dif AOD T/W
UVM
TUV3
TUV-UVM
TUV-UVM(%)
aod368
OzonUVM
92.5
day
TOZp = 253
TOZT = --

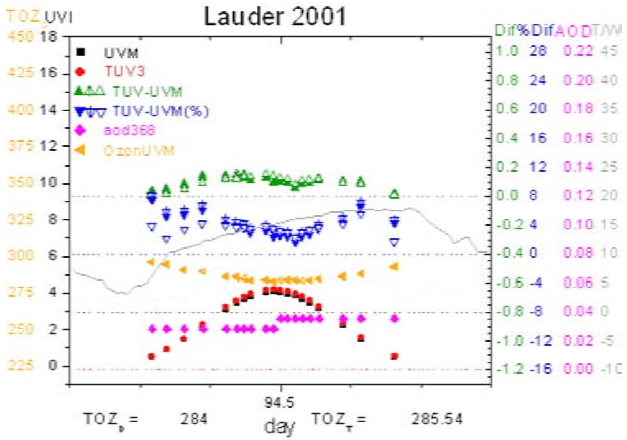
Lauder 2001
TOZ UVI
Dif%Dif AOD T/W
UVM
TUV3
TUV-UVM
TUV-UVM(%)
aod368
OzonUVM
94.5
day
TOZp = 284
TOZT = 285.54

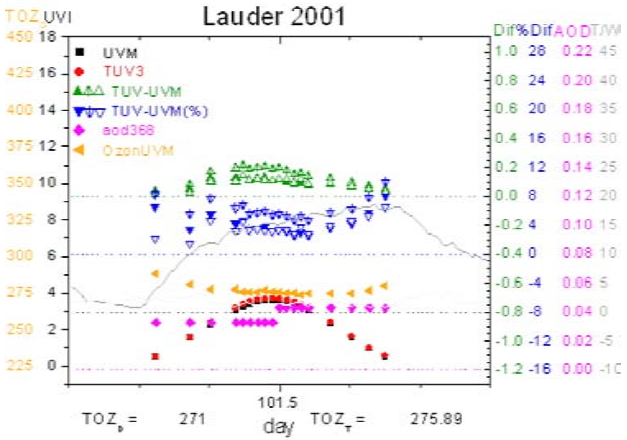
Lauder 2001
TOZ UVI
Dif%Dif AOD T/W
UVM
TUV3
TUV-UVM
TUV-UVM(%)
aod368
OzonUVM
101.5
day
TOZp = 271
TOZT = 275.89

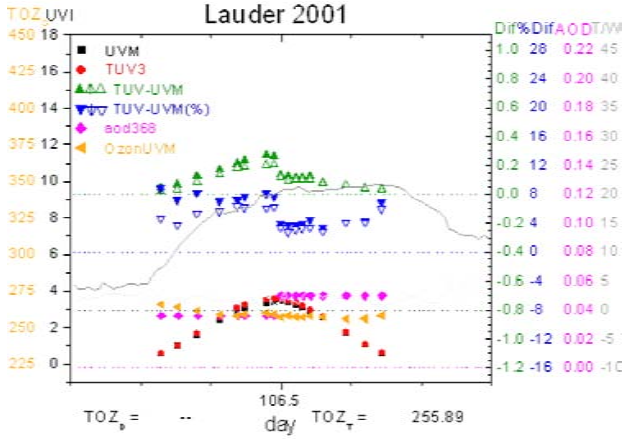
Lauder 2001
TOZ UVI
Dif% Dif AOD TJW
UVM
TUV3
TUV-UVM
TUV-UVM(%)
aod368
OzonUVM
106.5
day
TOZ$_p$ = --
TOZ$_T$ = 255.89

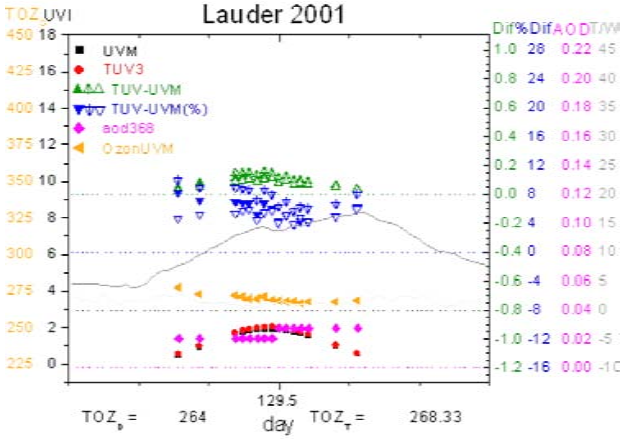
Lauder 2001
TOZ UVI
Dif% Dif AOD TJW
UVM
TUV3
TUV-UVM
TUV-UVM(%)
aod368
OzonUVM
129.5
day
TOZ$_p$ = 264
TOZ$_T$ = 268.33

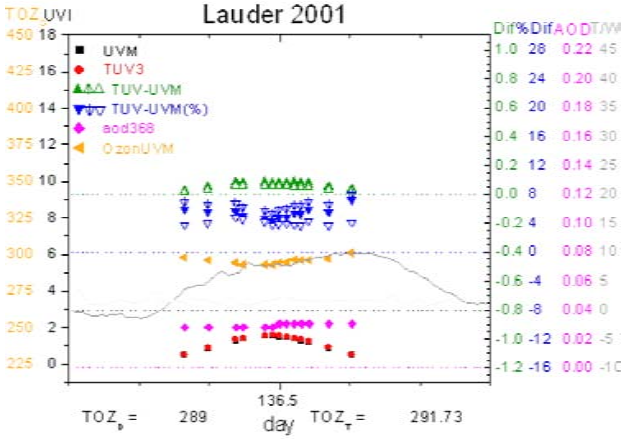
Lauder 2001
TOZ UVI
Dif% Dif AOD TJW
UVM
TUV3
TUV-UVM
TUV-UVM(%)
aod368
OzonUVM
136.5
day
TOZ$_p$ = 289
TOZ$_T$ = 291.73

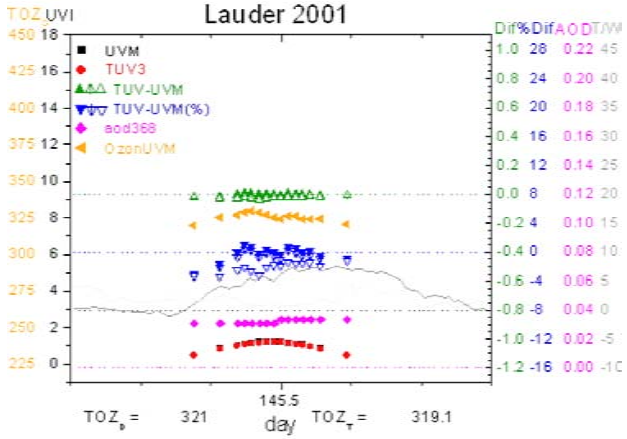
Lauder 2001
TOZ UVI
Dif% Dif AOD TJW
UVM
TUV3
TUV-UVM
TUV-UVM(%)
aod368
OzonUVM
145.5
day
TOZ$_p$ = 321
TOZ$_T$ = 319.1

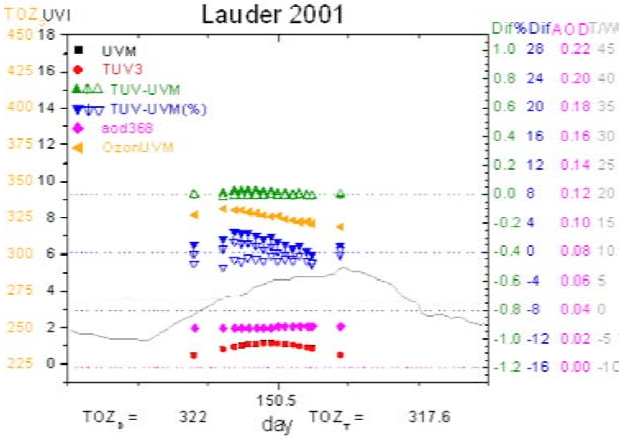
Lauder 2001
TOZ UVI
Dif% Dif AOD TJW
UVM
TUV3
TUV-UVM
TUV-UVM(%)
aod368
OzonUVM
150.5
day
TOZ$_p$ = 322
TOZ$_T$ = 317.6

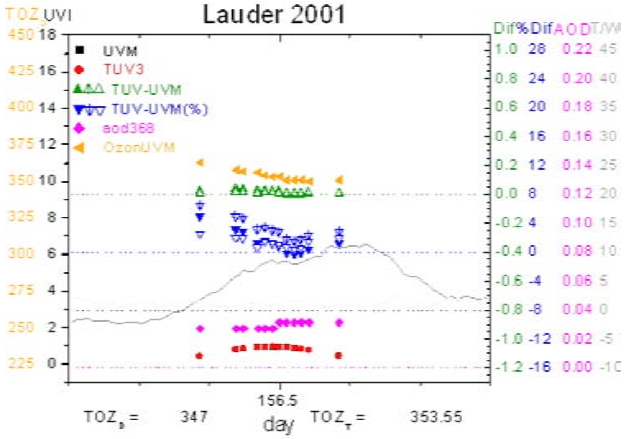
Lauder 2001
TOZ UVI
Dif% Dif AOD TJW
UVM
TUV3
TUV-UVM
TUV-UVM(%)
aod368
OzonUVM
156.5
day
TOZ$_p$ = 347
TOZ$_T$ = 353.55

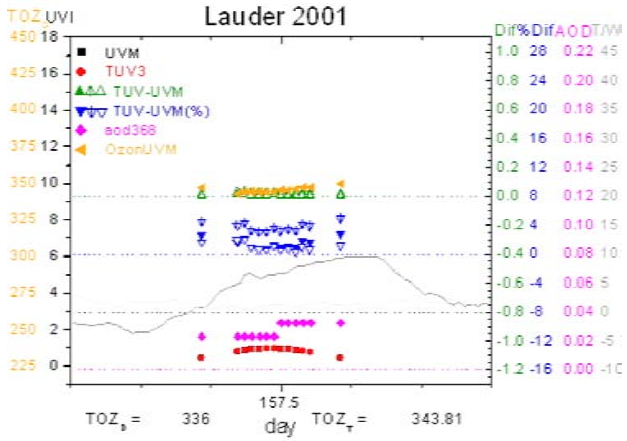
Lauder 2001
TOZ UVI
Dif% Dif AOD TJW
UVM
TUV3
TUV-UVM
TUV-UVM(%)
aod368
OzonUVM
157.5
day
TOZ$_p$ = 336
TOZ$_T$ = 343.81

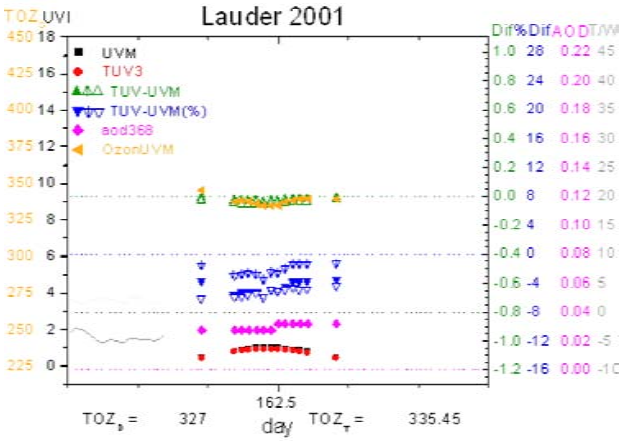
Lauder 2001
TOZ UVI
Dif% Dif AOD TJW
UVM
TUV3
TUV-UVM
TUV-UVM(%)
aod368
OzonUVM
162.5
day
TOZ$_p$ = 327
TOZ$_T$ = 335.45

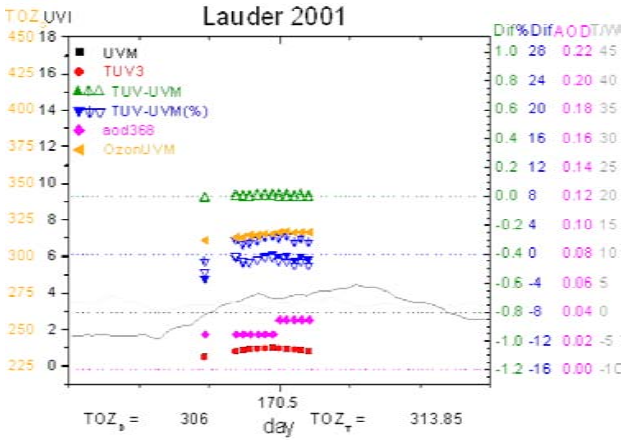
Lauder 2001
TOZ UVI
Dif% Dif AOD TJW
UVM
TUV3
TUV-UVM
TUV-UVM(%)
aod368
OzonUVM
170.5
day
TOZ$_p$ = 306
TOZ$_T$ = 313.85

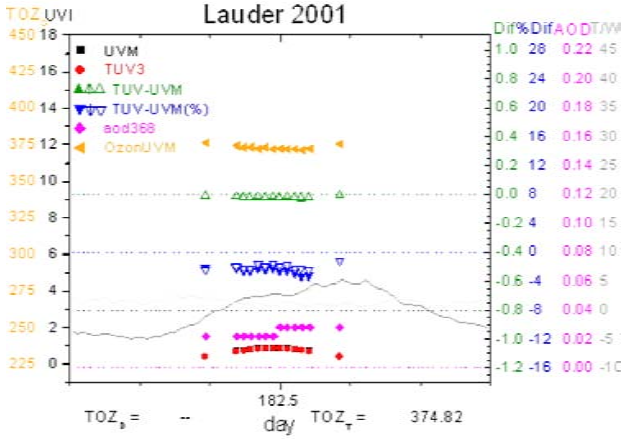
Lauder 2001
TOZ UVI
Dif%Dif AOD T/W
UVM
TUV3
TUV-UVM
TUV-UVM(%)
aod368
OzonUVM
182.5
day
TOZ$_b$ = --
TOZ$_T$ = 374.82

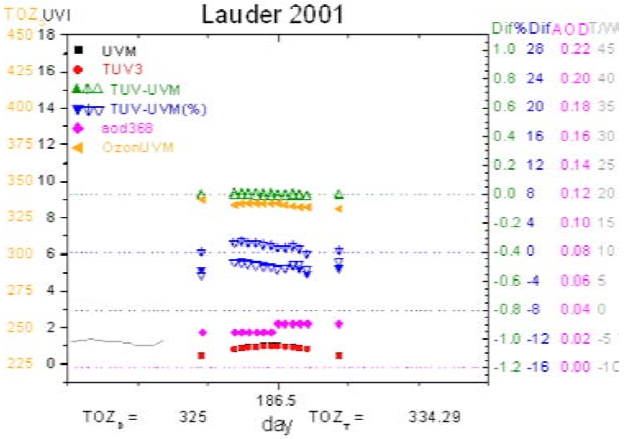
Lauder 2001
TOZ UVI
Dif%Dif AOD T/W
UVM
TUV3
TUV-UVM
TUV-UVM(%)
aod368
OzonUVM
186.5
day
TOZ$_b$ = 325
TOZ$_T$ = 334.29

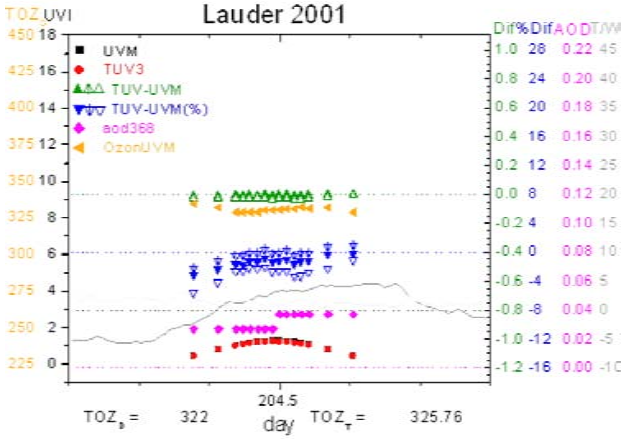
Lauder 2001
TOZ UVI
Dif%Dif AOD T/W
UVM
TUV3
TUV-UVM
TUV-UVM(%)
aod368
OzonUVM
204.5
day
TOZ$_b$ = 322
TOZ$_T$ = 325.76

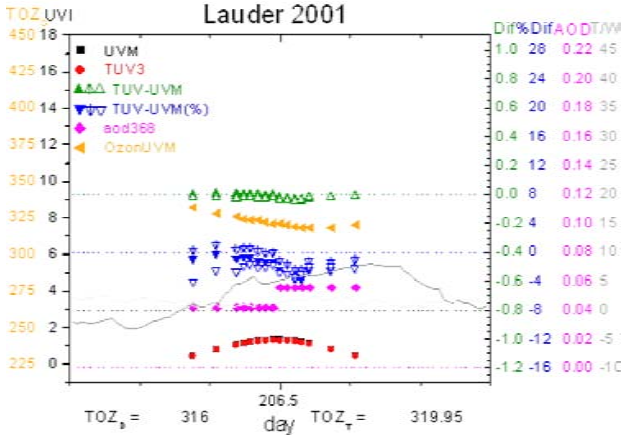
Lauder 2001
TOZ UVI
Dif%Dif AOD T/W
UVM
TUV3
TUV-UVM
TUV-UVM(%)
aod368
OzonUVM
206.5
day
TOZ$_b$ = 316
TOZ$_T$ = 319.95

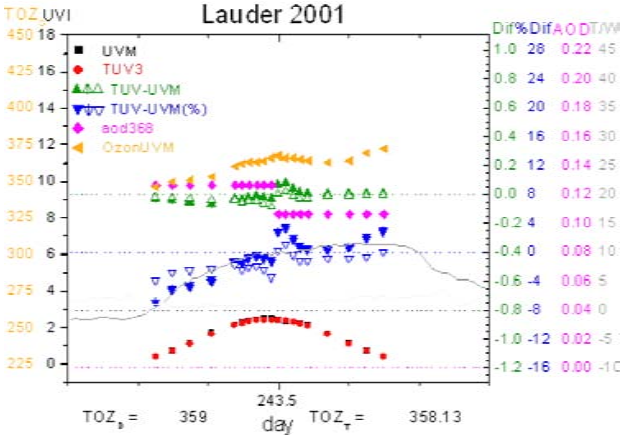
Lauder 2001
TOZ UVI
Dif%Dif AOD T/W
UVM
TUV3
TUV-UVM
TUV-UVM(%)
aod368
OzonUVM
243.5
day
TOZ$_b$ = 359
TOZ$_T$ = 358.13

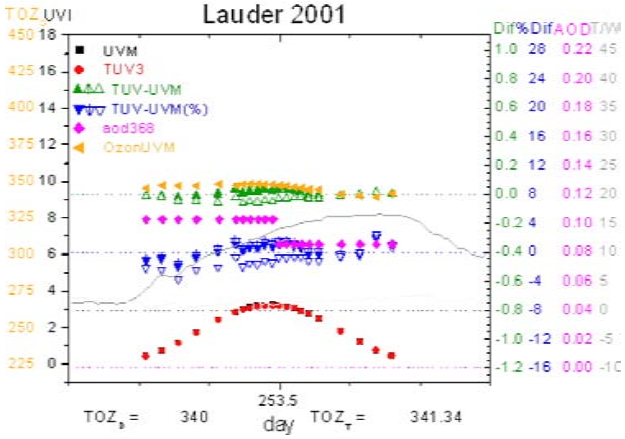
Lauder 2001
TOZ UVI
Dif%Dif AOD T/W
UVM
TUV3
TUV-UVM
TUV-UVM(%)
aod368
OzonUVM
253.5
day
TOZ$_b$ = 340
TOZ$_T$ = 341.34

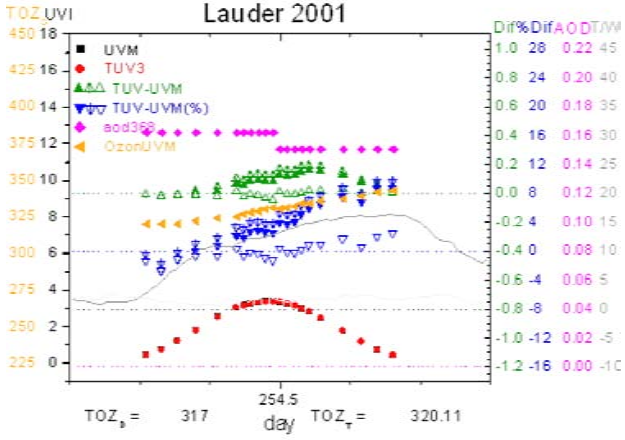
Lauder 2001
TOZ UVI
Dif%Dif AOD T/W
UVM
TUV3
TUV-UVM
TUV-UVM(%)
aod368
OzonUVM
254.5
day
TOZ$_b$ = 317
TOZ$_T$ = 320.11

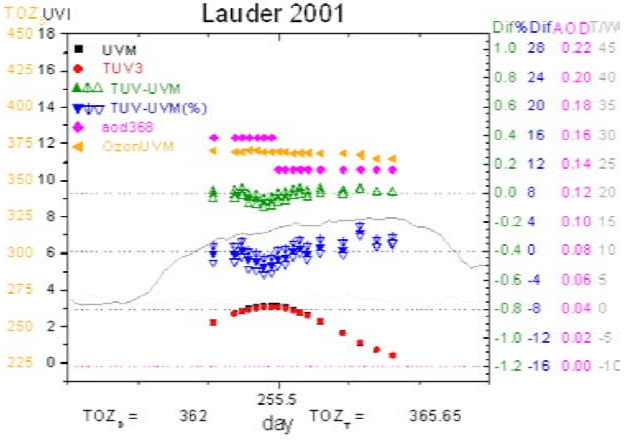
Lauder 2001
TOZ UVI
Dif%Dif AOD T/W
UVM
TUV3
TUV-UVM
TUV-UVM(%)
aod368
OzonUVM
255.5
day
TOZ$_b$ = 362
TOZ$_T$ = 365.65

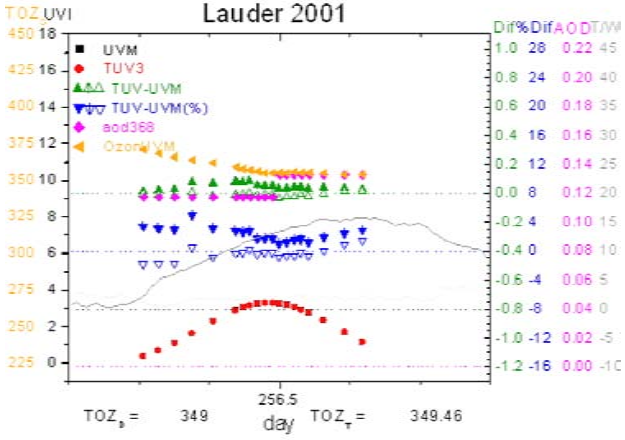
Lauder 2001
TOZ UVI
Dif%Dif AOD T/W
UVM
TUV3
TUV-UVM
TUV-UVM(%)
aod368
OzonUVM
256.5
day
TOZ$_b$ = 349
TOZ$_T$ = 349.46

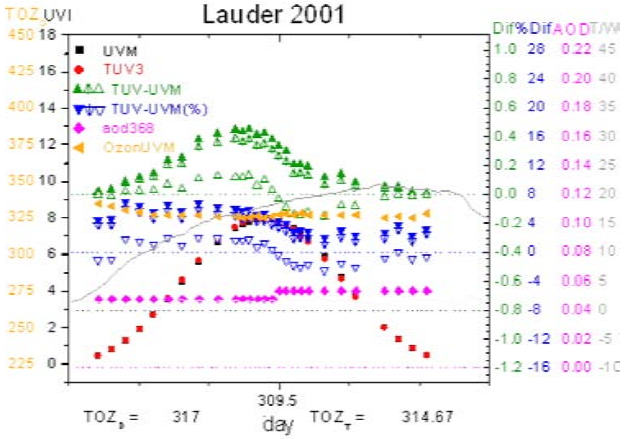
Lauder 2001
TOZ UVI
Dif% Dif AOD TJW
UVM
TUV3
TUV-UVM
TUV-UVM(%)
aod368
OzonUVM
309.5
day
TOZ$_b$ = 317
TOZ$_T$ = 314.67

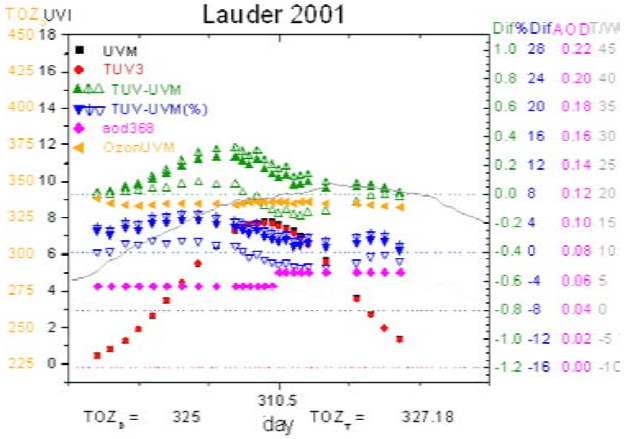
Lauder 2001
TOZ UVI
Dif% Dif AOD TJW
UVM
TUV3
TUV-UVM
TUV-UVM(%)
aod368
OzonUVM
310.5
day
TOZ$_b$ = 325
TOZ$_T$ = 327.18

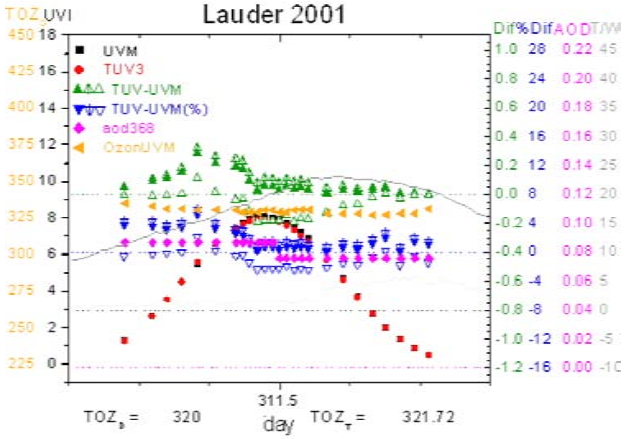
Lauder 2001
TOZ UVI
Dif% Dif AOD TJW
UVM
TUV3
TUV-UVM
TUV-UVM(%)
aod368
OzonUVM
311.5
day
TOZ$_b$ = 320
TOZ$_T$ = 321.72

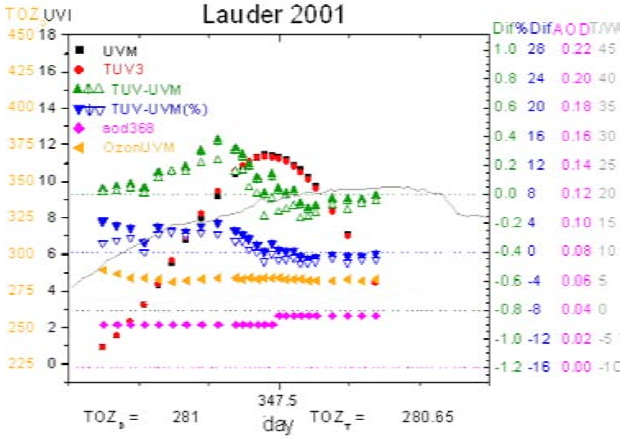
Lauder 2001
TOZ UVI
Dif% Dif AOD TJW
UVM
TUV3
TUV-UVM
TUV-UVM(%)
aod368
OzonUVM
347.5
day
TOZ$_b$ = 281
TOZ$_T$ = 280.65

D.2
Daily plots for clear days in Boulder 2000

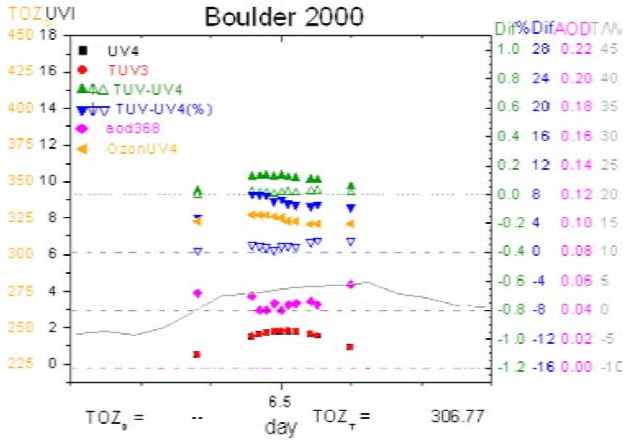
Boulder 2000
TOZ UVI
Dif% Dif AOD T
UV4
TUV3
TUV-UV4
TUV-UV4(%)
aod368
OzonUV4
6.5
day
TOZ0 = --
TOZT = 306.77

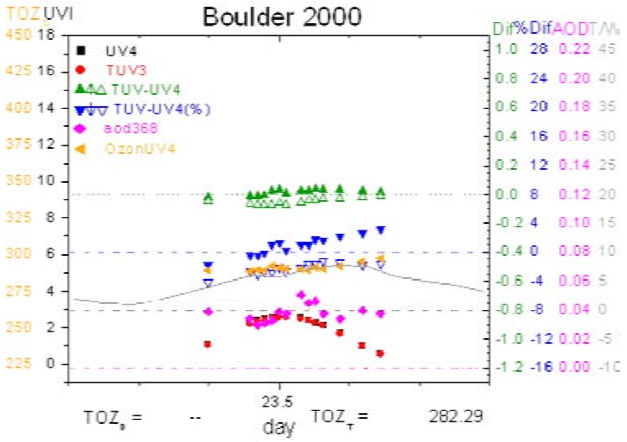
Boulder 2000
TOZ UVI
Dif% Dif AOD T
UV4
TUV3
TUV-UV4
TUV-UV4(%)
aod368
OzonUV4
23.5
day
TOZ0 = --
TOZT = 282.29

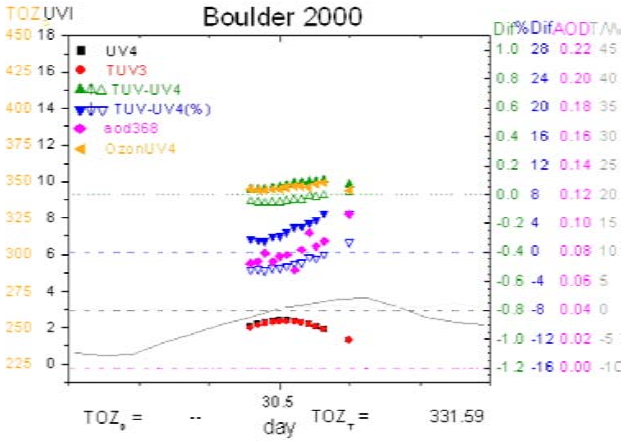
Boulder 2000
TOZ UVI
Dif% Dif AOD T
UV4
TUV3
TUV-UV4
TUV-UV4(%)
aod368
OzonUV4
30.5
day
TOZ0 = --
TOZT = 331.59

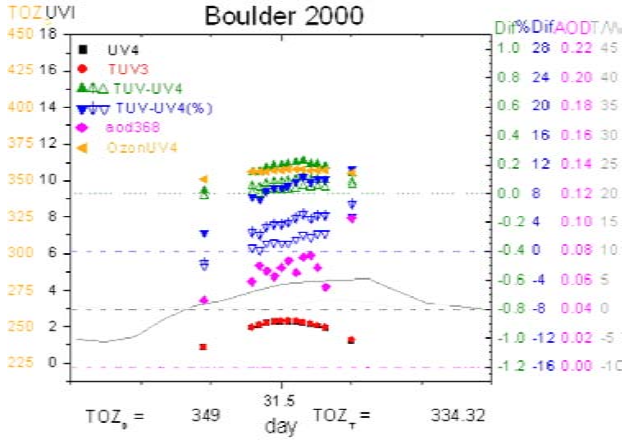
Boulder 2000
TOZ UVI
Dif% Dif AOD T
UV4
TUV3
TUV-UV4
TUV-UV4(%)
aod368
OzonUV4
31.5
day
TOZ0 = 349
TOZT = 334.32

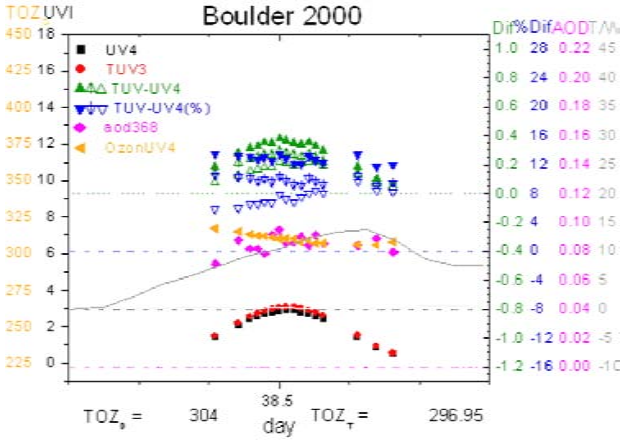
Boulder 2000
TOZ UVI
Dif% Dif AOD T
UV4
TUV3
TUV-UV4
TUV-UV4(%)
aod368
OzonUV4
38.5
day
TOZ0 = 304
TOZT = 296.95

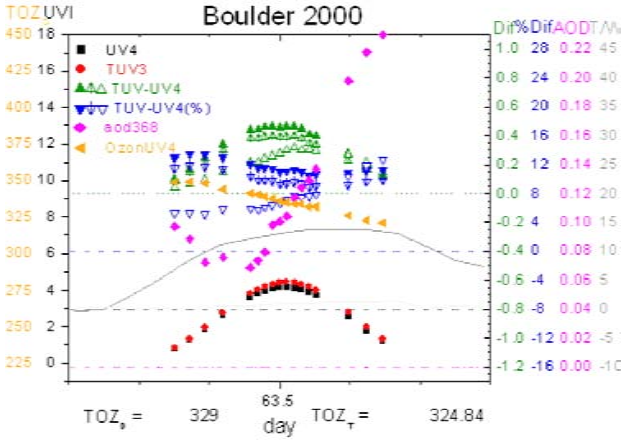
Boulder 2000
TOZ UVI
Dif% Dif AOD T
UV4
TUV3
TUV-UV4
TUV-UV4(%)
aod368
OzonUV4
63.5
day
TOZ0 = 329
TOZT = 324.84

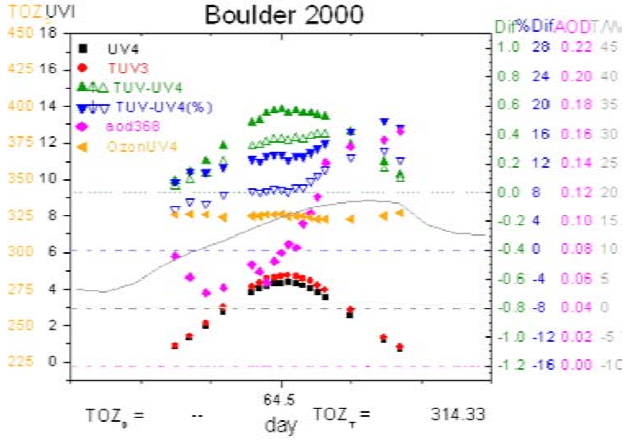
Boulder 2000
TOZ UVI
Dif% Dif AOD T
UV4
TUV3
TUV-UV4
TUV-UV4(%)
aod368
OzonUV4
64.5
day
TOZ0 = --
TOZT = 314.33

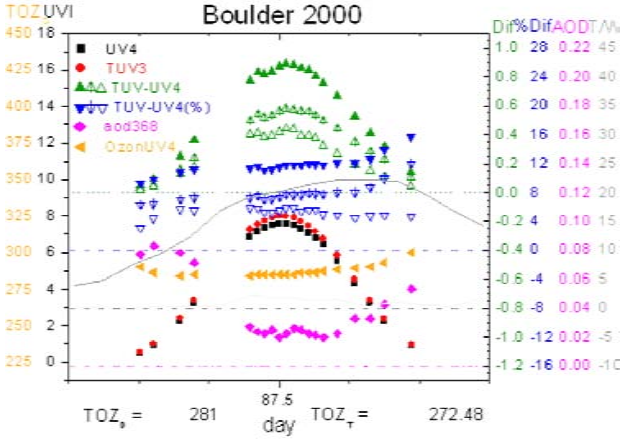
Boulder 2000
TOZ UVI
Dif% Dif AOD T
UV4
TUV3
TUV-UV4
TUV-UV4(%)
aod368
OzonUV4
87.5
day
TOZ0 = 281
TOZT = 272.48

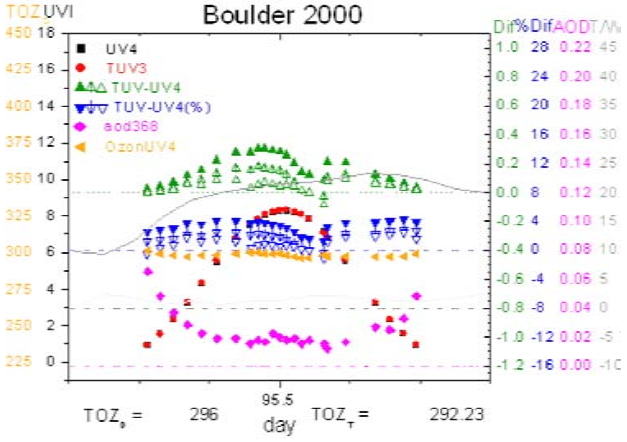
Boulder 2000
TOZ UVI
Dif% Dif AOD T
UV4
TUV3
TUV-UV4
TUV-UV4(%)
aod368
OzonUV4
95.5
day
TOZ0 = 296
TOZT = 292.23

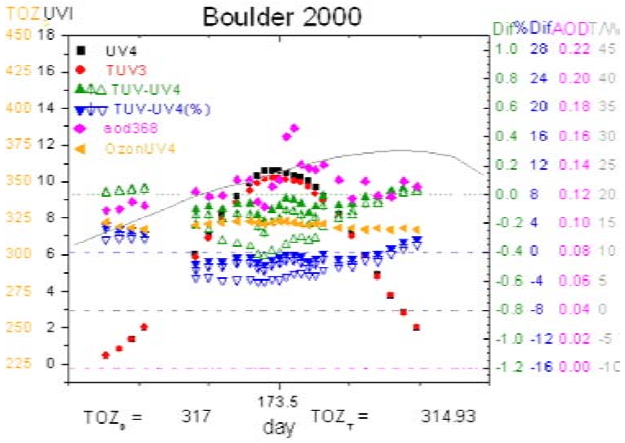
Boulder 2000
TOZ UVI
Dif% Dif AOD T/W
UV4
TUV3
TUV-UV4
TUV-UV4(%)
aod368
OzonUV4
173.5
day
TOZ$_o$ = 317
TOZ$_T$ = 314.93

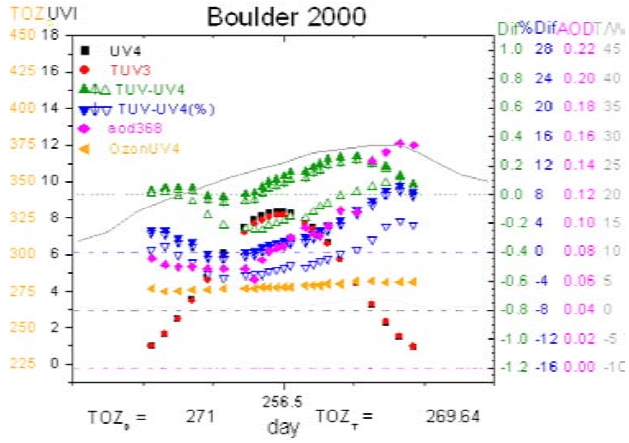
Boulder 2000
TOZ UVI
Dif% Dif AOD T/W
UV4
TUV3
TUV-UV4
TUV-UV4(%)
aod368
OzonUV4
256.5
day
TOZ$_o$ = 271
TOZ$_T$ = 269.64

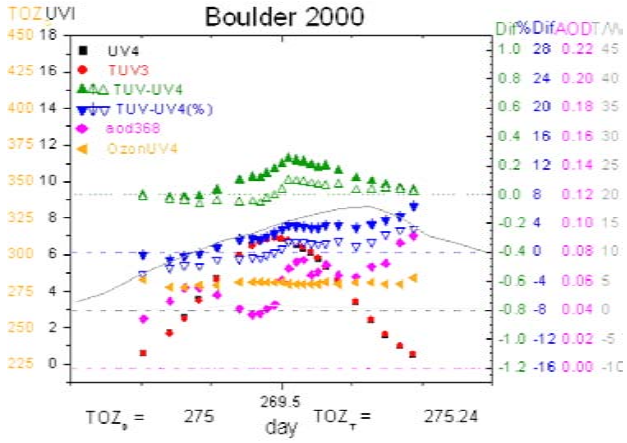
Boulder 2000
TOZ UVI
Dif% Dif AOD T/W
UV4
TUV3
TUV-UV4
TUV-UV4(%)
aod368
OzonUV4
269.5
day
TOZ$_o$ = 275
TOZ$_T$ = 275.24

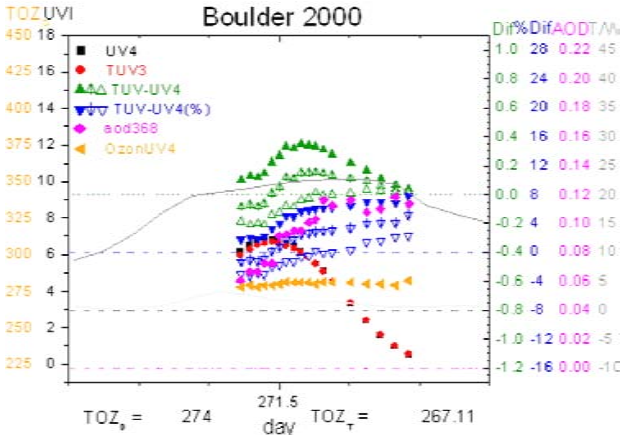
Boulder 2000
TOZ UVI
Dif% Dif AOD T/W
UV4
TUV3
TUV-UV4
TUV-UV4(%)
aod368
OzonUV4
271.5
day
TOZ$_o$ = 274
TOZ$_T$ = 267.11

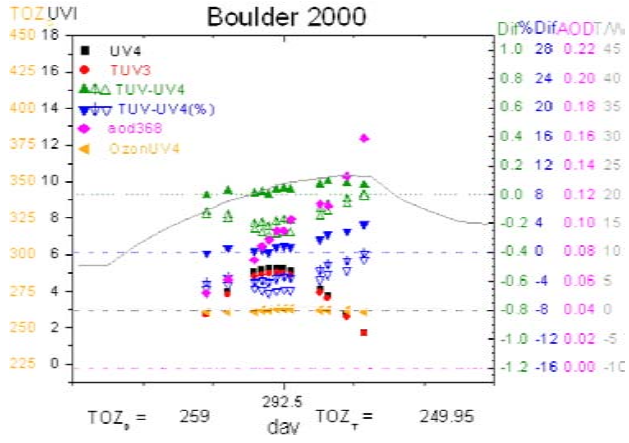
Boulder 2000
TOZ UVI
Dif% Dif AOD T/W
UV4
TUV3
TUV-UV4
TUV-UV4(%)
aod368
OzonUV4
292.5
day
TOZ$_o$ = 259
TOZ$_T$ = 249.95

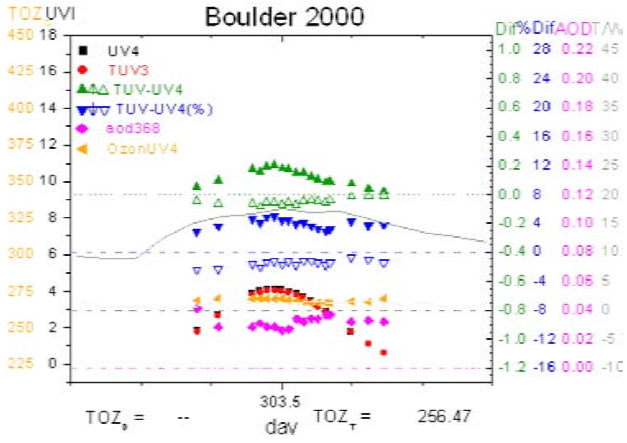
Boulder 2000
TOZ UVI
Dif% Dif AOD T/W
UV4
TUV3
TUV-UV4
TUV-UV4(%)
aod368
OzonUV4
303.5
day
TOZ$_o$ = --
TOZ$_T$ = 256.47

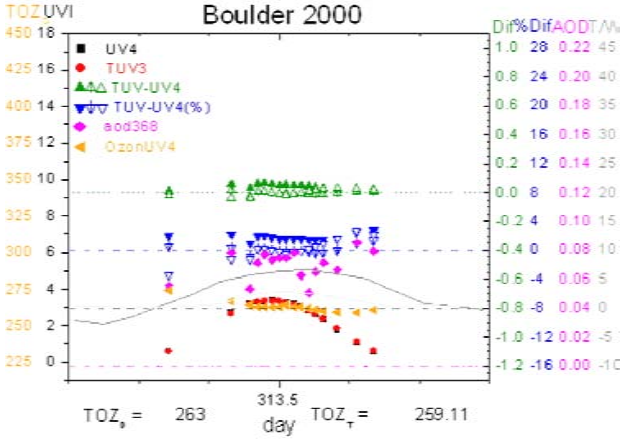
Boulder 2000
TOZ UVI
Dif% Dif AOD T/W
UV4
TUV3
TUV-UV4
TUV-UV4(%)
aod368
OzonUV4
313.5
day
TOZ$_o$ = 263
TOZ$_T$ = 259.11

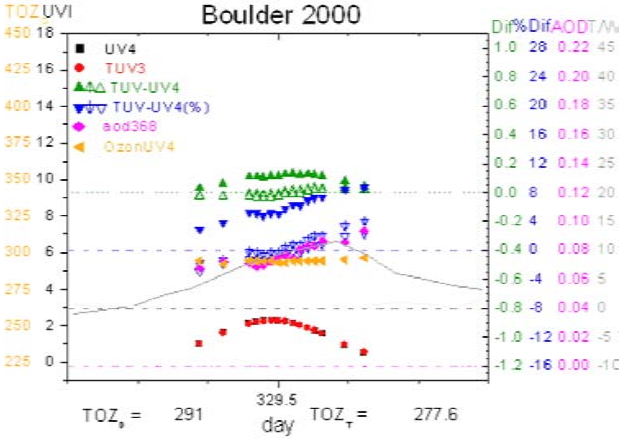
Boulder 2000
TOZ UVI
Dif% Dif AOD T/W
UV4
TUV3
TUV-UV4
TUV-UV4(%)
aod368
OzonUV4
329.5
day
TOZ$_o$ = 291
TOZ$_T$ = 277.6

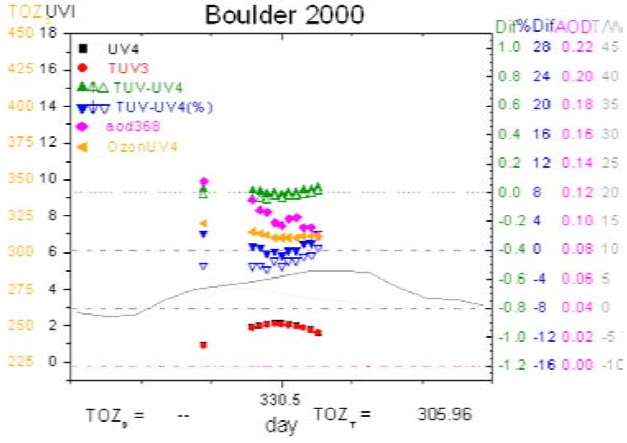
Boulder 2000
TOZ UVI
Dif% Dif AOD T/W
UV4
TUV3
TUV-UV4
TUV-UV4(%)
aod368
OzonUV4
330.5
day
TOZ$_o$ = --
TOZ$_T$ = 305.96

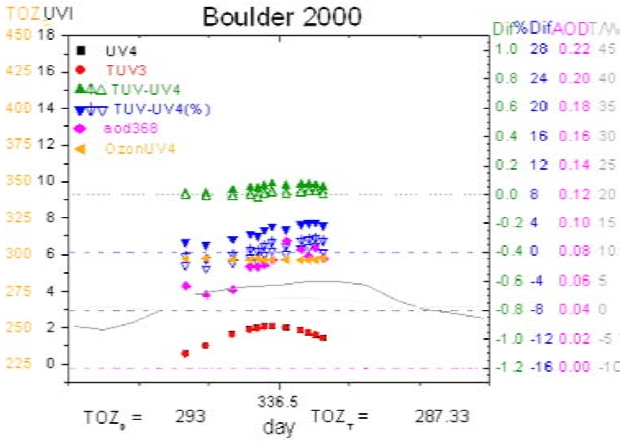
Boulder 2000
TOZ UVI
Dif% Dif AOD T /W
UV4
TUV3
TUV-UV4
TUV-UV4(%)
aod368
OzonUV4
336.5
day
TOZ$_0$ = 293
TOZ$_T$ = 287.33

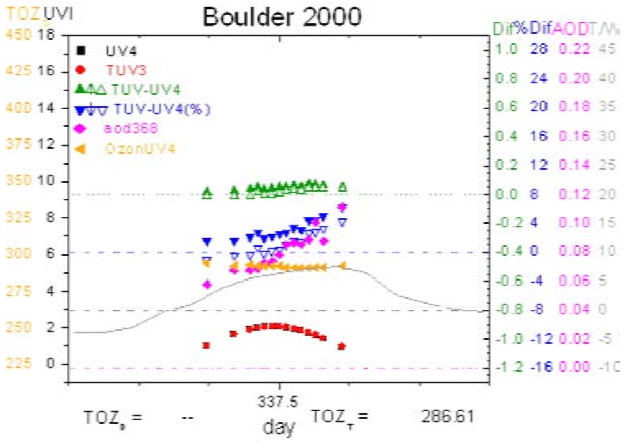
Boulder 2000
TOZ UVI
Dif% Dif AOD T /W
UV4
TUV3
TUV-UV4
TUV-UV4(%)
aod368
OzonUV4
337.5
day
TOZ$_0$ = --
TOZ$_T$ = 286.61

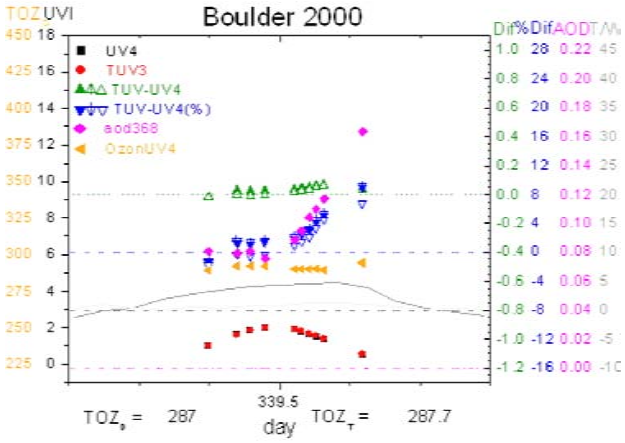
Boulder 2000
TOZ UVI
Dif% Dif AOD T /W
UV4
TUV3
TUV-UV4
TUV-UV4(%)
aod368
OzonUV4
339.5
day
TOZ$_0$ = 287
TOZ$_T$ = 287.7

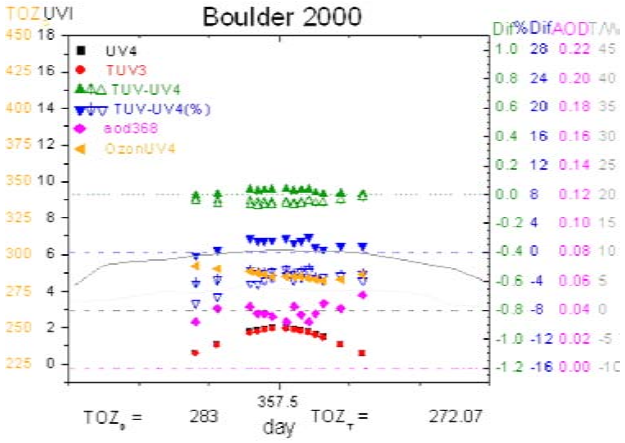
Boulder 2000
TOZ UVI
Dif% Dif AOD T /W
UV4
TUV3
TUV-UV4
TUV-UV4(%)
aod368
OzonUV4
357.5
day
TOZ$_0$ = 283
TOZ$_T$ = 272.07

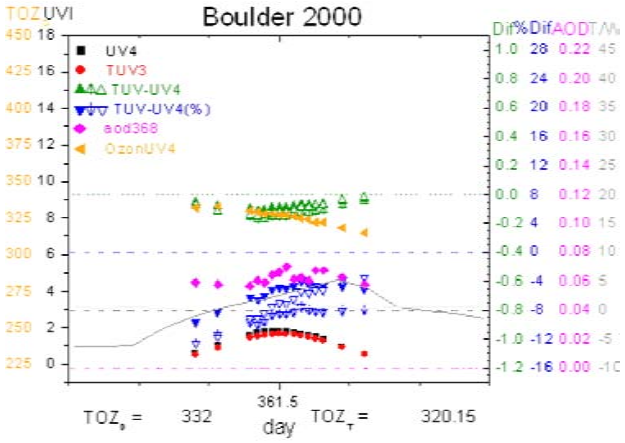
Boulder 2000
TOZ UVI
Dif% Dif AOD T /W
UV4
TUV3
TUV-UV4
TUV-UV4(%)
aod368
OzonUV4
361.5
day
TOZ$_0$ = 332
TOZ$_T$ = 320.15

D.3
Daily plots for clear days in Mauna Loa 2001

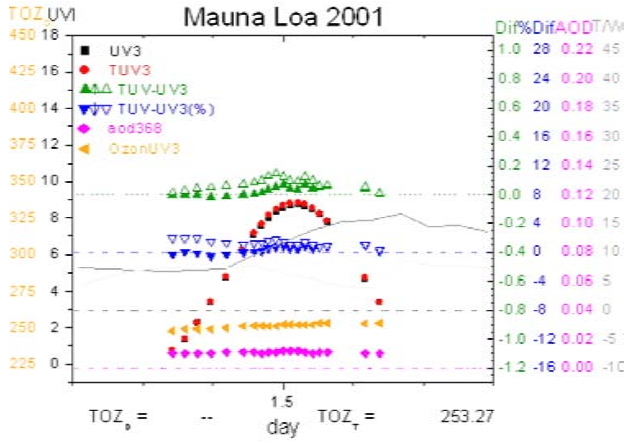
Mauna Loa 2001
TOZ UVI
Dif%Dif AOD T/W
UV3
TUV3
TUV-UV3
TUV-UV3(%)
aod368
OzonUV3
1.5
day
TOZ$_o$ = --
TOZ$_T$ = 253.27

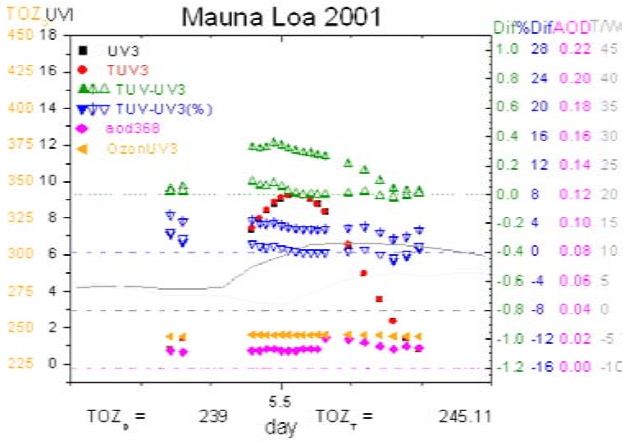
Mauna Loa 2001
TOZ UVI
Dif%Dif AOD T/W
UV3
TUV3
TUV-UV3
TUV-UV3(%)
aod368
OzonUV3
5.5
day
TOZ$_o$ = 239
TOZ$_T$ = 245.11

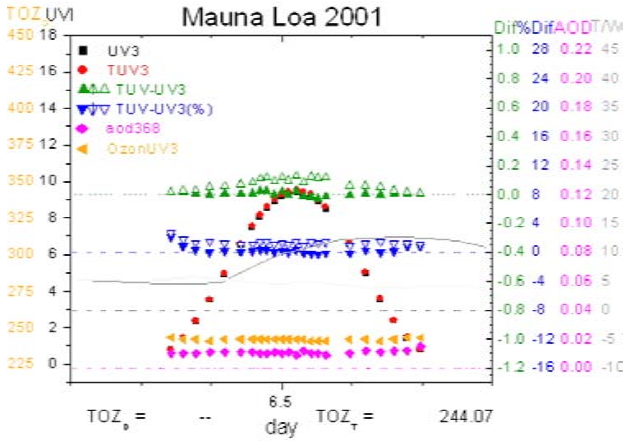
Mauna Loa 2001
TOZ UVI
Dif%Dif AOD T/W
UV3
TUV3
TUV-UV3
TUV-UV3(%)
aod368
OzonUV3
6.5
day
TOZ$_o$ = --
TOZ$_T$ = 244.07

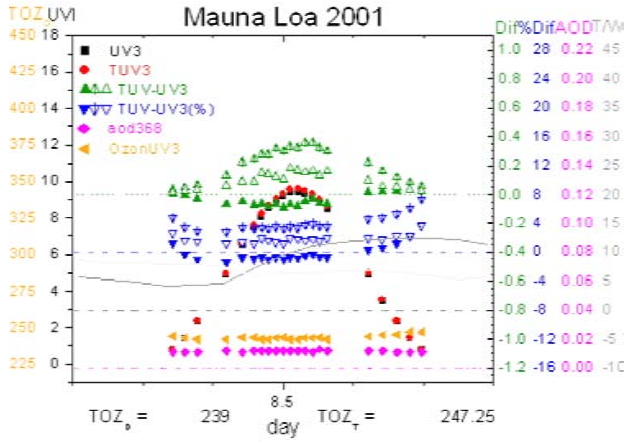
Mauna Loa 2001
TOZ UVI
Dif%Dif AOD T/W
UV3
TUV3
TUV-UV3
TUV-UV3(%)
aod368
OzonUV3
8.5
day
TOZ$_o$ = 239
TOZ$_T$ = 247.25

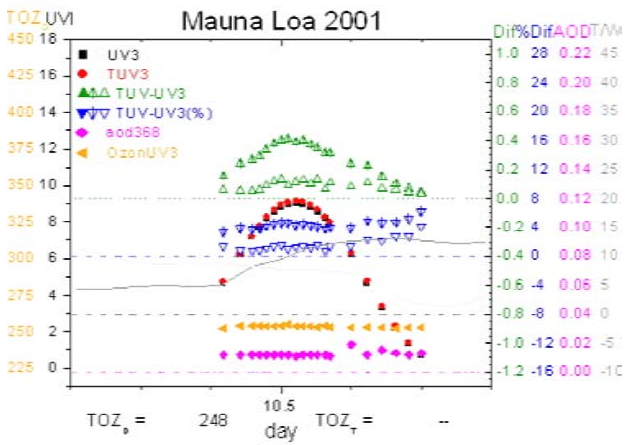
Mauna Loa 2001
TOZ UVI
Dif%Dif AOD T/W
UV3
TUV3
TUV-UV3
TUV-UV3(%)
aod368
OzonUV3
10.5
day
TOZ$_o$ = 248
TOZ$_T$ = --

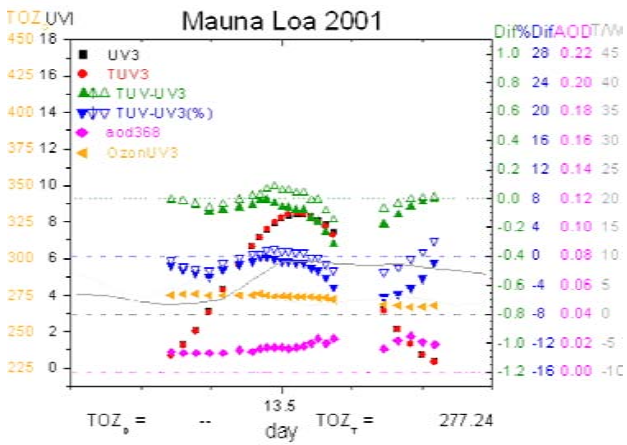
Mauna Loa 2001
TOZ UVI
Dif%Dif AOD T/W
UV3
TUV3
TUV-UV3
TUV-UV3(%)
aod368
OzonUV3
13.5
day
TOZ$_o$ = --
TOZ$_T$ = 277.24

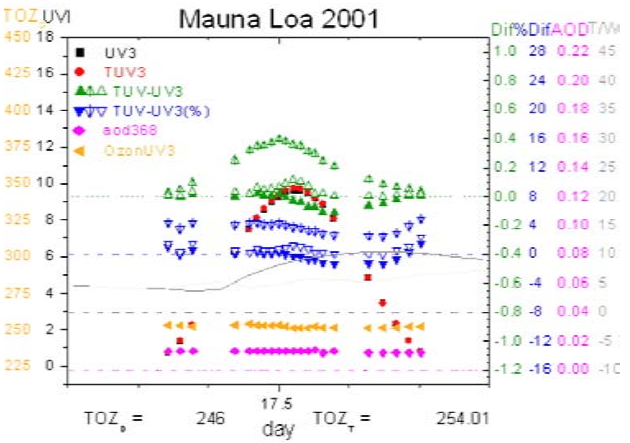
Mauna Loa 2001
TOZ UVI
Dif%Dif AOD T/W
UV3
TUV3
TUV-UV3
TUV-UV3(%)
aod368
OzonUV3
17.5
day
TOZ$_o$ = 246
TOZ$_T$ = 254.01

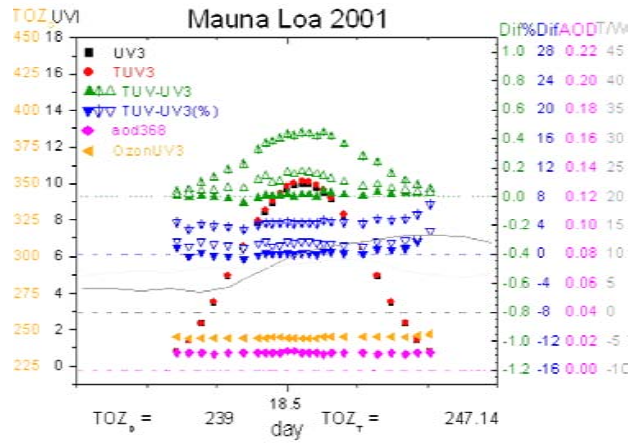
Mauna Loa 2001
TOZ UVI
Dif%Dif AOD T/W
UV3
TUV3
TUV-UV3
TUV-UV3(%)
aod368
OzonUV3
18.5
day
TOZ$_o$ = 239
TOZ$_T$ = 247.14

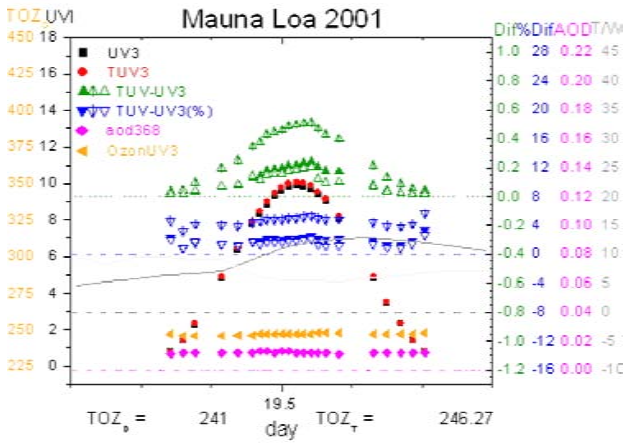
Mauna Loa 2001
TOZ UVI
Dif%Dif AOD T/W
UV3
TUV3
TUV-UV3
TUV-UV3(%)
aod368
OzonUV3
19.5
day
TOZ$_o$ = 241
TOZ$_T$ = 246.27

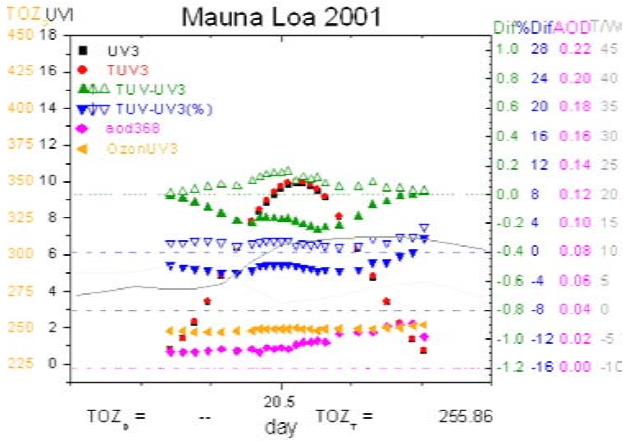
Mauna Loa 2001
TOZ UVI
Dif%Dif AOD T/W
UV3
TUV3
TUV-UV3
TUV-UV3(%)
aod368
OzonUV3
20.5
day
TOZ$_o$ = --
TOZ$_T$ = 255.86

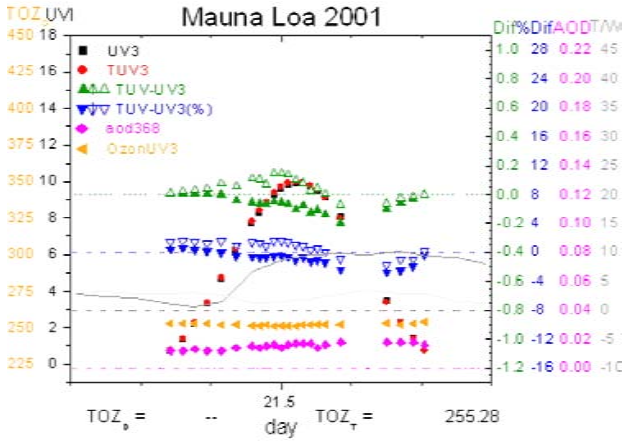
Mauna Loa 2001
TOZ UVI
Dif%Dif AOD T/W
UV3
TUV3
TUV-UV3
TUV-UV3(%)
aod368
OzonUV3
21.5
day
TOZ$_o$ = --
TOZ$_T$ = 255.28

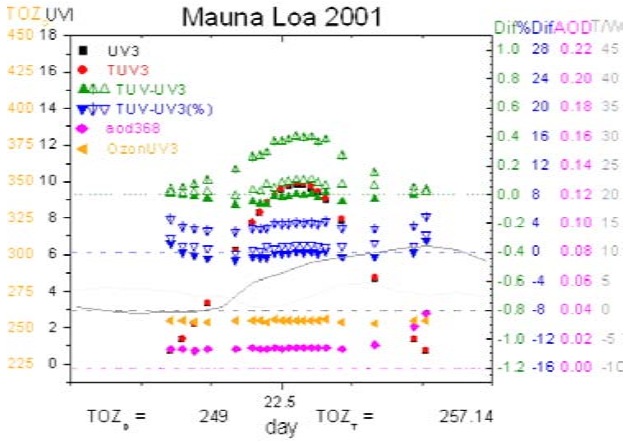
Mauna Loa 2001
TOZ UVI
Dif%Dif AOD T/W
UV3
TUV3
TUV-UV3
TUV-UV3(%)
aod368
OzonUV3
22.5
day
TOZ$_o$ = 249
TOZ$_T$ = 257.14

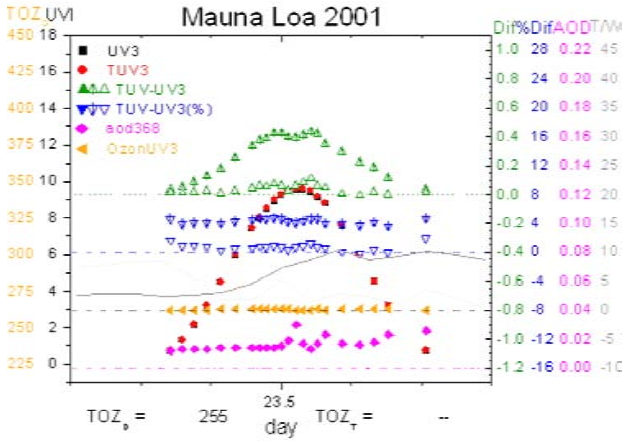
Mauna Loa 2001
TOZ UVI
Dif%Dif AOD T/W
UV3
TUV3
TUV-UV3
TUV-UV3(%)
aod368
OzonUV3
23.5
day
TOZ$_o$ = 255
TOZ$_T$ = --

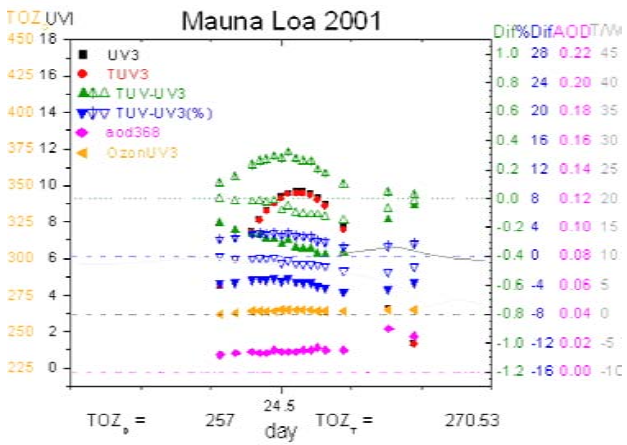
Mauna Loa 2001
TOZ UVI
Dif%Dif AOD T/W
UV3
TUV3
TUV-UV3
TUV-UV3(%)
aod368
OzonUV3
24.5
day
TOZ$_o$ = 257
TOZ$_T$ = 270.53

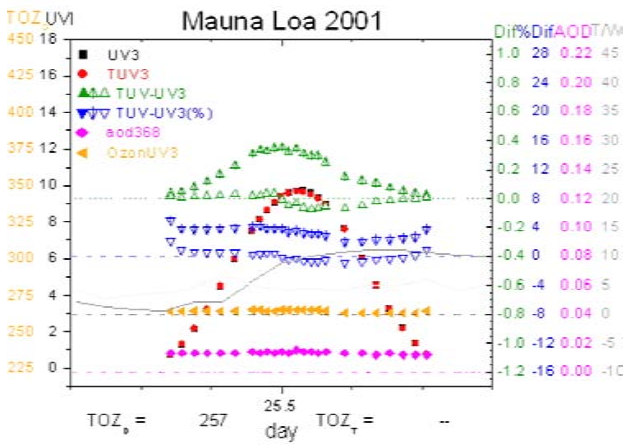
Mauna Loa 2001
TOZ UVI
Dif%Dif AOD T/W
UV3
TUV3
TUV-UV3
TUV-UV3(%)
aod368
OzonUV3
25.5
day
TOZ$_o$ = 257
TOZ$_T$ = --

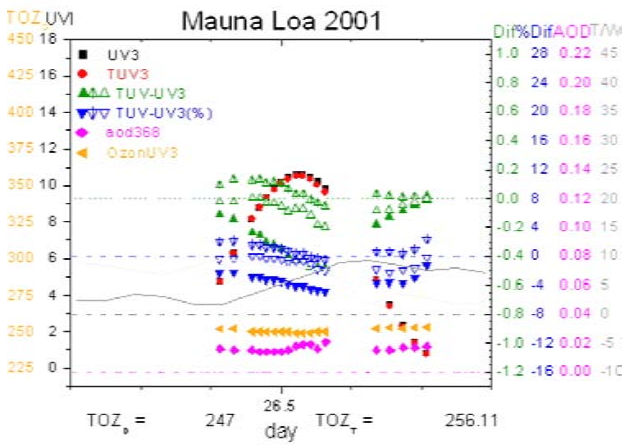
Mauna Loa 2001
TOZ UVI
Dif%Dif AOD T/W
UV3
TUV3
TUV-UV3
TUV-UV3(%)
aod368
OzonUV3
26.5
day
TOZ$_o$ = 247
TOZ$_T$ = 256.11

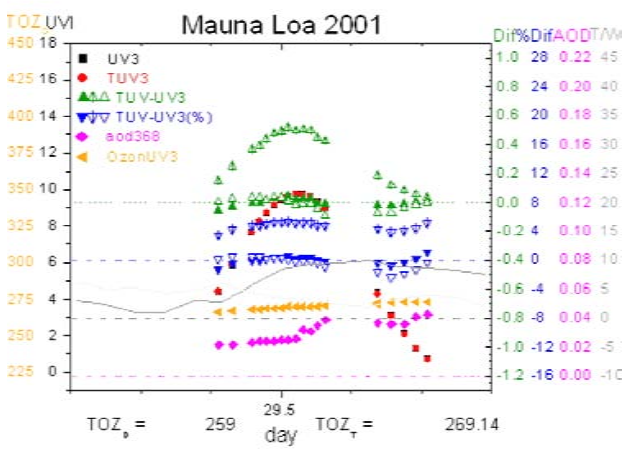
Mauna Loa 2001
TOZ UVI
Dif%Dif AOD T/W
UV3
TUV3
TUV-UV3
TUV-UV3(%)
aod368
OzonUV3
29.5
day
TOZ$_o$ = 259
TOZ$_T$ = 269.14

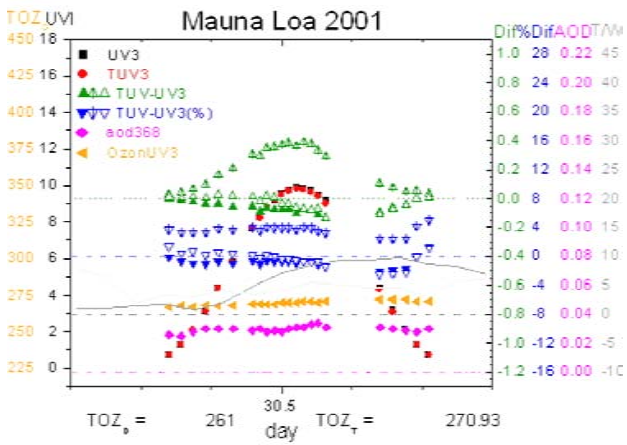
Mauna Loa 2001
TOZ UVI
Dif%Dif AOD T/W
UV3
TUV3
TUV-UV3
TUV-UV3(%)
aod368
OzonUV3
30.5
day
TOZ$_o$ = 261
TOZ$_T$ = 270.93

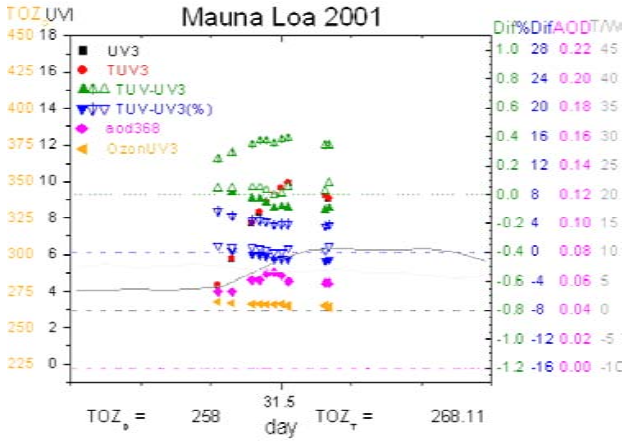
Mauna Loa 2001
TOZ UVI
Dif%Dif AOD T/W
UV3
TUV3
TUV-UV3
TUV-UV3(%)
aod368
OzonUV3
31.5
day
TOZ$_o$ = 258
TOZ$_T$ = 268.11

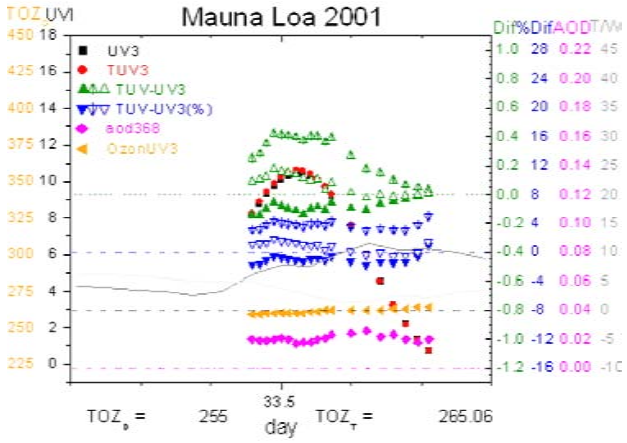
Mauna Loa 2001
TOZ UVI
Dif%Dif AOD T/W
UV3
TUV3
TUV-UV3
TUV-UV3(%)
aod368
OzonUV3
33.5
day
TOZ$_o$ = 255
TOZ$_T$ = 265.06

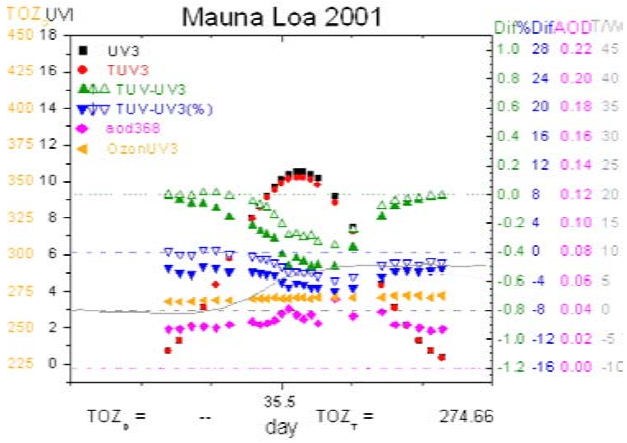
Mauna Loa 2001
TOZ UVI
Dif%Dif AOD T/W
UV3
TUV3
TUV-UV3
TUV-UV3(%)
aod368
OzonUV3
35.5
day
TOZ$_o$ = --
TOZ$_T$ = 274.66

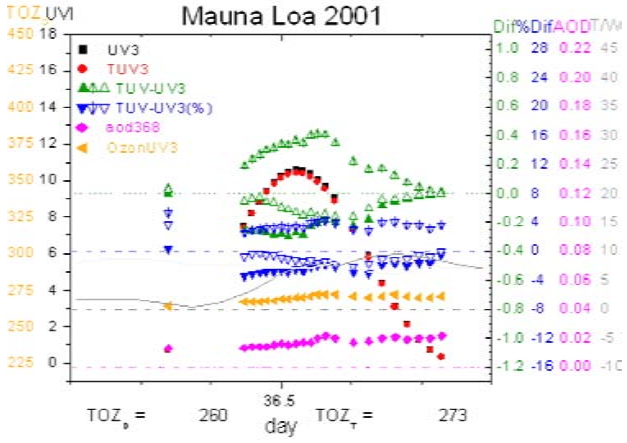
Mauna Loa 2001
TOZ UVI
Dif%Dif AOD T/W
UV3
TUV3
TUV-UV3
TUV-UV3(%)
aod368
OzonUV3
36.5
day
TOZ$_o$ = 260
TOZ$_T$ = 273

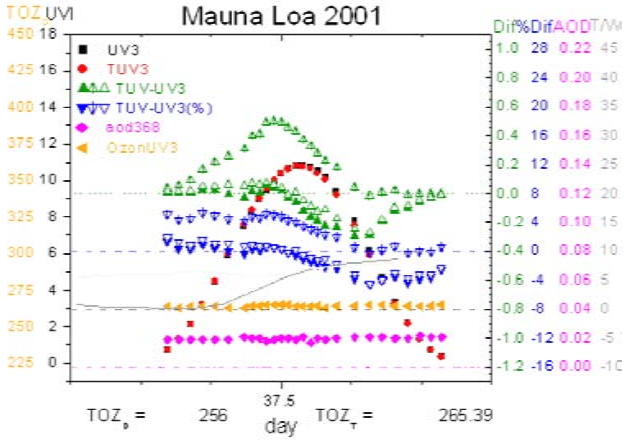
Mauna Loa 2001
TOZ UVI
Dif%Dif AOD T/W
UV3
TUV3
TUV-UV3
TUV-UV3(%)
aod368
OzonUV3
37.5
day
TOZ$_o$ = 256
TOZ$_T$ = 265.39

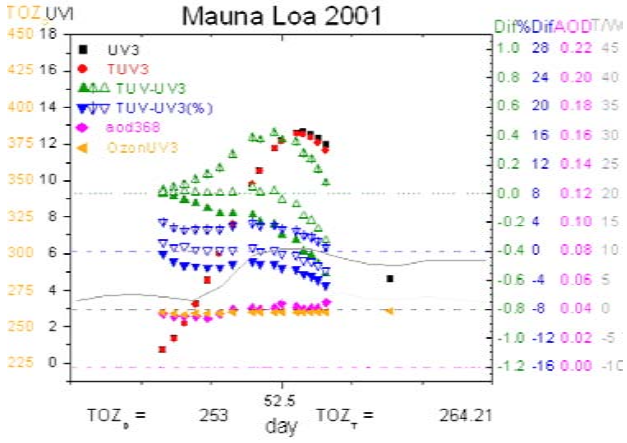
Mauna Loa 2001
TOZ UVI
Dif%Dif AOD T/W
UV3
TUV3
TUV-UV3
TUV-UV3(%)
aod368
OzonUV3
52.5
day
TOZ$_o$ = 253
TOZ$_T$ = 264.21

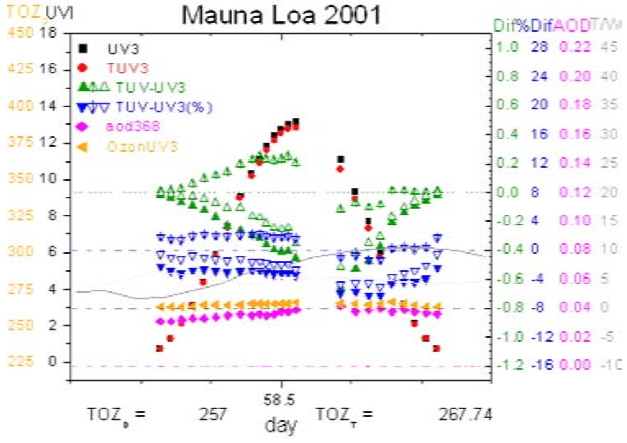
Mauna Loa 2001
TOZ UVI
Dif%Dif AOD T/W
UV3
TUV3
TUV-UV3
TUV-UV3(%)
aod368
OzonUV3
58.5
day
TOZ$_o$ = 257
TOZ$_T$ = 267.74

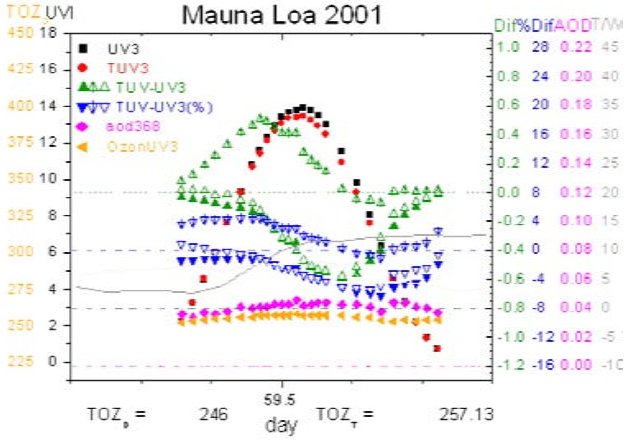
Mauna Loa 2001
TOZ UVI
Dif%Dif AOD T/W
UV3
TUV3
TUV-UV3
TUV-UV3(%)
aod368
OzonUV3
59.5
day
TOZ$_o$ = 246
TOZ$_T$ = 257.13

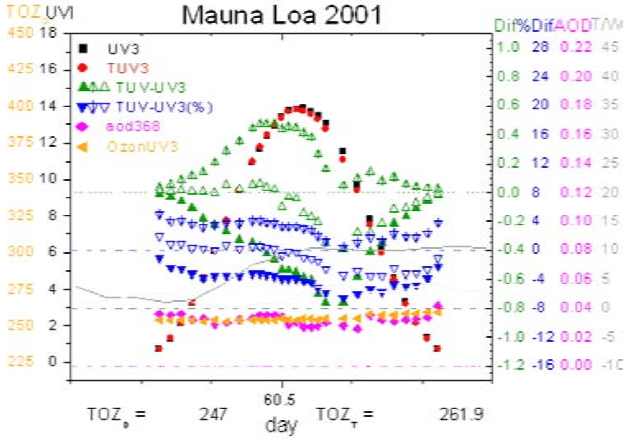
Mauna Loa 2001
TOZ UVI
Dif%Dif AOD T/W
UV3
TUV3
TUV-UV3
TUV-UV3(%)
aod368
OzonUV3
60.5
day
TOZ$_o$ = 247
TOZ$_T$ = 261.9

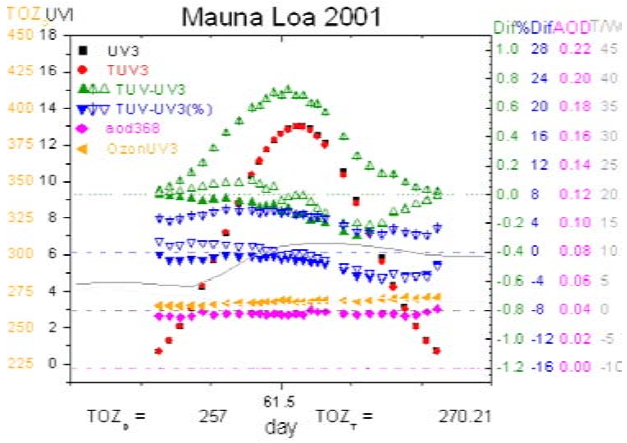
Mauna Loa 2001
TOZ UVI
Dif% Dif AOD T/W
UV3
TUV3
TUV-UV3
TUV-UV3(%)
aod368
OzonUV3
61.5
day
TOZ$_0$ = 257
TOZ$_T$ = 270.21

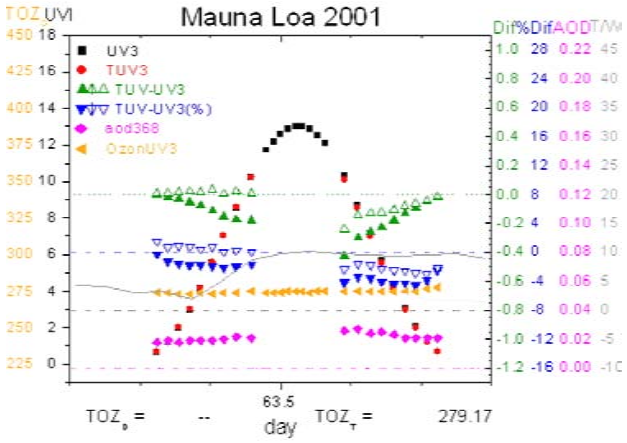
Mauna Loa 2001
TOZ UVI
Dif% Dif AOD T/W
UV3
TUV3
TUV-UV3
TUV-UV3(%)
aod368
OzonUV3
63.5
day
TOZ$_0$ = --
TOZ$_T$ = 279.17

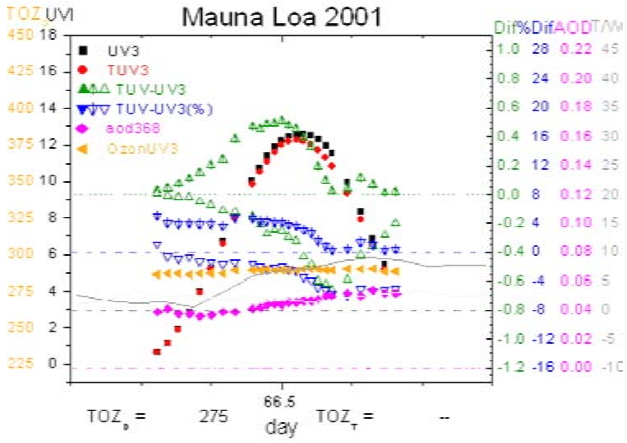
Mauna Loa 2001
TOZ UVI
Dif% Dif AOD T/W
UV3
TUV3
TUV-UV3
TUV-UV3(%)
aod368
OzonUV3
66.5
day
TOZ$_0$ = 275
TOZ$_T$ = --

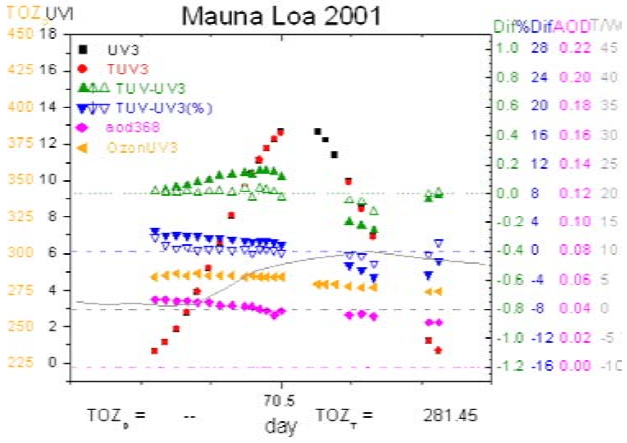
Mauna Loa 2001
TOZ UVI
Dif% Dif AOD T/W
UV3
TUV3
TUV-UV3
TUV-UV3(%)
aod368
OzonUV3
70.5
day
TOZ$_0$ = --
TOZ$_T$ = 281.45

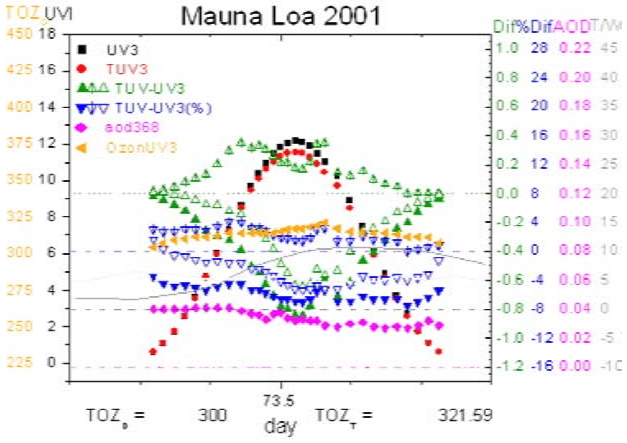
Mauna Loa 2001
TOZ UVI
Dif% Dif AOD T/W
UV3
TUV3
TUV-UV3
TUV-UV3(%)
aod368
OzonUV3
73.5
day
TOZ$_0$ = 300
TOZ$_T$ = 321.59

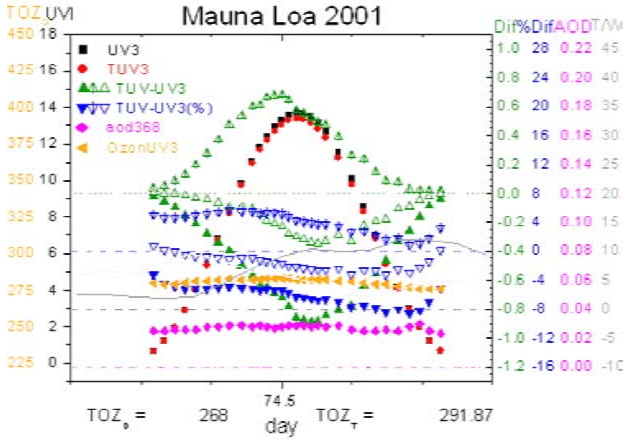
Mauna Loa 2001
TOZ UVI
Dif% Dif AOD T/W
UV3
TUV3
TUV-UV3
TUV-UV3(%)
aod368
OzonUV3
74.5
day
TOZ$_0$ = 268
TOZ$_T$ = 291.87

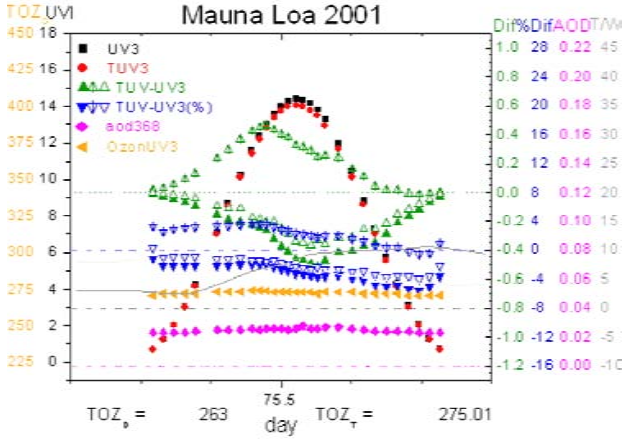
Mauna Loa 2001
TOZ UVI
Dif% Dif AOD T/W
UV3
TUV3
TUV-UV3
TUV-UV3(%)
aod368
OzonUV3
75.5
day
TOZ$_0$ = 263
TOZ$_T$ = 275.01

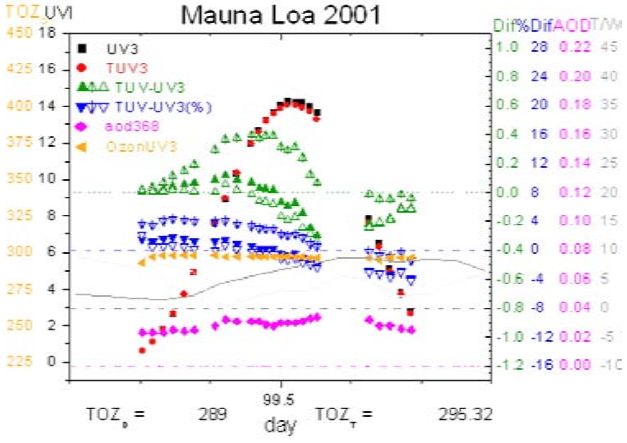
Mauna Loa 2001
TOZ UVI
Dif% Dif AOD T/W
UV3
TUV3
TUV-UV3
TUV-UV3(%)
aod368
OzonUV3
99.5
day
TOZ$_0$ = 289
TOZ$_T$ = 295.32

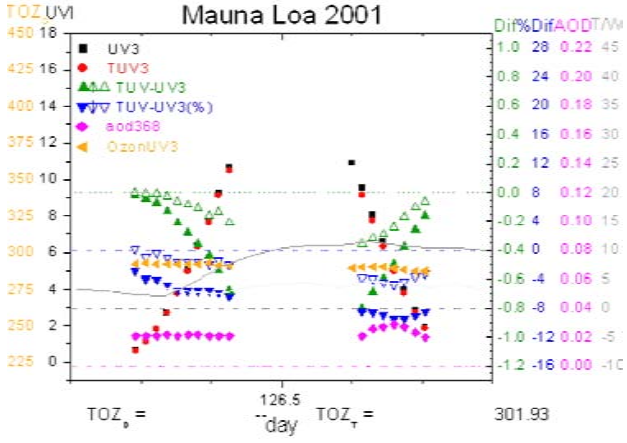
Mauna Loa 2001
TOZ UVI
Dif% Dif AOD T/W
UV3
TUV3
TUV-UV3
TUV-UV3(%)
aod368
OzonUV3
126.5
day
TOZ$_0$ = --
TOZ$_T$ = 301.93

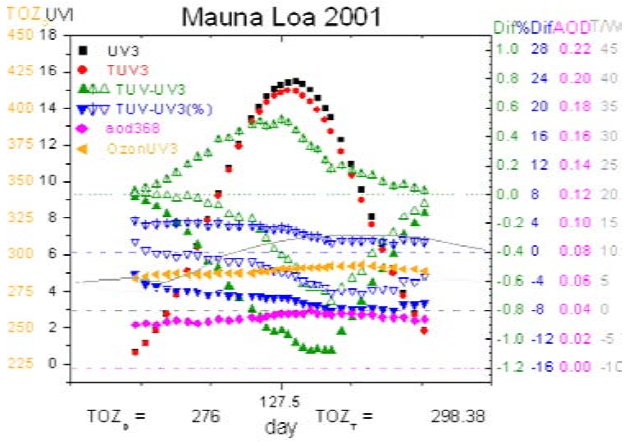
Mauna Loa 2001
TOZ UVI
Dif%Dif AOD T/W
UV3
TUV3
TUV-UV3
TUV-UV3(%)
aod368
OzonUV3
127.5
day
TOZ$_o$ = 276
TOZ$_T$ = 298.38

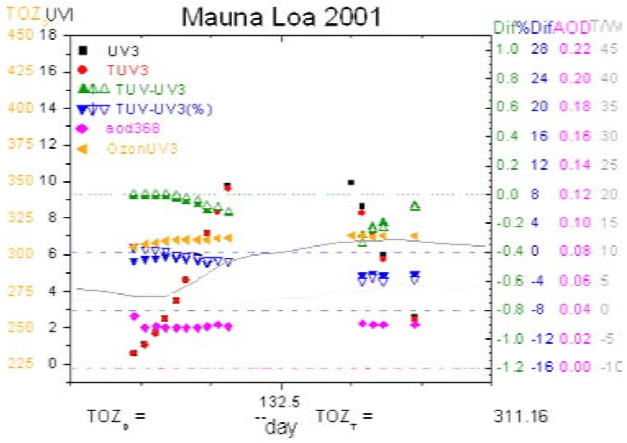
Mauna Loa 2001
TOZ UVI
Dif%Dif AOD T/W
UV3
TUV3
TUV-UV3
TUV-UV3(%)
aod368
OzonUV3
132.5
day
TOZ$_o$ =
TOZ$_T$ = 311.16

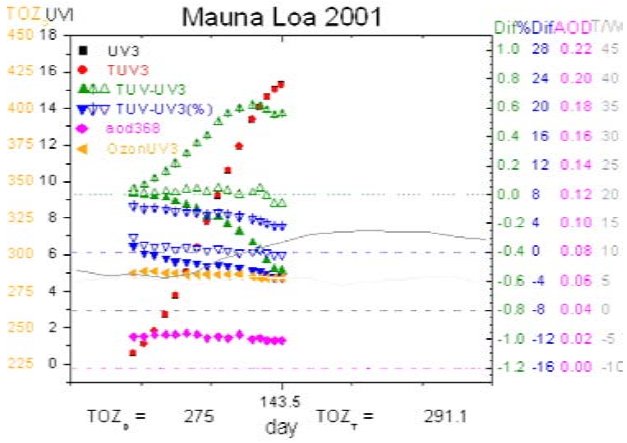
Mauna Loa 2001
TOZ UVI
Dif%Dif AOD T/W
UV3
TUV3
TUV-UV3
TUV-UV3(%)
aod368
OzonUV3
143.5
day
TOZ$_o$ = 275
TOZ$_T$ = 291.1

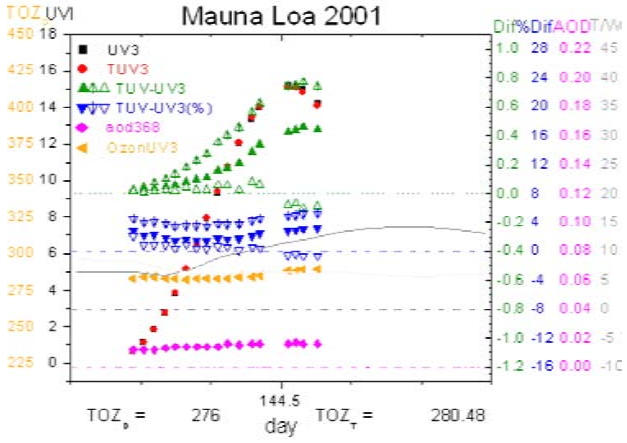
Mauna Loa 2001
TOZ UVI
Dif%Dif AOD T/W
UV3
TUV3
TUV-UV3
TUV-UV3(%)
aod368
OzonUV3
144.5
day
TOZ$_o$ = 276
TOZ$_T$ = 280.48

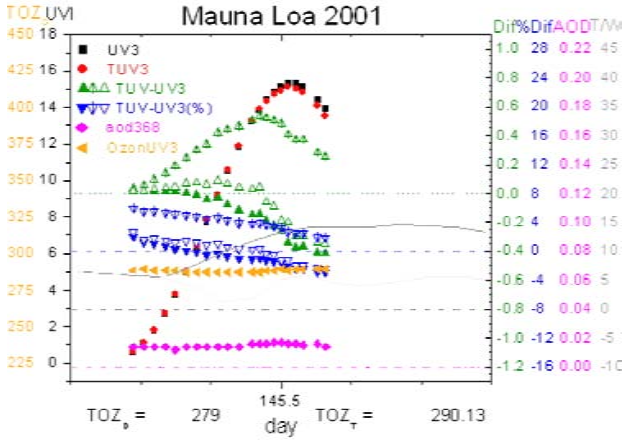
Mauna Loa 2001
TOZ UVI
Dif%Dif AOD T/W
UV3
TUV3
TUV-UV3
TUV-UV3(%)
aod368
OzonUV3
145.5
day
TOZ$_o$ = 279
TOZ$_T$ = 290.13

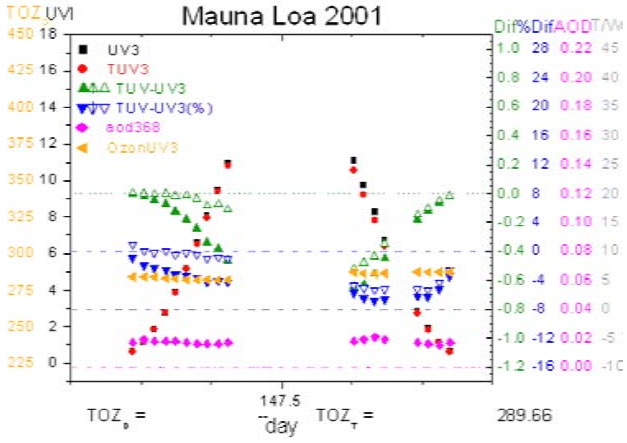
Mauna Loa 2001
TOZ UVI
Dif%Dif AOD T/W
UV3
TUV3
TUV-UV3
TUV-UV3(%)
aod368
OzonUV3
147.5
day
TOZ$_o$ =
TOZ$_T$ = 289.66

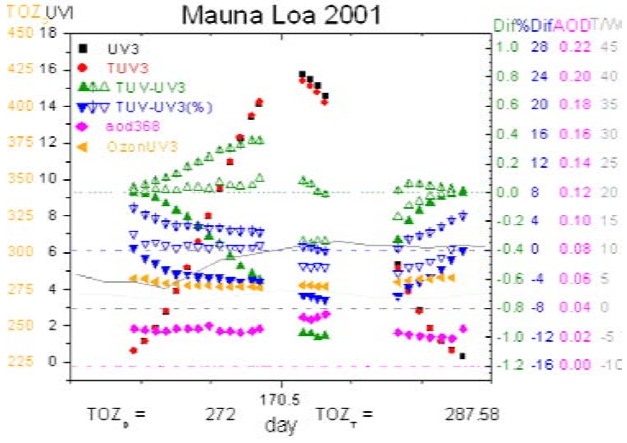
Mauna Loa 2001
TOZ UVI
Dif%Dif AOD T/W
UV3
TUV3
TUV-UV3
TUV-UV3(%)
aod368
OzonUV3
170.5
day
TOZ$_o$ = 272
TOZ$_T$ = 287.58

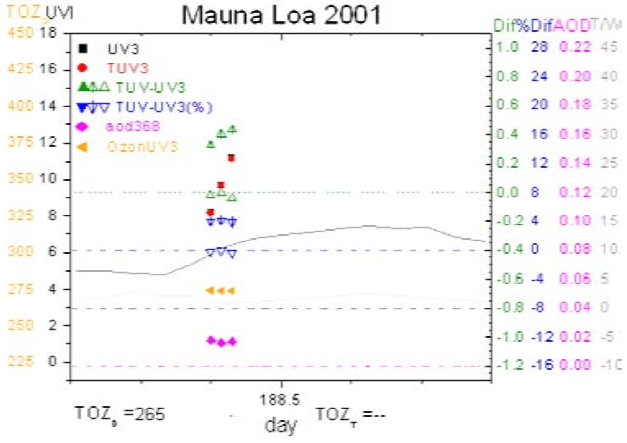
Mauna Loa 2001
TOZ UVI
Dif%Dif AOD T/W
UV3
TUV3
TUV-UV3
TUV-UV3(%)
aod368
OzonUV3
188.5
day
TOZ$_o$ =265
TOZ$_T$ =--

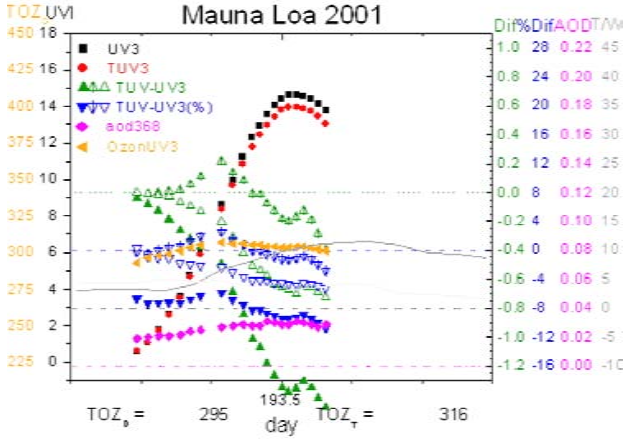
Mauna Loa 2001
TOZ UVI
Dif%Dif AOD T/W
UV3
TUV3
TUV-UV3
TUV-UV3(%)
aod368
OzonUV3
193.5
day
TOZ$_o$ = 295
TOZ$_T$ = 316

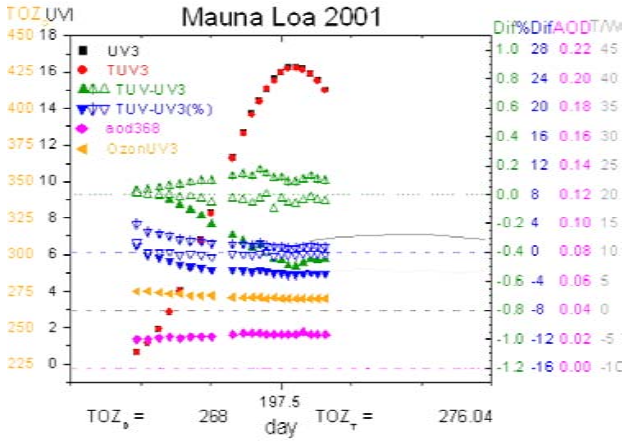
Mauna Loa 2001
TOZ UVI
Dif%Dif AOD T/W
UV3
TUV3
TUV-UV3
TUV-UV3(%)
aod368
OzonUV3
197.5
day
TOZ0 = 268
TOZT = 276.04

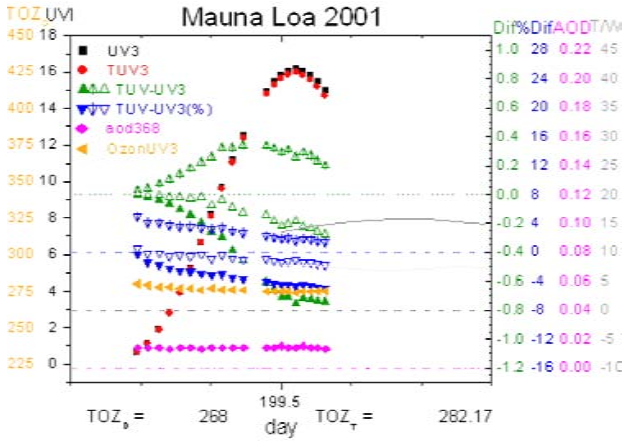
Mauna Loa 2001
TOZ UVI
Dif%Dif AOD T/W
UV3
TUV3
TUV-UV3
TUV-UV3(%)
aod368
OzonUV3
199.5
day
TOZ0 = 268
TOZT = 282.17

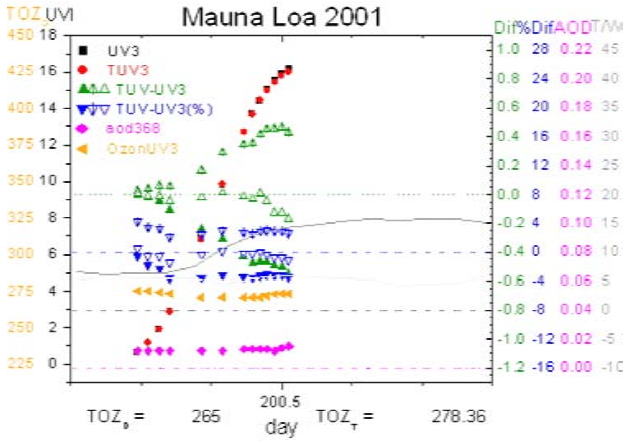
Mauna Loa 2001
TOZ UVI
Dif%Dif AOD T/W
UV3
TUV3
TUV-UV3
TUV-UV3(%)
aod368
OzonUV3
200.5
day
TOZ0 = 265
TOZT = 278.36

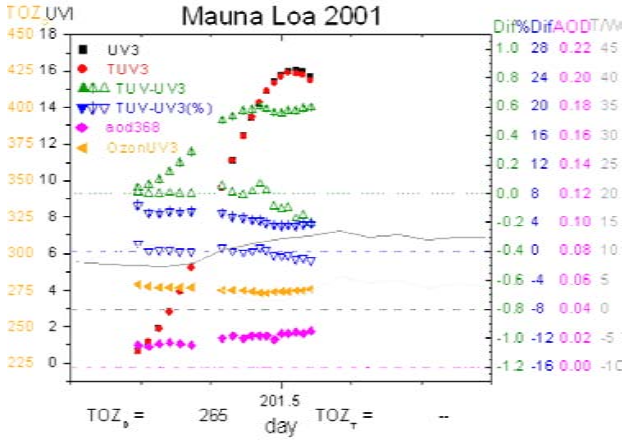
Mauna Loa 2001
TOZ UVI
Dif%Dif AOD T/W
UV3
TUV3
TUV-UV3
TUV-UV3(%)
aod368
OzonUV3
201.5
day
TOZ0 = 265
TOZT = --

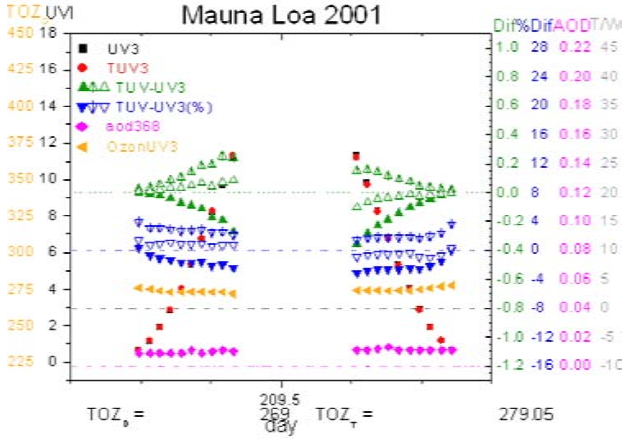
Mauna Loa 2001
TOZ UVI
Dif%Dif AOD T/W
UV3
TUV3
TUV-UV3
TUV-UV3(%)
aod368
OzonUV3
209.5
day
TOZ0 = 269
TOZT = 279.05

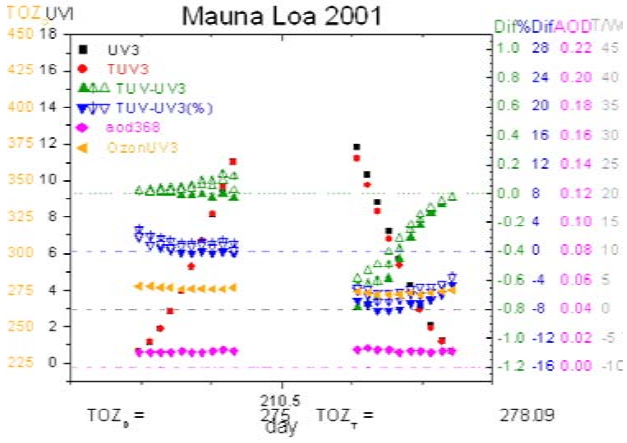
Mauna Loa 2001
TOZ UVI
Dif%Dif AOD T/W
UV3
TUV3
TUV-UV3
TUV-UV3(%)
aod368
OzonUV3
210.5
day
TOZ0 = 275
TOZT = 278.09

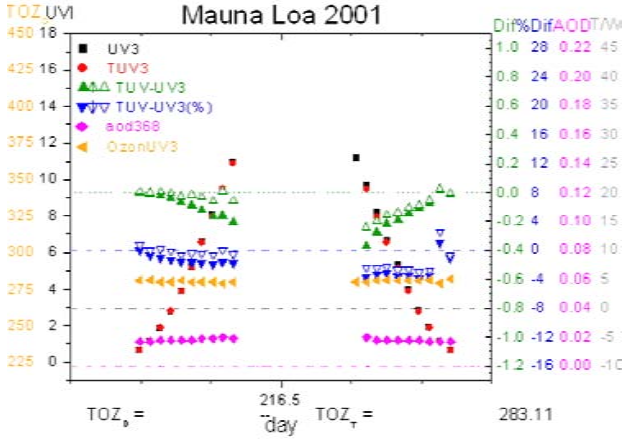
Mauna Loa 2001
TOZ UVI
Dif%Dif AOD T/W
UV3
TUV3
TUV-UV3
TUV-UV3(%)
aod368
OzonUV3
216.5
day
TOZ0 = --
TOZT = 283.11

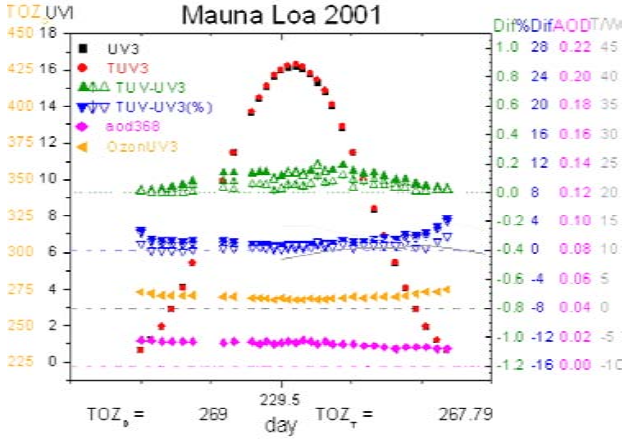
Mauna Loa 2001
TOZ UVI
Dif%Dif AOD T/W
UV3
TUV3
TUV-UV3
TUV-UV3(%)
aod368
OzonUV3
229.5
day
TOZ0 = 269
TOZT = 267.79

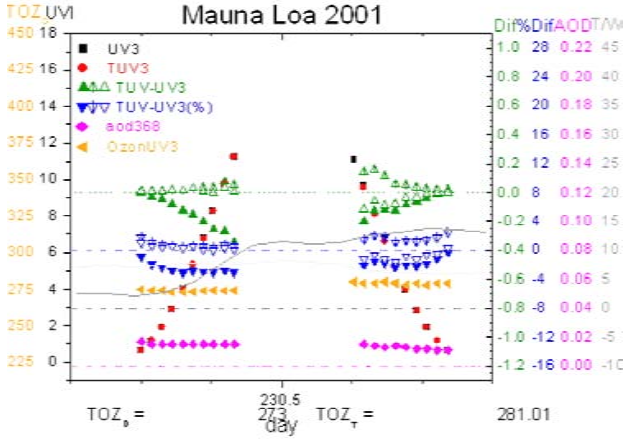
Mauna Loa 2001
TOZ UVI
Dif%Dif AOD T/W
UV3
TUV3
TUV-UV3
TUV-UV3(%)
aod368
OzonUV3
230.5
day
TOZ0 = 273
TOZT = 281.01

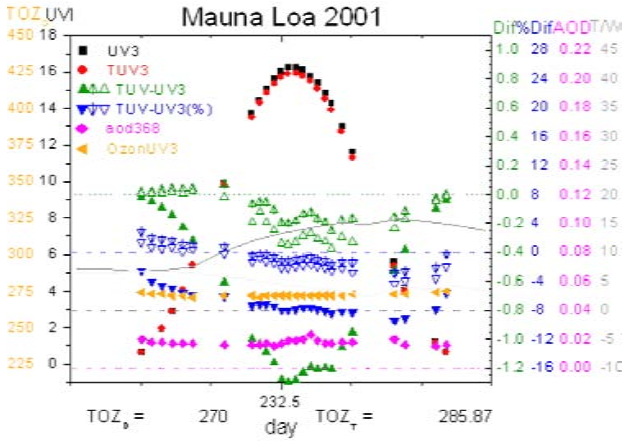
Mauna Loa 2001
TOZ UVI
Dif% Dif AOD T/W
UV3
TUV3
TUV-UV3
TUV-UV3(%)
aod368
OzonUV3
232.5
day
TOZ0 = 270
TOZT = 285.87

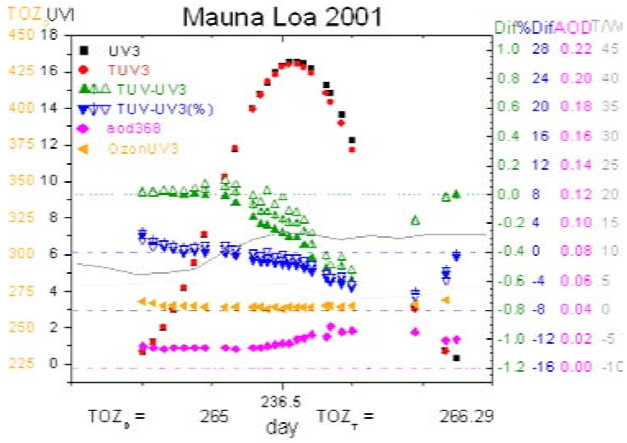
Mauna Loa 2001
TOZ UVI
Dif% Dif AOD T/W
UV3
TUV3
TUV-UV3
TUV-UV3(%)
aod368
OzonUV3
236.5
day
TOZ0 = 265
TOZT = 266.29

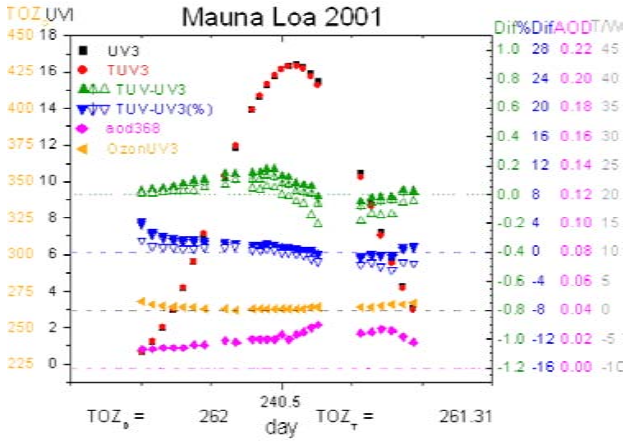
Mauna Loa 2001
TOZ UVI
Dif% Dif AOD T/W
UV3
TUV3
TUV-UV3
TUV-UV3(%)
aod368
OzonUV3
240.5
day
TOZ0 = 262
TOZT = 261.31

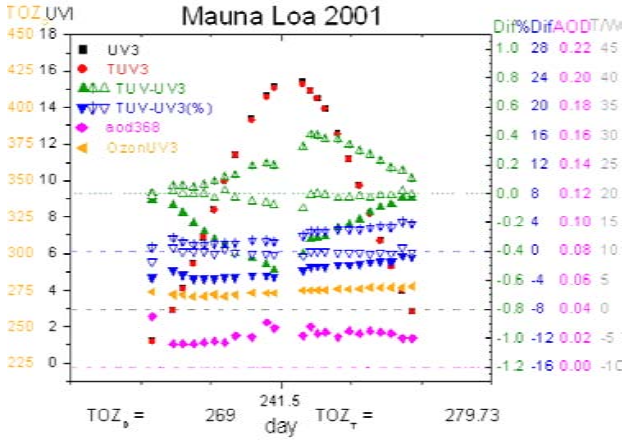
Mauna Loa 2001
TOZ UVI
Dif% Dif AOD T/W
UV3
TUV3
TUV-UV3
TUV-UV3(%)
aod368
OzonUV3
241.5
day
TOZ0 = 269
TOZT = 279.73

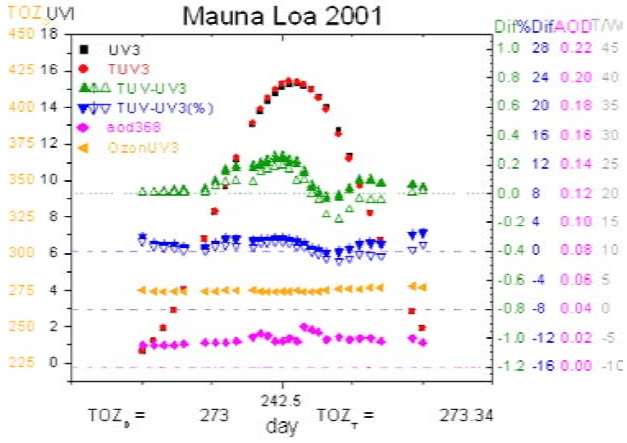
Mauna Loa 2001
TOZ UVI
Dif% Dif AOD T/W
UV3
TUV3
TUV-UV3
TUV-UV3(%)
aod368
OzonUV3
242.5
day
TOZ0 = 273
TOZT = 273.34

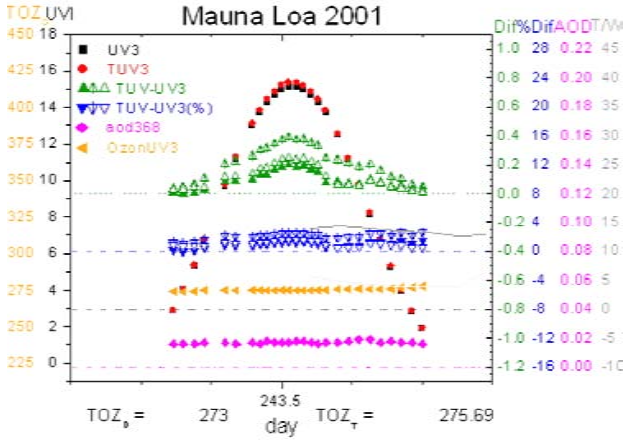
Mauna Loa 2001
TOZ UVI
Dif% Dif AOD T/W
UV3
TUV3
TUV-UV3
TUV-UV3(%)
aod368
OzonUV3
243.5
day
TOZ0 = 273
TOZT = 275.69

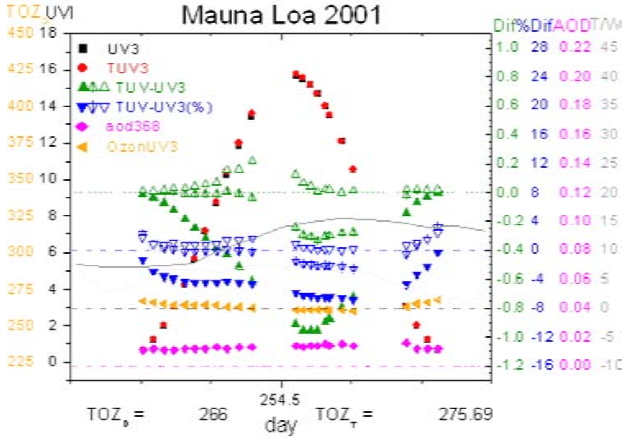
Mauna Loa 2001
TOZ UVI
Dif% Dif AOD T/W
UV3
TUV3
TUV-UV3
TUV-UV3(%)
aod368
OzonUV3
254.5
day
TOZ0 = 266
TOZT = 275.69

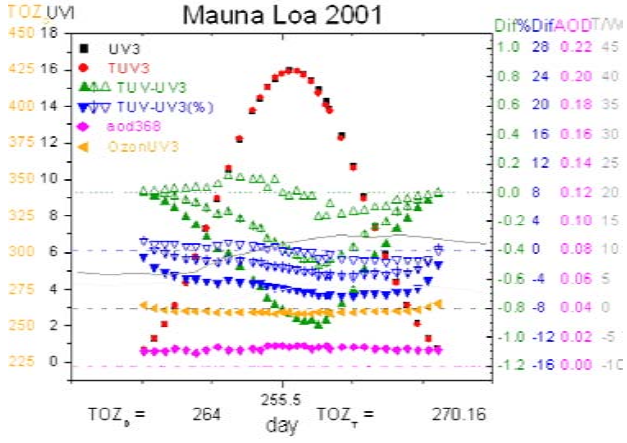
Mauna Loa 2001
TOZ UVI
Dif% Dif AOD T/W
UV3
TUV3
TUV-UV3
TUV-UV3(%)
aod368
OzonUV3
255.5
day
TOZ0 = 264
TOZT = 270.16

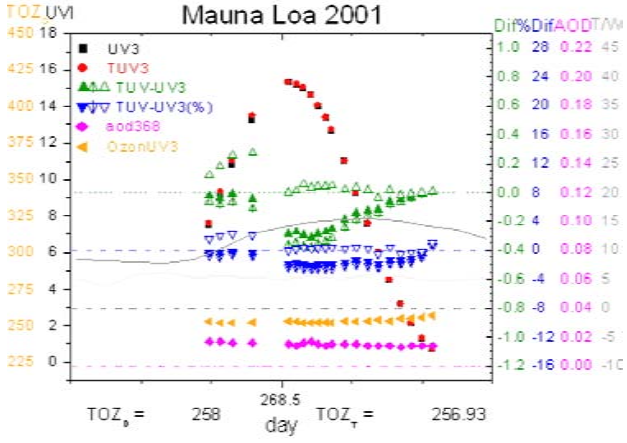
Mauna Loa 2001
TOZ UVI
Dif% Dif AOD T/W
UV3
TUV3
TUV-UV3
TUV-UV3(%)
aod368
OzonUV3
268.5
day
TOZ0 = 258
TOZT = 256.93

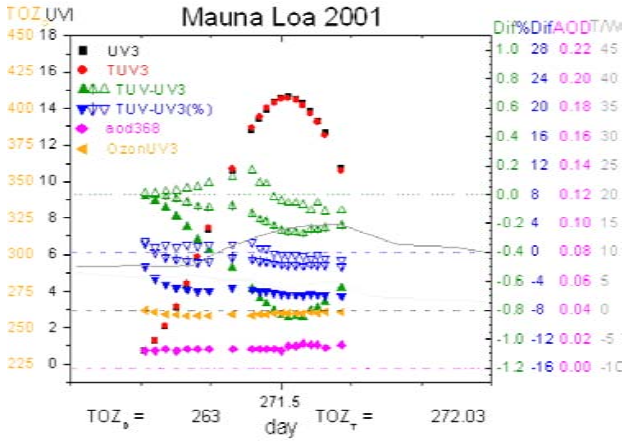
Mauna Loa 2001
UV3
TUV3
TUV-UV3
TUV-UV3(%)
aod368
OzonUV3
271.5
day
TOZ0 = 263
TOZT = 272.03

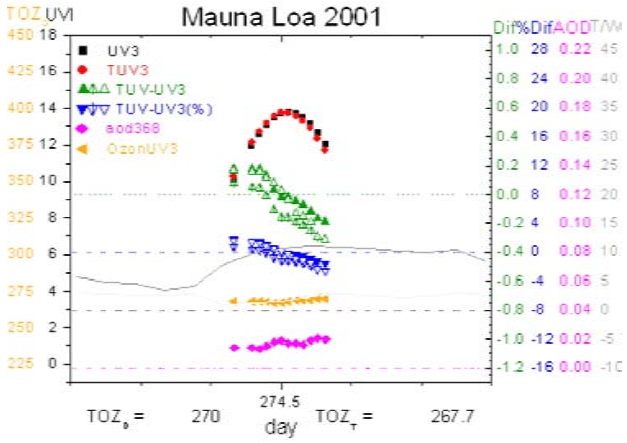
Mauna Loa 2001
UV3
TUV3
TUV-UV3
TUV-UV3(%)
aod368
OzonUV3
274.5
day
TOZ0 = 270
TOZT = 267.7

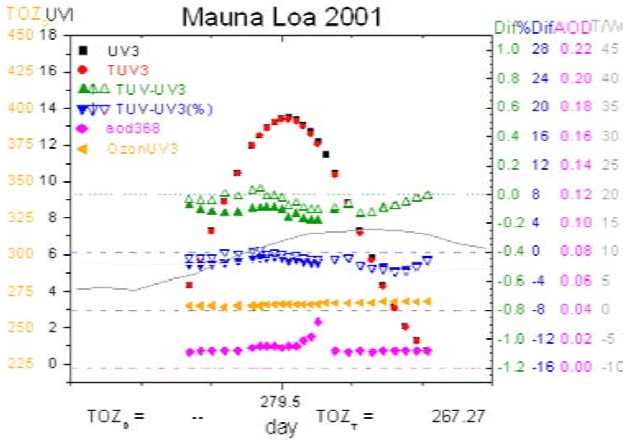
Mauna Loa 2001
UV3
TUV3
TUV-UV3
TUV-UV3(%)
aod368
OzonUV3
279.5
day
TOZ0 = --
TOZT = 267.27

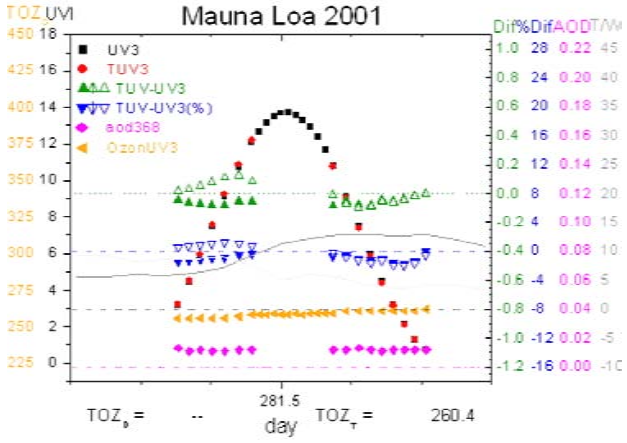
Mauna Loa 2001
UV3
TUV3
TUV-UV3
TUV-UV3(%)
aod368
OzonUV3
281.5
day
TOZ0 = --
TOZT = 260.4

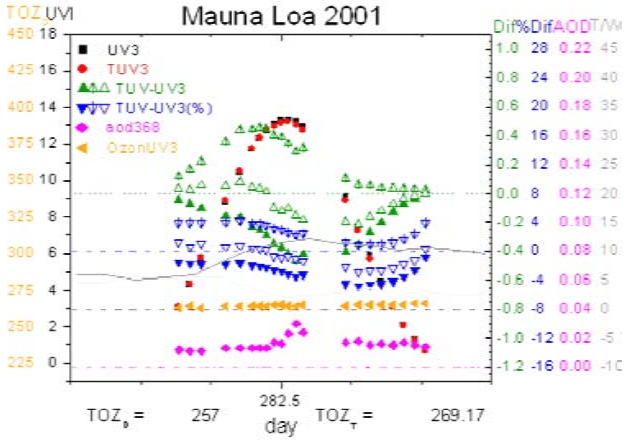
Mauna Loa 2001
UV3
TUV3
TUV-UV3
TUV-UV3(%)
aod368
OzonUV3
282.5
day
TOZ0 = 257
TOZT = 269.17

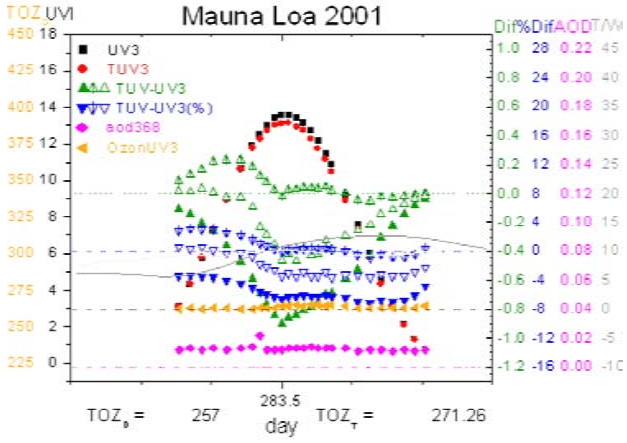
Mauna Loa 2001
UV3
TUV3
TUV-UV3
TUV-UV3(%)
aod368
OzonUV3
283.5
day
TOZ0 = 257
TOZT = 271.26

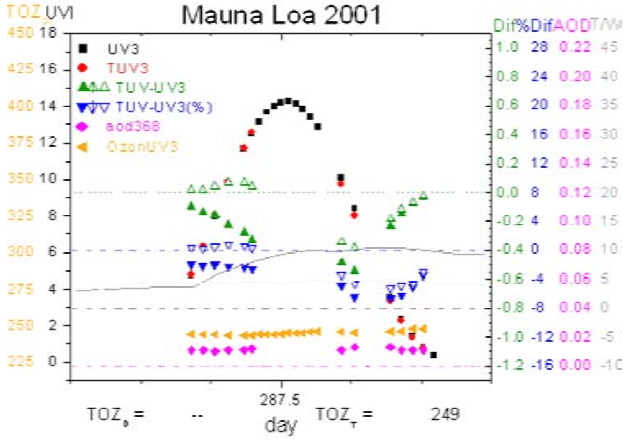
Mauna Loa 2001
UV3
TUV3
TUV-UV3
TUV-UV3(%)
aod368
OzonUV3
287.5
day
TOZ0 = --
TOZT = 249

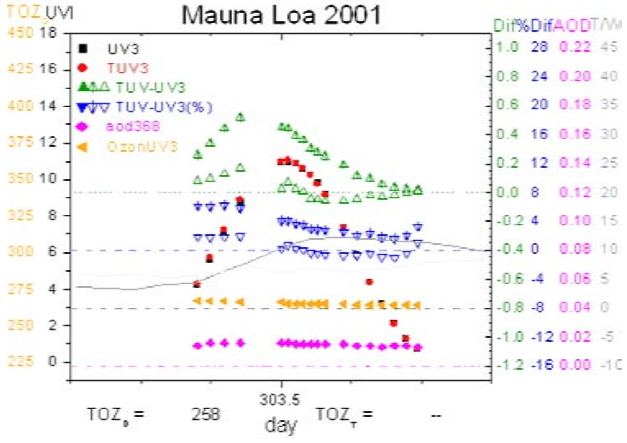
Mauna Loa 2001
UV3
TUV3
TUV-UV3
TUV-UV3(%)
aod368
OzonUV3
303.5
day
TOZ0 = 258
TOZT = --

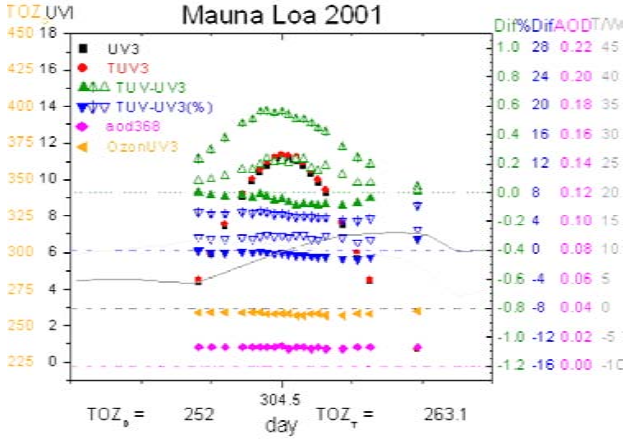
Mauna Loa 2001
UV3
TUV3
TUV-UV3
TUV-UV3(%)
aod368
OzonUV3
304.5
day
TOZ0 = 252
TOZT = 263.1

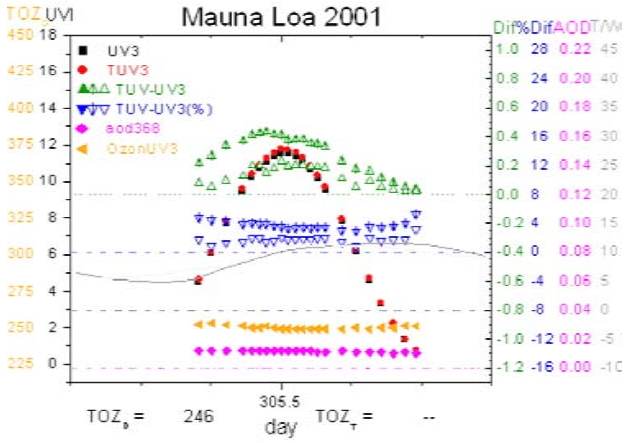
Mauna Loa 2001
TOZ UVI
Dif% Dif AOD T/W
UV3
TUV3
TUV-UV3
TUV-UV3(%)
aod368
OzonUV3
305.5
day
TOZ0 = 246
TOZT = --

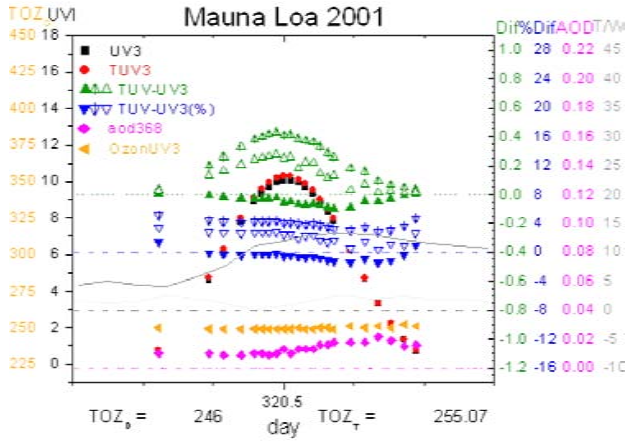
Mauna Loa 2001
TOZ UVI
Dif% Dif AOD T/W
UV3
TUV3
TUV-UV3
TUV-UV3(%)
aod368
OzonUV3
320.5
day
TOZ0 = 246
TOZT = 255.07

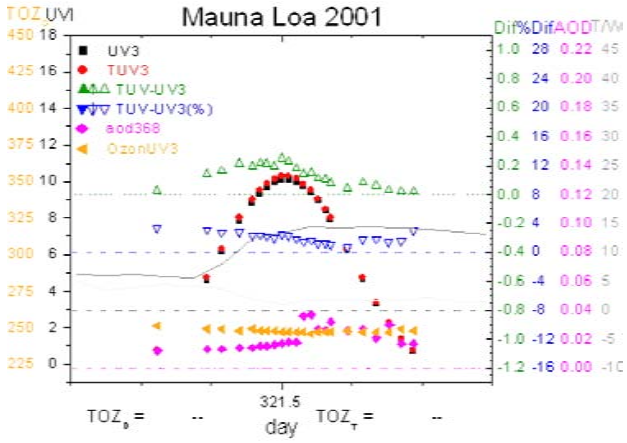
Mauna Loa 2001
TOZ UVI
Dif% Dif AOD T/W
UV3
TUV3
TUV-UV3
TUV-UV3(%)
aod368
OzonUV3
321.5
day
TOZ0 = --
TOZT = --

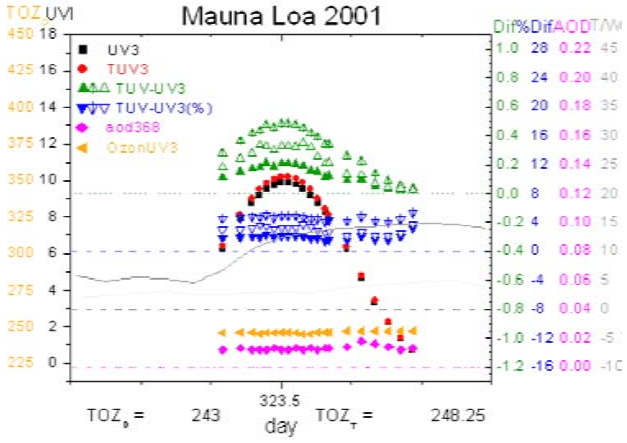
Mauna Loa 2001
TOZ UVI
Dif% Dif AOD T/W
UV3
TUV3
TUV-UV3
TUV-UV3(%)
aod368
OzonUV3
323.5
day
TOZ0 = 243
TOZT = 248.25

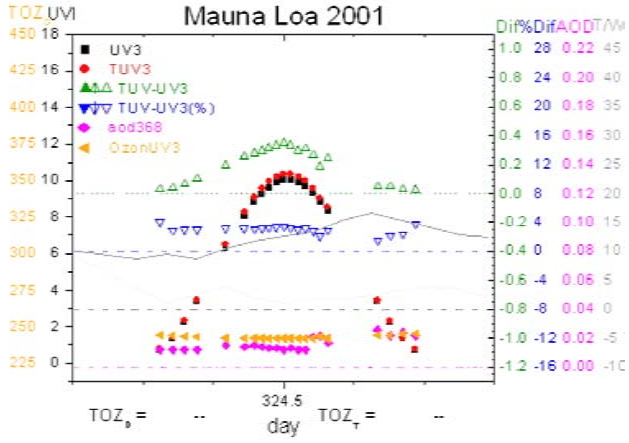
Mauna Loa 2001
TOZ UVI
Dif% Dif AOD T/W
UV3
TUV3
TUV-UV3
TUV-UV3(%)
aod368
OzonUV3
324.5
day
TOZ0 = --
TOZT = --

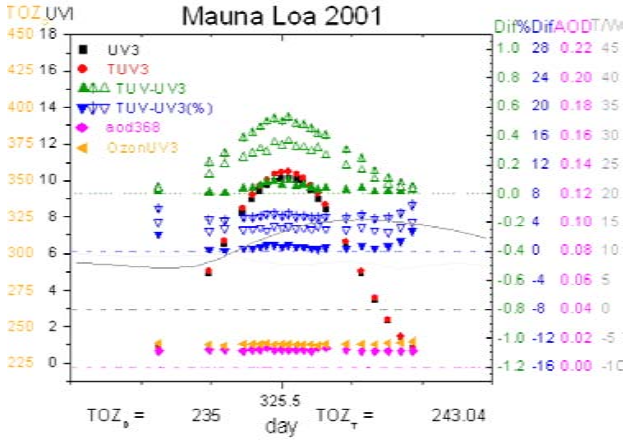
Mauna Loa 2001
TOZ UVI
Dif% Dif AOD T/W
UV3
TUV3
TUV-UV3
TUV-UV3(%)
aod368
OzonUV3
325.5
day
TOZ0 = 235
TOZT = 243.04

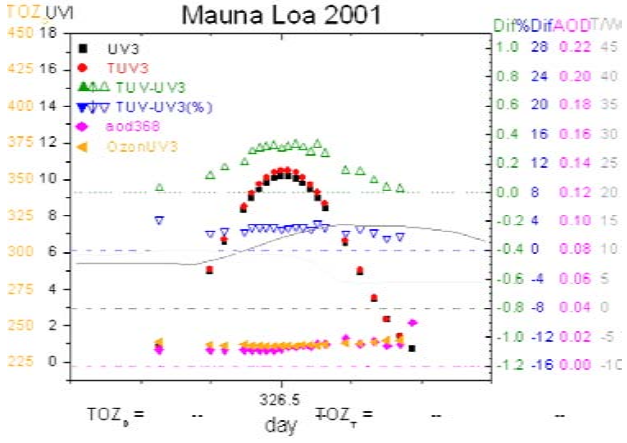
Mauna Loa 2001
TOZ UVI
Dif% Dif AOD T/W
UV3
TUV3
TUV-UV3
TUV-UV3(%)
aod368
OzonUV3
326.5
day
TOZ0 = --
TOZT = --

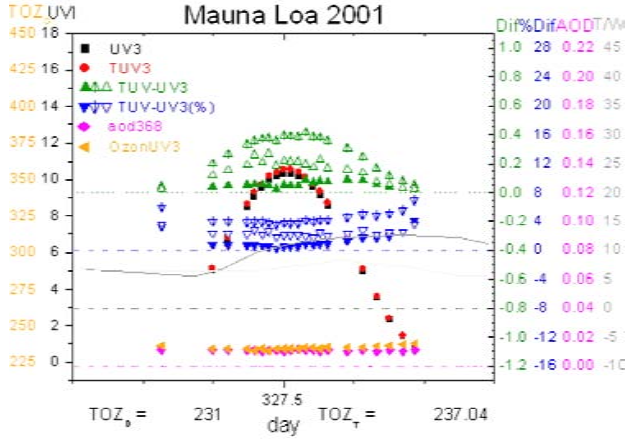
Mauna Loa 2001
TOZ UVI
Dif% Dif AOD T/W
UV3
TUV3
TUV-UV3
TUV-UV3(%)
aod368
OzonUV3
327.5
day
TOZ0 = 231
TOZT = 237.04

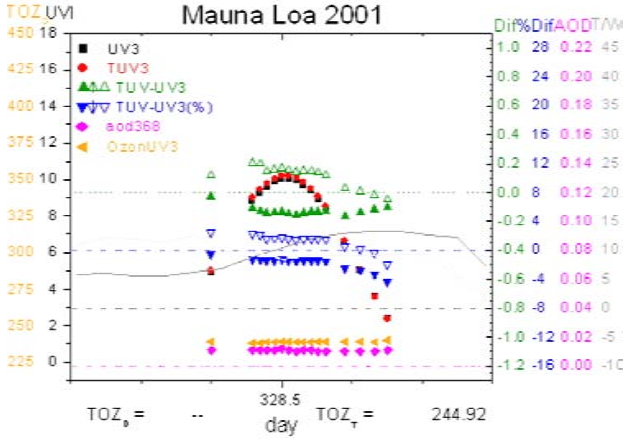
Mauna Loa 2001
TOZ UVI
Dif% Dif AOD T/W
UV3
TUV3
TUV-UV3
TUV-UV3(%)
aod368
OzonUV3
328.5
day
TOZ0 = --
TOZT = 244.92

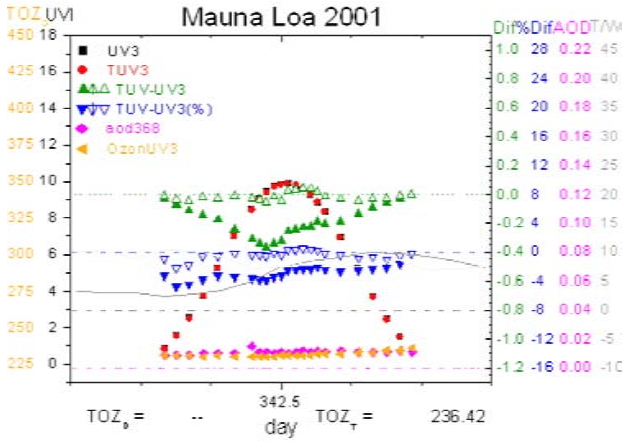
Mauna Loa 2001
TOZ UVI
Dif% Dif AOD T/W
UV3
TUV3
TUV-UV3
TUV-UV3(%)
aod368
OzonUV3
342.5
day
TOZ0 = --
TOZT = 236.42

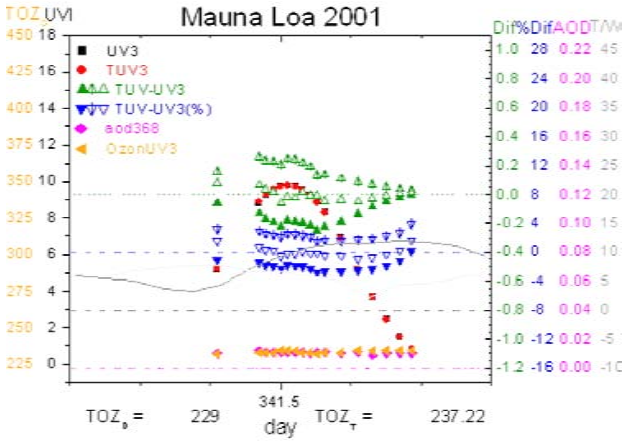
Mauna Loa 2001
TOZ UVI
Dif% Dif AOD T/W
UV3
TUV3
TUV-UV3
TUV-UV3(%)
aod368
OzonUV3
341.5
day
TOZ0 = 229
TOZT = 237.22

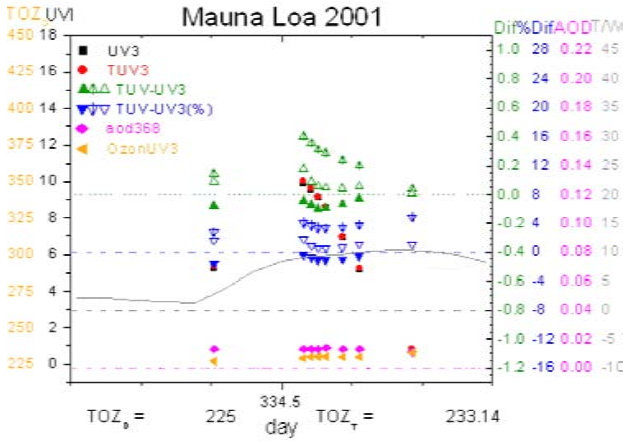
Mauna Loa 2001
TOZ UVI
Dif% Dif AOD T/W
UV3
TUV3
TUV-UV3
TUV-UV3(%)
aod368
OzonUV3
334.5
day
TOZ0 = 225
TOZT = 233.14

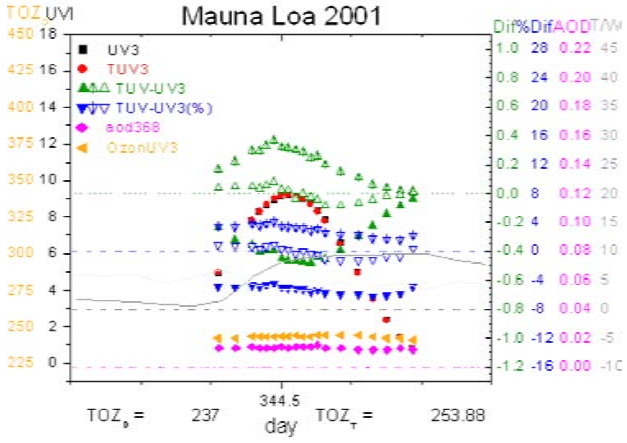
Mauna Loa 2001
TOZ UVI
Dif% Dif AOD T/W
UV3
TUV3
TUV-UV3
TUV-UV3(%)
aod368
OzonUV3
344.5
day
TOZ0 = 237
TOZT = 253.88

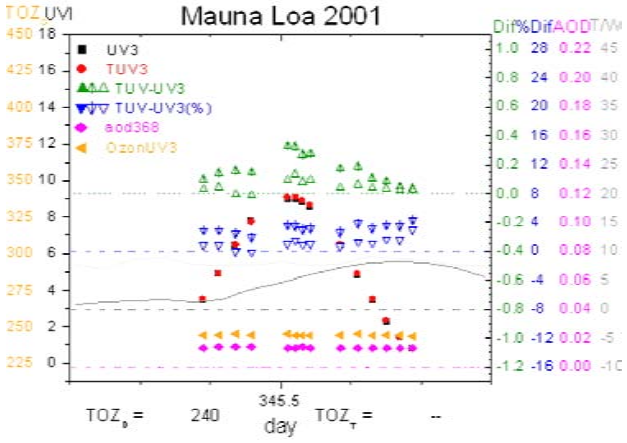
Mauna Loa 2001
TOZ UVI
Dif% Dif AOD T/W
UV3
TUV3
TUV-UV3
TUV-UV3(%)
aod368
OzonUV3
345.5
day
TOZ0 = 240
TOZT = --

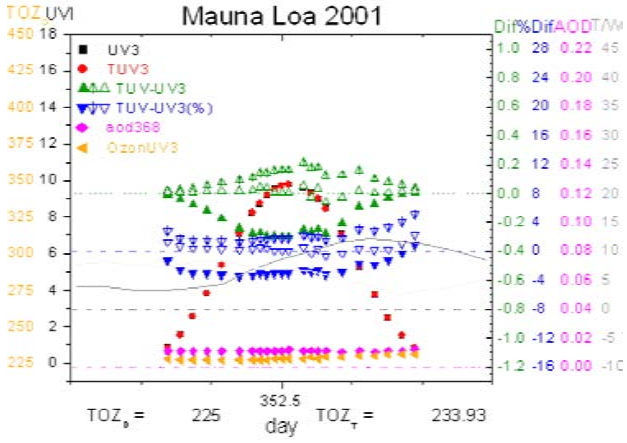
Mauna Loa 2001
TOZ UVI
Dif% Dif AOD T/W
UV3
TUV3
TUV-UV3
TUV-UV3(%)
aod368
OzonUV3
352.5
day
TOZ0 = 225
TOZT = 233.93

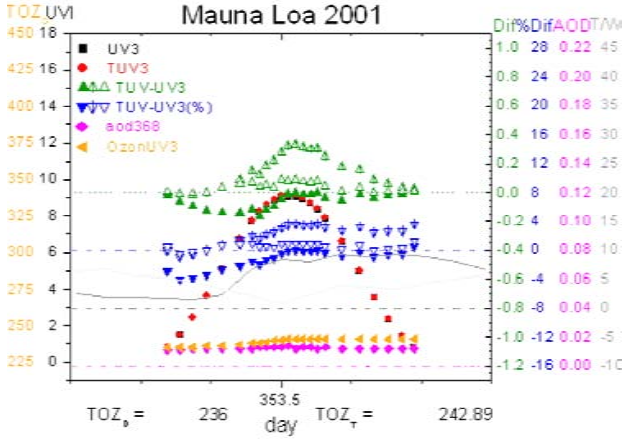
Mauna Loa 2001
TOZ UVI
Dif% Dif AOD T/W
UV3
TUV3
TUV-UV3
TUV-UV3(%)
aod368
OzonUV3
353.5
day
TOZ0 = 236
TOZT = 242.89

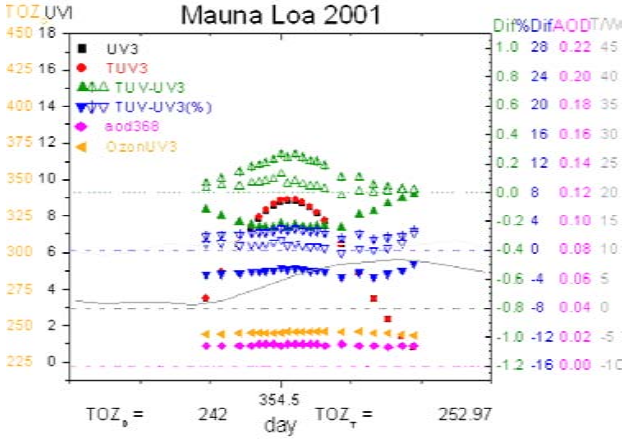
Mauna Loa 2001
TOZ UVI
Dif% Dif AOD T/W
UV3
TUV3
TUV-UV3
TUV-UV3(%)
aod368
OzonUV3
354.5
day
TOZ0 = 242
TOZT = 252.97

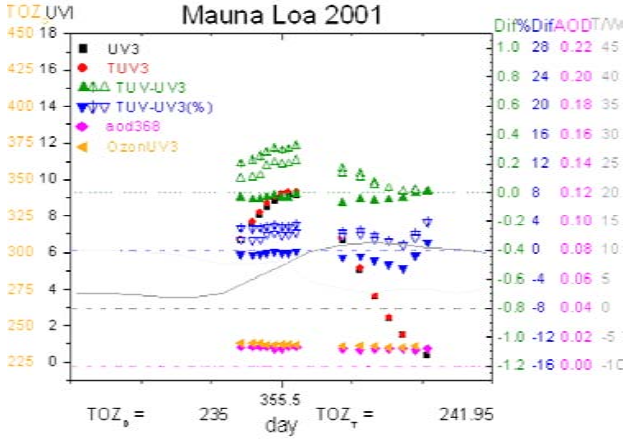
Mauna Loa 2001
TOZ UVI
Dif% Dif AOD T/W
UV3
TUV3
TUV-UV3
TUV-UV3(%)
aod368
OzonUV3
355.5
day
TOZ0 = 235
TOZT = 241.95

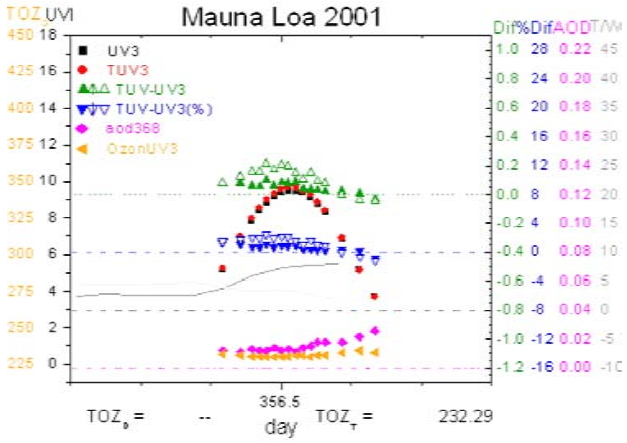
Mauna Loa 2001
TOZ UVI
Dif% Dif AOD T/W
UV3
TUV3
TUV-UV3
TUV-UV3(%)
aod368
OzonUV3
356.5
day
TOZ0 = --
TOZT = 232.29

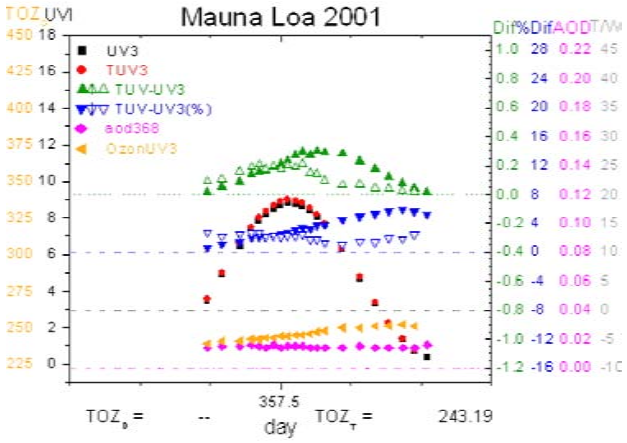
Mauna Loa 2001
TOZ UVI
Dif% Dif AOD T/W
UV3
TUV3
TUV-UV3
TUV-UV3(%)
aod368
OzonUV3
357.5
day
TOZ0 = --
TOZT = 243.19

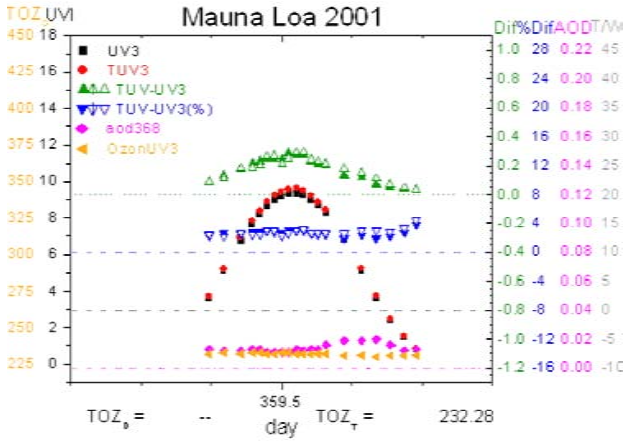
Mauna Loa 2001
TOZ UVI
Dif% Dif AOD T/W
UV3
TUV3
TUV-UV3
TUV-UV3(%)
aod368
OzonUV3
359.5
day
TOZ0 = --
TOZT = 232.28

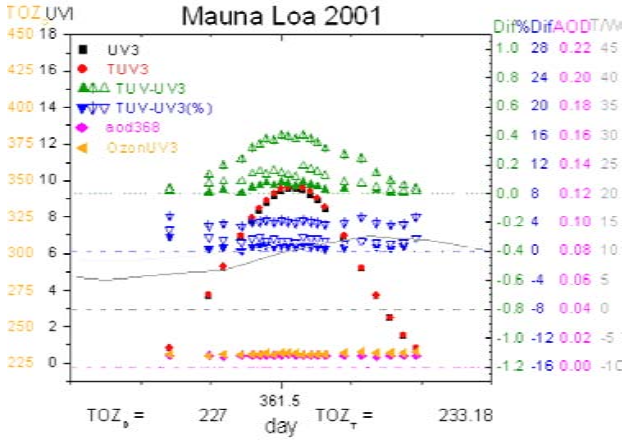
Mauna Loa 2001
TOZ UVI
Dif% Dif AOD T/W
UV3
TUV3
TUV-UV3
TUV-UV3(%)
aod368
OzonUV3
361.5
day
TOZ0 = 227
TOZT = 233.18

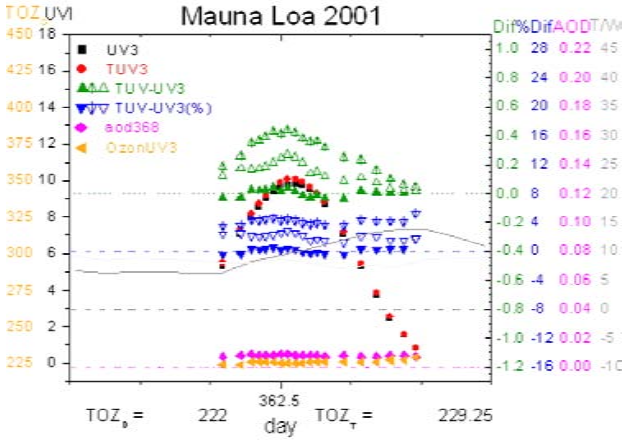
Mauna Loa 2001
TOZ UVI
Dif% Dif AOD T/W
UV3
TUV3
TUV-UV3
TUV-UV3(%)
aod368
OzonUV3
362.5
day
TOZ0 = 222
TOZT = 229.25

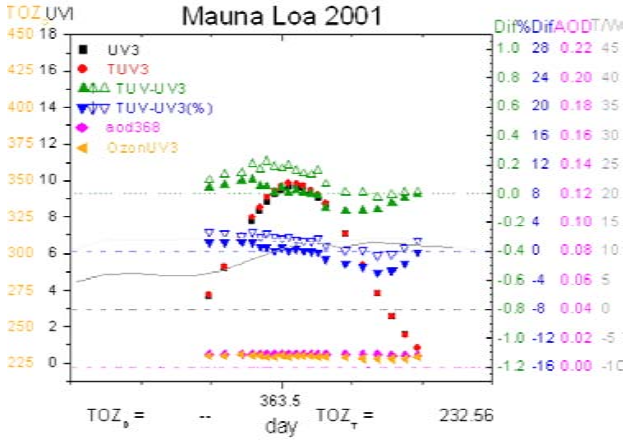
Mauna Loa 2001
TOZ UVI
Dif% Dif AOD T/W
UV3
TUV3
TUV-UV3
TUV-UV3(%)
aod368
OzonUV3
363.5
day
TOZ0 = --
TOZT = 232.56

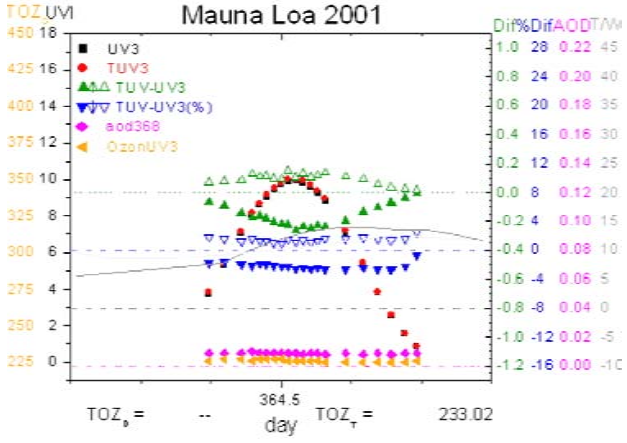
Mauna Loa 2001
TOZ UVI
Dif% Dif AOD T/W
UV3
TUV3
TUV-UV3
TUV-UV3(%)
aod368
OzonUV3
364.5
day
TOZ0 = --
TOZT = 233.02

D.4
Daily plots for clear days in Melbourne 2002

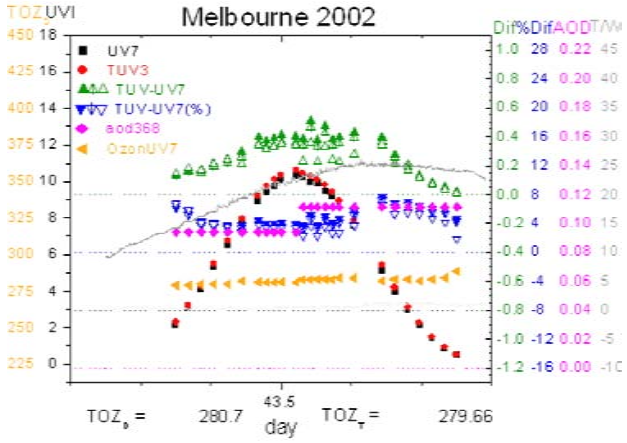
Melbourne 2002
TOZ UVI
Dif% Dif AOD T/W
UV7
TUV3
TUV-UV7
TUV-UV7(%)
aod368
OzonUV7
TOZ0 = 280.7
43.5
day
TOZT = 279.66

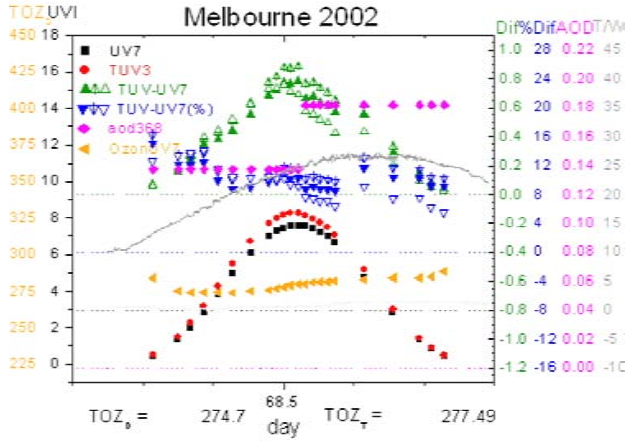
Melbourne 2002
TOZ UVI
Dif% Dif AOD T/W
UV7
TUV3
TUV-UV7
TUV-UV7(%)
aod368
OzonUV7
TOZ0 = 274.7
68.5
day
TOZT = 277.49

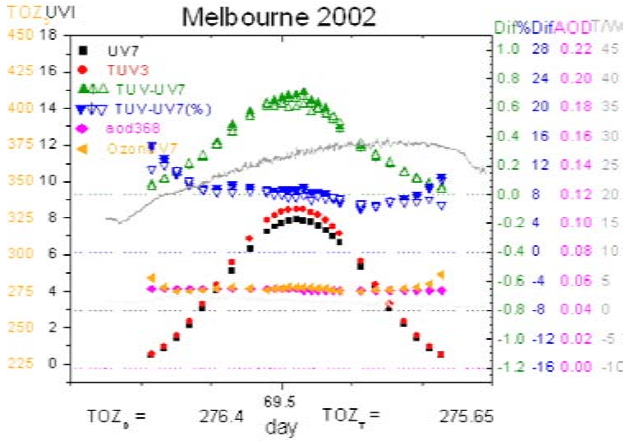
Melbourne 2002
TOZ UVI
Dif% Dif AOD T/W
UV7
TUV3
TUV-UV7
TUV-UV7(%)
aod368
OzonUV7
TOZ0 = 276.4
69.5
day
TOZT = 275.65

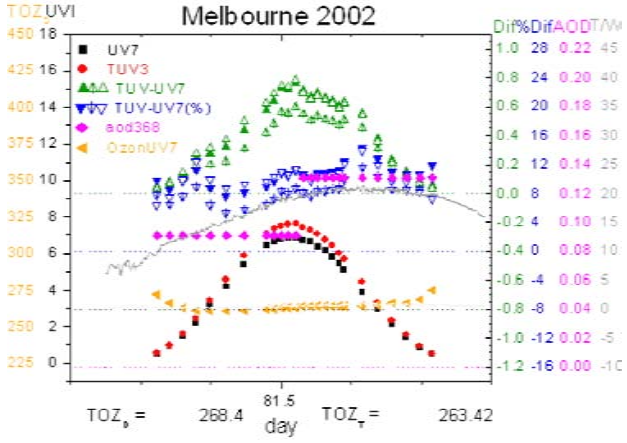
Melbourne 2002
TOZ UVI
Dif% Dif AOD T/W
UV7
TUV3
TUV-UV7
TUV-UV7(%)
aod368
OzonUV7
TOZ0 = 268.4
81.5
day
TOZT = 263.42

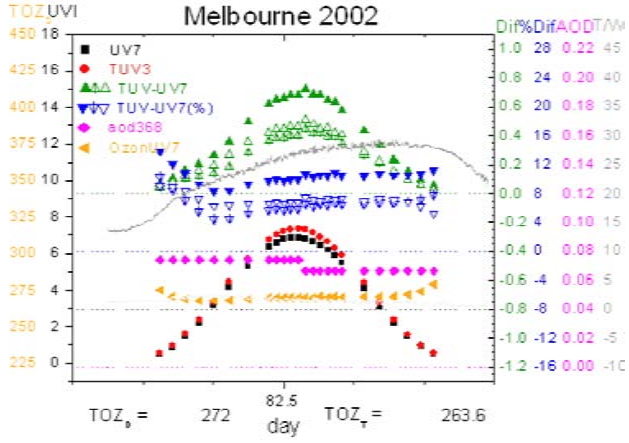
Melbourne 2002
TOZ UVI
Dif% Dif AOD T/W
UV7
TUV3
TUV-UV7
TUV-UV7(%)
aod368
OzonUV7
TOZ0 = 272
82.5
day
TOZT = 263.6

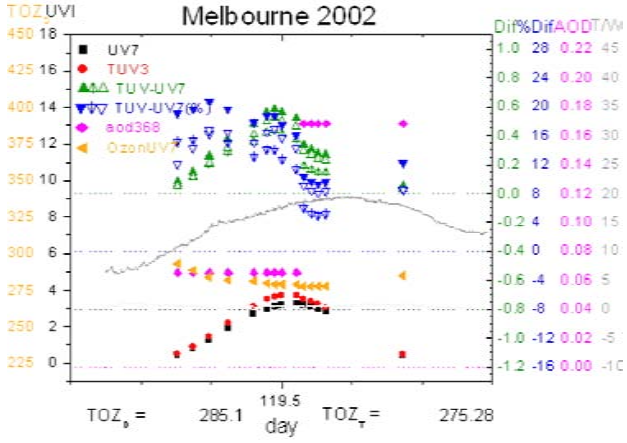
Melbourne 2002
TOZ UVI
Dif% Dif AOD T/W
UV7
TUV3
TUV-UV7
TUV-UV7(%)
aod368
OzonUV7
TOZ0 = 285.1
119.5
day
TOZT = 275.28

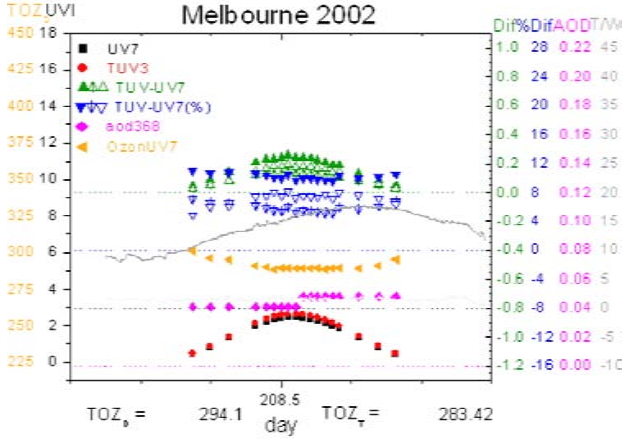
Melbourne 2002
TOZ UVI
Dif% Dif AOD T/W
UV7
TUV3
TUV-UV7
TUV-UV7(%)
aod368
OzonUV7
TOZ0 = 294.1
208.5
day
TOZT = 283.42

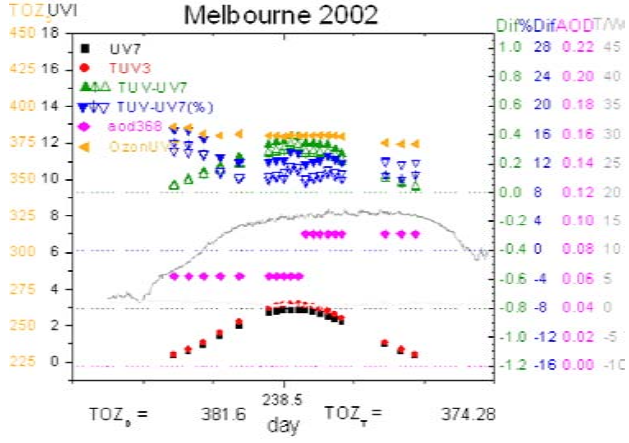
Melbourne 2002
TOZ UVI
Dif% Dif AOD T/W
UV7
TUV3
TUV-UV7
TUV-UV7(%)
aod368
OzonUV7
TOZ0 = 381.6
238.5
day
TOZT = 374.28

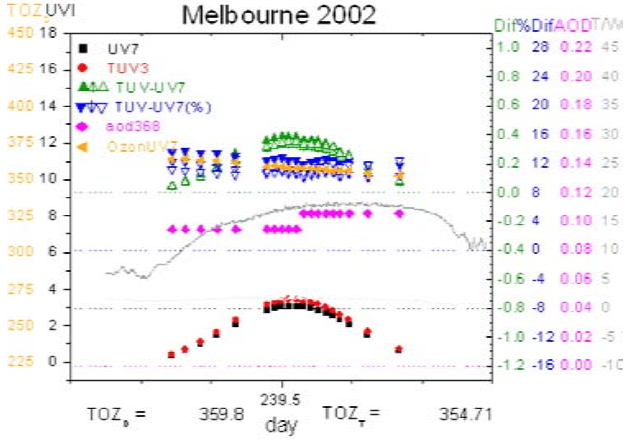
Melbourne 2002
TOZ UVI
Dif% Dif AOD T/W
UV7
TUV3
TUV-UV7
TUV-UV7(%)
aod368
OzonUV7
TOZ0 = 359.8
239.5
day
TOZT = 354.71

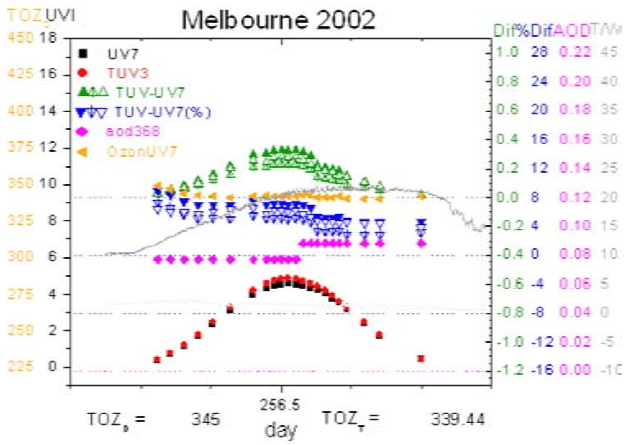
Melbourne 2002
TOZ UVI
Dif% Dif AOD T/W
UV7
TUV3
TUV-UV7
TUV-UV7(%)
aod368
OzonUV7
TOZ0 = 345
256.5
day
TOZT = 339.44

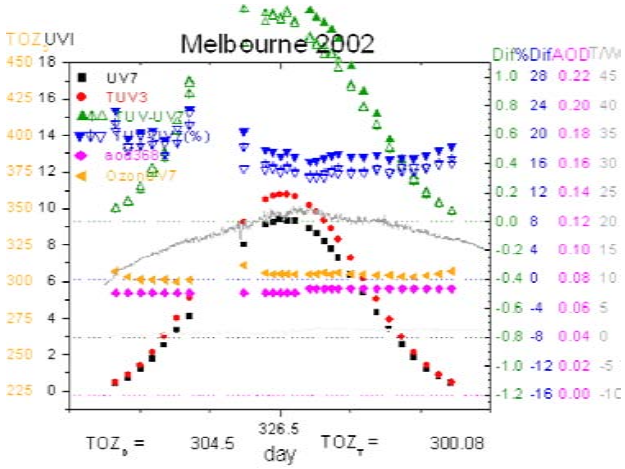
Melbourne 2002
TOZ UVI
Dif% Dif AOD T/W
UV7
TUV3
TUV-UV7
TUV-UV7(%)
aod368
OzonUV7
TOZ0 = 304.5
326.5
day
TOZT = 300.08

Annex E: Statistical Analysis of *TOZ* from TOMS in Catalonia, Spain

In Chapter 5 (Section 5.4.2), seasonal maps of typical UVI for the region of Catalonia are presented. For this, climatic values of *TOZ* from TOMS have been used. These have been derived from 25 years of data. Catalonia is seen by TOMS through 7 cells (see Figure E.1) although for that study one *TOZ* value representing the whole territory at each time was considered. In order to evaluate this simplification, here we present a basic statistic analysis of 25 years (1979-2003) of *TOZ* data from TOMS. From the obtained results, a discussion about the *TOZ* prediction for Catalonia is presented.

E.1 Data Analysis

Table E.1 shows the mean, minimum and maximum *TOZ* values for the 25-years time series for each cell. The mean annual *TOZ* values range from 318.4 to 323.2 DU, showing a tendency to increase from west to east and from north to south. Note that, from this, the largest systematic *TOZ* deviation between cells is 4.8 DU, which is well within the uncertainty associated to the *TOZ* measurement from TOMS (3%, see Table 4.6).

The minimum *TOZ* record for this period of time was between 181.3 and 198.1 DU and the maximum record was between 505 to 514 DU.

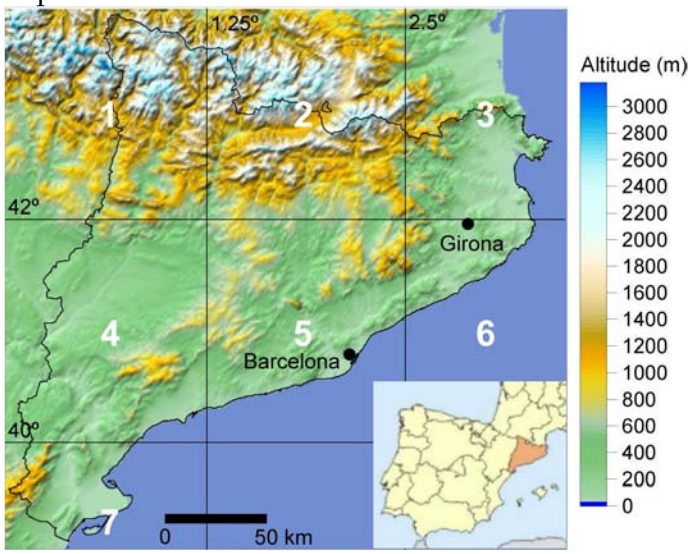

Figure E.1 (Same as Figure 5.1) Topographic map of Catalonia with 1 km resolution. The low-right square shows the situation of Catalonia in the Iberian Peninsula. Latitude and longitude lines are also shown. The numbers in white indicate the TOMS cells.

Table E.2 shows the linear regression coefficients among the seven time series. The correlation coefficients are always larger than 0.94, being the best correlations for the neighbour cells and the worst for the furthest cells.

Figure E.2 shows, as an example, the *TOZ* from the 7 cells plotted for the year 2002. Note that, despite the differences commented above, the *TOZ* for the seven cells follows the same day-to-day variation. Figure E.2 also shows the climatic *TOZ* values (used in Section 5.4.2) found through moving averages of ±5 days of 25 years of data and averaging together the values for the 7 cells. The error bars also displayed correspond to one standard deviation of the data. See that, as it has been noted for the climatic *TOZ* values for Girona (see Figure

Table E.1 Mean, minimum and maximum *TOZ* values (in DU) from the 25-year time series of *TOZ* from TOMS for each cell.

	Mean	Min	Max
1	318.4	190.1	505
2	319.4	192.1	508
3	323.2	198.1	512
4	320.1	184.2	509
5	321.1	187.2	514
6	323.1	188.2	507
7	320.3	181.3	509

Table E.2 Regression coefficients for the comparison of the 25-year time series of *TOZ* from TOMS for each cell against that for all the others

	1	2	3	4	5	6	7
1	1	0.989	0.966	0.982	0.973	0.952	0.953
2		1	0.987	0.976	0.982	0.971	0.951
3			1	0.960	0.978	0.983	0.941
4				1	0.988	0.963	0.983
5					1	0.987	0.978
6						1	0.960
7							1

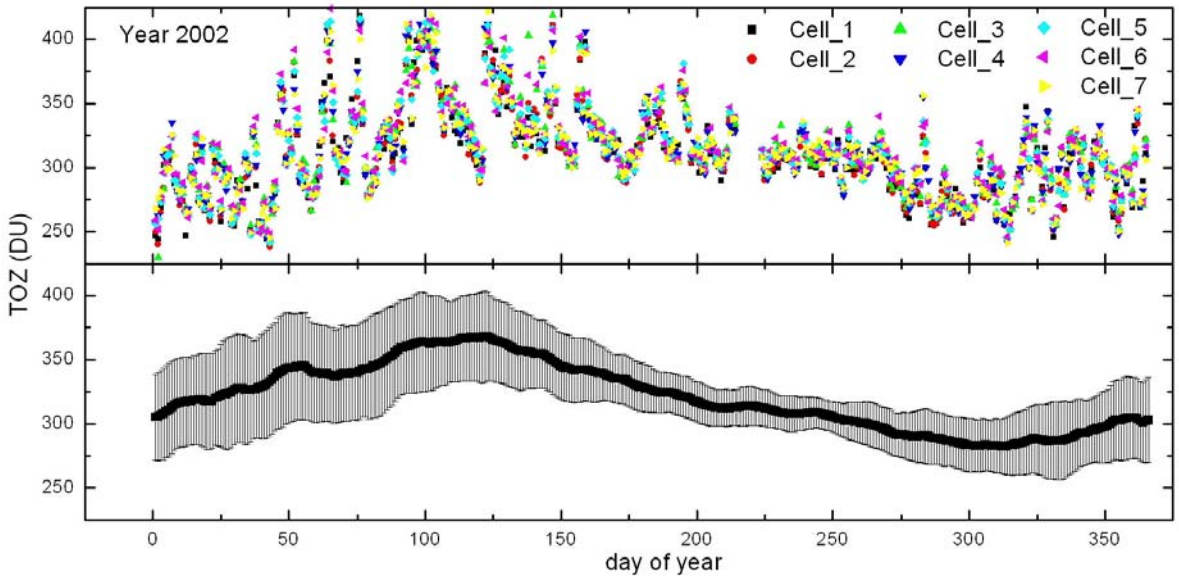

Figure E.2 Upper: Plot of the *TOZ* from TOMS for the 7 cells in Catalonia for 2002. Lower: Climatic *TOZ* (thick line) resulted from moving averages of ±5 days of the *TOZ* from all the cells and for 25 years. The intervals are given by one *SD*.

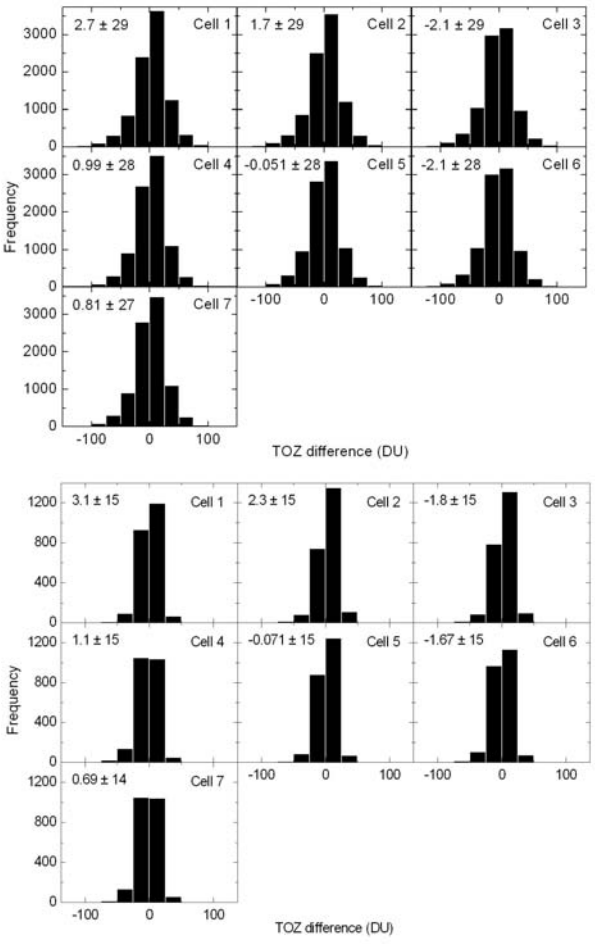

Figure E.3 Histograms of the differences between the climatic *TOZ* values in figure E.2 and the actual measured *TOZ* from TOMS for whole years (upper) and the summer season (lower) for the 25-year series. Mean ± *SD* values (in DU) are shown.

5.7), the standard deviations (*SD*) are much larger for winter (up to 44 DU) than for summer (up to 19 DU) which makes the climatic *TOZ* value for a summer day a better approach to the actual *TOZ* value at each cell.

This can be more clearly seen in the following analysis.

Figure E.3 shows the histograms of the differences between the climatic *TOZ* from Figure E.2 and the actual *TOZ* value for each cell for the whole 25-years series. Mean differences are small for all cells, from -2.1 to 2.7 DU although the *SD* of the differences are large, about 27-29 DU.

Moreover, despite for more than the 80% of the days (for each cell) the differences are within ±40 DU, the minimum and maximum differences found range from -168-157 to 118-135 DU, respectively, all these happening around winter-spring.

The same analysis but only for the summer season is also presented in Figure E.3. Note that the mean differences are also small (from -1.8 to 3.1). However, the *SD* values are as large as the half of those reported above (*SD* ≈ 15 DU) and minimum and maximum differences are also much smaller, from – 84-69 to 49-69 DU, respectively. Moreover, for the more than 80% of the days the differences are within ±20 DU.

These results show that the climatic *TOZ* has no significant systematic differences with the actual measured *TOZ* although differences can often be within ±40DU and peak differences can be very large. However, for the summer days, when UVI is larger and so it is more relevant to have a good estimation of *TOZ*, the differences between the climatic and the actual *TOZ* are greatly reduced.

E.2 Discussion about TOZ prediction

The above presented analysis, apart from being an evaluation about how representative is the climatic *TOZ* found, can also be used to derive the accuracy of the prediction of *TOZ* when considering the climatic *TOZ* as the predicted value.

To have an estimation of how good it would be this way of predicting *TOZ* for Catalonia we can compare the results from Figure E.3 with another approach to *TOZ* prediction commonly considered, which is the hypothesis of persistence. Usually this means that the *TOZ* from yesterday is considered as the predicted *TOZ* for tomorrow since the measured *TOZ* from today is usually not yet available when the prediction is performed. Figure E.4 shows, in an analogue way as Figure E.3, the histograms of the differences between *TOZ*[day-2] and *TOZ*[day]. When whole years are considered, the mean differences are very small, within ±0.022 DU with *SD* values similar to but slightly larger than those in Figure E.3, from 28 to 30 DU. Minimum and maximum differences are – 155-146 DU and 167-187 DU, respectively, although for more than 80% of the days the differences are within ±40 DU. Note that the results are very similar to those in Figure E.3.

When only the summer days are considered (see the histograms in Figure E.4), mean differences remain very small and within the same range (up to 0.015 DU), and *SD* values are much smaller although slightly larger than the corresponding values in Figure E.3, from 16 to 18 DU. Minimum and maximum differences are – 83-75 and 76-96 DU, respectively, although for more than 80% of summer days, the differences are within ±20 DU.

These results show that both ways of predicting the *TOZ* value (that is, using the climatic *TOZ* and the hypothesis of persistence) give, in average, similar results for the region of Catalonia. So, considering the climatic *TOZ* values for prediction purposes seems to be a reasonable option and it has the advantage that it does not depend on the real-time availability of *TOZ* measurements.

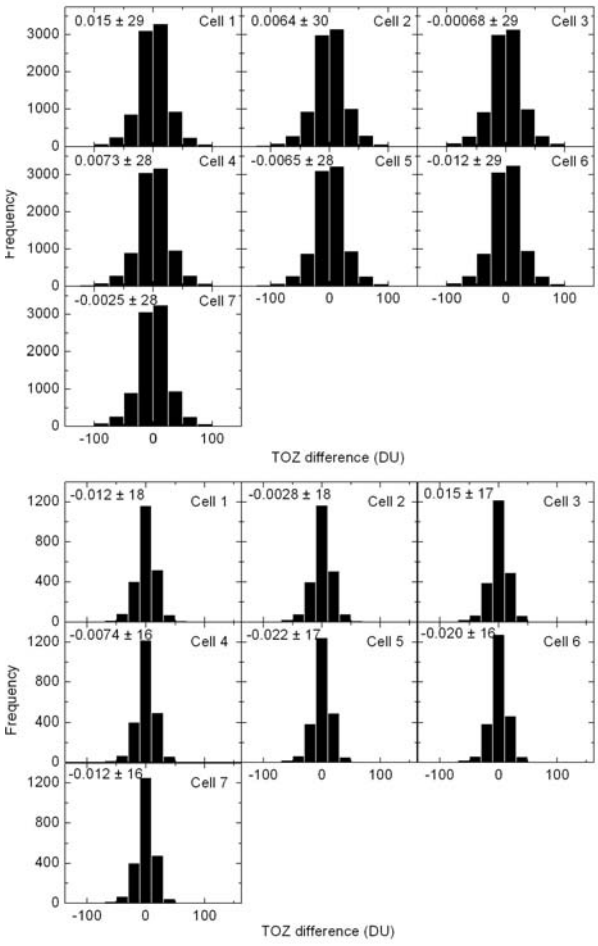

Figure E.4 Histograms of the *TOZ*[day -2] – *TOZ*[day] differences using the *TOZ* from TOMS for whole years (upper) and the summer season (lower) for the 25-year series. Mean ± *SD* values (in DU) are shown.